

INFORMATION TO USERS

This manuscript has been reproduced from the microfilm master. UMI films the text directly from the original or copy submitted. Thus, some thesis and dissertation copies are in typewriter face, while others may be from any type of computer printer.

The quality of this reproduction is dependent upon the quality of the copy submitted. Broken or indistinct print, colored or poor quality illustrations and photographs, print bleedthrough, substandard margins, and improper alignment can adversely affect reproduction.

In the unlikely event that the author did not send UMI a complete manuscript and there are missing pages, these will be noted. Also, if unauthorized copyright material had to be removed, a note will indicate the deletion.

Oversize materials (e.g., maps, drawings, charts) are reproduced by sectioning the original, beginning at the upper left-hand corner and continuing from left to right in equal sections with small overlaps.

Photographs included in the original manuscript have been reproduced xerographically in this copy. Higher quality 6" x 9" black and white photographic prints are available for any photographs or illustrations appearing in this copy for an additional charge. Contact UMI directly to order.

ProQuest Information and Learning
300 North Zeeb Road, Ann Arbor, MI 48106-1346 USA
800-521-0600

UMI[®]

University of Alberta

**Gas-Phase Ethylene/1-Hexene Copolymerization over MgCl_2 -Supported
Ziegler-Natta Catalysts**

by

Wei Liu



**A thesis submitted to the Faculty of Graduate Studies and Research in partial
fulfillment of the requirements for the degree of **Doctor of Philosophy****

in

Chemical Engineering

Department of Chemical and Materials Engineering

Edmonton, Alberta

Spring 2002



**National Library
of Canada**

**Acquisitions and
Bibliographic Services**

**395 Wellington Street
Ottawa ON K1A 0N4
Canada**

**Bibliothèque nationale
du Canada**

**Acquisitions et
services bibliographiques**

**395, rue Wellington
Ottawa ON K1A 0N4
Canada**

Your file Votre référence

Our file Notre référence

The author has granted a non-exclusive licence allowing the National Library of Canada to reproduce, loan, distribute or sell copies of this thesis in microform, paper or electronic formats.

The author retains ownership of the copyright in this thesis. Neither the thesis nor substantial extracts from it may be printed or otherwise reproduced without the author's permission.

L'auteur a accordé une licence non exclusive permettant à la Bibliothèque nationale du Canada de reproduire, prêter, distribuer ou vendre des copies de cette thèse sous la forme de microfiche/film, de reproduction sur papier ou sur format électronique.

L'auteur conserve la propriété du droit d'auteur qui protège cette thèse. Ni la thèse ni des extraits substantiels de celle-ci ne doivent être imprimés ou autrement reproduits sans son autorisation.

0-612-68599-3

Canada

University of Alberta

Library Release Form

Name of Author: Wei Liu

Title of Thesis: Gas-Phase Ethylene/1-Hexene Copolymerization over MgCl₂-Supported Ziegler-Natta Catalysts

Degree: Doctor of Philosophy

Year this Degree Granted: 2002

Permission is hereby granted to the University of Alberta Library to reproduce single copies of this thesis and to lend or sell such copies for private, scholarly or scientific research purposes only.

The author reserves all other publication and other rights in association with the copyright in the thesis, and except as herein provided, neither the thesis nor any substantial portion thereof may be printed or otherwise reproduced in any material from whatever without the author's prior written permission.



Wei Liu

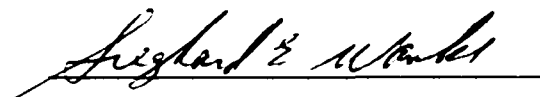
Suite 108, 9819-104St
Edmonton, Alberta
Canada, T5K 0Y8

Date: Dec. 20, 2001

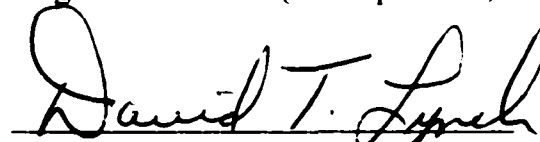
University of Alberta

Faculty of Graduate Studies and Research

The undersigned certify that they have read, and recommend to the Faculty of Graduate Studies and Research for acceptance, a thesis entitled **Gas-Phase Ethylene/1-Hexene Copolymerization over MgCl₂-Supported Ziegler-Natta Catalysts** submitted by **Wei Liu** in partial fulfillment of the requirements for the degree of **Doctor of Philosophy in Chemical Engineering**.



Sieghard E. Wanke (Co-Supervisor)



David T. Lynch (Co-Supervisor)



Phillip Y. K. Choi



Monica M. Palcic



João B. P. Soares

Date: Dec 20, 2001

ABSTRACT

The gas-phase ethylene/1-hexene copolymerization kinetics over morphology-controlled Ziegler-Natta catalysts were studied. In the first part of this study, spherically shaped MgCl_2 -supported TiCl_4 catalysts were synthesized by the emulsion quenching technique using various preparation conditions, e.g. different MgCl_2 : ethanol ratios and different amounts of electron donor, and the effects of the variation of catalyst preparation methods on catalytic activity and morphology of the nascent polyethylene were studied. It was found that electron donor was important in determining homopolymerization activities, nascent polymer morphologies and 1-hexene incorporation ability. Prepolymer with low yield (<100 g PE/gcat) was synthesized under mild conditions and was used as catalyst in the subsequent studies. Prepolymer particle growth process was examined by scanning electron microscopy and the effects of prepolymer size on the polymerization was studied.

In the kinetic study part, a new technique was used to achieve constant gas-phase composition during the 2-hour copolymerization runs in a 1-L reactor operated in the semi-batch mode of constant pressure. This technique allows the determination of the 1-hexene consumption; this rate of 1-hexene consumption provides direct evidence of the multi-site nature of supported Ziegler-Natta catalysts. The effects of temperature (60 to 90°C), 1-hexene, ethylene and hydrogen pressures (0 to 14 psi, 60 to 250 psi and 0 to 50 psi, respectively) and the length of runs on the activity profiles, 1-hexene consumption rates and polymer properties (e.g. molar mass, chemical composition and crystallinity) were determined.

Solubility of 1-hexene and ethylene in the polymer were found important in describing polymerization kinetics. In this study, solubilities of ethylene and 1-hexene were measured. The non-linear behavior of 1-hexene sorption was described using Flory-Huggins and Peng-Robinson equations. The sorption of 1-hexene in the 1-hexene/ethylene mixture was different from its solubility under pure 1-hexene conditions. This co-sorption of 1-hexene was indirectly estimated.

A three-site kinetic model based on kinetic understanding and polymer characterization was finally proposed. The first site is largely responsible for 1-hexene incorporation; this site is activated rapidly (<10 min) and deactivates in less than 1 hour. The other two sites are essentially ethylene homopolymerization sites. Langmuir-Hinshelwood adsorption theory was applied to describe the interaction of sorbed ethylene and 1-hexene with the catalytic sites. Simulation results showed that the model was successful in describing the observed rate profiles and copolymer compositions.

ACKNOWLEDGEMENTS

Many individuals have contributed in different ways to the completion of this thesis.

First of all, I would like to express my sincere gratitude to my advisors, Professor Sieghard Wanke and Professor David Lynch for their invaluable guidance and support during the entire course of this investigation. They inspired me in making the transition from student to researcher. I am deeply grateful for the kind help that Professor Wanke provided in my writing of this thesis.

I am thankful to those colleagues and department staff who provided direct assistance during this research project: Dr. Long Wu for the instruction and kind help in catalyst preparation studies; Ms. Naiyu Bu for the assistance in acquainting me with the polymerization reactor equipment, for providing valuable advice regarding my research, and for the doing the SEC measurements; Mr. MingQian Zhang for the TREF and solubility measurements; Ms. Tina Barker for doing SEM experiments and teaching me the operations; Mr. Walter Boddez and Mr. Richard Cooper for the great job in keeping all equipment running well; Ms. Andree Koenig for helping me set up the gas chromatograph; Mr. Jack Gibeau and Mr. Bob Barton for their willing in sharing their computer expertise; Mr. Ah-Dong Leu for X-ray diffraction measurements; and Mr. Bob Scott for the mechanical work. I would also like to thank Professor Jeff Stryker's group in the Department of Chemistry for letting me using the equipment and chemicals in their laboratory and Dr. GuiZhong Qi for giving me the instruction of NMR operations during weekends.

I wish to thank the many friends I made in Alberta during the last five years, who make my life more enjoyable.

Finally, I would like to dedicate this work to my parents, to express my forever gratitude for their deep love, support and encouragement all the time.

TABLE OF CONTENTS

CHAPTER 1. INTRODUCTION	1
CHAPTER 2. LITERATURE REVIEW	6
2.1 Catalytic Olefin Polymerization Process	6
2.2 Olefin Polymerization Catalysts	9
2.2.1 Phillips Catalysts	10
2.2.2 Ziegler-Natta Catalysts	11
2.2.3 Metallocene Catalysts	12
2.2.4 Other Olefin Polymerization Catalysts	14
2.3 Heterogeneous Ziegler-Natta Catalysts	14
2.3.1 The MgCl ₂ Support	15
2.3.2 Electron Donor	17
2.3.3 Cocatalyst and Active Centre	19
2.4 Kinetics of Polymerization	22
2.4.1 Slurry versus Gas-Phase Reactions	23
2.4.2 Active Centre Studies	24
2.4.3 Cocatalyst	25
2.4.4 Influence of Hydrogen	26
2.4.5 Catalyst Deactivation	28
2.4.6 Prepolymerization	30
2.4.7 Comonomer and Copolymerization	31
2.5 Modeling Description of Kinetic Behaviors	32
2.5.1 Variables in Modeling Polymerization Kinetics	33
2.5.2 Adsorption Theory	34
2.5.3 Multi-Site Theory	36
2.6 Characterization of LLDPE	41
2.6.1 Physical Structure Characterization	41
2.6.2 Chemical Structure Analysis	44

CHAPTER 3. EXPERIMENTAL PROCEDURE AND CONDITIONS	49
3.1 Catalyst Preparation	49
3.1.1 Preparation of Spherical MgCl ₂ Support Particles by Melt Quenching Method	49
3.1.2 Dealcoholation Treatment	50
3.1.3 Catalyst Preparation	51
3.2 Prepolymerization and Polymerization	56
3.2.2 Prepolymerization	56
3.2.2 Polymerization	56
3.3 Controlling 1-Hexene Concentration in the Gas Phase	59
3.4 Characterization Techniques	62
3.4.1 Nuclear Magnetic Resonance (NMR)	62
3.4.2 Size Exclusion Chromatography (SEC or GPC)	65
3.4.3 Scanning Electron Microscopy (SEM)	65
3.4.4 Temperature Rising Elution Fractionation (TREF)	66
3.4.5 Differential Scanning Calorimetry (DSC)	69
 CHAPTER 4. RESULTS OF MgCl₂/TiCl₄ CATALYST SYNTHESIS	 71
4.1 General Rules of Obtaining Spherical Catalyst Particles	71
4.2 Influence of Catalyst Composition on Activity and Product Morphology	75
4.2.1 Effects of C ₂ H ₅ OH/MgCl ₂ on Activity and Bulk Density	75
4.2.2 Effects of Ti Distribution on Activity and Bulk Density	78
4.2.3 Effects of Dibutyl Phthalate on Activity and Bulk Density	81
4.2.4 Effects of Dibutyl Phthalate on Copolymerization	84
 CHAPTER 5. PREPOLYMER STUDIES	 87
5.1 Polymer Growth on the Catalysts	87
5.2 Prepolymer Size Effects	96

CHAPTER 6. KINETICS OF ETHYLENE/1-HEXENE COPOLYMERIZATION	102
6.1 Reproducibility of Copolymerization Experiments	102
6.2 Effects of Prepolymerized Catalyst Amount	107
6.3 Effects of Monomer/Comonomer Concentrations on Kinetics	109
6.3.1 Constant Ethylene Pressure	109
6.3.2 Constant 1-Hexene/Ethylene Ratios	115
6.3.3 Constant 1-Hexene Pressure	117
6.4 Effects of Hydrogen	118
6.5 Effects of Temperature	122
6.6 Effects of Length of Runs	126
6.7 Comparison of Homopolymerization and Copolymerization in Gas Phase and Slurry Phase	127
 CHAPTER 7. NASCENT COPOLYMER PROPERTIES AND SOLUBILITIES	 132
7.1 Molar Mass and Its Distribution	132
7.1.1 Comparison of Homo- and Copolymerization	132
7.1.2 Comonomer Effects on Molar Masses	132
7.1.3 Effects of Hydrogen	134
7.1.4 Effects of Temperature	134
7.1.5 Effects of Length of Runs	134
7.2 Chemical Composition of LLDPE	136
7.2.1 Results from ¹³ C-NMR Measurement	136
7.2.2 1-Hexene Distribution in Polymer from TREF Analyses	139
7.3 Crystallinity	141
7.3.1 General Features of DSC Curves	141
7.3.2 Effects of Comonomer Concentration	143
7.3.3 Effects of Hydrogen	144
7.3.4 Effects of Temperature	144

7.4	Solubility	146
7.4.1	Solubility of Ethylene and 1-Hexene in Nascent Polymer	146
7.4.2	Modeling of Ethylene and 1-Hexene Concentration in Polymer	148
7.4.3	Co-solubility Estimation	152
 CHAPTER 8. KINETICS INTERPRETATION OF ETHYLENE/ 1-HEXENE COPOLYMERIZATION		 157
8.1	Multiple Site Nature	157
8.2	Modeling of Copolymerization	160
8.3	Model Fitting Procedure and Results	166
8.4	Comments on Model	184
8.4.1	Model Improvements	184
8.4.2	Additional Comparison of Model and Experimental Results	185
 CHAPTER 9. CONCLUSIONS AND RECOMMENDATIONS		 188
8.1	Conclusions	188
8.2	Recommendations	191
 REFERENCES		 192
 APPENDIX A: ANALYSIS OF GAS-PHASE COMPOSITION IN REACTOR BY GAS CHROMATOGRAPHY		 213
A.1	Gas Chromatography System	213
A.2	Determination of Response Factors	214
A.3	Control of 1-Hexene Composition	215

APPENDIX B: 1-HEXENE PHYSICAL AND THERMODYNAMIC PROPERTIES	217
B.1 Vapor Pressure of 1-Hexene	217
B.2 Density of 1-Hexene Liquid	217
B.3 PVT Properties of 1-Hexene	217
APPENDIX C: CALCULATION OF 1-HEXENE REACTION RATE	220
APPENDIX D: SUMMARY OF SUPPORT AND CATALYST PREPARATION AND HOMO-CO-POLYMERIZATION RUNS	224

LIST OF TABLES

Table 1.1	Summary the Largest Polyethylene Producers (Brown, 2000).	1
Table 2.1	Comparison of the Features of Different Polyolefin Catalysts.	12
Table 4.1	Summary of Activities and Product Bulk Densities for Various Catalysts.	76
Table 4.2	Summary of Copolymerization Activities for Catalysts with Different DBP Contents.	84
Table 5.1	X-ray Quantitative Analysis of Catalyst and Prepolymer with Different Yields.	93
Table 6.1	Summary of Copolymerization Results for Reproducibility Study.	104
Table 6.2	Experimental Results in Studying the Effects of Catalyst Amount on Kinetics.	107
Table 6.3	Copolymerization Results at Different Ethylene and 1-Hexene Pressures.	110
Table 6.4	Summary of Polymerization Runs at Different Hydrogen Pressures.	119
Table 6.5	Experimental Results of Copolymerization under Different Temperatures.	123
Table 6.6	Experimental Conditions and Results for Homo- and Copolymerization Runs in Slurry Phase and Gas Phase.	128
Table 7.1	Molar Masses and Polydispersity o Homopolymer and Copolymer under Similar Reaction Conditions.	133
Table 7.2	Summary of Reaction Conditions and DSC Analysis Results.	142
Table 8.1	Complete Parameters Used for Multi-Site Model Simulations.	170
Table A.1	Experimental Results of Response Factor Determination.	215
Table C.1	Calculation of 1-Hexene Incorporation Rate of Run GasCo40.	223
Table D.1	Summary of Support Preparation Results.	225
Table D.2	Summary of Catalyst Preparation Results.	226
Table D.3	Summary of Prepolymerization Runs.	227
Table D.4	Summary of Copolymerization Runs.	228
Table D.5	Summary of Homopolymerization Runs.	231

LIST OF FIGURES

Figure 1.1	Relationship between short chain branching length and the toughness of Union Carbide LLDPEs (James, 1986)	3
Figure 3.1	Schematic Diagram of Catalyst Preparation Procedure	53
Figure 3.2 (a)	Optical micrograph of MgCl₂ support particles	55
Figure 3.2 (b)	Scanning electron micrograph of catalyst particles	55
Figure 3.3	Schematic diagram of the copolymerization equipment	57
Figure 3.4	Concentration change of 1-hexene in the gas phase during the first experiment when 1-hexene was only added once at the beginning	61
Figure 3.5	Estimated rate of 1-hexene disappearance based on derivative of fitting curve in Figure 3.4	61
Figure 3.6 (a)	Control result of the second run based on the predictions shown in Figure 3.5 and on-line modification	63
Figure 3.6 (b)	Actual 1-hexene addition process in the second run (GasCo42)	63
Figure 3.7	X-ray mapping of catalyst Cat-4 (see Appendix D for catalyst preparation summary) surface and cross section	67
Figure 3.8	X-ray microanalysis spectrum of catalyst Cat-4	68
Figure 3.9	TREF profile for sample GasCo08 (see Appendix E)	69
Figure 3.10	DSC endothermic curve of copolymer GasCo46 (see Appendix E)	70
Figure 4.1	SEM image of support (Support-17) with EtOH/MgCl₂ mole ratio of 3.5	73
Figure 4.2	SEM image of support (Support-18) from emulsion before steady state was established. (120°C for 20 minutes).	73
Figure 4.3	SEM image of support (Support-15) operated at 130°C and 590 rpm.	74
Figure 4.4	SEM image of support (Support-16) operated at 115°C and 1000 rpm.	74
Figure 4.5	Catalyst (Cat-4) made form Support-16 shown in Figure 4.4. Fines observed in Figure 4.4 disappeared during the introduction of Ti and subsequent washings.	75
Figure 4.6	Dependence of catalyst activity and polymer bulk density on support C₂H₅OH/MgCl₂ ratio.	77
Figure 4.7	Dependence of catalyst activity on titanium content.	78

Figure 4.8	X-ray mapping observation of internal Cat-4 particles.	79
Figure 4.9	Internal structure of Polymer A made with Cat-5.	80
Figure 4.10	Internal structure of Polymer B made with Cat-4.	80
Figure 4.11	Relationship between DBP/MgCl₂ and bulk density.	82
Figure 4.12	Dependence of average homopolymerization rate on DBP/MgCl₂.	82
Figure 4.13	Effects of DBP content on 1-hexene incorporation ability.	86
Figure 5.1	Typical reaction profile of prepolymerization run.	88
Figure 5.2	Particle growth observation. Color pictures are x-ray dot mappings of elements Mg (blue), Cl (red) and Ti (yellow). Black/white pictures are SEM micrographs of catalyst and prepolymers.	90
Figure 5.3	Concentration differences of Cl, Mg and Ti between outer layer and inner part.	94
Figure 5.4	Particle growth model under mild conditions.	95
Figure 5.5	Polymerization profiles of prepolymers with different particle size under same conditions.	97
Figure 5.6	Polymer particle size and average polymerization rate as functions of prepolymer particle size.	98
Figure 5.7	Dependence of M_w on prepolymer size.	99
Figure 5.8	Dependence of polydispersity Q on prepolymer size.	99
Figure 6.1	Comparison of reaction profiles of two runs with comonomer control (GasCo15) and without control (GasCo14).	105
Figure 6.2	Comparison of reaction profiles of two runs (GasCo18 and GasCo40) under similar reaction conditions.	106
Figure 6.3	Comparison of ethylene reaction profiles for different amounts of catalyst.	108
Figure 6.4	Comparison of 1-hexene consumption rates at different Al/Ti ratios based on GC analysis.	108
Figure 6.5	Ethylene rate profiles at P_{C2}=60 psi and different 1-hexene pressures.	111
Figure 6.6	Ethylene rate profiles at P_{C2}=150 psi and different 1-hexene pressures.	111
Figure 6.7	Ethylene rate profiles at P_{C2}=250 psi and different 1-hexene pressures.	112

Figure 6.8	Dependence of average rate of PE production on ethylene and 1-hexene pressures.	113
Figure 6.9	Dependence of 1-hexene consumption rate on ethylene and 1-hexene pressures.	114
Figure 6.10	Ethylene rate profiles at constant C_6/C_2 ratio.	115
Figure 6.11	Dependence of ethylene reaction rates in the early stages and in the end of runs on ethylene pressure with constant C_6/C_2 ratio.	116
Figure 6.12	Dependence of overall 1-hexene consumption rates on 1-hexene pressure with constant C_6/C_2 ratio.	116
Figure 6.13	The power order relations between pressure and average reaction activity at constant 1-hexene pressures.	117
Figure 6.14	Dependence of average 1-hexene consumption rate on ethylene pressure at constant 1-hexene pressures.	119
Figure 6.15	Rate profiles of copolymerization at different hydrogen concentrations.	120
Figure 6.16	Hydrogen effects on ethylene and 1-hexene reaction rates.	121
Figure 6.17	Hydrogen effects on reaction rate ratio of 1-hexene/ethylene.	121
Figure 6.18	Rate profiles of copolymerization at different reaction temperatures.	123
Figure 6.19	Dependence of average reaction rates of 1-hexene and ethylene on reaction temperature.	124
Figure 6.20	Dependence of 1-hexene/ethylene reaction rate ratio on reaction temperature.	125
Figure 6.21	Arrhenius plot of the average copolymerization rate.	125
Figure 6.22	Ethylene rate profiles with different length of runs. $P_{C_2}=150$ psi, $P_{C_6}=14$ psi, $T = 70^\circ\text{C}$.	126
Figure 6.23	Dependence of polymer yield and average 1-hexene amount dissolved and incorporated in polymer on length of runs.	127
Figure 6.24	Plot of R_p versus time according to first-order decay law, eq. (6.2).	128
Figure 6.25	Comparison of ethylene homo- and copolymerization rate profiles in gas-phase (a) and slurry-phase (b) operations.	130
Figure 7.1	Relationship between 1-hexene pressure and molar mass and polydispersity ($P_{C_2} = 60$ psi).	133

Figure 7.2	Effects of hydrogen on molar mass and polydispersity (Runs GasCo42, 59, 60 and 61).	135
Figure 7.3	Effects of temperature on molar mass and polydispersity. (Runs GasCo60, 62, 64 and 65).	135
Figure 7.4	Effects of run lengths on M_n and M_w.	136
Figure 7.5	1-Hexene content of the product as a function of 1-hexene pressure In the reactor.	137
Figure 7.6	1-Hexene content in the copolymer as a function of hydrogen pressure.	138
Figure 7.7	1-Hexene content in the copolymer as a function of reaction temperature.	138
Figure 7.8	Short chain branching distribution (SCBD) of copolymers produced under ethylene pressure of 60 psi.	139
Figure 7.9	Comparison of average SCB contents measured by ^{13}C-NMR and TREF.	140
Figure 7.10	DSC endotherms of nascent LLDPE samples.	143
Figure 7.11	Dependence of crystallinity on 1-hexene content in polymer.	144
Figure 7.12	Dependence of crystallinity on hydrogen.	145
Figure 7.13	Dependence of crystallinity on reaction temperature.	145
Figure 7.14	Solubility of ethylene in GasCo38 as a function of ethylene pressure at different temperatures.	146
Figure 7.15	Solubility of 1-hexene in GasCo38 as a function of 1-hexene pressure at different temperatures.	147
Figure 7.16	Comparison of the 1-hexene solubilities of commercial polyethylenes and GasCo38 at 69°C. The data of commercial polyethylene are obtained from Moore (2000).	148
Figure 7.17	Flory-Huggins interaction parameter as a function of 1-hexene pressure.	152
Figure 7.18	Experimental results and Flory-Huggins/Peng-Robinson simulations for 1-hexene solubility at different pressure and temperatures for GasCo38.	153
Figure 7.19	Comparison of calculated co-solubility of 1-hexene in polymers and the measurement solubility of 1-hexene in GasCo38.	154
Figure 7.20	Co-solubility of 1-hexene in the product based on C_6/C_2 ratio	155
Figure 7.21	Co-solubility of 1-hexene in the presence of hydrogen.	155
Figure 7.22	Co-solubility of 1-hexene at different reaction temperatures.	156

Figure 8.1	Long homopolymerization run (GasHo13).	158
Figure 8.2	Multiple-site nature of catalyst observed from molar mass distribution Curve. (1: dissolved polymer, 2: non-dissolved, 3: whole sample.)	159
Figure 8.3	Deconvolution result of GPC curve of sample GasCo36 (P_{C_2}=60 psi, P_{C_6} =9.3 psi) by three Gaussian Peaks.	160
Figure 8.4	1-Hexene average reaction rate for run GasCo40 (P_{C_2}=60 psi, P_{C_6}=3.4 psi)	167
Figure 8.5(a)	Comparison of ethylene reaction profile and model prediction for GasCo40 (P_{C_6}= 3.4 psi, P_{C_2}= 60 psi).	171
Figure 8.5(b)	Comparison of ethylene reaction profile and model prediction for GasCo18 (P_{C_6}= 3.7 psi, P_{C_2}= 60 psi).	171
Figure 8.5(c)	Comparison of ethylene reaction profile and model prediction for GasCo35 (P_{C_6}= 5.1 psi, P_{C_2}= 60 psi).	172
Figure 8.5(d)	Comparison of ethylene reaction profile and model prediction for GasCo34 (P_{C_6}= 6.4 psi, P_{C_2}= 60 psi).	172
Figure 8.5(e)	Comparison of ethylene reaction profile and model prediction for GasCo39 (P_{C_6}= 7.5 psi, P_{C_2}= 60 psi).	173
Figure 8.5(f)	Comparison of ethylene reaction profile and model prediction for GasCo36 (P_{C_6}= 9.3 psi, P_{C_2}= 60 psi).	173
Figure 8.5(g)	Comparison of ethylene reaction profile and model prediction for GasCo38 (P_{C_6}= 11.5 psi, P_{C_2}= 60 psi).	174
Figure 8.6(a)	Comparison of ethylene reaction profile and model prediction for GasCo15 (P_{C_6}= 5.9 psi, P_{C_2}= 107 psi).	174
Figure 8.6(b)	Comparison of ethylene reaction profile and model prediction for GasCo53 (P_{C_6}= 14.0 psi, P_{C_2}= 105 psi).	175
Figure 8.7	Comparison of ethylene reaction profile and model prediction for GasCo24 (P_{C_6}= 11.5 psi, P_{C_2}= 200 psi).	175
Figure 8.8(a)	Comparison of ethylene reaction profile and model prediction for GasCo45 (P_{C_6}= 3.2 psi, P_{C_2}= 150 psi).	176
Figure 8.8(b)	Comparison of ethylene reaction profile and model prediction for GasCo44 (P_{C_6}= 6.4 psi, P_{C_2}= 150 psi).	176

Figure 8.8(c)	Comparison of ethylene reaction profile and model prediction for GasCo20 (P_{C_6}= 8.3 psi, P_{C_2}= 150 psi).	177
Figure 8.8(d)	Comparison of ethylene reaction profile and model prediction for GasCo42 (P_{C_6}= 12.5 psi, P_{C_2}= 150 psi).	177
Figure 8.8(e)	Comparison of ethylene reaction profile and model prediction for GasCo46 (P_{C_6}= 14.0 psi, P_{C_2}= 150 psi).	178
Figure 8.9(a)	Comparison of ethylene reaction profile and model prediction for GasCo51 (P_{C_6}= 6.3 psi, P_{C_2}= 250 psi).	178
Figure 8.9(b)	Comparison of ethylene reaction profile and model prediction for GasCo48 (P_{C_6}= 8.1 psi, P_{C_2}= 250 psi).	179
Figure 8.9(c)	Comparison of ethylene reaction profile and model prediction for GasCo52 (P_{C_6}= 11.7 psi, P_{C_2}= 250 psi).	179
Figure 8.9(d)	Comparison of ethylene reaction profile and model prediction for GasCo26 (P_{C_6}= 13.8 psi, P_{C_2}= 250 psi).	180
Figure 8.9(e)	Comparison of ethylene reaction profile and model prediction for GasCo50 (P_{C_6}= 14.1 psi, P_{C_2}= 250 psi).	180
Figure 8.10(a)	1-Hexene reaction rate and the simulation curve for run GasCo34 (P_{C_2}= 60 psi, P_{C_6} = 6.4 psi).	181
Figure 8.10(b)	1-Hexene reaction rate and the simulation curve for run GasCo35 (P_{C_2}= 60 psi, P_{C_6} = 5.1 psi).	181
Figure 8.10(c)	1-Hexene reaction rate and the simulation curve for run GasCo36 (P_{C_2}= 60 psi, P_{C_6} = 9.3 psi).	182
Figure 8.10(d)	1-Hexene reaction rate and the simulation curve for run GasCo40 (P_{C_2}= 60 psi, P_{C_6} = 3.4 psi).	182
Figure 8.10(e)	1-Hexene reaction rate and the simulation curve for run GasCo42 (P_{C_2}= 150 psi, P_{C_6} = 12.5 psi).	183
Figure 8.10(f)	1-Hexene reaction rate and the simulation curve for run GasCo44 (P_{C_2}= 150 psi, P_{C_6} = 6.2 psi).	183
Figure 8.11	Comparison of 1-hexene content measured from ^{13}C-NMR and model predictions.	185

Figure 8.12	Comparison of experimental profile and simulation results of homopolymerization GasHo 13 ($P_{C_2}=200$ psi, $P_{C_6}=0$ psi) by applying kinetic parameters listed in Table 8.1.	186
Figure A.1	Dependence of response factor on flow rate of GC sample gas.	216
Figure B.1	Comparison of different equations of state (ideal-gas law, PR, RKS) at $T=70^\circ\text{C}$.	219

ABBREVIATIONS AND NOMENCLATURE

Abbreviations

¹³ C-NMR	Carbon-13 nuclear magnetic resonance
AES	Auger electron spectroscopy
AFM	Atomic force microscopy
ASTM	American Society for Testing and Materials
BD	Bulk density
CCD	Chemical composition distribution
CRYSTAF	Crystallization analysis fractionation
DBP	Di-n-butyl phthalate
DEAC	Diethylaluminum
DSC	Differential scanning calorimetry
EB	Ethyl benzoate
ED	Electron donor
FID	Flame ionization detector
FTIR	Fourier Transform Infrared
GC	Gas chromatography
GPC	Gel permeation Chromatography
HDPE	High-density polyethylene
IPRAL	Isoprenylaluminum
LDPE	Low-density polyethylene
LLDPE	Linear low-density polyethylene
MAO	Methyl aluminoxane
MDPE	Medium-density polyethylene
MI (MFI)	Melt index
MM	Molar mass
MMD	Molar mass distribution
PE	Polyethylene
SANS	Small-angle neutron scattering
SCB	Short chain branch

SCBD	Short chain branch distribution
SEC	Size exclusion chromatography
SEM	Scanning electron microscopy
TEA	Triethylaluminum
TEM	Transmission electron microscope
THHAL	Tri-n-hexylaluminum
TIBAL	Tri-isobutylaluminum
TNOAL	Tri-n-octylaluminum
TREF	Temperature rising elution fractionation
UHMWPE	Ultra high-density polyethylene
VLDPE	Very low-density polyethylene
XPS	X-ray photoelectron spectroscopy

Nomenclature

[A]	Cocatalyst concentration
[C*]	Concentration of active centre
[H₂]	Hydrogen concentration
[M]	Monomer concentration
[TEA]	Triethylaluminum concentration
<i>a</i>	Activity
<i>C*</i>	Active centre
<i>f</i>	Fugacity of solvent
<i>f</i>	Relative response factor
<i>f</i>^o	Fugacity of solvent at standard state
<i>H</i>	Heat of fusion of polyethylene
<i>H_c</i>	Heat of fusion for 100% crystalline polyethylene
<i>k*</i>	Henry's constant
<i>k'</i>	Reaction centre formation rate constant
<i>k'_{a1}</i>	Spontaneous deactivation rate constant for active site
<i>k'_{a2}</i>	Ethylene assisted deactivation constant for active site
<i>K₁</i>	Langmuir-type adsorption equilibrium constant for ethylene

K_2	Langmuir-type adsorption equilibrium constant for 1-hexene
K_A	Adsorption equilibrium constant for cocatalyst
k_a	Adsorption rate constant
k_t^A	Chain transfer rate constant to cocatalyst
k_d	Deactivation rate constant
k_D	Desorption rate constant
k_{d1}	Spontaneous deactivation rate constant for potential site
k_{d2}	Ethylene assisted deactivation constant for potential site
k_t^H	Chain transfer rate constant to hydrogen
k_i	Initiation rate constant
k_{i1}	Initiation rate constant by ethylene
k_{i2}	Initiation rate constant by 1-hexene
K_M	Adsorption equilibrium constant for monomer
k_t^m	Chain transfer rate constant to monomer
k_p	Propagation rate constant
k_{p1}	Ethylene propagation rate constant
k_{p2}	1-Hexene propagation rate constant
k_s	Spontaneous chain transfer rate constant
k_{tr}	Chain transfer rate constant
k_β	β -Agostic interaction rate constant
M_n	Number average molar mass
M_w	Weight average molar mass
P^0	Pressure of solvent at reference state
Q	Polydispersity
R_∞	Ethylene polymerization rate at long times
R_{max}	The maximum rate of polymerization
R_p	Ethylene polymerization rate
R_{p0}	Ethylene polymerization rate in the absence of hydrogen
R_{p1}	Propagation rate constant for ethylene
$R_{p1,n}$	Ethylene propagation rate constant for Site n
R_{p2}	Propagation rate constant for 1-hexene

$R_{p2,1}$	1-Hexene propagation rate constant for Site 1
S	Potential active site
S	Solubility
S^*	Active site
S_0	Number of potential sites per unit mass of catalyst
S_v	Vacant potential site
S_v^*	Vacant active site
T_R	Reduced temperature
V_0	Initial volume of polymer
X_n	Average chain length
χ	Flory-Huggins interaction parameter for solvent
χ_c	Crystallinity
ϕ	volume fraction of penetrant in polymer
θ_1	Fraction of sites occupied by ethylene
θ_2	Fraction of sites occupied by 1-hexene
θ_M	Fraction of sites occupied by monomer molecules
ω	Acentric factor

CHAPTER 1. INTRODUCTION

Polyethylene (PE) is the world largest synthetic polymer in terms of annual production and is widely used throughout the world due to its versatile properties and low cost. The demand for all types of PE first surpassed 50 million tons in 2000 (Robinson, 2001). Some of the most important PE producers and their prospective market shares in 2001 are listed in Table 1.1.

Table 1.1 Summary the Largest Polyethylene Producers (Brown, 2000).

Company	Share (wt%)
Dow	12.44
ExxonMobil	10.56
Elenac (Shell-BASF)	5.03
Equistar	4.74
Phillips Chevron	3.75
Borealis	3.55
BP Amoco	2.76
DSM	2.76
Formosa PC	2.67
Ato-Fina	2.27
Nova	2.27
Solvay	2.17
Others	45.01

There are three general types of PE resins: low-density PE (LDPE), linear low-density PE (LLDPE), and high-density PE (HDPE). Specialty grades of commercial PE also include very low-density PE (VLDPE), medium-density PE (MDPE), and ultra high-molecular weight PE (UHMWPE). HDPE has essentially unbranched straight chains, which pack tightly, giving a high degree of crystallinity. With the presence of short chain branches in LDPE and LLDPE, the crystallinity is reduced. The density ranges for the three main types of PE resins are from 0.910 to 0.930 g/cm³ for LDPE, 0.910 to 0.940 g/cm³ for LLDPE, and 0.941 to 0.97 g/cm³ for HDPE (Maraschin, 2001).

The production of polyolefins started with the free-radical high-pressure (up to 300 MPa) process for polyethylene, which was discovered by Imperial Chemical Industries (ICI) in the 1930's. The product from this high-pressure process resulted in highly branched LDPE (0.910-0.925g/cm³). This type of polyethylene often has 0.5-5 long chain branches per 1000 carbon atoms (Seppala, 1985) and contains a varying number of short chain branches with 2-8 carbon atoms, most often 4 (James, 1986). The discoveries of Ziegler-Natta catalysts and Phillip type catalysts during the 1950's led to a new approach for production of polyolefins at significantly reduced pressures (i.e. < 2 MPa) and lower temperatures (i.e. <100°C). Because of the coordination polymerization mechanism, the ethylene monomer units insert in a regular fashion at an active site on the catalyst, leading to a linear structure, lower branch content and thus higher density products (HDPE). The LDPE and HDPE address different markets, since they have different physical properties. LDPE is mainly used as thin films and HDPE is mostly used in extrusion products. The first commercialization of linear low-density polyethylene (LLDPE) began as early as in 1960 in Canada. The product is called SCLAIR (Dyer et al., 1997). The emergence of LLDPE came from the consideration of producing low density PE films (Dyer et al., 1997) and lowering production cost of LDPE (Nowlin, 1985). To produce LLDPE using Ziegler-Natta catalysts, comonomers such as 1-butene, 1-hexene, or 1-octene are copolymerized with ethylene to give short chain branches. LLDPE has replaced many applications of LDPE in the market.

LLDPE, as the name implies, is characterized by linear molecules without long chain branches. Short chain branches in LDPE are generated primarily through a free-radical, backbiting mechanism. Short chain branches in LLDPE are the result of copolymerization of ethylene with other α -olefins. Propylene, for example, gives a short chain branch of one carbon atom, 1-butene or 1-hexene give short chain branches of two and four carbon atoms, respectively.

Commercial LLDPE products are available based on propylene, 1-butene, 1-hexene, 1-octene. The selection of a comonomer for LLDPE is based on process compatibility, cost,

and product properties. James (1986) summarized qualitatively the physical property changes of Union Carbide LLDPE products with the increase in length of short chain branches. As shown in Figure 1.1, for products of lower melt index (high molecular weight), toughness depends strongly on the comonomer type, at least up to 1-hexene. Above 1-hexene, the increase is less significant. For higher melt-index (lower molecular weight) products, the dependence is much less significant. Other scientists (Kioka, et al., 1994) reported that tear strength and impact strength both improved as short-chain branch length increased.

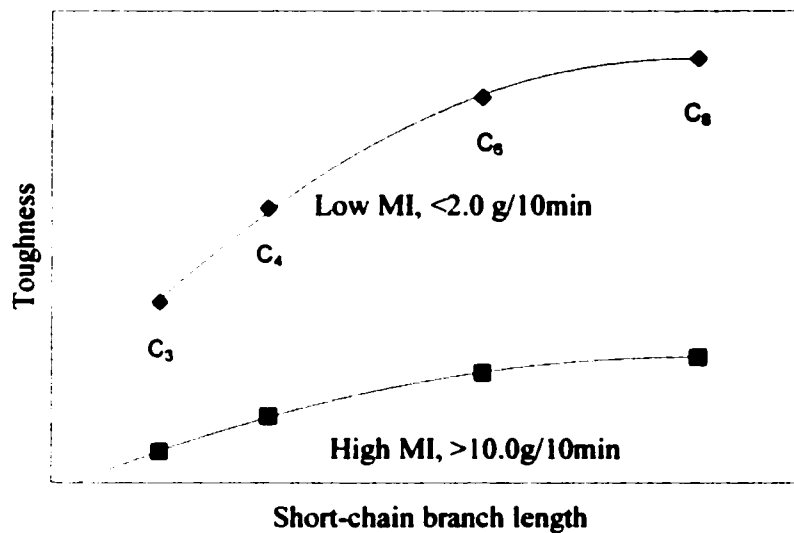


Figure 1.1 Relationship between short chain branch length and the toughness of Union Carbide LLDPEs (James, 1986).

The LDPE/LLDPE markets typically are divided into several applications areas: film, injection molding (i.e. cans and other containers), wire and cable, rotational molding (i.e. large agricultural tank), blow molding (i.e. bottles) and others, among which the film product is the largest part. LLDPE is now a big global business segment with an estimated sales value of US\$10.9 billion in 1999 (Buckalew and Schumacher, 2000). The global consumption of LLDPE has grown at an average rate of 8% per year since 1995 (Buckalew and Schumacher, 2000). The success of LLDPE in the marketplace has been, to a large extent, due to its improved physical properties of LLDPE over LDPE (James, 1986). For example, at the same density level, melting point, modulus and tensile

strength of LLDPE are significant higher than those of LDPE. As a result, LLDPE can be used at higher temperatures and allows the use of thinner parts.

The end-use properties of PE products are much dependent on the choice of catalysts. Furthermore, good catalysts can also optimize the polymerization process and improve economics. As a result, tremendous efforts have been made in catalyst research and development in the past five decades. In the earliest days, most plants manufactured their own catalysts in situ by the reduction of liquid TiCl_4 with organoaluminum compounds to form $\beta\text{-TiCl}_3$ which they followed by proper heat treatment to convert it to the more desirable $\delta\text{-TiCl}_3$ (Chien et al., 1982). Subsequently, Stauffer Chemicals manufactured and marketed unsupported heterogeneous $\delta\text{-TiCl}_3\text{-}0.33\text{AlCl}_3$ catalysts. In these catalysts only a small fraction of Ti is involved in the polymerization; the catalyst residues have to be removed from the PE product.

A large proportion of polyethylene is produced via slurry and gas phase processes. The nature of these processes requires heterogeneous catalysts. At present, supported catalysts are preferred. A catalyst support is important in obtaining high specific activity. Higher activity of supported TiCl_4 catalysts in comparison with non-supported TiCl_3 catalysts mainly came from higher number of active centres (Giannini, 1981). Today's high activity MgCl_2 -supported Ziegler-Natta catalysts (Z-N catalysts) leave no more than 10 ppm titanium and 30 ppm chlorine in the polymer formed (Choi and Ray, 1985). A review of various catalysts is presented in Chapter 2.

In spite of a half-century research on Z-N catalysts, there are still large areas of basic knowledge where depth of understanding is lacking. The fundamental questions include an understanding of the polymerization mechanism, structure of active centres, the influence of catalyst composition and type on the polymerization kinetics, the effects of reaction conditions on the properties of polymer and the effects of monomer solubility on growing polymers. The objectives of this work are to prepare and study the latest generation of TiCl_4 catalysts and establish the kinetics of copolymerization in the gas phase over these highly active catalysts.

In the first part of this work, spherically shaped MgCl_2 -supported TiCl_4 catalysts were synthesized using various preparation conditions, e.g. different MgCl_2 : ethanol ratios and different amounts of electron donor, and the effects of the variations in catalyst preparation methods on catalytic activity and morphology of the nascent polyethylene were studied.

In the second part, ethylene/1-hexene copolymerization rates during gas-phase polymerization using prepolymerized MgCl_2 -supported TiCl_4 catalysts were measured. The effects of temperature, and 1-hexene, ethylene and hydrogen concentrations on the activity profiles were determined. Obtaining activity profiles at constant gas-phase concentration of 1-hexene is a challenging experimental task and a novel technique to achieve such operation was developed. Various techniques were used to characterize the nascent LLDPE products, including scanning electron microscopy (SEM) for observation of product morphology, size exclusion chromatography (SEC) for determination of molecular weight, carbon-13 nuclear magnetic resonance (^{13}C -NMR) and temperature rising elution fractionation (TREF) for measurements of chemical composition of polymer and differential scanning calorimetry (DSC) for analysis of melting point and crystallinity.

In the final part of this study, a kinetic model is proposed based on the experimental results and previous work by other scientists. The simulation results are discussed and summarized.

CHAPTER 2. LITERATURE REVIEW

Catalytic olefin polymerization has become a huge industry in the past five decades since the discovery of catalysts by Ziegler (Ziegler et al., 1953), Natta (Natta et al., 1955) and Hogan and Banks (1958). It is not possible to review all the massive literature in this area; hence, this review will be restricted to a brief introduction to industrial catalytic olefin polymerization processes, a general overview of types of catalysts used for olefin polymerization with a more detailed review of supported Ziegler-Natta catalysts, general kinetic observation, selected kinetic models and copolymer characterization studies. The emphasis of this review will be on supported Ziegler-Natta catalysts and gas-phase ethylene polymerization.

2.1 Catalytic Olefin Polymerization Processes

Olefin polymerization processes can be classified into at least five types: high-pressure processes, bulk-phase processes, solution processes, slurry processes and gas-phase processes. Among these five processes, gas-phase processes have the largest production capability (Xie et al., 1994) due to their versatility. Despite the commercial success of gas-phase ethylene polymerization, fundamental studies of gas-phase polymerization are fairly limited. Only a small fraction of research studies are done using gas-phase reactors. This is because gas-phase reactors are not easy to construct and operate, and heat transfer problems are not easy to solve (Lynch and Wanke, 1991).

The first commercial PE was produced by a high-pressure process, which was discovered by Imperial Chemical Industries in the 1930s. High-pressure processes are carried out at 120-300 MPa and at temperature above the melting temperature of polyethylene. Tubular reactors are often used in this process and the product is a low density polyethylene (LDPE). This process involves a free radical chain polymerization mechanism and long chain branching is a recognizable feature of LDPE.

In slurry-phase process, a catalyst is suspended in a hydrocarbon medium, such as isobutane. Polymerization takes place at a temperature below the melting point of the

polymer, typically less than 110°C. The polymer product is solid particles which are suspended in the hydrocarbon diluent (also called suspension process). Different reactor configurations and diluents are used by different companies in industry (James, 1986; Al-Sammerrai and Al-Nidawy, 1989). Typical residence times are between 0.5 and 1.5 hours.

The bulk-phase process is similar to the slurry process except that the liquefied monomer becomes the reaction medium. This process is not used in ethylene polymerization because ethylene cannot be liquefied at typical reaction temperature ($T_{C,C_2H_4} = 9^\circ\text{C}$). Polypropylene can be produced by this process and polymerization of propylene is carried out at 55-75°C and at a pressure close to its vapor pressure. The polymer formed on the suspended catalyst particles is insoluble and precipitates out from the monomer liquid. The advantage of this process is the high monomer concentration and elimination of inert solvent recovery (Choi and Ray, 1985).

In the solution-phase process, the produced polymer is dissolved in the liquid phase; the catalyst may or may not be dissolved. Polymerization takes place in a hydrocarbon solvent above the melting temperature of the polymer, generally between 140 and 300°C. The solution process provides a wider operation temperature range than either slurry or gas-phase processes, which may improve control of molar mass (James, 1986). Shorter residence time allows small volume reactors and quick product transitions. However, solvent recovery by evaporation is energy consuming and molar mass is limited because the viscosity of the solvent-polymer mixture increases sharply with molar mass.

Patents for gas-phase ethylene polymerization were filed as early as 1957, but the first commercial plant using a gas-phase fluidized bed process did not begin operation until 1968 (Al-Sammerrai and Al-Nidawy, 1989). The main obstacles in the commercialization of gas-phase polymerization processes were the difficulties encountered in designing a heterogeneous gas-solid reaction system and controlling polymer properties. Extraordinary expansion of gas-phase processes happened during 1980s after Union Carbide's introduction of its fluid-bed UNIPOL process, which was

the leader in gas-phase ethylene polymerization. In the UNIPOL-PE process, purified gaseous ethylene and comonomer are fed continuously into a fluidized bed reactor; catalyst is added continuously. The reaction temperature is below 100°C, and pressure below 2 MPa. Circulated by a small compressor, the recycle gas stream serves multiple functions in the reactor, e.g. it fluidizes the polymer bed, provides reactants for polymerization, and removes the heat of reaction by circulating the gas stream passing through a cooler before being returned to the reactor. Polyethylene, in solid granular form, is removed directly. The granular product, with or without additives, is ready for packaging and shipping. The size and shape of the granules make them suitable for handling and processing by the user; pelletizing is an alternative (Karol, 1995; James, 1986; Al-Sammerrai and Al-Nidawy, 1989; Frederik et al., 1994; Xie et al., 1994). Production of LLDPE using gas-phase processes is more difficult than production of HDPE because the difference between the melting point and reaction temperature is smaller for LLDPE. The catalyst types and equipment design developed for HDPE cannot be used to produce LLDPE because of the potential agglomeration of polymer particles. According to Karol (1995), the key to the success of the UNIPOL technology for LLDPE production is the suitable catalyst that can operate at low temperature and low pressure. In the UNIPOL process, it is essential that the bed always contain polymer particles to prevent the formation of localized hot spots (Xie et al., 1994). The operating temperature for the production of LLDPE in the gas-phase is below 90°C (Xie et al., 1994).

To eliminate the risk of hot spots forming and prevent catalyst bursting into fines at the beginning of the reaction, BP Chemicals introduced a two-step gas-phase process (Chinh and Dumain, 1991). Before the catalysts are brought into the fluidized-bed reactor, they are first exposed to mild reaction conditions (low temperature and low monomer concentration, slurry or gas phase) in a stirred tank reactor for prepolymerization. Prepolymerization gives the advantages of polymer particle control and catalyst activity control.

Different production processes were compared by James (1986). In the slurry phase, the produced polymer's density is limited. As density decreases, resin solubility increases. At a density of about 0.93 g/cm^3 , sufficient dissolution occurs to foul the reactor. Thus, slurry processes are not very flexible for LLDPE production. Solution-based processes provide polyethylenes over a broad range of densities, but are limited in the range of melt index. As the melt index decreases (large molar mass), solution viscosity increases. At some point, the increased viscosity limits reactor operability and productivity. The gas-phase process is not subject to the solubility and viscosity problems inherent in solution or slurry processes and provides the greatest product versatility. Gas-phase process can produce a complete range of PE with densities from $0.91\text{-}0.97 \text{ g/cm}^3$ and melt index from <0.01 to $>100 \text{ g/min}$ (James, 1986). Furthermore, gas-phase process can reduce construction costs by up to 30% and operation costs by up to 35% over liquid-phase processes (James, 1986). The only disadvantage is the narrow range of operating temperatures, which places special demands in the catalysts for gas-phase processes.

A new nanoscale polymerization attracted researchers recently. The background lies in the precise control of the primary properties of polymer molecular crystalline structure. Kageyama et al. (1999) reported the production of crystalline polyethylene fibres with a diameter 30 to 50 nm by the polymerization of ethylene with titanocene (TiCp_2) supported by a fibrous mesoporous silica in conjunction with MAO as cocatalyst. The new type mesoporous silica has a honeycomb-like framework with a uniform, controllable pore diameter from 15 to 100 \AA , which is smaller than lamellar length of PE crystals. The growing PE chains are thus prevented from folding within the silica pores and extended-chain crystal fibres are formed. This kind of molecule has unexpected ultrahigh molar mass, a higher density 1.01 g/cm^3 due to more crystalline part. This technique is called "extrusion polymerization".

2.2 Olefin Polymerization Catalysts

The high-pressure process for ethylene polymerization discussed in Section 2.1 follows free radical polymerization mechanism and no catalyst is needed (using initiator instead). All other processes (bulk-phase, gas-phase, etc) follow the coordination polymerization

mechanism and the catalyst is the key part in controlling polymerization behavior and product properties.

A good olefin polymerization catalyst should have the following properties (Dall'Occo et. al., 1988)

- Good shelf life (no significant deactivation during storage).
- Free flowing particles for easy feeding to reactor.
- Low sensitivity to poisons.
- High productivity, no reactor fouling.
- Easy control of molar mass and its distribution, chain branches, particle morphology (i.e. particle size, particle size distribution, and bulk density).

The synthesis of a high performance polymer usually requires a good control of primary polymer properties. Excellent polymer particle morphology control is desirable because it also simplifies the post-processing steps, such as extrusion or spinning, and will be discussed more in the next part.

There are three families of olefin polymerization catalysts used in industry. Chromium oxide-based catalyst system (i.e. Phillips catalysts) and Ziegler-Natta catalyst system both were discovered in the 1950s and have been commercialized since then. Single-site catalysts emerged in the late 1970s.

2.2.1. Phillips Catalysts

A highly active olefin polymerization catalyst based on chromium supported on silica or alumina was discovered by Hogan and Banks at Phillips Petroleum in the 1950s (Hogan and Banks, 1958). It is often referred to as Phillips catalyst. They are active for olefin polymerization in the absence of additional cocatalyst. These catalysts have been used commercially for many years, particularly in slurry and gas phase polymerization processes (Jenny and Maddox, 1998). This kind of chromium oxide catalysts is the most active oxide-based catalyst systems (Beach and Kissin, 1986). The chromium compounds are activated by calcination at 500-700°C in a dry oxidizing environment and then

reduced with carbon monoxide or alkylaluminum compounds. Kinetics of ethylene polymerization contains three steps. The first step is an induction period of 10-30 min. This period can be shortened or even eliminated if the catalyst is first reduced. In the next step, catalyst activity is rapidly increased. In the final step, the catalyst exhibits high and stable activity followed by decay. The molar mass (MM) is best controlled by temperature. In addition, the pore size affects the MM. Larger pore size silica led to lower MM (Pullukat and Hoff, 1999). Compared to $MgCl_2$ -supported $TiCl_4$ catalysts, silica supported Phillips catalysts have the following advantages (Pullukat and Hoff, 1999):

- Lower chloride residue resulting in less color and lower corrosiveness toward dies and other parts of processing machinery.
- More uniform polymerization rates without the need for prepolymerization.
- Lower catalyst manufacturing cost and less toxic waste during catalyst synthesis.

2.2.2 Ziegler-Natta Catalysts

Ziegler-Natta catalysts (sometimes also called Ziegler catalysts) are named after German chemist Karl Ziegler and Italian chemical engineer Giulio Natta for their landmark discoveries in the 1950s. Over the last five decades, significant developments have occurred in this system in terms of catalyst design, process technology and mechanistic understanding. At present, Ziegler-Natta catalysts are the world most widely used catalyst for producing olefin polymers, although it is witnessing more and more challenges from newly developed single-site catalysts. Ziegler-Natta catalyst contains a range of active sites, which given polydispersity a wide range, from 2 for homogeneous catalysts, to 5-30 for heterogeneous catalysts (Beach and Kissin, 1986).

The majority of Ziegler-Natta catalysts consist of two components. One of the components is a transition metal compound, typically a titanium, vanadium, or zirconium compound, such as $TiCl_x$ ($x=2,3,4$), $Ti(OR)_4$, VCl_4 , $ZrCl_4$. The other component of the catalysts is an organometallic compound, such as $Al(C_2H_5)_3$, $Al(i-C_4H_9)_3$, $Al(C_2H_5)_2Cl$, or $Al(C_2H_5)Cl_2$. Alone, neither of the above two components can polymerize alkenes. According to their solubilities, Ziegler-Natta catalysts can be classified as homogeneous catalysts, pseudo-homogeneous catalysts, and heterogeneous catalysts (Kissin, 1985). For

homogeneous Ziegler-Natta catalysts, transition metal compound, organometallic compound and their interaction products are all soluble in the reaction medium. Some examples are $(C_5H_5)_2TiCl_2/Al(C_2H_5)_2Cl$, $VCl_4/Al(C_2H_5)_2Cl$ and $(C_5H_5)_2ZrCl_2/(CH_3AlO)_n$ (Kissin, 1985). If the starting catalyst's components are soluble but their interaction products are insoluble forms, they are called pseudo-homogeneous catalysts. Some examples are $TiCl_4/Al(C_2H_5)_3$ and $VCl_4/Al(C_2H_5)_2Cl$. The most important class is heterogeneous Ziegler-Natta catalysts that are insoluble. Examples are $TiCl_3/Al(C_2H_5)_3$, $VCl_3/Al(i-C_4H_9)_3$, and $TiCl_4/MgCl_2/silica /Al(C_2H_5)_3$. Modern commercial Ziegler-Natta catalysts are heterogeneous which also contain supports and modifiers. Detailed description of heterogeneous catalysts will be illustrated in Part 2.3.

Ziegler-Natta catalysts used in the gas-phase process must satisfy further requirements: high level of productivity (10^6 g polymer/ g transition metal), molar mass must be controlled by temperature and chain transfer agents, and good morphology control (Karol, 1995). Titanium based Ziegler-Natta catalysts are usually used for producing ethylene homopolymers; chromium and vanadium catalysts have better incorporation rates of comonomers and are often used in copolymerization production. The general comparison of different catalysts was provided by Karol (1995) as indicated in Table 2.1.

Table 2.1 Comparison of the Features of Different Polyolefin Catalysts (Karol, 1995)

Catalyst Parameters	Titanium Mg/Ti/ED	Vanadium $VCl_3(THF)_3$	Chromium CrO_3	Zirconocene Cp_2ZrCl
Productivity	H	H	H	H
H ₂ Response	M	H	L	M, H
MMD	Narrow	Medium to Broad		Very Narrow
Comonomer Incorporation	M	H	H	L, M, H
Decay Rate	M	L, M	L	L

ED: electron donor; H: high; M: moderate; L: low; MMD: molar mass distribution.

2.2.3 Metallocene Catalysts

Metallocene catalysts have been the subjects of extensive research and commercial development since the discovery by Sinn and Kaminsky (1980). The breakthrough was

the use of methyl aluminoxane (MAO) as cocatalyst to active group 4 bis (cyclopentadienyl) metallocene complexes. The term of metallocene has been used to describe these new catalysts because most of catalysts are based on metal compounds that include π -bound cyclopentadienyl (Cp) ring structures. Polymers produced via homogeneous metallocene catalysts have very narrow molar mass distribution (polydispersity around 2), which leads to products with higher impact resistance and higher resistance to stress cracking. The key features of these catalysts are their single site nature and their versatility for polymer molecular structure control. In order for metallocene catalysts to be used in the existing and prevailing slurry and gas-phase processes, a procedure for heterogenizing the catalysts on a support is necessary to obtain morphology control. In recent years, a variety of supports, such as silica, zeolite, alumina, magnesium dichloride and styrene-divinylbenzene, have been used.

Compared to Ziegler-Natta catalysts and Phillips catalysts, metallocene catalysts produce polymers with narrow molar mass distribution (MMD). The drawback of this characteristics is that the polymer products show bad flow ability at molten states, which is unfavorable during blow and extrusion processes. Thus, the primary use for metallocene based polyethylene is used as a blending resin with traditional Phillips or Ziegler-Natta based polyethylenes (Buckalew and Schumacher, 2000). In order to take advantage of both the metallocene and Ziegler-Natta catalysts, researchers (Cho et al., 1998) try to prepare Ziegler-Natta/metallocene hybrid catalysts on modified $MgCl_2$ supports.

The metallocene catalyst systems usually employ MAO as cocatalysts. The requirement of large amount of expensive MAO with low efficiency compared to small amounts of cocatalysts used in Ziegler-Natta systems is another shortcoming of the metallocene/MAO systems (Bajgur and Sivaram, 2000). Therefore studies on MAO-free system have received much attention after 1980s.

Since more and more non-metallocene-type single-site catalysts are now being explored and used, the “single-site” catalysts rather than metallocene catalysts should be used.

2.2.4 Other Olefin Polymerization Catalysts

Traditional catalysts (Ziegler-Natta and Phillips catalyst systems) as well as newly developed single-site catalyst systems are quite sensitive, easily poisoned, and require air-free and moisture-free environments. As a result, a substantial cost in the production of polyolefins is incurred in the purification of monomer and comonomer feeds. Younkin et al. (2000) attempted to find a new catalyst family that could tolerate many function groups and still produce olefin macromolecules. The nickel type complexes they developed are a family of neutral (most Ziegler-Natta and single-site catalysts have cationic metal centres), single component (no cocatalyst is required) catalysts, which have activity as high as 2000 kg/(mol Ni-h-100 psi ethylene) at low temperatures and can produce PE with $M_w > 250,000$ and with polydispersity between 1.5-3.0. These catalysts can maintain activity of 540 kg/(mol Ni-h-100 psi ethylene) in the toluene solution containing 10 vol% water.

Another exciting discovery is the tandem catalyst developed by Komon et al. (2000), which can produce ethylene/1-butene and ethylene/1-hexene copolymers from a single feedstock of ethylene. The catalyst has dual functionalities: one function of the catalyst is provided by a special nickel-borane compound which produces linear 1-alkenes from ethylene; and the second function is obtained by a commercial Ti-type homogeneous catalyst which is efficient in copolymerizing 1-alkenes with ethylene. These two parts work together on ethylene and produce a single copolymer product. The copolymer composition can be controlled via Ti/Ni ratio and temperature.

2.3 Heterogeneous Ziegler-Natta Catalysts

A Ziegler-Natta catalyst is a complex formed by reaction of a transition metal compound (halide, alkoxide, or alkyl) of Group 4 to 10 transition metals with a metal alkyl or alkyl halide of Group 1 and 13 base metals. The former component is often called catalyst and the latter the cocatalyst (Boor, 1979).

The first generation Ziegler-Natta catalyst were based on $3\text{TiCl}_3 \cdot \text{AlCl}_3$ and $\text{Al}(\text{C}_2\text{H}_5)_2\text{Cl}$ and had low activity and yielded polymers with low stereoregularity. The introduction of

a Lewis base into the catalyst system gave rise to the second generation catalysts, which were more active and produced polymers with higher stereospecificity. The activity of first and second generation catalysts, however, was not sufficiently high and washing treatments of the polymer were required for removing of catalyst residues (Gupta, 1999). The third generation catalyst, which is the main topic in this study, is composed of TiCl_4 supported on MgCl_2 , with trialkylaluminum as cocatalyst and a Lewis base as electron donor (Soga and Shiono, 1997). This type of catalyst was first developed by Shell International Research in 1968 (Gerbasi et al., 1984) and the technology using this catalyst was first commercialized by Montedison and Mitsui Petrochemical (Terano and Kataoka, 1988). This third generation catalyst is highly successful in industrial production of polyethylene and polypropylene because of extremely high activity, high selectivity, good control of molar mass distribution and chemical composition, and good morphology of nascent polymer particles (Soga and Shiono, 1997; Gupta, 1999).

2.3.1 The MgCl_2 Support

A supported Ziegler-Natta catalyst includes a support material, a transition metal compound, and an electron donor and/or base metal alkyl or alkyl halides. Many materials, such as SiO_2 , MgO and Al_2O_3 , have been used as catalyst supports; but MgCl_2 , unlike inert supports, plays an important role in creating catalytic sites (Bosowska and Nowakowska, 1998), making it one of the most widely used and most effective support materials for Ziegler-Natta catalysts (Dusseault and Hsu, 1993a).

Unlike the magnesium atoms in the bulk, which have sixfold coordination, the cations located at the side surface of the crystal edges are coordinatively unsaturated and therefore can form bonds with adsorbed molecules. Such unsaturated atoms can form halogen bridge bonds with titanium halides resulting in the formation of strongly bonded surface complexes (Galli et al., 1984; Koranyi et al., 1999). As a result, higher activity can arise from a more efficient use of the transition metal atoms. Many researchers (Kashiwa, 1980; Gerbasi, 1984; Barbe et al., 1987; Puhakka et al., 1995) suggested that the similarity between MgCl_2 and TiCl_3 crystal structures led to the enhancement of catalyst activity. Others (Galli et al., 1983; Karol et al., 1988; Soga et al., 1984) did not

agree that the similarity of crystal structures between MgCl_2 and TiCl_3 was the main reason. According to Giannini (1981) and Dusseault and Hsu (1993a), magnesium chloride donates electrons to the more electronegative titanium, stabilizing the coordination of monomer, resulting in a higher propagation rate during polymerization.

The structure of MgCl_2 cannot only improve the catalyst activity but also influence the comonomer incorporation ability for ethylene/ α -olefin copolymerization. Ko et al. (1997) found that different MgCl_2 structures influenced the comonomer incorporation ability on polymer chains. Only those supports with thermal treatment (dealcoholation) showed the comonomer enhancement effect.

Another aspect of the versatility of MgCl_2 support is its capability to replicate the $\text{TiCl}_4/\text{MgCl}_2$ catalyst particle morphologies in to the polymer particles. The goal regarding the control of the polymer morphology was once the most ambitious and most difficult job in the industrial area (Galli et al, 1984). Only Montedison has applied the technology of producing nascent polymer granules to be directly used for extrusion or other applications without palletizing. This technology requires producing spherical polymer particles with high bulk densities. Unfortunately, this technology is still not completely successful (Russell, 2000).

In spite of the lack of understanding of the reasons regarding to the effects of MgCl_2 support on catalysts, it is well known that in order to obtain a successful catalyst, MgCl_2 must first be converted to the form which can efficiently incorporate TiCl_4 , a process referred to as activation. This is done by many methods, such as ball milling, spray drying, chemical conversion and emulsion quenching.

From the late 1970s to 1980s, a main method in obtaining active MgCl_2 support has been done by ball milling (Dusseault and Hsu, 1993a), at least in academia. Ball milling can be carried out with TiCl_4 alone or with an electron donor. During ball milling (usually lasting tens of hours), MgCl_2 crystallites break up, crystallite sizes are reduced and structural defects increase, leading to more TiCl_4 located on the defects, which is

regarded as the potential active site. Introduction of electron donors may stabilize the MgCl_2 crystallites by coordination effect (Keszler et al., 1980; Sergeev et al., 1983). Typically, co-milling MgCl_2 with TiCl_4 results in an average titanium content of around 4 wt% (Kashiwa, 1980).

The emulsion quenching technique (also called melt quenching) is the process used in the current study and will be discussed in detail. This method of producing porous spherical MgCl_2 particles was first reported and patented by Montedison Company in 1983 (Ferraris et al., 1983). This method consists of forming an emulsion of molten $\text{MgCl}_2 \cdot n\text{C}_2\text{H}_5\text{OH}$ adduct in a hydrocarbon liquid, followed by rapid solidification. The general procedure is that a preset amount of anhydrous MgCl_2 , anhydrous $\text{C}_2\text{H}_5\text{OH}$ (usual mole ratio $\text{MgCl}_2 : \text{C}_2\text{H}_5\text{OH} = 1 : 3$) and Vaseline are loaded into an autoclave reactor under an inert gas atmosphere. The reaction mass is then heated to 120°C , at which temperature the $\text{MgCl}_2 \cdot 3\text{C}_2\text{H}_5\text{OH}$ complex is melted. With the help of vigorous stirring rate (e.g. 3,000 ~ 10,000 rpm), an emulsion is formed. This emulsion is then passed through a small-diameter tube and quenched in heptane at -40°C . Vaseline inside the support particle is removed by washing with heptane. The obtained spherical $\text{MgCl}_2 \cdot 3\text{C}_2\text{H}_5\text{OH}$ particles typically have sizes between 10 and 350 μm (Sacchetti et al., 1993). The support complex is further heated to temperatures from 30 to 180°C to decrease the alcohol content (called dealcoholation) and increase support porosity. After suitable treatment with TiCl_4 and electron donors, the catalyst shows very high activity and can produce spherical polyethylene product with high bulk density (e.g. Wu, et al., 1999).

Other MgCl_2 activation methods such as the chemical reaction method, recrystallization method, and spray drying method, have recently been discussed in detail by Wu (1999).

2.3.2 Electron Donor

The early MgCl_2 -supported catalysts were very active but not stereospecific enough to be employed for the polymerization of propylene on an industrial scale. A lot of research work has been done to remove this limitation. A solution to this problem was finally found by adding electron donor compounds into the catalyst. Electron donors or Lewis

bases are often used internally (added in the process of making catalyst) or externally (adding during the polymerization). Various types of Lewis bases are employed to increase stereospecificity, such as amines, ethers, and esters. The most widely used ones are benzoates or phthalates. Many papers have been published concerning the roles of electron donors on propylene catalytic polymerization. Introduction of an internal donor can increase the stereoregularity of poly(α -olefins), while polymerization rates may decrease (Xu et al., 1998; Guyot et al. 1988; Chien and Hu 1987; Busico et al., 1985) or increase (Huang and Rempel, 1995; Kang et al., 1990; Chien and Hu 1987). The effects of electron donors on ethylene homopolymerization or ethylene/ α -olefin copolymerization have not been studied in detail because there is no need for stereospecificity consideration in ethylene polymers. However, electron donors may also play an important role in creating active sites for ethylene polymerization (Bosowska and Nowakowska, 1998). Sacchetti et al. (1993) synthesized a $\text{MgCl}_2/\text{ED}/\text{TiCl}_4$ catalyst, which can be used for either propylene or ethylene polymerization. They mentioned in their patent that catalysts containing internal donors may produce LLDPE with restricted molar mass distribution, but no detailed study and explanation were given.

The function of electron donors (ED) in the catalyst has been widely investigated. Many researchers found that ED such as ethyl benzoate (EB) or phthalates can affect support crystallites. Increasing ED amounts, at least at some stage, can stabilize the decreased MgCl_2 crystal size (Keszler et al., 1980; Sergeev et al., 1983; Bosowska and Nowakowska, 1998). In general, surface energy increases with decreases in crystal size. The increase of the surface energy accelerates the aggregation of small particles (called Ostwald ripening). Internal donor such as EB may lower the surface energy of disordered MgCl_2 by forming a complex with MgCl_2 , interrupts the increase of particle size, and thus increases the defects of MgCl_2 crystals, making more active sites (Kashiwa, 1980; Park and Lee, 1992; Dusseult and Hsu, 1993a).

It is still not very clear how electron donors coordinate with MgCl_2 , TiCl_4 or cocatalysts and participate in polymerization reactions. Sergeev et al. (1983) found that a $\text{TiCl}_4 \cdot \text{EB}$ complex showed no activity in polymerization while it was active after being supported

in MgCl₂. Thus, he suggested that TiCl₄ and EB were not combined, but both occupied separate centres in MgCl₂. Xiao et al. (1986) observed that when TiCl₄-EB complex was milled with MgCl₂, the complex decomposed and a MgCl₂/EB surface complex formed. Terano and Kataoka's (1989) and Busico et al. (1985) also agreed that TiCl₄ and EB are not combined in the catalyst. In contrast, the irreversible complexation of EB with TiCl₄, and the stability of TiCl₄-EB complex at room temperature strongly suggest the existence of a TiCl₄-EB complex in the catalyst. Guyot et al. (1988), through infrared analysis, found that a ternary complex of TiCl₄-ED-MgCl₂ was formed as well as two binary complexes (TiCl₄-MgCl₂ and TiCl₄-ED). Using x-ray spectroscopy, Jones and Oldman (1988) suggested that the structure of active centre is Ti bound to MgCl₂ via a double bridge while EB is bonded to Ti. Xu et al. (1998) studied the effect of internal electron donor dibutyl phthalate on catalyst formation and found that the internal donor could interact with both Mg and Ti atoms.

Soga and Shiono (1997), by summarizing other people's work, suggested that internal donors could block TiCl₄ fixation to certain parts of the MgCl₂ crystallite which form non-stereospecific sites and help the formation of isospecific sites.

2.3.3 Cocatalyst and Active Centre

The active sites are considered to be transition metal atoms, usually titanium atoms in Ziegler-Natta catalysts. From the above review in Part 2.3.1, it is known that TiCl₄ can react with the defects of magnesium chloride structure. The Ti⁺⁴ adsorbed on the support is not an active site but it is a potential reaction centre (Zakharov et al., 1985). It can be activated only after being treated by a cocatalyst such as triethylaluminum (TEA). The activation of the triethylaluminum is twofold; first, it reduces Ti⁺⁴ to Ti⁺³, followed by alkylation of the Ti⁺³ according to the below mechanism (Malatesta, 1959):



Oligomers (from reaction 4) found after alkylation reactions confirmed this mechanism (Malatesta, 1959). Koranyi et al. (1999), by applying modern surface science technology, such as Auger electron spectroscopy (AES), x-ray photoelectron spectroscopy (XPS), supported the above mechanism that AlEt_3 reduced and alkylated the TiCl_4 to TiCl_2Et .

Kohara et al. (1979) found that when cocatalyst $\text{Al}(\text{Et})_3$ was washed away from the original TiCl_3 catalyst, it showed no activity for propylene polymerization. If it washed away during polymerization, the reaction did not stop, but the polymerization rate was lower. Thus, he suggested that the cocatalyst was actually part of the reaction centres and did not leave the active sites. Sindelar et al. (1996), however, argued that the cocatalyst could form a ternary system with the support and TiCl_4 to influence the catalytic behavior without directly participating in the reaction.

Catalyst preparation methods and reaction time strongly influence the titanium oxidation states. Baulin et al. (1980) found the Ti oxidation state on their MgCl_2 -supported catalysts before activation by cocatalyst was uniformly +4. Chien et al. (1982) determined Ti oxidation states by redox titration method and found that the $\text{MgCl}_2/\text{EB-AlEt}_3/\text{TiCl}_4$ catalyst they made had Ti^{+2} , Ti^{+3} , Ti^{+4} ions. Hasebe et al. (1997a) studied the oxidation state of titanium chloride in $\text{MgCl}_2/\text{TiCl}_4/\text{TEA}$ catalyst system and found that the reduction of titanium chloride continued with the reaction time. However, the average oxidation value of the supported catalyst after the reaction (10 min) was larger than +3. Thus, quite a few of the titanium cations were still at the state of +4. Chien, et al. (1989), however, found that Ti oxidation distribution did not change significantly after a few minutes during polymerization or aging.

The type of cocatalysts can also have a dramatic effect on the olefin polymerization behavior. Aluminum alkyls are the most commonly used cocatalysts, and the trialkyl aluminum compounds are usually preferred to halogen containing analogues (Lynch et al., 1991). The influence of different aluminum alkyls on the ethylene polymerization over $\text{SiO}_2/\text{MgCl}_2$ -supported TiCl_4 catalysts was investigated by Lynch et al. (1991). Experimental results showed that *tri-n*-hexylaluminum (TNHAL) and *tri-n*-

octylaluminum (TNOAL) had the highest effectiveness in increasing catalyst activities, triethylaluminum (TEA) had the lowest effectiveness, and diethylaluminum chloride (DEAC), tri-isobutylaluminum (TIBAL) and isoprenylaluminum (IPRAL) were intermediate in their effectiveness. It was also found that the shapes of the activity-time profiles were very dependent on the choice of cocatalysts. A decay-type profile was observed when TEA was used, while a constant activity profile was observed when TNOAL was the cocatalyst. Chien et al. (1989) attributed these cocatalyst effects to the formation of different Ti oxidation state distributions in the catalysts.

Typically alkyl aluminum is used in excess of the stoichiometric ratio with respect to the molar concentration of active centres. Some of the aluminum alkyl serves as scavenger of impurities. The optimum Al/Ti ratio is reported around 10 to 30 for polypropylene polymerization rates (Dusseult and Hsu, 1993a). Lynch and Wanke (1991) found that the ethylene gas-phase polymerization was independent of cocatalyst amount if Al/Ti >10. Kissin (1985) suggested that Al concentration in solution was the key to influencing the catalyst behavior in slurry reactions. For a gas-phase reaction, Lynch and Wanke (1991) regarded that it was not reliable to check cocatalyst concentration because the gas-phase alkyl concentration was limited by relatively low vapor pressure of the higher molar mass alkyls.

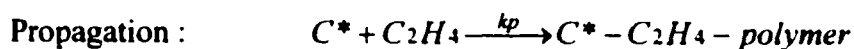
Excess aluminum alkyl would reduce further Ti^{+3} to Ti^{+2} . Many researchers (Soga et al., 1982; Karol et al., 1988; Nowlin et al., 1988) studied ethylene homo and copolymerizations and found that Ti^{+2} only polymerize ethylene while Ti^{+3} would polymerize both ethylene and higher α -olefins (e.g. propylene, butene, hexene). Kashiwa and Yoshitake (1984) also found that Ti^{+2} was not active for propylene polymerization but showed activity after it was oxidized to Ti^{+3} .

Ti spatial distribution on the support is another important feature which influences the catalyst performance. Hasebe et al. (1997b), using scanning Auger electron microscopy, found that the distribution of titanium was uneven on the support surface. They also inferred that various states of titanium clusters existed. Experimental results from Chung

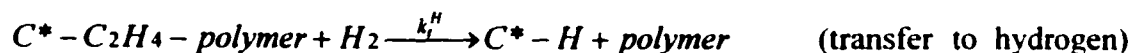
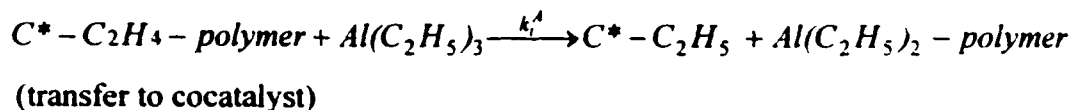
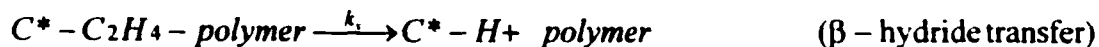
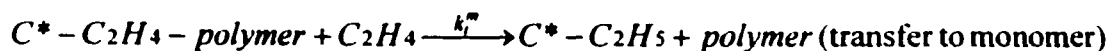
et al. (1996) showed that the produced ethylene had the maximum bulk density when Ti was evenly distributed on the support and when the Ti/Mg ratio on the catalyst surface was similar to that of the entire catalyst particle. Chu et al. (1999) studied the influence of Ti^{+3} structure on the comonomer incorporation ability in ethylene/1-hexene copolymers. Experimental results indicated that Ti^{+3} atoms dispersed on the surface of $MgCl_2$ surface had two existing structures: isolated ions and multinuclear species. The first state produced ethylene rich polymer with high molar mass. The multinuclear species increased 1-hexene incorporation and produced polymer with lower molar mass (MM) and broader molar mass distribution (MMD).

2.4 Kinetics of Polymerization

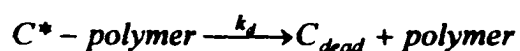
The observed kinetics of Ziegler-Natta catalytic polymerization is the overall reflection of three parts: chemical reaction on the active sites, the change of catalyst activity during polymerization, and mass and heat transfer influences. The reaction profile can be the acceleration type, decay type and hybrid of the two, i.e. reaction rate increases to a maximum and then decreases. Many factors can influence the reaction behaviors, e.g. types of catalyst support, physical structures and chemical compositions of catalysts, cocatalysts, temperature, impurities and reaction phase (e.g. slurry phase, gas phase). The general scheme for olefin polymerization on Ziegler-Natta catalyst is (Kissin, 1985):



Chain Transfer:



Deactivation of reaction sites:



Several mechanisms have been proposed for the propagation step. The widely accepted one is the Cossee's mono-metallic mechanism (Cossee, 1964). In Cossee's theory, the monomer is coordinated at the vacant orbital of a six-coordinate Ti centre followed by inserting into the polymer chain. The migration of the polymer chain to its original position is required to obtain isotactic propagation. Since the transition metal alone cannot reach high activity, a cocatalyst is always required and cocatalyst amounts influence significantly the catalyst activity. Other researchers proposed a bimetallic centre mechanism: Ti coordinates with cocatalysts to form the true centre (Doi et al., 1983).

In the section below, a detailed review will be given regarding to the influences of reactor type, active centre, deactivation, hydrogen, and cocatalyst on polymerization kinetics. Finally, prepolymerization and copolymerization studies will be discussed.

2.4.1 Slurry versus Gas-Phase Reactions

Gas-phase reaction processes are very successful in industry. However, slurry reactors are most commonly used in laboratory studies for the evaluation of new catalysts and for the polymerization studies. This is due to the relatively easy construction and operation of slurry-phase reactors as well as the good heat transfer in slurry-phase reactions (Lynch and Wanke, 1991). Gas-phase polymerization results are harder to reproduce than slurry results (Jejelowo et al., 1991; Bu et al., 1995). Due to these difficulties, the results from slurry operations are frequently used to predict the activity of catalysts for gas-phase operations (Jejelowo et al., 1991). Jejelowo et al. (1991) compared ethylene polymerization in gas-phase and slurry-phase operations using same catalysts and found that the kinetic behavior for the same catalysts was very process-dependent. Although the initial reaction rate could be similar for gas-phase and slurry-phase reactions, catalyst decayed much faster for gas-phase reactions. It was suggested that the fast deactivation of catalyst in gas-phase reactor was due to temperature increase from heat-transfer limitations in gas-phase, fast rate of Ti^{4+} reduction and higher cocatalyst concentration on

the surface of catalyst particles. Increasing temperature caused decreases in the overall rate of polymerization in gas-phase operation but led to the increases in slurry-phase operations. It can be seen that the catalytic behavior observed in slurry reactors cannot be directly used for the prediction under gas-phase conditions.

2.4.2 Active Centre Studies

For catalyst preparation, it is required that Ti component is not agglomerated but evenly dispersed on the support. The formation of transition metal clusters on the surface of the support limits the number of active sites, resulting in inefficient use of Ti (Dupuy and Spitz, 1997). Keii et al. (1982) found that in the region of Ti contents >2 wt%, the catalyst activity per unit weight of Ti decreased hyperbolically, which suggested that excess Ti over 2 wt% was largely inactive for polymerization. Cunningham et al. (1988) found that in the catalyst preparation, the proper washing with hot heptane after TiCl_4 refluxing was very important. The excess of TiCl_4 hindered the formation of highly active sites.

Decreasing polymerization rate with increasing polymerization time is a common phenomenon but the causes are not known. This decrease of polymerization rate is either due to the reduction of polymerization ability of active pieces (e.g. lower propagation rate constant, k_p) or due to the decreasing number of active sites. Since the specific propagation rate constant cannot be estimated without knowing the concentration of reaction centres, a lot of work has been done to try to measure the concentration of active centres. This can mainly be done from kinetic data analysis or by tagging the polymer chain with radioactive species.

The first method is carried out only for very short polymerization times when it is assumed that no transfer reactions occur. A plot of yield/ M_n versus yield is constructed and the y-intercept approximates C^* (Dusseault and Hsu, 1993a).

The second method is based on the assumption that one poisoning molecule (such as ^{14}CO or $^{14}\text{CO}_2$) deactivates only one site. Thus, the polymer product is analyzed to find

C^* , and subsequently k_p (Dusseault and Hsu, 1993a; Mejzlik et al. 1988). Marques et al. (1988) studied the ethylene polymerization kinetics over $MgCl_2$ -supported $TiCl_4$ catalysts using ^{14}CO radio-tagging technique. They found that only about 5-16% of the available titanium atoms were active as polymerization centres. The number of active centres was time dependent, increasing with the time of polymerization (0-2h) and the propagation constant decreased with time. Jaber and Fink (1995), however, found that polymerization time and temperature did not change the $[C^*]$, and $[C^*]$ in ethylene homopolymerization and in ethylene/1-hexene copolymerization were almost the same. The maximum number of active centres was generated when Al/Ti ratio was about 50. Chien and Kuo (1986) found that not all active titanium reacted with ^{14}CO equally. The choice of poisoning/tagging compound appeared to influence the final results.

It should be mentioned that, the accuracy of the ^{14}CO radioactive labeling method is determined by the extent of chain transfer processes. If transfer reactions are significant, the values of k_p would be underestimated since the presence of transfer reaction would inflate the C^* values. Thus, short time polymerization experiments should be carried out at times smaller than chain lifetimes or more than one method should be used to determine active centre concentrations (Marques et al., 1998).

2.4.3 Cocatalyst

A cocatalyst is always required to obtain high activity Ziegler-Natta catalysts. Different types of cocatalysts have different effects on kinetic behaviors (Lynch et al., 1991). The functions of cocatalyst are (1) to reduce and alkylate the $TiCl_4$ to form reaction centre, (2) to act as impurity scavenger, and (3) to act as chain transfer agent. The reaction between catalyst and cocatalyst is rapid and is complete in less than 5 minutes (Böhm, 1978).

Dusseault and Hsu (1993a, 1993b) studied the effect of triethylaluminum (TEA) cocatalyst on gas-phase ethylene polymerization over $MgCl_2/EB/TiCl_4$ catalyst system. Increasing Al/Ti ratio from 10 to 130, increased productivity monotonically. The catalyst deactivation rate was, however, increased at high Al/Ti ratios (Dusseault and Hsu, 1993a,

1993b; Chien and Kuo, 1986). Dumas and Hsu (1989) found that at Al/Ti=15, there existed an optimum for propylene polymerization. Marques et al. (1993) showed that the maximum rate appeared at Al/Ti=100 for TEA cocatalyst and 400 for TIBAL. Jejelowo et al. (1991) found that polymerization rates in gas-phase and slurry-phase reactions were relatively independent of Al/Ti ratio, which was varied from 7 to 142.

The exact mechanism of cocatalyst reaction is unknown, but it may be seen as a competitive reaction with monomer for the adsorption at active sites. The bulkier the alkyl groups, the less likely the alkyl aluminum will undergo transfer. Keii (1972, 1982, 1986) found that at low cocatalyst concentration the polymerization rate over Ziegler-Natta catalysts can be approximated by Langmuir-type expressions:

$$R_p = k_p[M] \frac{K_A[A]}{1 + K_A[A]}$$

or

$$R_p = k_p[M] \frac{K_A[A]}{(1 + K_A[A])^2}$$

where $[M]$ is the monomer concentration in bulk phase, $[A]$ is the cocatalyst concentration, K_A is the adsorption equilibrium constant for the cocatalyst, and k_p is the lumped reaction rate constant. Other researchers (Choi and Ray, 1985; Marques et al., 1993) also arrived at similar expressions of polymerization rate with respect to cocatalyst concentration.

Cocatalyst effects as a chain transfer agent was studied by Keii (1986). The relationship between molecular weight of polypropylene and cocatalyst TEA (triethylaluminum) was given by the expression

$$(\overline{M}_n)^{-1} = k(K_A[TEA] + \frac{1}{K_A[TEA]})$$

2.4.4 Influence of Hydrogen

The effects of hydrogen on rate of olefin polymerization with Ziegler-Natta catalysts are complex. It depends on the type of monomer, catalyst, cocatalyst and polymerization

conditions. Hydrogen can increase, decrease or not affect the polymerization rates (Soares and Hamielec, 1996a). Introducing hydrogen usually restrains the ethylene polymerization rate and decreases the polymer molecular weight (Keii, 1988; Kioka and Kashiwa, 1991; Salajka et al., 1993; Huang et al. 1997) but can either increase or decrease polymerization rate if the monomer alkenes are longer than three carbons (Kioka and Kashiwa, 1991; Chien and Kuo, 1986; Marques et al., 1993). In some special conditions, hydrogen can also increase ethylene copolymerization rate. Jaber and Ray (1993) found that for solution copolymerization of ethylene, reaction rate increased at moderate hydrogen concentration but decreased at high hydrogen concentration.

The general expressions of ethylene polymerization rate with respect to hydrogen concentration is (Keii, 1986; Kissin, 1989a):

$$R_p = \frac{R_{p0}}{1 + a[H_2]^{0.5}}$$

where a is a data fitting constant, R_{p0} is the polymerization rate in the absence of hydrogen. From the above equation, it can be seen that polymerization rate would be slower at higher hydrogen concentration.

Huang et al. (1997) studied hydrogen effects on gas-phase ethylene/1-butene copolymerization over $MgCl_2/SiO_2$ -supported $TiCl_4$ Catalysts. They found that the dependence of reaction rate on hydrogen concentration could be expressed by linear combination of Keii's Langmuir adsorption expressions (Keii, 1986) as given by:

$$R_p = \frac{a_1 R_{p0}}{1 + a_2 [H_2]^{0.5}} + a_3 (R_{p0} - a_4 [H_2]^{0.5})$$

where a_1 to a_4 are experimental determined parameters.

The dependence of molar mass on hydrogen concentration is usually given as (Keii, 1988; Jaber and Ray, 1993; Huang et al., 1997)

$$\overline{M}_n^H = \frac{\overline{M}_n^0}{1 + a[H_2]^m}$$

m is usually between 0.5 and 1.

The exact mechanism of hydrogen effect is still unclear. Some researchers (Chien and Nozaki, 1991) suggested that hydrogen could oxidize Ti^{+2} to Ti^{+3} , thus increasing the rate for propylene polymerization. Many others (Choi and Ray, 1985; Keii, 1988; Kissin, 1989b) found that the effect of hydrogen on reaction rate was reversible. The catalyst activity can be fully recovered after hydrogen was removed from the polymerization system. The reversibility of the hydrogen effect suggested that the rate decrease is caused by some equilibrium process rather than by irreversible reactions of active centres (Kissin, 1989b).

2.4.5 Catalyst Deactivation

As mentioned earlier, many supported Ziegler-Natta catalytic systems are subject to rapid decay. The deactivation can be explained as (1) lowering of activity of active centres due to structure change; (2) reduced number of active centres; (3) monomer diffusion limitation due to encapsulation of the catalyst in the semicrystalline polymer.

Murachev et al. (1993) found that increasing Al/Ti ratio, further reduced the Ti and resulted in lower activity. By introducing oxidants, the activity could be recovered. Ti^{+2} ions are believed to be inactive in α -olefin polymerization but active in ethylene polymerization at lower reaction rate level. The aging effect of catalyst observed by Keii (1982) strongly suggested the role of TEA in the deactivation of catalysts: reducing Ti^{+3} to Ti^{+2} . Wu et al. (1996) found that the decay rate in the gas phase was always faster than in slurry operations and the average oxidation states of Ti ions was lower in gas-phase than in slurry process.

According to Weber et al. (1988) and Chien et al. (1989), the deactivation of the Ziegler-Natta catalysts was not related to the change in the oxidation states of titanium. It was found that TEA reduced the Ti oxidation state at the beginning of catalyst activation. Ti oxidation states remained unchanged during the reaction. Aging of activated catalyst caused no changes in the distribution of Ti^{+n} , whereas the catalyst activity decayed

rapidly. They proposed that the reaction decay was due to the decrease of the number of active centres.

Guyot et al. (1993) proposed that deactivation was due to catalyst structural change: the occupied monomer will not insert into the growing chain, instead it eliminates one hydrogen to the growing chain and forms a π complex with Ti to form an inactive center. This inactive center can be reactivate by hydrogen and cocatalysts.

Czaja et al. (1999) also found the deactivation rate in slurry phase reaction was always lower than in the gas phase. The deactivation rate was only dependent on the catalyst concentration. Mass transfer resistance of monomer to the active sites seemed to be a probable reason for the decay.

Analysis of kinetic data resulted in the conclusion that different order decay reactions existed. Keii (1982) described the decay as third-order at polymerization times less than 10 minutes, while at times beyond 3 hours first-order kinetics best represented the situation. Chien and Kuo (1986) found that first order decay was applicable at low Al/Ti ratios (<42) and second order for high Al/Ti ratios for propylene polymerization. For ethylene polymerization, second order deactivation was observed when Al/Ti>80. For gas-phase ethylene polymerization, a gradual transition from first to second order deactivation was observed by Dusseault and Hsu (1993a) as the Al/Ti ratio increased.

Second-order decay implies a simultaneous reaction between two active centres bound to the surface of support. This only appears reasonable for adjacent sites as described by Chien et al. (1989) as



where P and P' represent two growing polymer chains.

Pino et al. (1985) reported that the decay rate was proportional to $[TEA]^{1/2}$. Because of the continuance of decay in the absence of polymerization, over reduction by TEA of Ti^{+3} to Ti^{+2} was thought by many to be the main route for deactivation. This may explain why

decay is faster at higher Al/Ti ratios and why at high temperature ($>70^{\circ}\text{C}$) using DEAC, a weaker reducing agent, results in a more active catalyst than when using TEA at the same conditions (Dusseault and Hsu, 1993a).

2.4.6 Prepolymerization

Prepolymerization is a polymerization reaction under mild reaction conditions (i.e. low ethylene concentration and low reaction temperature) to obtain polymer with a low yield (e.g. <100 g PE/gcat). This obtained prepolymer is later used as catalyst in subsequent polymerization reactions. Prepolymerization is generally used to control highly active polymerization to produce nascent polymer with good morphology and to avoid overheating at the beginning of the reaction. Prepolymerization has no effects on the characteristics of polymer products (M_w , tacticities, melting points, etc). Unexpectedly, researchers found that prepolymerization can increase the catalyst activity and influence comonomer consumption rate (Yano et al. 1986; Xu et al. 1990; Wu et al. 1996; Soares, and Hamielec, 1996a; Czaja and Krol, 1998; Wu, 1999; Chu et al. 2000).

Yano et al. (1986) and Czaja and Krol (1998) suggested that the higher catalyst activity after prepolymerization came from the more active sites exposed to monomer due to uniform fragmentation during the prepolymerization stage. Prepolymerization had no effects on the nature of active sites (rate constants did not change after prepolymerization). Xu et al. (1990), however, assumed that the nature of the active centres formed by the prepolymerization differed from the original catalyst system. Soares and Hamielec (1996a) proposed that higher rate constants, complete break up of the original particles, and high porosity all might be the reasons for higher polymerization rates.

Chu et al. (2000) found that prepolymerization with ethylene/1-hexene showed an increment of the reactivity of 1-hexene during later copolymerization and a lower fraction of ethylene-rich polymer but did not change molar mass and molar mass distribution. They (Chu et al., 2000) summarized the possible explanations of the rate enhancement effect of prepolymerization: (1) controlled fracturing of the catalyst during

prepolymerization, resulting in exposing more active sites; (2) activation of dormant sites or formation of additional sites; (3) change of the distribution of the titanium oxidation states or alternation of the association state of titanium; and (4) reduction of mass diffusion resistances of monomer through the prepolymer layer.

Czaja and Krol (1999) reported that prepolymerization controlled the fragmentation of catalysts under mild conditions, and that polymer morphology and activity were improved. Wu (1999) further found that not all prepolymerization reactions could produce polymer with good morphology. For gas-phase prepolymerization, prepolymer particles were totally broken into fine powders and flakes, even at low ethylene pressures and low temperatures. Generally, slurry prepolymerization at lower temperatures are required to produce prepolymer particles with higher bulk density.

2.4.7 Comonomer and Copolymerization

Compared to ethylene or propylene homopolymerization, not much work has been done on the copolymerization kinetics studies, especially for gas-phase operation. This is because the control of gas-phase composition is much more difficult (Han-Aderekun et al., 1997a) and concentration of the comonomer in the produced polymer must be considered (Bukatov et al., 1988).

Two opposite kinetic phenomena have been reported for the comonomer effect on reaction rates. Some researchers (Munoz-Escalona et al, 1987; Karol et al., 1993; Calabro and Lo, 1988; Han-Aderekun et al., 1997b; Ko et al., 1997) found that introduction of comonomer increased overall ethylene reaction rates, others (Kryzhanovskii et al., 1990; Chien and Nozaki, 1993; Hingyckx et al., 1998; Bialek and Czaja, 2000) found it decreased reaction rate. Karol et al. (1993) reported that ethylene polymerization rate increased in the presence of α -olefin. The magnitude of this increment depended on comonomer types. For ethylene/1-butene and ethylene/1-hexene copolymerization, a second order dependency on ethylene pressure was found. The formation of new active centres due to the stronger coordination of α -olefin was assumed to be the cause of this rate enhancement. Munoz-Escalona et al. (1987) suggested that physical effects such as

reduced diffusion resistance and increased monomer solubilities were the reasons for the observed rate enhancement in the presence of 1-hexene. Other researchers (Calabro and Lo, 1988; Han-Aderekun et al., 1997b) argued that diffusion theory alone was not sufficient to account for the enhancement effects. Ko et al. (1997) examined the comonomer enhancement effects for different MgCl_2 -supported TiCl_4 catalysts. They found that the comonomer enhancement was very catalyst dependent; thermal treatment of the $\text{MgCl}_2/\text{THF}/\text{TiCl}_4$ catalysts enhanced catalyst activity. It was suggested that the increasing rate effect came from a change of catalyst nature caused by heat treatment, which formed new active sites that could be activated by comonomer.

Kryzhanovskii et al. (1990) found that introduction of 1-hexene into the reaction medium reduced the ethylene reaction order from second-order for homopolymerization to first-order for copolymerization. Bialek and Czaja (2000) compared two types of catalysts for ethylene copolymerization. They found that introduction of comonomers (1-pentene, 1-hexene, 1-octene, 1-decene, 1-dodecene) decreased the catalysts activities for all catalysts. The catalyst activity did not depend on the type of comonomer used but depend on the comonomer concentration in the feed. The incorporation of α -olefin in the polymer chain was found to be dependent on the type and concentration of comonomer as well as the type of catalyst. Vanadium catalyst showed higher incorporation rates for comonomer than titanium-based Ziegler-Natta catalysts. The comonomer reactivity decreased with the increase of the size of comonomers. Hingyckx et al. (1998) also found a negative comonomer effect for $\text{MgCl}_2/\text{THF}/\text{TiCl}_4$ catalyst system. The reason was attributed to the formation of inactive sites resulting from the irreversible complexation of the 1-octene with active sites. Chien and Nozaki (1993) found that 1-hexene decreased polymerization rates for homogeneous Ziegler-Natta catalyst system whereas increased reaction rate for heterogeneous system. They attributed these differences to the different change in Ti oxidation states.

2.5 Modeling Description of Kinetic Behaviors

The composition of supported Ziegler-Natta catalysts is complicated and each component appears to have more than one function in determining the kinetics. As a result,

polymerization kinetics is not easily generalized. The situation is further complicated by the existence of multiple active centres. Over the past decades researchers attempted to develop a general model for Ziegler-Natta polymerization but with limited success. A brief review of some of the kinetic modeling is presented below.

2.5.1 Variables in Modeling Polymerization Kinetics

The three main variables included in the modeling of polymerization kinetics over Ziegler-Natta catalysts are monomer concentrations, temperature and number of active site types. The concentration of active sites is usually not used explicitly in the models; it is lumped with the rate constants. Isothermal operation is usually attempted for investigation of temperature effects; however, temperature effects are included in models which account for heat and mass transfer effects. Models with heat and mass transfer limitations will not be discussed in this review; such models have recently been reviewed by McKenna and Soares (2001). The monomer concentrations used in the models are usually assumed to be equal to or directly proportional to the monomer concentrations in the bulk phase next to the heterogeneous Ziegler-Natta catalysts.

The concentration of reactants adjacent to the active site should be used for modeling the rate of catalytic reactions. During slurry and gas-phase olefin polymerization the polymer grows around or over the catalyst particle. The catalyst particle fractures during the initial stages of polymerization. In some recent work with modeling Ziegler-Natta catalysts, Kim and Somorjai (2000) determined that the polymer deposits over the active sites and that polymerization continues below the previously formed polymer, i.e. the concentration of monomer next to the active site is the concentration of monomer absorbed in the previously formed polymer. For ethylene homopolymerization, the equilibrium concentration of sorbed ethylene is well modeled by Henry's law (Michaels and Bixler, 1961; Hutchinson and Ray, 1990; Chen, 1993; McKenna, 1998; Moore and Wanke, 2001); hence the usual assumption that the concentration is proportional to the bulk-phase concentration is valid. However, the single component sorption of 1-butene and 1-hexene cannot be described by Henry's law at the concentrations typically used in copolymerization (Yoon et al., 1996; Budzien et al., 1998a; McKenna, 1998; Moore and

Wanke, 2001). Adsorbed concentrations of 1-butene and 1-hexene at partial pressures approaching their vapor pressures are much higher than the values obtained by extrapolation of Henry's law using constants obtained at low partial pressure (Moore and Wanke, 2001).

The sorption phenomena are more complicated in the presence of two monomers since the interactions between the monomers can affect the solubility (Chen, 1993; Moore and Wanke, 2001). Preliminary measurements of 1-hexene and ethylene co-solubility at 1-hexene pressures close to its vapor pressure in polyethylene by Moore and Wanke (2001) showed very complex behavior. Very little data on such co-solubilities at conditions close to those encountered during industrial gas-phase copolymerization are available in the open literature.

2.5.2 Adsorption Theory

The interaction of monomers in the vicinity of the active sites with the active sites is frequently described by adsorption theory which is commonly used in heterogeneous catalyst system. The exact form of the resulting kinetic expressions differs depending on the specific adsorption steps. Normally, the reaction occurs only after monomer is adsorbed from the bulk phase onto the active sites and the Langmuir-Hinshelwood model is usually used to describe the adsorption process.

Burfield (1972) assumed that polymerization was not fast enough to break up the equilibrium of monomer adsorption onto catalyst surface. They describe the rate as

$$R_p = k_p C^* \theta_M$$

k_p is the propagation rate constant, C^* is the concentration of active sites, and θ_M is the fraction of sites occupied by monomer molecules, which by the Langmuir-Hinshelwood model is given by

$$\theta_M = \frac{K_M [M]}{(1 + K_M [M] + K_A [A])}$$

K_M and K_A are the adsorption equilibrium constants for monomer and aluminum alkyl, respectively and $[A]$ is the cocatalyst concentration.

Böhm (1978b) disagreed with the assumption of adsorption and desorption equilibria between monomer and aluminum alkyl made by Burfield (1972). He argued that for the assumption to be true, the adsorption and desorption rate constants for monomer would be unrealistically high in comparison to the propagation rate constant. He derived an extensive reaction model based on the Rideal mechanism, obtaining the rate expression:

$$R_p = \frac{k_p k_a [M][C^*]}{(k_p + k_D + k_a [M])(1 + b/a + c/a)}$$

where k_a and k_D are adsorption and desorption rates constants and $[C^*]$ is the concentration of active centres. The $(1 + b/a + c/a)$ term describes the various surface adsorption processes that may occur. The model was validated for ethylene polymerization over $Mg(OC_2H_5)_2$ -supported catalysts.

Keii (1986) decoupled the reaction profile into two parts: an initial stage during which the reaction rate increased, and a decay stage of the reaction rate. Based on Langmuir-Hinshelwood adsorption theory, the first stage can be expressed as

$$R_p = k_p [M][C^*]$$

$$\frac{d[C^*]}{dt} = \frac{k'[M]K_A[A]}{1 + K_A[A]}$$

where k' is reaction centre formation rate constant. In this stage, the rate increase is due to the increase of reaction centres. In the second decay stage, reaction centres are considered unchanged where the rate constant is a function of time:

$$R_p' = k_p [M][C^*] \frac{K_A[A]}{(1 + K_A[A])^2}$$

When $K_A[A]$ is much larger than 1, the equation is simplified to:

$$R_p' = \frac{k_p [M][C^*]}{K_A[A]}$$

Thus, the increasing cocatalyst concentration decreases the reaction rate.

Bu et al. (1995) found that the overall reaction order was a strong function of temperature and the ethylene reaction order extended from less than 1.0 to more than 1.5. No single

Bu et al. (1995) found that the overall reaction order was a strong function of temperature and the ethylene reaction order extended from less than 1.0 to more than 1.5. No single Langmuir-Hinshelwood equation could meet the experimental results. Thus, a dual site mechanism was proposed to with Langmuir-Hinshelwood expression of each site. This model was able to describe the observed reaction orders.

2.5.3 Multi-Site Theory

Broad molar mass distribution (MMD), broad chemical composition distribution (CCD), and reaction rate decay are usually observed in heterogeneous Ziegler-Natta catalytic system. These phenomena cannot be explained by transport model alone (Ray, 1988) and multiple site nature of the catalyst has to be considered.

The postulate that catalysts contain different types of sites is usually not based on direct kinetic observations, but on unusual broadnesses of MMD and CCD. Researchers have deconvoluted the MMD curves and CCD curves and have attributed the various deconvolution curves to different sites. Reaction rate profiles can then be simulated by assigning various kinetic parameters to each site. Two types of approaches are discussed below. One approach, represented by Soares and coworkers, developed the multi-site model mainly from CCD spectrum based on Stockmayer's distribution theory; the other approach, led by Kissin, decoupled the MMD chromatograph from Flory's distribution equation (Flory distribution is actually a particular solution of Stockmayer's distribution).

Soares Multi-Layer Model

For Soares approach, the prototype of the model was first put forward in 1995 (Soares and Hamielec, 1995a); it was called multi-layer model because the growing polymer particle was treated as a sphere with multiple layers. In each layer, the average numbers were used to calculate balance relations in each time interval. The volume of each layer was updated according to the amount of polymer formed in that time interval. The reactions involved in this multi-layer model included the usual steps such as site formation, initiation, propagation, and transfer to hydrogen, deactivation reactions were not included. Simplifications, such as equating initiation rate for each site to propagation

constants and neglecting hydrogen transfer resistance, were made. One key part of this model was that each type of catalyst site produced polymer with MMD and CCD that followed Stockmayer's bivariate distribution.

Simulation results (Soares and Hamielec, 1995a) showed: (1) a decrease of molar mass (MM) with increasing mass transfer resistance, but polydispersities were not influenced significantly even for very high activity catalyst under strong mass transfer limitations; (2) a significant decrease of monomer concentration towards the centre of the particle at low monomer diffusivity resulted in longer chain length in the outer layers; (3) a considerable decreases in MM with increasing initial sizes of the particles; (4) that concentration gradients were highest at the beginning of the reaction; (5) that the multi-grain model alone could not explain the observed broad MMD and CCD; (6) that for copolymerization with significant transfer problems, copolymer composition would be a function of both radial position in the particle and length of polymerization; (7) that broad CCD and MMD can be obtained with a three-site model.

Later, Soares and coworkers (Soares et al., 1996 and Soares, 1998) used Flory's distribution equation to model multi-site phenomena from MMD curve and Stockmayer's bivariate distribution to simulate CCD curve. The MMD can be measured by size exclusion chromatography (SEC), while the CCD can be obtained by temperature rising elution fractionation (TREF) or crystallization analysis fractionation (CRYSTAF). A five-site model was presented and it was suggested that 4 to 7 types are normally necessary to obtain good fit of SEC analysis results. They also emphasized that although more than four site types were used in mathematical model, not all of them may have distinct chemical structures.

Kissin's Multi-Site Model

Kissin (1993) applied Flory's distribution theory and proposed a multi-site model by his SEC deconvoluting technique. Simulation results for activity profiles using a five-centre model (Kissin, 1993) showed that the five centres differed widely in their kinetics. The first centre formed very rapidly and decayed very rapidly. This centre produced polymer

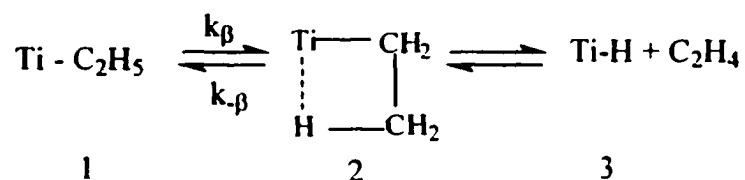
with lowest MM. Types 4 and 5 centres were more stable and could produce high MM polymer. Types 2 and 3 had properties between Types 1 and 4.

Later, Kissin (1995) applied his theory to result from ethylene/1-hexene copolymerization experiments. He found that the copolymerization reaction was faster than homopolymerization at the same slurry reaction conditions. The average 1-hexene content in the copolymer decreased with time. The 1-hexene content in the copolymer decreased from 4.2 mol% in a 5 min run to 0.8 mol% in a 120 min run. The change in the copolymer composition suggested that the active centres which readily react with 1-hexene deactivated more rapidly. Only the copolymer molecules with relative low 1-hexene contents were formed at later stages of the polymerization reaction. Applying the same kinetic model and computation procedures, the characteristics of active centres were evaluated for copolymerization. The first reaction centre decayed rapidly but it had the highest 1-hexene incorporation ratio; the 1-hexene content in the polymer for this site was as high as 25 mol% and the weight average molar mass (M_w) was less than 10,000. The yield from this type of sites was less than 5 wt% of the total yield in a one-hour run. The populations of second and third active centres decayed at lower rates. 1-Hexene incorporation from Sites 2 and 3 were 3.0 and 0.8 mol%, respectively. The combined PE yield from Sites 2 and 3 was 45% of the total yield. Sites 4 and 5 were most stable, producing the highest MM polymer and nearly linear polymer molecules with 1-hexene content less than 0.2 mol%. It was assumed that each type of active site produced polymer with a polydispersity of 2. Introducing external donor to the catalyst influenced the distribution of different centres significantly. Sites 1 and 2 disappeared with increasing amount of the donor. Thus, the MMD would be narrow and move to higher MM direction.

Kissin et al. (1999a, 1999b) further investigated the multi-site nature of Ziegler-Natta catalysts for ethylene/1-hexene copolymerization. Since Sites 1, 2 and 3 were found to have higher comonomer incorporation rate, the rate enhancement due to 1-hexene appearance should come mainly from these sites. Whereas Sites 4 and 5, which were essentially homopolymerization sites, should have lower reaction rate at the presence of

1-hexene. To confirm these assumptions, a two-step polymerization method was designed. In the first stage, ethylene homopolymerization was carried out under mild conditions for 3 to 4 h to deactivate the first 3 types of sites. The second stage was the normal copolymerization. Experimental results showed reduced reaction rates and lower 1-hexene incorporation, as expected for Sites 4 and 5. Addition of hydrogen to the reactor affected the activity of the sites differently. Activities of Sites 1, 2, and 3 in copolymerization reactions were less affected, whereas the amount of polymer made by Sites 4 and 5 was significantly reduced. As a result, the 1-hexene content in copolymers increased with increasing hydrogen concentration.

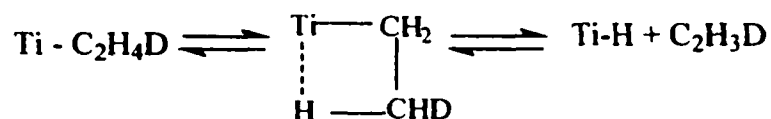
Many researchers found that the overall reaction order of ethylene was higher than unity (Wu et al., 1999; Kissin et al., 1999a and 1999b; Han-Adebkun and Ray, 1997; Bu et al., 1995) and close to 1 in the presence of higher α -olefin. Kissin et al. (1999a and 1999b) tried to develop a mechanism to explain this observation. They assumed that the stability of the Ti-C₂H₅ coordination stage could be unusually stable by β -agostic interaction between the hydrogen atom and Ti atom (structure 2):



This hypothesis has been confirmed by quantum-mechanical calculations of other researchers (Ciardelli et al. 1994). The equilibrium constant for the above reaction is quite high. Only the uncoordinated Ti-C₂H₅ group is capable of reacting with ethylene. When H occupies the Ti vacancy, it is inert for propagation reactions. Under this assumption, the high reaction order with respect to the ethylene concentration is the result of a low concentration of active Ti-C₂H₅ sites. This effect can be alternatively presented as a very slow chain initiation reaction with ethylene. The rate depression effect of hydrogen is also explained by β -agostic model. The chain transfer reaction with hydrogen leads to the formation of Ti-H bond (structure 3 in the model). Reinitiation by ethylene forms β -agostic intermediate which is very stable. Thus the number of active site

decreases in the presence of hydrogen. When an α -olefin is present, it inserts into the Ti-H bond with an immediate formation of Ti-polymer bond, bypassing the non-reactive β -agostic coordination state, and thus increasing the number of active centres.

This scheme predicts that if deuterium is used instead of hydrogen as a chain transfer agent, not only should chain ends contain deuterium atoms, but some hydrogen atoms in ethylene molecules should be replaced with deuterium atoms and deuterated ethylene should be present both in the remaining monomer and in polymer chains. Experiments (Kissin et al., 1999b, 1999c) showed that deuterized ethane and ethylene exist in the system and 3.3% of ethylene in gas phase had deuterium atom in it and 80% of ethane contained one, two or three deuterium atoms. Deuterated ethylene is formed via the scheme below:



IR and ^{13}C -NMR spectra (Kissin et al., 1999b, 1999c) of the polymers produced in the presence of D_2 showed that besides replacement of $-\text{CH}_3$ chain end with $-\text{CH}_2\text{D}$ chain ends, it also displayed a number of additional features associated $-\text{CHD}-$ and $-\text{CD}_2-$ groups.

Other Multi-Site Models

Dumas and Hsu (1989) proposed another kind of multi-site model based on statistical argument. They suggested that the different Ti locations on the support were the main reason for the distribution of propagation and deactivation rates. Their simulation results showed that the number of active site type could be from 2 to 100. No chemical explanation was given.

Recently Shariati et al. (1999) developed a two-site model for ethylene polymerization in slurry phase over a polymer-supported Ziegler-Natta catalysts. They proposed that each type of site corresponded to Ti in a different oxidation state. The model includes activation of active sites, propagation, deactivation, chain transfer by hydrogen and the

effect of monomer diffusion through the polymer layer around the catalyst particle to the active centres.

Wu (1999) carried out gas-phase ethylene homopolymerization over $\text{MgCl}_2/\text{ED}/\text{TiCl}_4$ catalysts. In order to avoid active site concentration variance with time due to catalyst activation and deactivation, ethylene pressure was varied during one single run. The kinetics was described by a two-site model. This model was able to describe most of the observed trends of rate profiles, such as single maximum at low reaction temperatures and double maximum at higher temperatures, the S-shaped initial acceleration period at low temperature and low ethylene pressure, and the broadnesses of the two rate maximum of rate profiles.

2.6. Characterization of LLDPE

Polymer characterization is essential for the understanding of catalyst behavior, polymerization kinetics, as well as the determination of polymer properties. The characterization methods reviewed in this section are divided into two parts: physical structure characterization methods and chemical structure analysis methods.

2.6.1 Physical Structure Characterization

This part covers the determination of internal structure of nascent polymer particles, physical properties of LLDPE (e.g. crystallinity, melting temperature and viscosity), and finally the relationship between melt index and molar mass.

Internal Structure of Nascent Polymer Particle

Noristi et al. (1994) found that MgCl_2 -supported Ziegler-Natta catalyst particles consisted of primary crystallites made of quasi-hexagonal thin platelets with an average size of 10-40 nm. The presence of secondary structures was not clearly detected by electron microscopy and could only be inferred by surface area and pore volume values. Scanning electron microscope (SEM) and transmission electron microscope (TEM) observation showed that catalyst fragments were uniformly dispersed in the polymer particle throughout the whole growth process. TEM examination of microtomed polymer particle

slices found that the size of catalyst fragments was much smaller than the catalyst's primary crystallites. The catalyst broke up at the beginning of the reaction and became smaller and smaller as the polymerization went on. This conclusion was different from the findings of Kakugo et al. (1989a, 1989b), who concluded that catalyst crystallites retained their sizes in the course of polymerization and the primary polymer particles grew as reactions proceeded.

Kakugo et al. (1989a, 1989b) also observed by TEM that the primary particle size of polymers was around 0.2-0.35 μm . This was consistent with the findings of Putanov et al. (1989), who observed the primary particle sizes of 0.15-0.2 μm , but the size of globules on the surfaces of particles were found to be about 1 μm (Kakugo et al., 1989a, 1989b). In the core of the individual primary polymer particles there existed one or a few catalyst fragments. These findings revealed that the polymer globules observed on the particle surface were not primary but secondary structures.

Munoz-Escalona and Parada (1980) applied SEM and TEM to observe the morphology of growing polymer particles during propylene polymerization. It was found that initially, the polymer grew on the catalyst surface in form of dots. As the polymerization continued, the dots grew and covered the catalyst surface. In the next reaction stage, polymerization rate increased due to fracture of the catalyst particles, which was caused by mechanical stresses from the growing polymer. Finally, the globular morphology went to wormlike morphology as the polymerization continued. The cobweb morphology was also observed (Graff et al., 1970; Muoz-Escalona and Parada, 1980; Wu, 1999) due to further stretching of the growing globules. Weickert et al. (1999) found that increasing reaction temperature resulted in more open porous polymer particle structures.

Wu (1999) studied the morphology replication phenomena of MgCl_2 -supported TiCl_4 catalyst by SEM. He found that if cracks initially existed on the catalyst surface, they would replicate on the surface of final polymer particles. This morphology replication is one of the characteristics of morphology-controlled Ziegler-Natta catalysts. However, the prepolymer of this kind of catalyst did not show any cracks on the surface. Wu (1999)

suggested mass transfer limitations might be the reason for the disappearance of cracks. Since more polymer was produced near the surface during prepolymerization, the surface cracks were filled up by polymer. In later polymerization, growing polymer in the interior would generate expansion force and force particle breaking up at the weakest point which corresponded to the initial cracks. The inside structure of PE particle was found to have two kinds of globules—loosely connected groups and tightly bounded groups. Wu (1999) suggested that these two different structures corresponded to two different catalytic sites, which had different activities.

Physical Properties

Among various properties the solution viscosity and the melt viscosity are predominantly affected by long chain branching, while the properties related to the crystallinity such as density, crystalline melting point, rigidity, hardness, permeability, chemical resistance and so on, are predominantly affected by the short chain branching (Shirayama et al., 1971). Shirayama et al. (1971) studied the effects of various comonomers on the properties of LLDPE. Polymer samples were first fractionated by TREF before being analyzed. Experimental results showed that side chain lengths less than 16 carbons did not affect the melting index-intrinsic viscosity ($[\eta]$) relationship. Short chain branch (SCB) did not affect significantly the melt extensibility or melt tension. Branches smaller than C_3 could be accommodated in the lattice. The branches larger than C_4 would be excluded from the lattice. Copolymers with longer branches had lower crystallinity. Bulkier branches exerted a larger hindrance effect on crystal formation. Small branches were nearly as effective as large branches in decreasing polymer's melting point at the same crystallinity level. Later, Alamo et al. (1984) arrived at similar conclusions; they found that polymer properties such as melting temperature, density, enthalpy of fusion, were dependent on comonomer concentration but independent of comonomer type for Ziegler-type LLDPE. It should be stressed here that crystalline melting point of a copolymer is very much influenced by the uniformity of composition and the branching distribution. Chu and Park (1997) found that melting temperature and heat of fusion were dependent on comonomer type if the concentrations of comonomer were similar for metallocene based LLDPE. The heat of fusion and melting temperature decreased in the

order: polyethylene > ethylene/propylene copolymer > ethylene/butene copolymer > ethylene/hexene copolymer > ethylene/octene copolymer.

Wignall et al. (1996) applied small-angle neutron scattering (SANS) to study the phase separation phenomenon in LLDPE. Experiments showed that LLDPE contained a dispersed minority phase which consisted of highly branched amorphous copolymer. These findings supported the prediction of liquid-liquid phase separation for compositionally polydisperse LLDPE; highly branched molecules in the distribution may phase segregate, even if the overall branch content is low. Loos et al. (1999), applying atomic force microscopy (AFM) to study the formation of crystals during polymerization and found that besides crystalline phase and amorphous phase an intermediate phase might exist.

Melt Index and Molecular Weight

Melt Index (MI or MFI) is defined as the amount of polymer that flows through a die in a give time at preset temperature and pressure. This parameter is widely used in industry because it reflects the processibility of polymer. Usually a higher MI corresponds to low MM (molar mass). Bremner and Rudin (1990) tried to correlate the relationship between MI and MM for commercial polyethylene. They found that for 1-octene LLDPE, equation $MI^1 = GM_w^{3.4}$ gave a reasonable fit to the experimental result, in which G is a fitted parameter. For butene LLDPE, M_w could not be reasonable predicted, M_v was used and the relationship with MI was $M_v = -10332 \times \ln MI + 76829$. Huang et al. (1997) found that the equation $MI^1 = GM_w^{3.4}$ provided an excellent fit for their laboratory-prepared 1-butene LLDPE. The validity for the expressions was strongly dependent on polydispersity and processing history.

2.6.2 Chemical Structure Analysis

Comonomer concentration and its distribution in copolymer are very important parameters in determining product properties. Generally, ^{13}C -NMR, FTIR and IR are the main tools for concentration detection; and TREF, DSC and CRYSTAF are used for comonomer distribution studies.

Carbon-13 Nuclear Magnetic Resonance (^{13}C -NMR)

Carbon-13 Nuclear Magnetic Resonance or ^{13}C -NMR is generally considered an absolute method for PE quantitative analysis (De Pooter et al., 1991). Solution ^{13}C -NMR is generally regarded as a reliable analytical technique for identifying and quantifying all of the branching features of polyolefins. However, it suffers from several drawbacks. The first is that the sample must be dissolved in an appropriate solvent. As a result, insoluble polyolefins and cross-linked systems are not amenable to this approach. The second problem is its relatively low sensitivity; long data acquisition times are commonly required to obtain satisfactory quantitative results. With the help of modern technology, high temperature solid-state ^{13}C -NMR was used recently to analyze LLDPE and overcome the above mentioned drawbacks (Guo et al., 2000). By applying solid-state ^{13}C -NMR, comonomer type can be rapidly determined at room temperature by distinguishing of comonomer resonance at different frequencies. Quantitative determination, which requires higher temperatures, such as 200°C (polymer is actually in the melted state at this temperature), gives satisfactory results comparable to solution ^{13}C -NMR. Solid-state ^{13}C -NMR can also undertake some other tasks and provide useful information about the bulk structures, such as branch location, crystallinity and chain packing. Branch location study showed that for ethylene/1-hexene copolymer, the side chains are totally excluded from the crystalline regions (Guo et al., 2000).

Fourier Transform Infrared (FTIR)

Neves et al. (1993) analyzed the comonomer concentration of the fractionated ethylene/1-butene LLDPE by FTIR. Preparative TREF was applied to fractionate the LLDPE sample according to different crystallizabilities. Fourier transform infrared (FTIR) was used to determine the branching degree of each fraction. The concentration of methyl group was determined from the absorbance band at 1378 cm^{-1} .

The infrared spectroscopic method for short chain branching normally focuses on the absorption band at 1378 cm^{-1} , which has some limitations since it cannot differentiate short chain branches from end groups. Blitz and McFaddin (1994) used other IR frequency methods to qualify and quantify comonomer concentrations in LLDPE. They

found that ethyl branches (1-butene comonomer) could be characterized by an adsorption at 770 cm^{-1} , butyl branches (1-hexene comonomer) at 893 cm^{-1} . To quantify comonomer contents, a Fourier self-deconvolution method was applied. Calculation showed that FTIR and NMR data were in quantitative agreement. The advantage of this technique is that FTIR is less costly and faster than NMR spectroscopy.

Temperature Rising Elution Fractionation (TREF)

Temperature rising elution fractionation (TREF) is a method for separating semicrystalline polymers according to their different solubilities and crystallizabilities. TREF only fractionates semicrystalline polymers and is not applicable to amorphous polymers. TREF fractionates polymer chains according to the molecular structure that affects crystallinity. In LLDPE, the incorporation of comonomer into the linear polyethylene chains results in irregularities that influence the crystallizability of polymer. In the precipitation step, polymer solute settles on inert support particles such as Chromosorb P or glass beads. The layers that are closer to the surface of the support are precipitated at higher temperature and therefore are more crystalline than external layers. Co-crystallization should be avoided, this is accomplished by very slow cooling, e.g. 1.5°C/h (Soares and Hamielec, 1995b; Zhang et al., 2000). Solvent type does not seem to play a significant role (Soares and Hamielec, 1995b). The elution temperature is virtually molar mass (MM) independent for values larger than 10,000. Molecules with MM below 500 remain in the solution at room temperature and highly branched material (the degree of branching exceeds 48 methyls per 1000 carbon atoms) will not crystallize at room temperature, regardless of its MM (Wild et al., 1982).

Mingozzi and Nascetti (1996) compared the comonomer composition distribution for Ziegler-Natta type LLDPE and single-site type LLDPE by applying TREF. Experimental results showed compositional heterogeneity as a consequence of the different content and sequence distribution of 1-butene along the chains for both types of LLDPE.

Mingozzi and Nascetti (1996) found that the MM increased at high TREF extraction temperature, while Neves et al. (1993) suggested that this discrepancy was not significant

in view of the uncertainties present in a high temperature SEC analysis. Zhang et al. (2000) clearly showed the MM increased with increasing TREF elution temperature for LLDPE made with Ziegler-Natta catalyst. For metallocene-based LLDPEs MM did not show the same trend.

Differential Scanning Calorimetry (DSC)

Shanks and Amarasinghe (2000) studied the comonomer intramolecular distribution by DSC. HDPE endotherms showed a single peak, which meant the crystalline lamella were quite uniform. After fractionation of LLDPE samples by TREF, the DSC endotherms showed multi peaks for either Ziegler-Natta LLDPE or single-site LLDPE. This meant the copolymers exhibited a wide range of comonomer distribution, which was consistent with the discovery by Stark (1996). Neves et al. (1993) characterized the fractionated ethylene/1-butene LLDPE by DSC, FTIR and SEC. DSC analysis showed that the melting temperature increased linearly with the TREF extraction temperature in the low temperature range and maintained constant after extraction temperature was higher than 80°C. This result agreed with FTIR results that melting point was low because the molecules contained more comonomer, reducing crystalline order of the polymer. Crystallinity calculations revealed that when extraction temperature was less than 90°C, crystallinity degree increased with the increase of extraction temperature because of the lower comonomer contents. At the temperature about 90°C, crystallinity decreased with increasing solution temperature. The author explained that this was due to different crystal lamellae formed below 90°C and above 90°C,

Recently, a new stepwise crystallization method “successive nucleation/annealing (SNA)” was applied to differentiate and compare methylene sequence distribution for LLDPE in DSC analysis (Zhang et al., 2000). It was assumed that the neighbouring sequence on the polymer chain could crystallize independently and the melting point was a function of crystallite size. Analyses found multiple peak curves for both Ziegler-Natta LLDPE and single-site LLDPEs. After separating polymer samples by TREF, SNA-DSC endotherms of each fraction also found multiple peaks for both Ziegler-Natta samples and single-site samples, which meant short chain branch (SCB) along individual macro chain

backbone was not uniform. Further experiments (Zhang et al., 2000) showed that intermolecular heterogeneity was found in the Ziegler-Natta sample, while single-site sample was intermolecularly homogeneous.

Crystallization Analysis Fractionation (CRYSTAF)

Monrabal (1994) proposed a new technique similar to TREF for determining the chemical composition information in LLDPE, which was called CRYSTAF (crystallization analysis fractionation). The analysis of CRYSTAF was carried out by monitoring the polymer solution concentration during crystallization by controlled cooling. As temperature goes down, most crystalline fractions, composed of molecules with zero or very few branches will precipitate first, resulting a decrease in the solution concentration. This is followed by precipitation of fractions of increasing branch content as temperature continues to decrease. The last data point, corresponding to the lowest temperature of crystallization cycle, represents the fraction that has not crystallized and remains soluble. The derivative of the concentration curve can be associated with short chain branching distribution (SCBD).

Comparison experiments with TREF showed that the results were similar (Monrabal, 1994). The advantage of CRYSTAF is that this approach only requires one temperature cycle to perform SCBD analysis, simplifying the equipment and reducing analysis time (Monrabal, 1994).

CHAPTER 3. EXPERIMENTAL PROCEDURES AND CONDITIONS

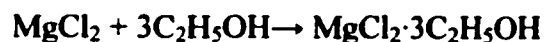
Catalyst preparation methods, polymerization procedures, control of comonomer feeding and polymer characterization techniques are described in this chapter. The catalyst preparation methods include the preparation of spherical MgCl_2 support particles, the thermal treatment of fresh support particles, TiCl_4/ED addition, activation and Ti content analyses. The polymerization part stresses gas-phase analysis techniques and comonomer addition equipment. Composition control illustrates gas sampling and feed control procedures. Polymer characterization techniques include ^{13}C -NMR, SEM, GPC (or SEC) and TREF methods.

3.1 Catalyst Preparation

The catalyst preparation procedure in this study is mainly based on the method developed by Wu et al. (1999). The experimental procedures and experimental conditions which are different from previous studies will be emphasized. The detailed information of catalyst preparation equipment and materials has been published elsewhere (Wu, 1999; Wu et al., 1999).

3.1.1 Preparation of Spherical MgCl_2 Support Particle by Melt Quenching Method

The following method was used to prepare spherical MgCl_2 particles which were used as catalyst supports. About 200 g Vaseline oil (from Fluka) was loaded into a one-litre, jacketed Pyrex mixing vessel (Büchi Laboratory AutoClave, BEP280) fitted with a Rushton turbine stirrer. The reactor was kept under vacuum overnight. The reactor was then heated to 80°C , keeping vacuum for 1 h to remove moisture inside the oil; 20 g of magnesium dichloride (98% purity and 1.5 wt % of water, from Aldrich) and 38 mL anhydrous ethyl alcohol (from Aldrich) were charged separately into the reactor under nitrogen protection while the temperature of the Vaseline was decreased to 60°C (too much ethanol vaporizes if added at the temperature above its boiling point). After the ethanol was charged, it reacted with MgCl_2 quickly and severely, causing the suspension temperature to increase 5 to 7°C in 30 seconds. The exothermic reaction is



After MgCl_2 and $\text{C}_2\text{H}_5\text{OH}$ were charged, the mixture was heated from $\sim 67^\circ\text{C}$ to 120°C in 2 h, while increasing the stirring rate from 200 rpm to 800-900 rpm. At about 120°C , an emulsion of $\text{MgCl}_2 \cdot 3\text{C}_2\text{H}_5\text{OH}$ melted complex in Vaseline was formed at the high stirring rate. A 3:1 molar ratio of ethanol to MgCl_2 was chosen because the resulting complex melts at temperature between $100\text{-}130^\circ\text{C}$ (Sacchetti et al., 1993). Higher ethanol: MgCl_2 ratio results in particles which are easily broken, and at lower ratios, the support particles have lower porosities and surface areas.

The exit port of the reactor was connected through a ball valve to a Teflon tubing with an inside diameter of 1.5 mm and length of about 3 m. The other end of the tubing was dipped into 1.5 L anhydrous heptane (from Aldrich) contained in a 3-L flask. The heptane and flask were cooled below -30°C by a bath of an ethylene glycol-water mixture; the bath was precooled by liquid nitrogen.

After keeping the emulsion at 120°C for more than 1 h, the reactor pressure was increased to 4 to 5 bars by introduction of nitrogen gas. The emulsion was forced out by opening the ball valve and flowed through the Teflon tubing, which was externally heated to 120°C , and then into the cold stirred heptane, where it solidified. The final temperature of the heptane after introduction of the emulsion was less than 0°C . The whole procedure for preparing and quenching the emulsion took about 6 h. The Vaseline in the emulsion was removed with heptane wash at $40\text{-}60^\circ\text{C}$ and the resulting solid product was dried under vacuum at room temperature. The obtained support morphology was examined using an optical microscope (Olympus PEM 3). The density, as measured by a pycnometer (AccuPyc 1330, Micromeritics Instrument Co.), was about 1.3 g/cm^3 . The summary of all the support preparation conditions is given in Appendix D, Table D.1.

3.1.2 Dealcoholation Treatment

The fresh spherical support was transferred into a glass tube with a fritted disk at the bottom. The transfer was done in a glove box because exposure to moisture must be avoided at all stages of the support and catalyst preparations. The tube was heated by

heating rate and temperature was increased slowly from room temperature to 130°C in 3 to 6 h. A desired amount of ethanol was removed from the MgCl₂-ethanol by purging with nitrogen. The mass differences between the support sample before thermal dealcoholation and after dealcoholation were measured to estimate the amount of ethanol which has been removed. The exact composition of MgCl₂·xC₂H₅OH complex after dealcoholation was determined by the sintering method which is described below. According to Sacchetti et al. (1993), dealcoholation increases the support porosity and the C₂H₅OH: MgCl₂ mole ratio after treatment should not be greater than 2. The partially dealcoholated support particles were then treated with TiCl₄.

The sintering method which is used in determining the composition of MgCl₂·xC₂H₅OH complex was developed in this study based on the reaction scheme provided by Magalhaes et al. (1991), i.e.



The method consisted of the following steps:

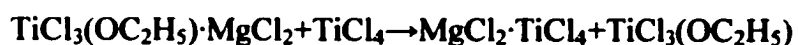
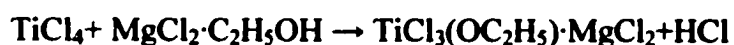
1. Placed about 0.1 g of partially dealcoholated support in a 125 mm long Pyrex tube with screw cap.
2. Heated the tube in a flame while swirling gently until the support sample was liquefied.
3. Continued to heat until the ethanol had boiled off and the remaining solid became a small chunk or fine powder.
4. Kept heating the solid until white smoke (HCl vapor) could be seen rising from the solid.
5. Cooled the tube after smoking stopped and closed the cap quickly.
6. Weighted the sintered sample and calculated the initial ethanol content according to the above reaction scheme.

3.1.3 Catalyst Preparation

The MgCl₂-supported TiCl₄ catalysts were prepared by adding 3 g of dealcoholated support complex and 60 mL of anhydrous heptane into a 300 mL glass flask. While

maintaining the temperature below 0°C, about 90 mL TiCl₄ (99.9%, from Aldrich) was added drop-wise in flask over a 3 –5 h period while stirring slowly or swirling gently. The TiCl₄ addition rate was found to have important effect on final polymer bulk densities. The slow addition of TiCl₄ was first regarded as a method of avoiding support particle break up (Wu, 1999), but was later found to have no influence on the morphology of the catalyst. Even if the support particles were added quickly into pure TiCl₄ at higher temperature, the obtained catalyst showed spherical shape and could produce spherical prepolymer. However, the obtained polymers had lower bulk density compared with the polymer which was produced by the catalyst with drop-wise TiCl₄ addition.

After the TiCl₄ addition, the temperature slowly increased to 40°C and a desired amount of electron donor, di-*n*-butyl phthalate (DBP, from Fluka) diluted to 10% heptane solution, was added drop-wise into the system over a 0.5 h period. The suspension system turned bright yellow immediately after the DBP addition was started. After the DBP was totally added, the mixture was heated to 110°C and kept at this temperature for 1 h while the color of the suspension became darker (light yellow brown or dark brown). After the mixture was cooled, the liquid phase was siphoned out and neat 100 mL TiCl₄ was added at room temperature over a 1 h period, followed by heating to 120°C and maintaining at that temperature for 1 h. The second TiCl₄ treatment helped remove inert Ti complexes from the catalyst support. The activation reactions are



The soluble TiCl₄ in the catalyst particles was removed by washing 10~15 times in heptane at 60°C. Finally, the catalyst products were dried under vacuum at room temperature. The complete schematic procedure from support quenching technique to catalyst preparation is shown in Figure 3.1.

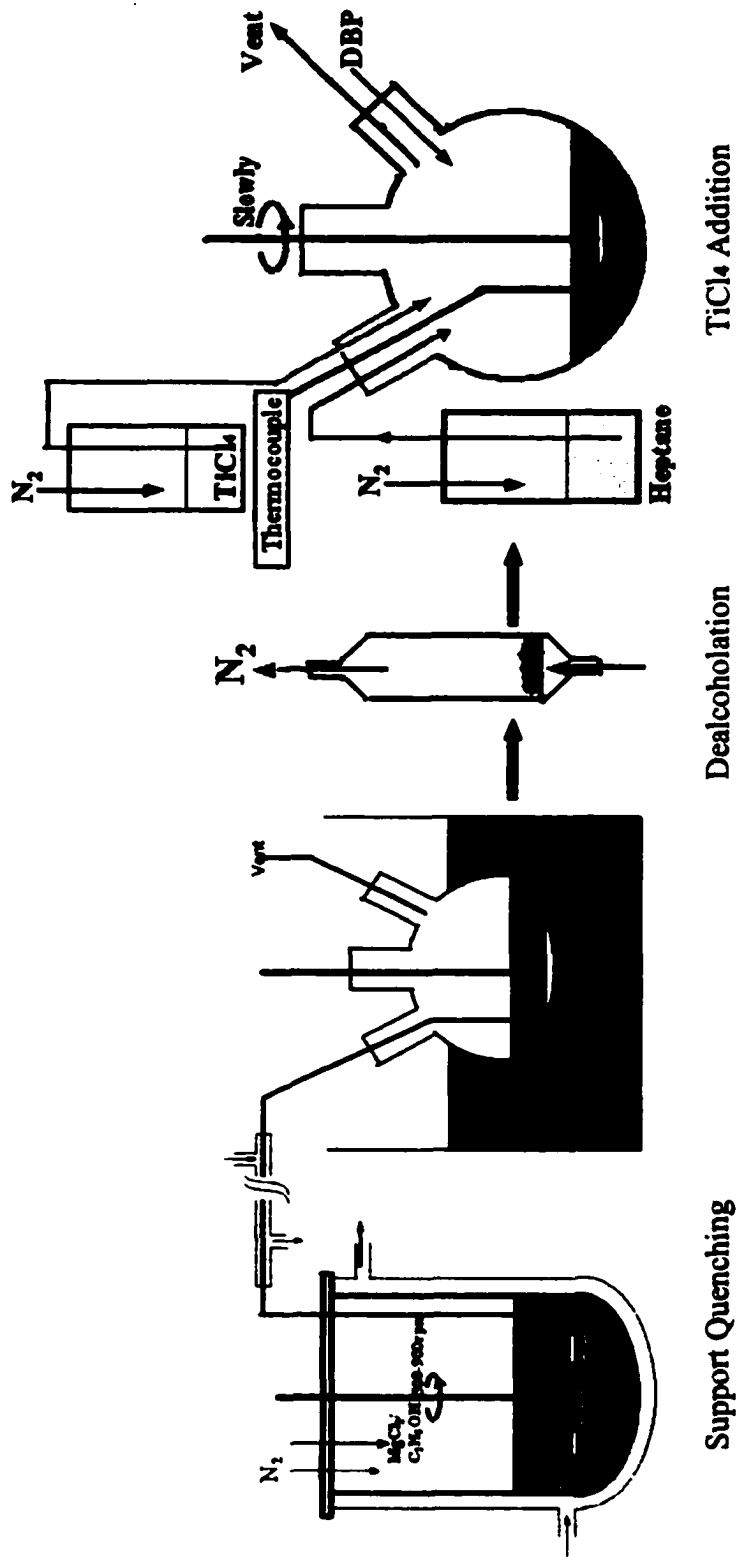


Figure 3.1. Schematic Diagram of Catalyst Preparation Procedure

The shapes of support and catalyst particles were observed using an optical microscope and a scanning electron microscope (SEM). Figure 3.2 shows an optical micrograph of the support particles (before dealcoholation, Figure 3.2a) and a scanning electron micrograph of the resulting catalyst particles (Figure 3.2b).

Quantitative Ti contents was determined by colorimetric analysis method (Vogel, 1961).

This method consisted of the following steps:

1. Weighted out 100 mg sample in the glove box and placed in a 40 mL Pyrex test tube with screw cap.
2. Added 4 mL of concentrated sulfuric acid (95%, from Fisher Scientific), heated up and kept boiling for 2 min, allowed to cool to room temperature.
3. Cautiously added 20 mL H₂O, cooled again to room temperature and then transferred the colorless solution to a 100 mL Kjeldahl flask.
4. Carefully added 5 mL concentrated H₂SO₄ and 50 mL H₂O, allowed to cool to room temperature.
5. Added 7 mL hydrogen peroxide (30% stabilized, from Fisher Scientific).
6. Added more H₂O to make up to the volume mark.
7. Move about 2 mL solution into a 0.5 cm crystal cell (from Fisher Scientific) and measured the absorbance at 410 nm using UV-VIS Recording Spectrophotometer (from Shimadzu, model UV-160), and finally determined the Ti content from calibration curve.

All catalysts made in this work have Ti content between 1.8 wt% and 6 wt%. The spatial distributions of the Ti in some porous support particles were also determined by energy dispersion x-ray analysis (see Section 3.4). The compositions and preparation conditions of the catalysts prepared in this study are summarized in Appendix D, Table D.2.

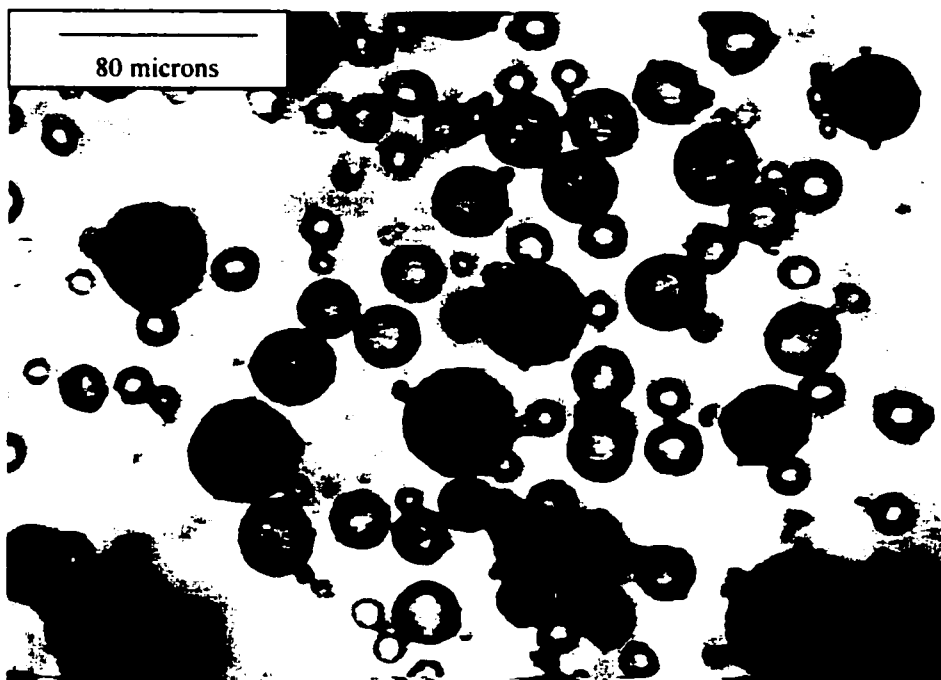


Figure 3.2. (a) Optical micrograph of MgCl_2 support particles.

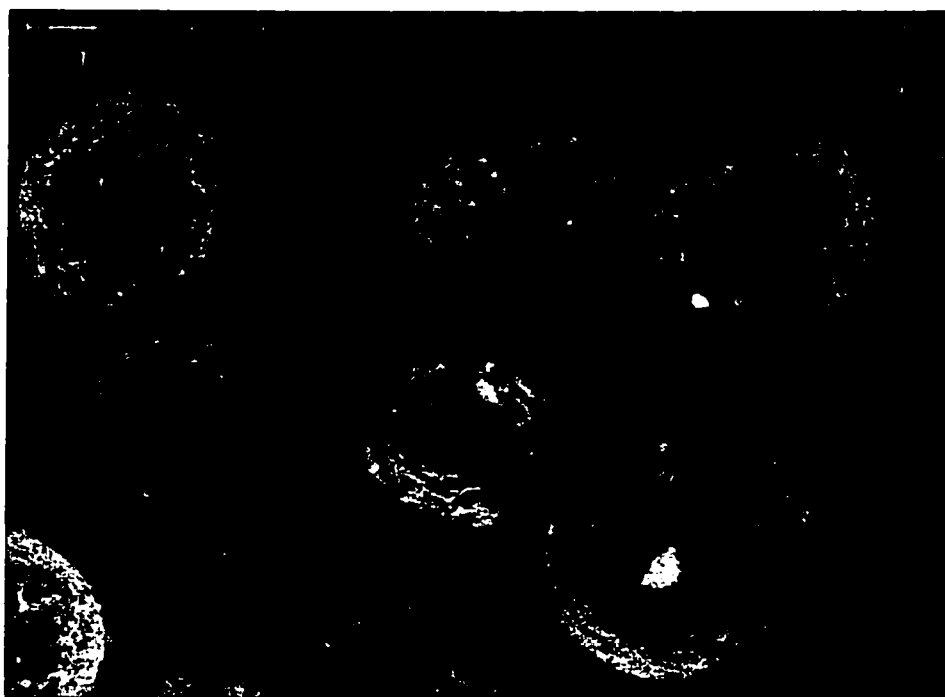


Figure 3.2 (b) Scanning electron micrograph of catalyst particles.

3.2 Prepolymerization and Polymerization

3.2.1 Prepolymerization

Prepolymerization is used before gas-phase polymerization to control the polymer morphology if the catalyst particles are fragile and/or to prevent overheating during rapid polymerization reactions. During prepolymerization, the catalyst particles are exposed to mild polymerization conditions, usually in a slurry, and a small amount of polymer is produced, typically 20 to 100 g of polymer per gram of catalyst. The prepolymerization produces stable particles which are used as catalysts in subsequent polymerization under more severe conditions. In this research, prepolymerization was carried out in a 1-L stirred, glass autoclave with a circulating cooling jacket. The reactor was evacuated overnight at 80°C after leak tests. About 300 mL heptane was fed into the reactor under N₂ protection. About 0.3 mL triethylaluminum (TEA) and 100 mg catalyst, which were drawn into separate Hamilton Gastight syringes in a glove box, were injected into the reactor via a syringe port. The reaction temperature was controlled at 30°C, ethylene pressure was between 55-138 kPa (8-20 psi), and hydrogen pressure was about 70 kPa (10 psi). The reaction condition was monitored by a PC. When the amount of produced prepolymer was about 10 g, the product was removed from the reactor under nitrogen protection into a special vial. The prepolymer was dried under nitrogen flow in the vial and stored in the glove box for further polymerization use.

A summary of all the prepolymerization runs is given in Appendix D, Table D.3.

3.2.2 Polymerization

A 1-L stainless semibatch reactor built and described by Lynch and Wanke (1991) was used for polymerization experiments. The reactor system was modified for gas chromatography (GC) analysis. A heat gun was used in order to keep the GC sampling valve (Swagelok metering valve, SS2-A) at high temperature. The schematic diagram of the reaction equipment is shown in Figure 3.3. The heat gun was mounted above the reactor and the distance and angle between heat gun and sampling port could be adjusted. The power of heat gun was controlled by a voltage transformer (0-140V). The GC sampling tubing which connected the GC equipment, Hewlett Packard (hp) 5890 series II

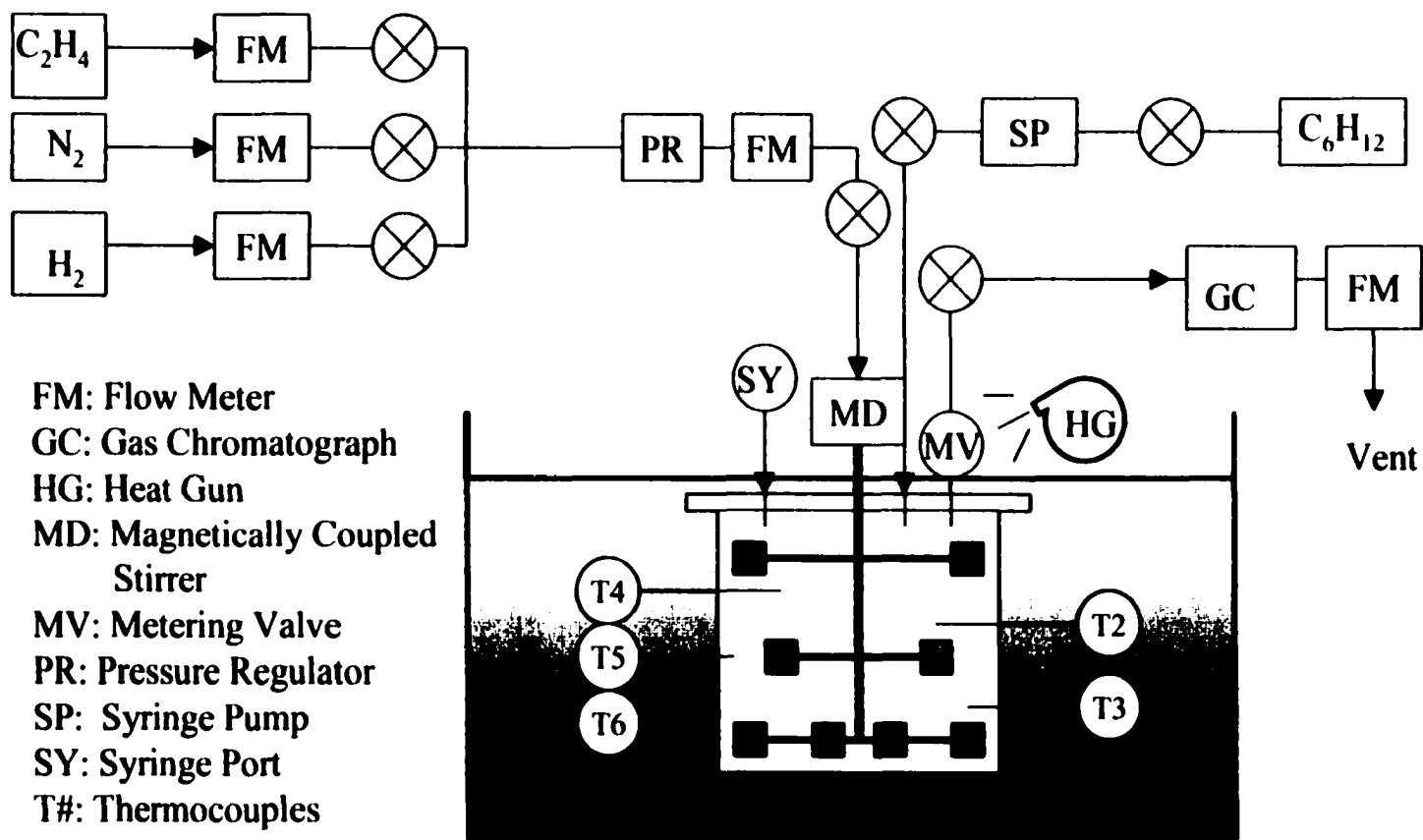


Figure 3.3 Schematic diagram of the copolymerization equipment

and the GC sampling valve was a 1.15 m long Teflon tubing with outside diameter 1.6 mm (1/16") and inside diameter 0.25 mm (0.01"). An hp 3390A integrator was used for calculating sample compositions. The GC parameters and the determination of ethylene/1-hexene response factors are described in Appendix A.

The reason for heating the GC sampling port is that the saturation pressure for 1-hexene is very temperature dependent; it is 3.5 psi at 24°C and 18 psi at 70°C (see Appendix B for the properties of 1-hexene). In this study, the reaction temperature was kept between 60 and 90°C (usually 70°C) in order to obtain relatively high 1-hexene concentration in the reactor. Since the sampling port was above the oil bath, its temperature was lower than that in the reactor which was merged in the oil bath. This reduced temperature at the GC sampling valve would lead to condensation of 1-hexene inside the valve and thus affect the accuracy and the reproducibility of the GC analysis.

In addition, the partial pressure of 1-hexene in the reactor should never exceed 20% of the total pressure during the runs because the gas sample from the reactor was transferred to GC at room temperature and near atmosphere pressures (about 13.7 psi in Edmonton). Under these conditions, the saturation pressure of 1-hexene is 3.5 psi and accounts for 25% of the total sampling pressure ($3.5 \text{ psi}/13.7 \text{ psi} = 25\%$). Higher 1-hexene concentration in the reactor would lead to condensation of 1-hexene in the Teflon tubing.

In gas-phase polymerization, the start-up procedure for each run consisted of placing a 200 g NaCl (crystalline, from Fisher Scientific) seed bed into the clean reactor, leak testing the reactor with N₂ at 400 psi and evacuating overnight at 90°C. The reactor was cooled to the desired reaction temperature by controlling the oil bath temperature before reaction. After the desired amount of TEA had been injected into the reactor, the heat gun was switched on. The salt bed was stirred for 5 min before the next step. About 0.1 g prepolymer which was previously put into the catalyst holder in the glove box was blown into the reactor with nitrogen through a port in the flange on the top of the reactor. The total nitrogen pressure in the reactor after adding prepolymer was kept a little above ambient pressure (<15 psi). A preset amount of 1-hexene was pumped into the reactor

with an ISCO 500D high-pressure syringe pump. Finally, the desired amount of hydrogen was added into the reactor, followed by continually addition of ethylene to maintain the total pressure. The additions of catalyst, 1-hexene, and hydrogen and the start of ethylene flow were carried out in less than 8 min. The stirring speed of the reactor during polymerization was about 204 rpm. The experimental runs lasted 0.5 to 8 h, usually 2 h.

The data acquisition system used for the prepolymerization was also used for polymerization. Data recorded by the PC included ethylene flow rate, reaction pressure and temperature at different locations in the reactor. The GC sampling valve was always opened during copolymerization runs. The flow rate of sampling gas was also monitored by PC and the value was subtracted from ethylene flow rate in later calculations. The change in 1-hexene composition in the reactor with time were measured by GC. If controlling of 1-hexene gas phase concentration in the reactor was required, 1-hexene was added periodically into the reactor using the ISCO 500D syringe pump. After polymerization, the reactor was disassembled and polymer product was rinsed with water to remove salt and kept in the oven at 60°C overnight to degas any remaining comonomer dissolved in the nascent copolymer.

A summary of gas-phase copolymerization runs is given in Appendix D, Table D.4; gas-phase homopolymerization runs and slurry-phase runs are described in Table D.5.

3.3 Controlling 1-Hexene Concentration in the Gas Phase

For Ziegler-Natta copolymerization reactions, comonomer concentration in the reactor is very important for the kinetic studies but it is not easily controlled, especially in laboratory reactors. The common methods are either to carry out the reaction in slurry phase where excessive amount of comonomer is added and the comonomer concentration is essentially constant during reaction, or adding desired amount of comonomer once at the beginning of the reaction in gas-phase polymerization. Not much work has been published on controlling the comonomer composition in laboratory gas-phase copolymerization studies. Han-Adebekun et al. (1997) reported a design and control methodology for gas-phase copolymerization in a stirred bed reactor. A Fourier transform infrared spectrometer

(FTIR) was used to monitor the composition ratio change of comonomer to monomer according to their specific adsorption bands and a feed-back PI controller was used for the control of comonomer feeding rate. There was a 20% drift from the set point in the first 10 min; after the initial period, the control error was very small. No detailed copolymerization kinetics were reported. Gas chromatography (GC) is usually used for gas composition detection in gas-phase commercial copolymerization processes (Han-Adebekun et al., 1997); however, it is seldom found for composition control in laboratory experiments. Chen (1993) applied GC analyses to measure gas-phase composition for ethylene/propylene copolymerization and controlled the composition by a PI controller. Experimental results showed that the control error in the first 20 min was large (30% deviation from set point).

In this study, a GC was used to monitor 1-hexene content in the gas phase and a new methodology was applied to control the gas composition manually. Two experiments were required to obtain one run at constant 1-hexene concentrations. In the first experiment, an amount of 1-hexene was added into the reactor at the beginning of run which resulted in the desired 1-hexene /ethylene mole ratio. No additional 1-hexene was added during the run. Care has to be taken so that the amount of 1-hexene in the reactor did not result in the presence of liquid 1-hexene. The Antoine equation (see Appendix B) was used to estimate the saturation pressure as a function of temperature. This allowed the determination of the maximum amount of 1-hexene which could be added to the reactor and still ensure gas-phase operations. Changes in the 1-hexene/ethylene mole ratio were monitored by GC during the run. An example of 1-hexene composition changes with reaction time is shown in Figure 3.4. The rate of disappearance of 1-hexene from the gas phase can be estimated by differentiation of the 1-hexene/ethylene ratio with time. Such a calculated rate of 1-hexene disappearance is shown in Figure 3.5. As shown in Figures 3.4 and 3.5, the rate of 1-hexene disappearance is at a maximum close to the start of the experiment and rapidly decreases during the first half hour and levels off after about 2 hours. It has to be emphasized that the rate of 1-hexene disappearance from the gas phase is not the reaction rate of 1-hexene because the value also includes 1-hexene loss in the sampling stream as well as 1-hexene which dissolves in the polymer produced

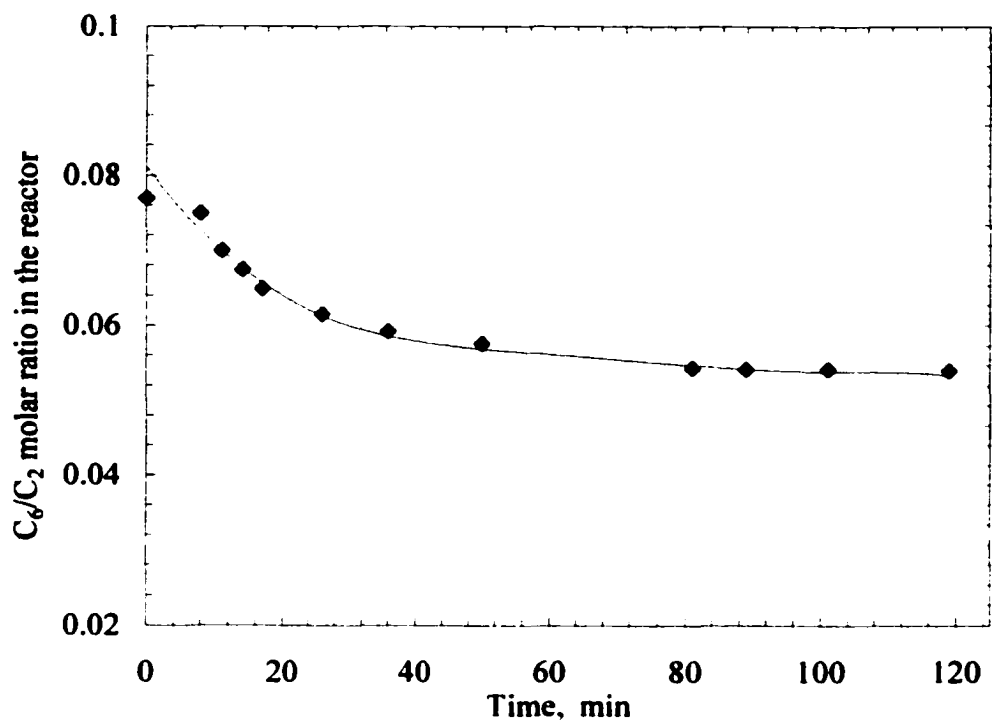


Figure 3.4 Concentration change of 1-hexene in gas phase during the first experiment (GasCo41) when 1-hexene was only added once at the beginning.

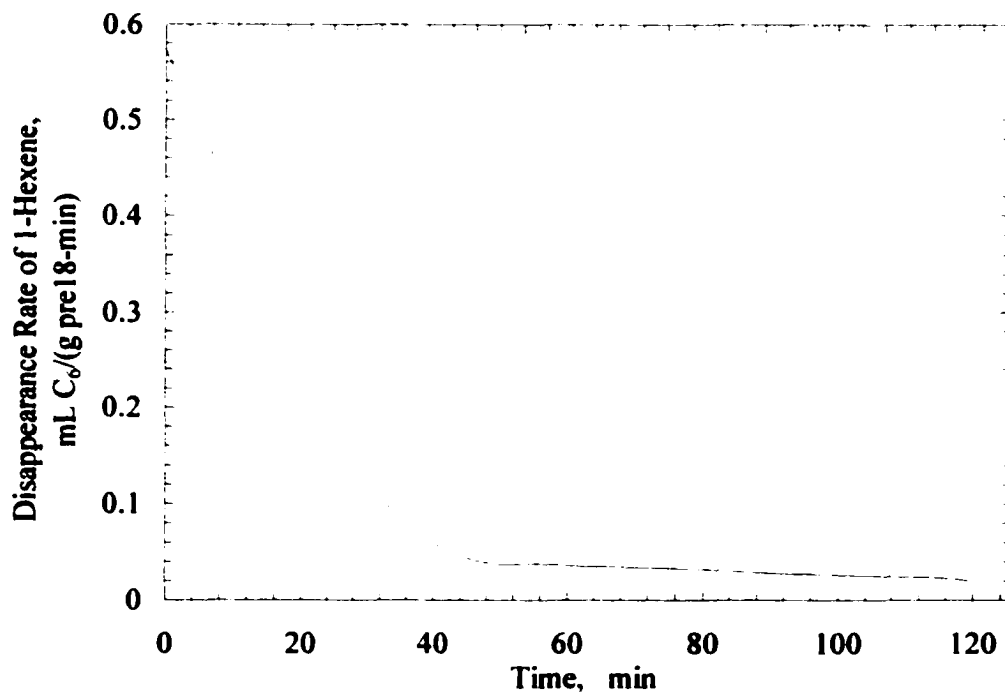


Figure 3.5 Estimated rate of 1-hexene disappearance based on derivative of fitting curve in Figure 3.4.

during the run.

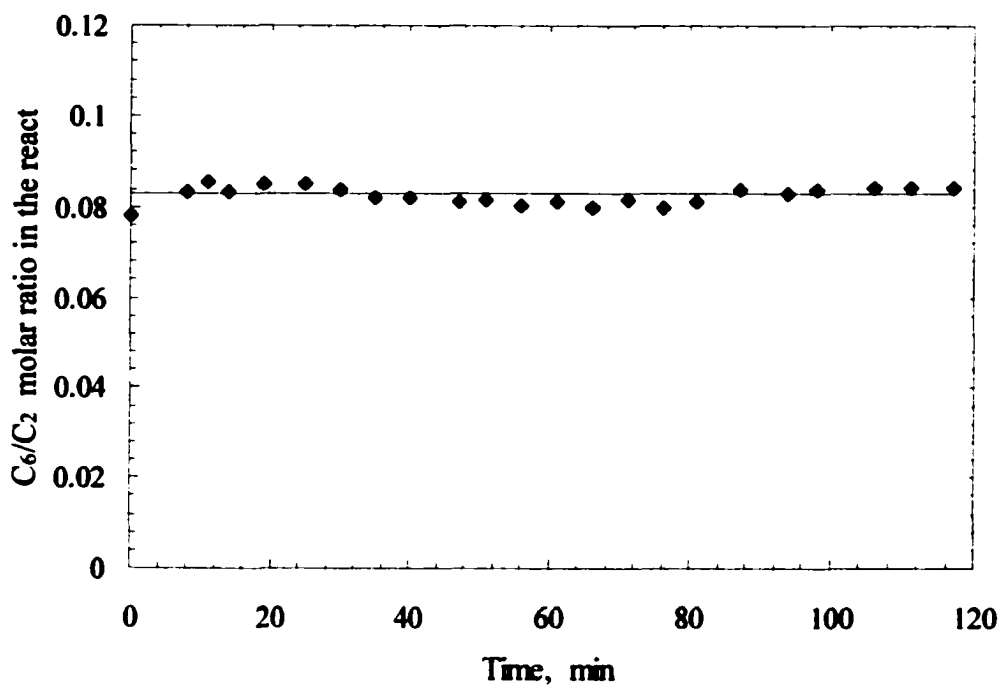
A second experiment was carried out with the initial conditions similar to those in the first run, but 1-hexene was added periodically during the second run at a rate approximately equal to the rate of disappearance obtained from the first run. Total pressure and temperature in the second run were similar to those in the first run. The second run was used to calculate the rate of 1-hexene reaction as a function of time. The procedure used to calculate the 1-hexene reaction rate is described in detail in Appendix C.

Normally one GC analysis required 2.5 min. After calculation of the comonomer content according to GC analysis, the deviation from the set point was obtained and the subsequent feeding rate of 1-hexene was adjusted. Generally, the actual feeding rate in the first half hour was higher than the pre-calculated value because the predicted feeding rate was based on lower comonomer concentration and because more 1-hexene dissolved in polymer under higher 1-hexene pressure; in the later stage of the reaction, the feeding rate was always lower than that calculated because the reaction rate was depressed more by higher comonomer concentration. In Figure 3.6, typical changes of 1-hexene/ethylene molar ratio with time as a result of 1-hexene addition during the run are shown. The variations in 1-hexene/ethylene ratio were usually less than $\pm 5\%$. This figure indicates clearly that an approximately constant comonomer concentration was maintained over the entire duration of the reaction by the intermittent addition of 1-hexene.

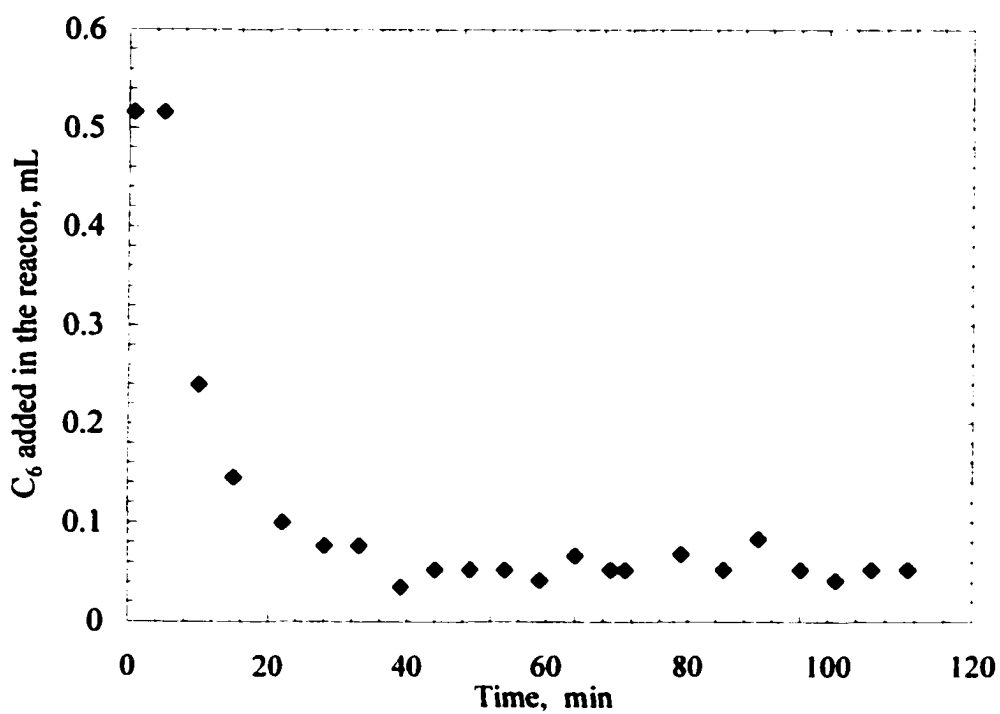
3.4 Characterization Techniques

3.4.1 Nuclear Magnetic Resonance (NMR)

In this study, high-resolution ^{13}C -NMR was used to measure comonomer content in copolymer products. Samples were dissolved in 1,2,4-trichlorobenzene and analyzed by Varian Unity 500 MHz NMR at 120°C . The data collection time was 1.3 s, delay time was set for 10 s and the pulse signal angle was given at 90° . The resulting polymer spectrum was analyzed according to ASTM D5017-96 and the procedure of De Pooter et al. (1991). However, the liquid sample preparation procedure was different from the ASTM method because most polymer samples would not dissolve properly if the ASTM



(a)



(b)

Figure 3.6. (a) Control results of the second run (GasCo42) based on the predictions shown in Figure 3.5. (b) Actual 1-hexene addition process in the second run.

method was used; Bialek and Czaja (2000) also reported the same problem with the ASTM method of specimen preparation. As a result, a modified method based on ASTM D5017-96 was developed and the procedure used to prepare NMR specimen is described below:

1. 0.05 to 0.2 g of polyethylene sample with 4-5 g 1,2,4-trichlorobenzene (spectrophotometric grade, from Aldrich) and ≤ 0.004 g antioxidant (2-*tert*-butyl-4 methylphenol, from Aldrich) were added into a 10-mL one-neck flask. The amount of solute added was dependent on the molar mass of the polymer sample (more solvent per mass of polymer for high M_w). The flask was kept in an oven with swing equipment at temperature between 140 to 160°C for 5 to 15 h.
2. The transfer of the dissolved sample was done by one of the following two methods.

Method 1: Attached NMR tube to a funnel by a special Teflon tubing. Put this whole assembly in another oven at 130°C. Quickly moved the hot flask from the first oven, toppled over the flask, letting the viscous liquid stream down slowly into the funnel. Since the temperature went down quickly with the opened oven door, a pair of scissors was used to cut off the cooling “gel” after 1.5 g of solution was moved into the funnel. Closed the door for 15-30 min until the gel melted again. Using a piece of copper wire to move air at the bottom of NMR tube and have polymer settle to the bottom of in the tube. The final length of polymer solution in the tube should be around 4.5 cm. A copper hook was used to remove excess polymer from the tube. Filled the top of gel with 0.5 cm deuterized benzene solution (D_6).

Method 2: If the polymer solution was too viscous to be transferred into the NMR tube, it would be cooled in the flask. A hook or small scoop was used to move the gel out of the flask on a plate. Cut 1.5 g of gel into small pieces and then put them into NMR tube with the help of copper wire.

3. After the sample solution was transferred in to the NMR tube, cleaned the top 3 cm of the tube so as to have a polymer free zone for sealing. After the opening was sealed, moved the tube into oven again, and heated to 130-140°C. When the

gel was melted, turned upside down and let the melt set down and mixed with the D₆. After 3-4 times, the solution was homogeneous and was ready for NMR examination.

3.4.2 Size Exclusion Chromatography (SEC or GPC)

The molar masses and polydispersity of ethylene prepolymer, homopolymer and copolymer were measured by Size Exclusion Chromatography (SEC). A Waters 150C GPC equipped with a differential refractometer and a series of four Shodex GPC/UT-800M columns was used initially. The columns and the detector were maintained at 140°C. Later, samples were analyzed by Waters Alliance GPCV 2000 and three Waters Styrag HT6E columns plus one guard column. Millennium 2000 system was used for processing data. The columns and the detector were maintained at 145°C. The solvent, HPLC-grade 1,2,4-trichlorobenzene, was pumped through the columns at 1.0 cm³/min. The solvent contained approximately 0.25 g/L of antioxidant 2,6-*tert*-butyl-methylphenol. The polymer concentrations in the solution were between 0.4 and 0.7 g/L. The calibration was done using standard samples of polystyrene and polyethylene with narrow polydispersities.

3.4.3 Scanning Electron Microscopy (SEM)

The catalyst samples for SEM observations were prepared in the glove box and sealed with plastic bags, then transferred into the carbon evaporator (Hitachi, HUS-4) for coating, and finally into the microscope. To obtain samples suitable for the examination of cross-section microstructure, prepolymer or catalyst particles were first embedded in epoxy resins (from West System Inc, resin 105:hardener 205 = 5:1) to form a suitable support matrix for further microtoming and to avoid interactions with air and moisture. After allowing the resin to harden for the 8 hours, the resin sample was sliced into thin pieces (<0.3 mm). These thin pieces were quickly carbon coated to minimize exposure to oxygen and moisture.

The SEM equipment was a Hitachi S-2700 SEM model using PGT software for image acquisition. An accelerating voltage of 10 kV was used. Increasing electron energy and

scanning time may result in the accumulation of electrons on the surface of specimen which leads to charging problem. When SEM electron beam interacts with the specimen, some of the charge injected by the beam is emitted in the form of the backscattered and secondary electrons while other fraction of charge remains in the specimen. This charge flows to ground if the specimen is a conductor and a suitable connection exists. Since polymer samples are not good conductors, carbon coating (or gold coating) is needed for making the specimen electron conductible. If some place is not appropriately coated and the ground path is thus blocked, the specimen is quickly charged. This charged area acts as an electron mirror and SEM loses its ability to “see” the detailed structures.

The Imix system with a PRISM IG (Intrinsic Germanium) detector was used for x-ray microanalysis (x-ray quantitative analysis and x-ray dot mapping). Higher electron energy is needed (accelerating voltage 20 kV) to produce x-ray signals strong enough for chemical analysis.

Typical Ti distribution of a sample catalyst is shown in Figure 3.7. It can be seen that the distribution is quite even on the surface and along the cross section. Figure 3.8 is a sample of x-ray quantitative analysis spectrum and Ti content measured is 4.2 wt % which is comparable to the value 3.5 wt% obtained via the colorimetric method.

3.4.4 Temperature Rising Elution Fractionation (TREF)

The TREF system used for characterization of LLDPE products was a custom-built apparatus which has been detailed described by Lacombe (1995) and Zhang (1999).

The general TREF procedures for sample analysis in this study are

1. **Crystallization Step:** About 5-10 mg polymer samples were weighted in a glass bottle (15-20 mL), o-xylene was added till the solute concentration of 0.001 gPE/mL was obtained. Then, about 1.5 g of glass beads (80-100 mesh) was added into the mixture. With the help of magnetic stirrer, the slurry was heated slowly to 125°C in a silicone oil bath and maintained at the temperature for 2 h to ensure the complete dissolution of polymer. Further heating of 2 h at 125°C without stirring, the solution was then

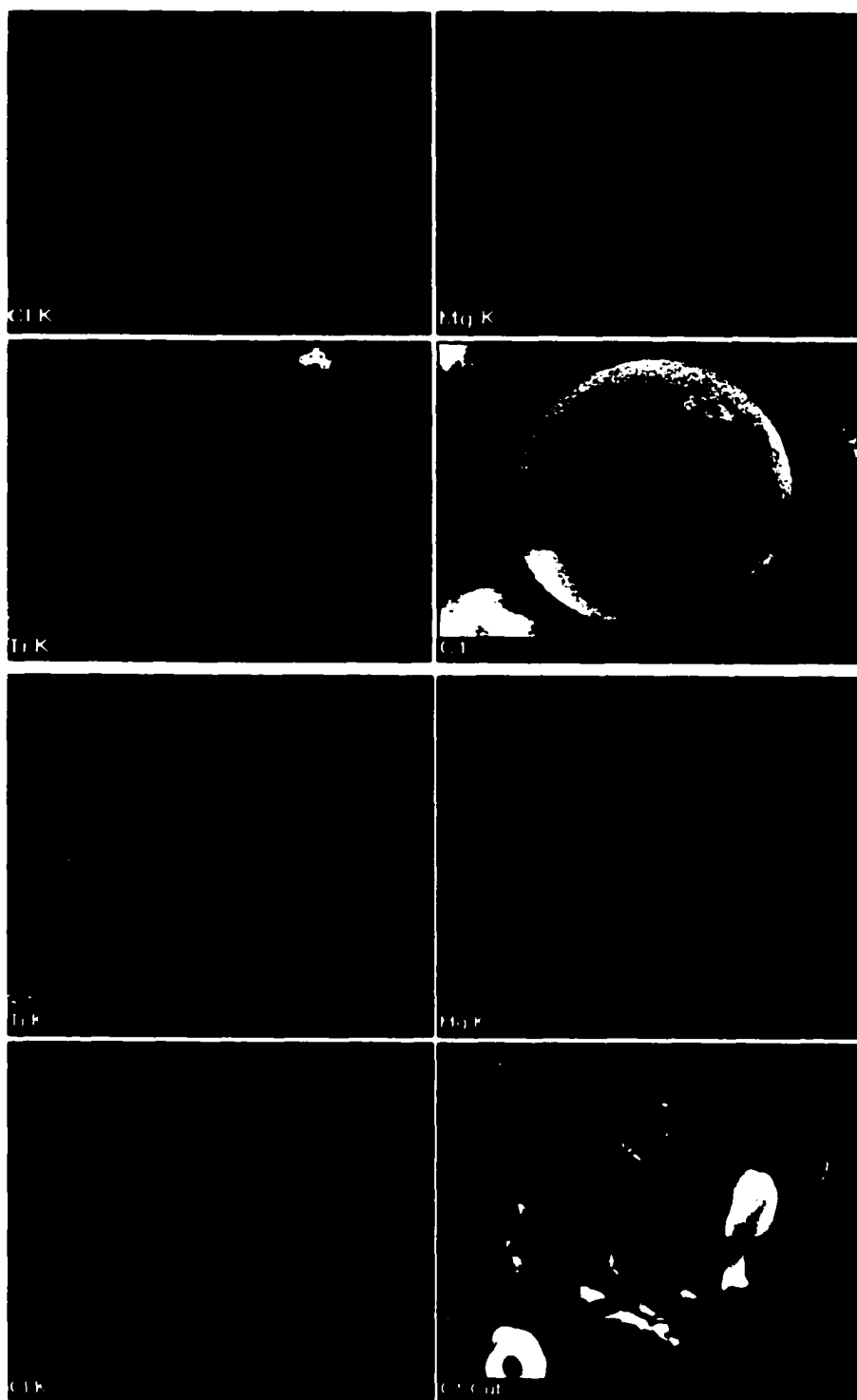


Figure 3.7 X-ray dot mappings of surface (top images) and cross-section (bottom images) of catalyst Cat-5. The yellow, blue and red dots represent Ti, Mg and Cl elements, respectively.

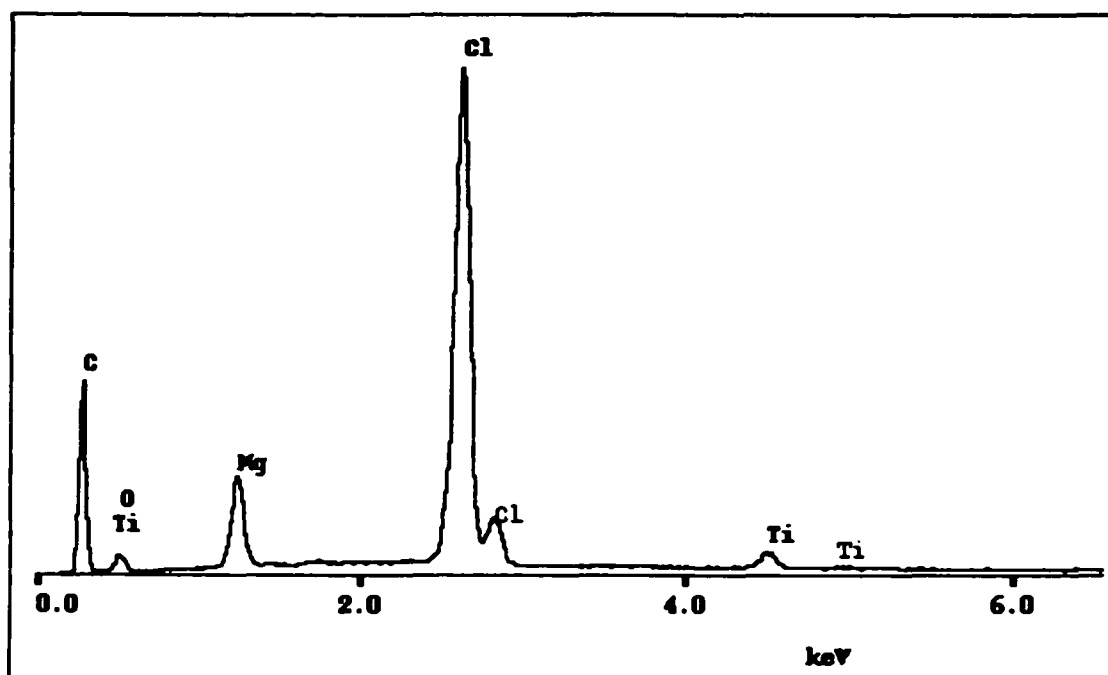


Figure 3.8 X-ray microanalysis spectrum of catalyst Cat-4.

slowly cooled down to -8°C at a cooling rate of $1.5^{\circ}\text{C}/\text{h}$. The crystallized sample was then transferred to a TREF column for elution.

2. **Elution Step:** During this step, the column temperature was increased from 0°C to 125°C at a heating rate of $1^{\circ}\text{C}/\text{min}$ while the *o*-dichlorobenzene solvent was pumped through the column continuously at a constant flow rate of $1.0\text{ mL}/\text{min}$. During the heating, LLDPE molecules dissolved and were eluted by the solvent flow. Samples with higher SCB content dissolve first and were eluted at lower temperatures. The eluted polymer species were detected with an on-line IR detector tuned at 2859cm^{-1} . A typical elution run would last about 2.5 h.

Figure 3.9 gives an example of TREF spectrum of one copolymer sample. This figure can be converted to SCB distribution according to the method described by Zhang (1999).

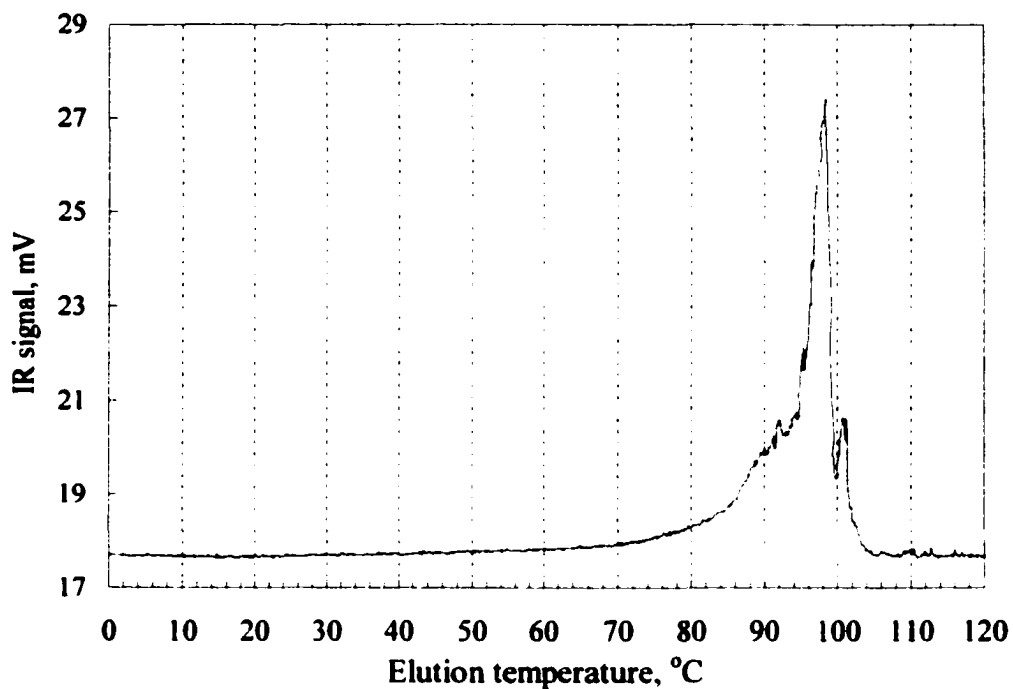


Figure 3.9. TREF profile for sample GasCo08.

3.4.5 Differential Scanning Calorimetry (DSC)

Crystallinity was determined with a Perkin-Elmer DSC-4 system. Sample sizes varied from 5 to 15 mg. Polymer sample was heated from room temperature to 170°C at a rate of 10°C/min. The heat of fusion values were determined from the peak of the DSC endothermic spectra. The mass fraction of crystals, χ_c , can be calculated from the heat of fusion:

$$\chi_c = H/H_c$$

where H_c is the heat of fusion for 100% crystalline polyethylene; H_c is chosen 291 J/g according to other researcher's work (Chien and Nozaki, 1993; Parker et al., 1996). A typical DSC curve is shown in Figure 3.10.

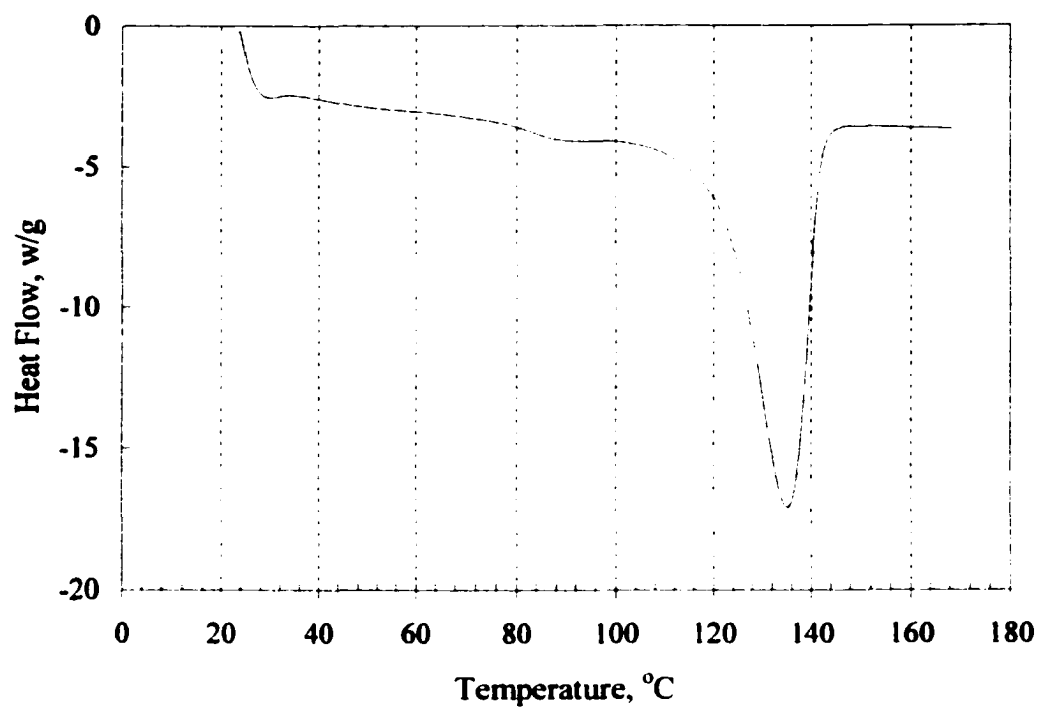


Figure 3.10 DSC endothermic curve of copolymer GasCo46.

CHAPTER 4. RESULTS OF $\text{MgCl}_2/\text{TiCl}_4$ CATALYST SYNTHESIS

The newest generation of Ziegler-Natta catalysts is characterized by their morphology-controlled property (Forte and Coutinho, 1996). Polymers with irregular shape and low bulk density are not commercially desirable because they are difficult to handle. If the polymer is to be stored or sold in granular form, significantly larger amounts of storage and shipping space is required for handling these materials. Even if the granular form polymer is to be pelletized prior to shipping, the processing of a given quantity of the low bulk density material through the pelletizing equipment requires significantly longer processing time than would the same quantity of high bulk density materials.

Very high activity MgCl_2 -supported Ziegler-Natta catalysts have been widely used in industry and many patents reported their inventions of catalyst preparation method which could produce polyolefins with good morphology. Some of them were reviewed in Chapter 2. However, a complete study on the influences of catalyst's composition and preparation history on the control of polymer morphology and reaction behavior is seldom found for ethylene polymerization. The object in this part of the current work is the preparation of morphology-controlled MgCl_2 -supported TiCl_4 catalysts, and to study the factors that affect the polymer morphologies and homopolymerization activities. Finally, the relationship between catalyst and copolymerization behavior was probed.

4.1 General Rules of Obtaining Spherical Catalyst Particles

Reproducible preparation of Ziegler-Natta catalysts require a lot of 'know-how' and sometimes "the reproduction of some experimental finding is as important as finding itself" (Kissin, 1985). The catalyst preparation method in this study generally followed the procedure described by Wu (1999). However, modifications were made to improve the reproducibility. Some general rules for catalyst preparation based on observations made in the current study are summarized below:

1. In the support preparation step, the $\text{C}_2\text{H}_5\text{OH}/\text{MgCl}_2$ ratio is very important for obtaining suitable supports. At high ratios (>3.5), it is difficult to control the spherical morphology and the obtained support particles break easily. SEM images of the

support with $C_2H_5OH/MgCl_2$ ratio about 3.5 are shown in Figure 4.1. It can be seen that the all particles are irregular. At low ratios (<2.5), it is not possible to obtain the adduct in a totally melted form before it precipitates. Usually the $C_2H_5OH/MgCl_2$ ratio was kept around 2.8~3.2 in the current study.

2. Emulsion steady state was established after 0.5 h of stirring at $120^\circ C$. Spherical droplets were not completely formed if the emulsion was quenched before steady state was established. As shown in Figure 4.2, quite a few of the particles have irregular shapes if the mixing time was short.
3. The support size was affected by the emulsion temperature and stirring speed. The general stirring speed kept between 500 and 1000 rpm (lower stirring speed at higher temperature). Higher emulsion temperature required lower stirring speed to get the same sizes (see Figure 4.3 and Figure 4.4). For the support shown in Figure 4.3, the emulsion temperature was $130^\circ C$ and the stirring rate was 590 rpm; the support in Figure 4.4 was made at $110^\circ C$ and stirring rate was 1000 rpm. The obtained supports had similar size.
4. Fines were usually part of the support product; however, they were often eliminated during the $TiCl_4$ treatment. Reaction between $TiCl_4$ and ethanol is rapid and highly exothermic (Forte and Coutinho, 1996). When adding $TiCl_4$ to the support suspended in heptane, ethanol in the support reacted rapidly with the $TiCl_4$ (see Chapter 3). The small fines were further broken due to this rapid reaction and appeared to be eliminated in subsequent washings. The catalyst made from support shown in Figure 4.4 is shown in Figure 4.5. No fines were observed in the final catalyst. Similar results were shown in Figure 3.2. Furthermore, to avoid breaking of the spherical particle, it is important to keep the titaniation procedure slow (i.e. adding $TiCl_4$ drop-wise to the support suspension) and to keep the system at low temperature (e.g. $< 0^\circ C$).

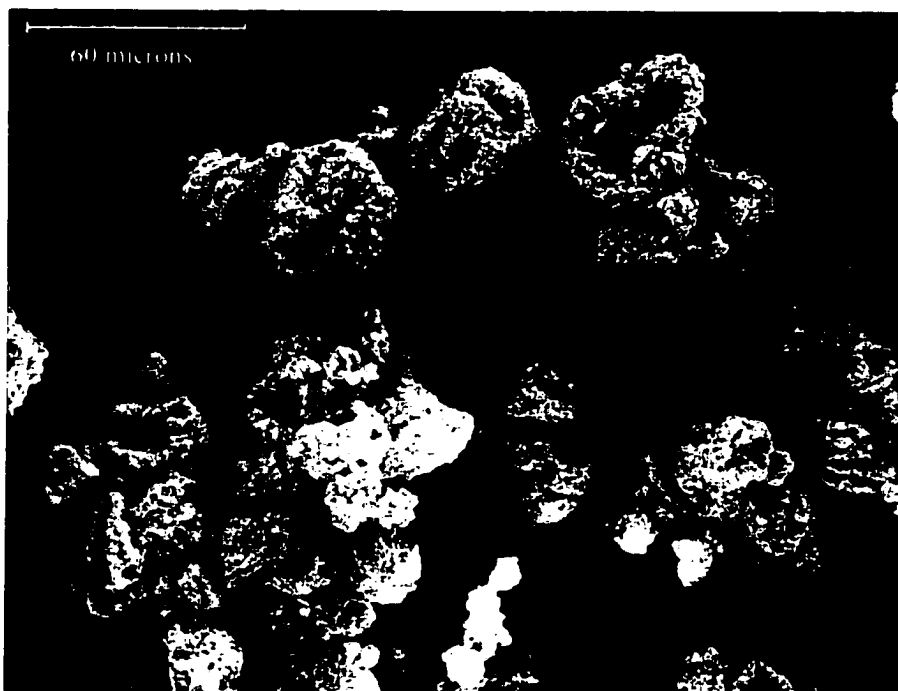


Figure 4.1 SEM image of support (Support-17) with EtOH/MgCl₂ mole ratio about 3.5.

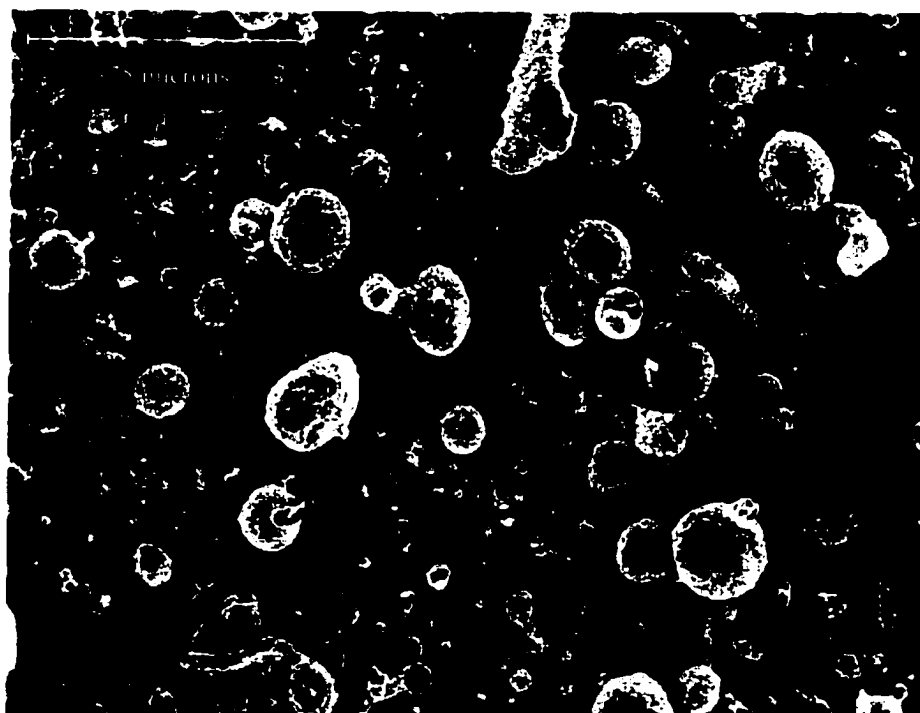


Figure 4.2 SEM picture of support (Support-18) from emulsion before steady state was established. (120°C for 20 minutes).

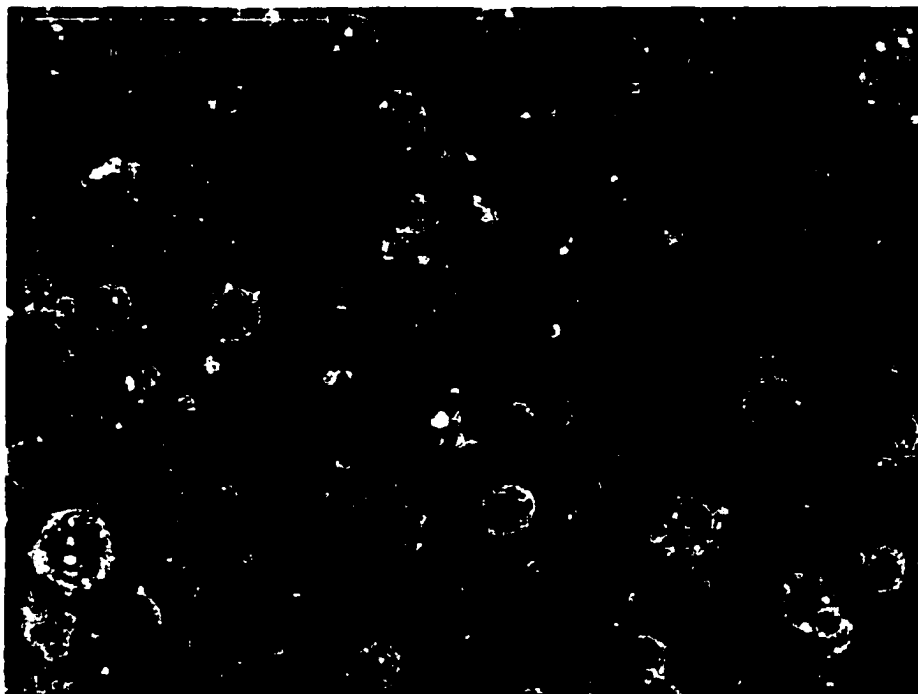


Figure 4.3 SEM image for the support (Support-15) operated at 130°C and 590 rpm stirring rate.

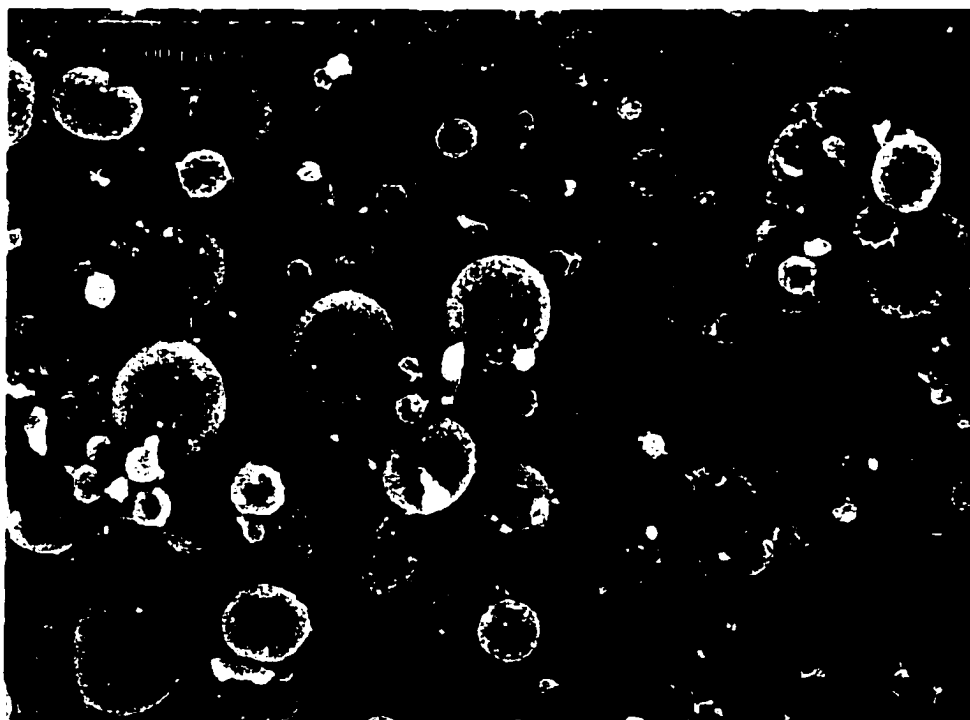


Figure 4.4 SEM image for the support (Support-16) operated at 115°C and 1000 rpm.

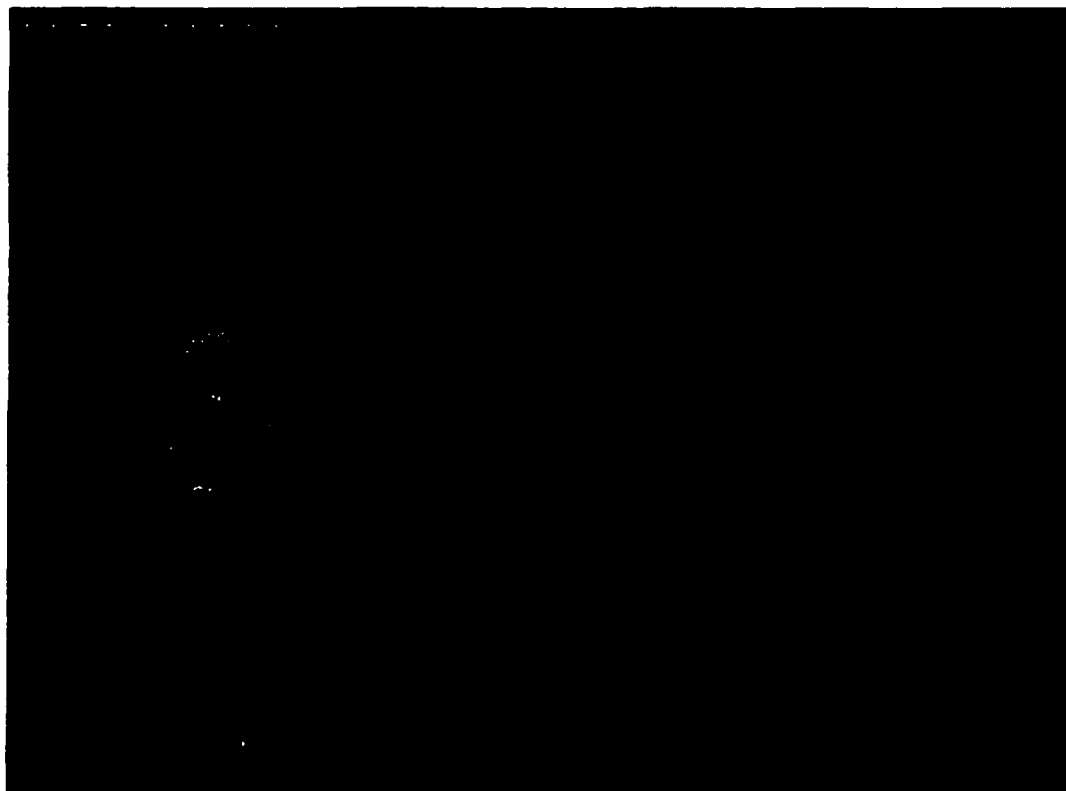


Figure 4.5 Catalyst (Cat-4) made from Support-16 shown in Figure 4.4. Fines observed in support disappeared during the introduction of Ti and subsequent washings.

4.2 Influence of Catalyst Composition on Activity and Product Morphology

The effects of $C_2H_5OH/MgCl_2$ ratio, Ti content and the amount of electron donor on catalytic activity and polymer morphology are presented in this section. The methods for ethanol and titanium content determination were described in the previous chapter. Electron donor content was calculated for the amount of DBP added. Experimental results were summarized in Table 4.1. Detailed catalyst preparation procedures have given in Chapter 3.

4.2.1 Effects of $C_2H_5OH/MgCl_2$ on Activity and Bulk Density

Partial dealcoholation before treatment with $TiCl_4$ is generally used in $MgCl_2/EtOH$ supported catalyst preparation (Sacchetti et al., 1993; Chung et al., 1996; Shin et al., 1995; Parada et al., 1999). The effect of the degree of dealcoholation on catalyst activity and polymer bulk density have been studied and the results are listed in Table 4.1 and plotted in Figure 4.6.

Table 4.1 Summary of Activities and Product Bulk Densities for Various Catalysts.

Catalyst No.	C ₂ H ₅ OH /MgCl ₂	Ti Content Wt%	DBP/MgCl ₂	Activity, kg PE/(gcat-h-100psi ethylene) (Run No.)			Bulk Density ¹ , g/cm ³	
				Homo, Slurry	Homo, Gas phase	Copolymerization	Slurry	Gas phase
Cat-1	0.34	2.1	0.03	5.0 (Slu-6)	1.1 (GasHo8)	1.7 (GasCo6)	0.31	0.35
Cat-2	1.1	2.0	0.12	--	1.7 (GasHo11)	3.2 (GasCo8)	--	0.35
Cat-3	1.4	4.0	0.05	2.9 (Slu-7)	1.8 (GasHo10)	4.5 (GasCo4)	Broken	0.38
Cat-4	1.5	3.5	0.07	3.4 (Slu-8)	1.9 (GasHo7), 1.6 (GasHo12)	3.5 (GasCo9)	Broken	0.4, 0.38
Cat-5	1.45	3.1	0.06	2.0-2.5 (Slu-1 –Slu-5)	1.6 (GasHo12)	--	0.29-0.34	0.38
Cat-6	1.8	5.5	--	3.3 (Slu-11)	1.2 (GasHo2)	--	0.31	0.36
Cat-7	1.8	6.5	0	15.3 (Slu-13)	0.7 (GasHo1)	2.7 (GasCo10)	0.23	0.25
Cat-8	1.9	1.8	0.08	3.4 (Slu-12)	2.2 (GasHo3)	--	0.31	0.37
Cat-9	2.5	1.9	0.08	--	0.1 (GasHo9)	--	--	0.35
Cat-10	2.8	4.3	0.09	0.3 (Slu-10)	--	--	0.35	--

¹Bulk density was measured only for the spherical product. Most of copolymer products were broken particles.

Examination of the Figure 4.6 shows that neither activity nor bulk density are well correlated with the $C_2H_5OH/MgCl_2$ ratio. This result is different from the work of Parada et al. (1999) who found that the catalyst activity was inversely proportional to the degrees of dealcoholation. However, the two catalysts (Cat-9 and Cat-10) made from supports with high $C_2H_5OH/MgCl_2$ ratio (≥ 2.5) after dealcoholation both had very low activities.

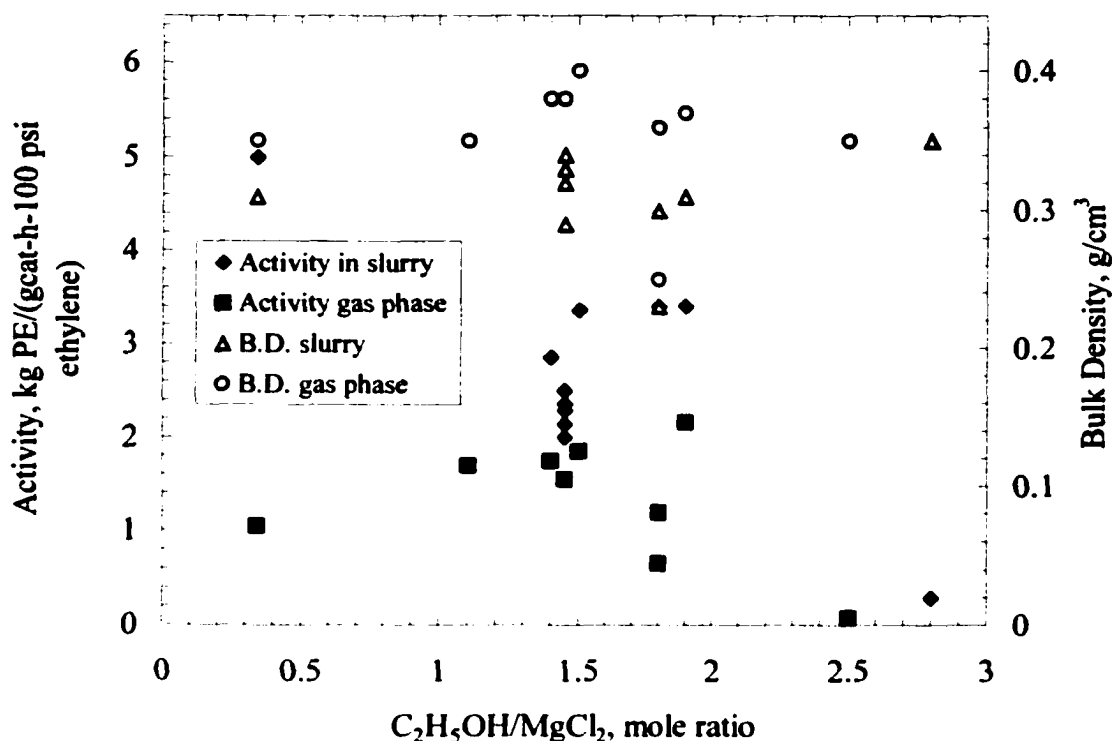


Figure 4.6 Dependence of catalyst activity and polymer bulk density on support $C_2H_5OH/MgCl_2$ ratio.

Ethanol in the support has two functions: first as a solvent for spherical support formation; and second, destroying the $MgCl_2$ lattice, i.e., increasing the crystal defects and thus forming potential sites on which active Ti can be anchored. During the catalyst impregnation process, the ethanol is replaced by Ti. As mentioned in the previous chapter, the $TiCl_4$ can react with ethanol and form titanium chloride alkoxide complex:



This ethoxide is inactive for olefin polymerization (Chung et al., 1996; Parada et al., 1999) and must be removed from the support. $TiCl_3(OC_2H_5)$ is soluble in hot $TiCl_4$ and

thus can be washed out of support by fresh and excess TiCl_4 at elevated temperature. If the ethanol content of the support is high, it may be difficult to totally remove the alkoxide from the inside of the catalyst, which may result in low activity. Therefore, the removal of alcohol is very important to achieve high activities. Sacchetti et al. (1993) suggested in a patent that the $\text{C}_2\text{H}_5\text{OH}/\text{MgCl}_2$ ratio in the support before titanation should not exceed 2; otherwise activity would be low. They attributed the lower activity to the lower porosity and surface area of the support. Parada et al. (1999) found that dealcoholation affected the capacity of interaction of the TiCl_4 with the MgCl_2 . Higher dealcoholation degree led to higher Ti content. This was not the case in our experiments. No clear trend between dealcoholation degree and titanium amount is evident in the results shown in Table 4.1.

4.2.2 Effects of Ti Distribution on Activity and Bulk Density

No correlation between average activity and Ti content was observed (see Figure 4.7). The presence of inactive Ti as well as variation in electron donor content may be the cause.

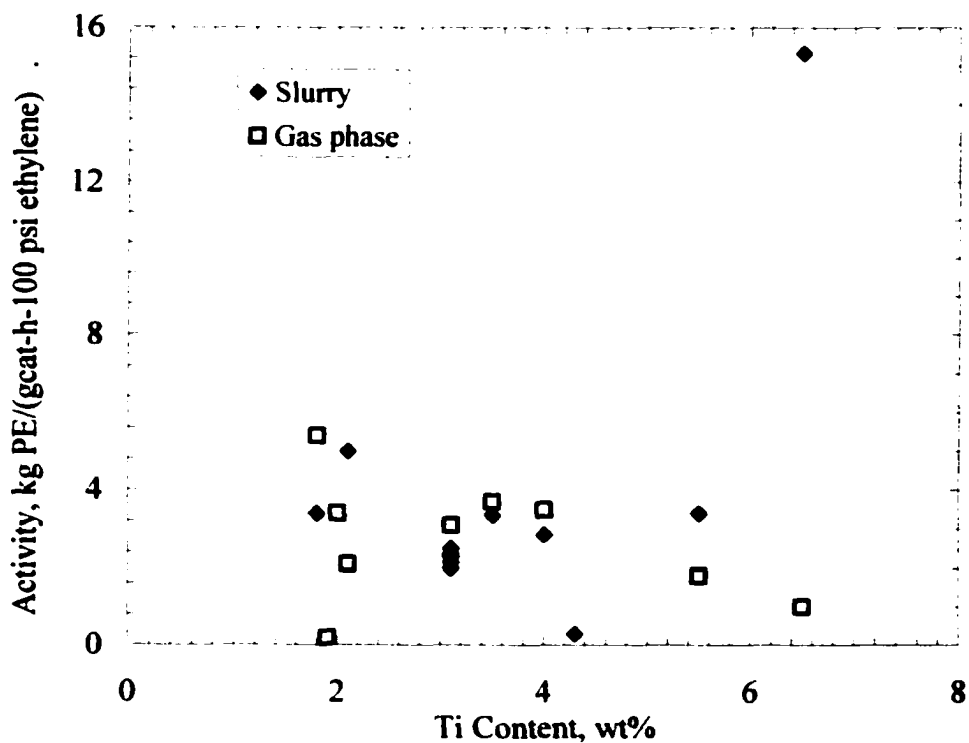


Figure 4.7 Dependence of catalyst activity on titanium content.

It is generally believed that the poor morphology comes from the uneven distribution of Ti throughout the catalyst particle. Chung et al. (1997) found that the bulk density of produced polyethylene was at maximum when Ti/Mg ratio on the catalyst surface is similar to that of the entire catalyst. When the Ti/Mg ratio on the surface was higher than that of the entire catalyst, the bulk density was low. In this study, x-ray dot mapping technique was used to directly observe the element distribution on the surface and on the cross section of catalyst Cat-5 (see Figure 3.7). In Figure 4.8, element distribution image for a cross section of Cat-4 is given. A relatively even distribution of Ti throughout the catalyst particles can be seen in both pictures. The x-ray quantitative analyses showed that the Ti contents for both catalysts were also similar. The x-ray quantitative analysis for Cat-5 yielded a Ti content at the surface of 4.8% and an average of 4.1% in the cross section. Analysis for Cat-4 showed that Ti content at the surface was 4.7 % and cross section average was 4.2 %.

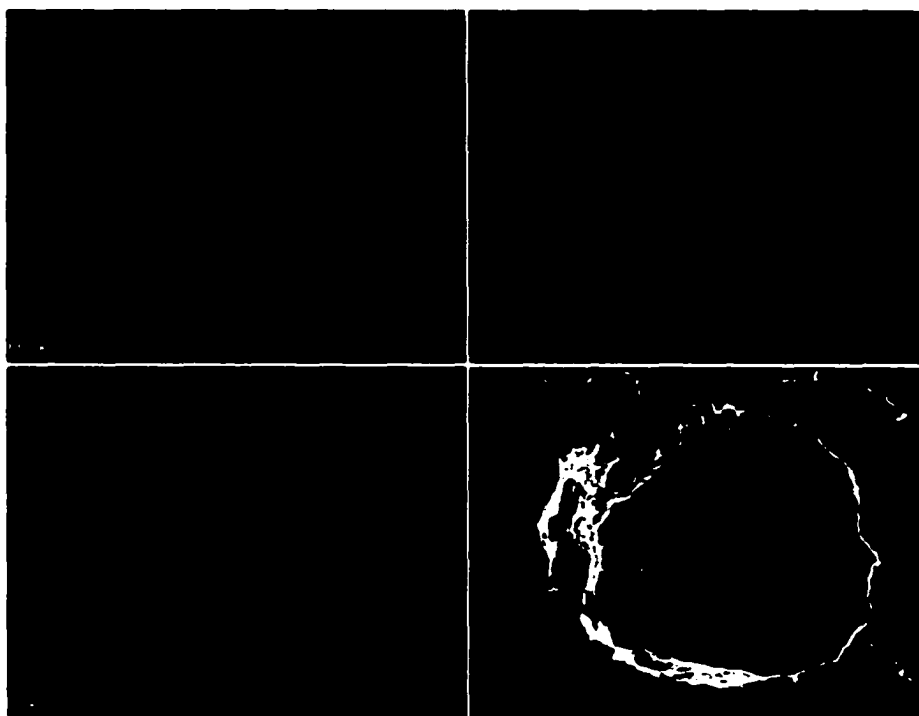


Figure 4.8 X-ray mapping observation of internal Cat-4 particle.

Gas-phase homopolymerization (70°C, $P_{C_2H_4}=200$ psi, 2-h run) using these two catalysts produced polyethylene particles with different structures (Figure 4.9 and Figure 4.10). Figure 4.9 shows the internal structure of the polyethylene made with Cat-5 (Polymer A



Figure 4.9 Internal structure of Polymer A made with Cat-5.

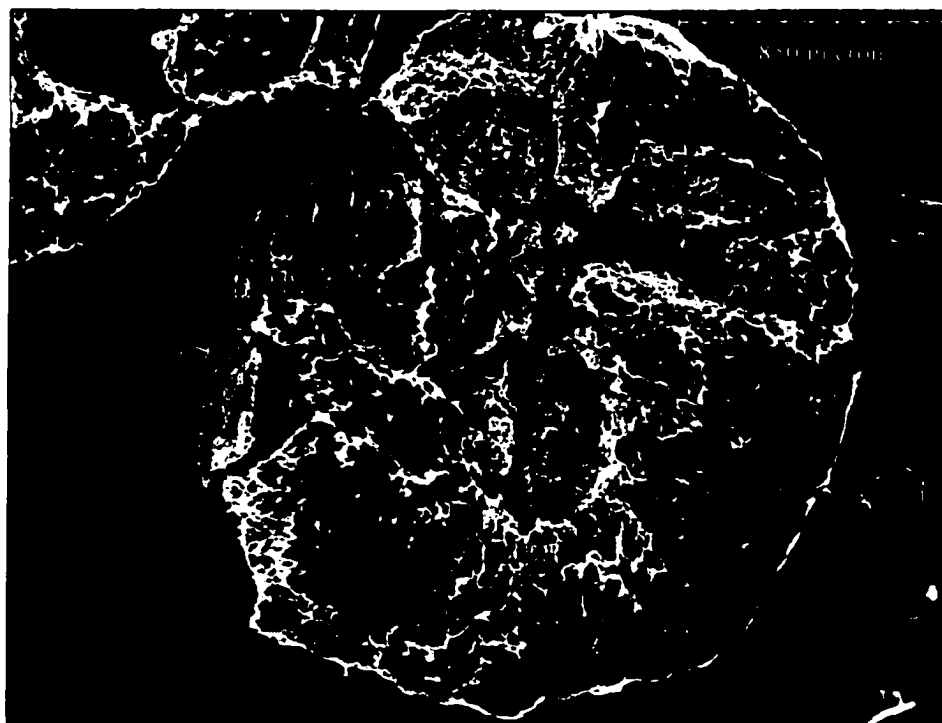


Figure 4.10. Internal structure of Polymer B made with Cat-4.

with bulk density 0.33 g/cm³) and Figure 4.10 shows the internal structure of the polyethylene made with Cat-4 (Polymer B with bulk density 0.40 g/cm³). It can be seen clearly that Polymer B had a denser structure than Polymer A. Hence, parameters other than Ti distribution play a dominant role in controlling nascent particle morphology.

4.2.3 Effects of Dibutyl Phthalate on Activity and Bulk Density

Electron donors, like ethyl benzoate (EB) and dibutyl phthalate (DBP), are widely used in propylene and other α -olefin polymerization to produce stereoregular product because they can increase catalyst activity, as well as stereoregularity (Soga and Shiono, 1997). Electron donors have seldom found application in ethylene polymerization. The present study found that the DBP affects polymerization behavior and polyethylene morphology. The effect of DBP concentration on bulk density and catalytic activity are shown in Figures 4.11 and 4.12. The C₂H₅OH/MgCl₂ ratios for the supports used were less than 2 since higher values resulted in low activity (see Section 4.2.1).

In Figure 4.11, catalyst prepared from supports not containing any DBP produced polymers with low bulk densities and the catalyst particle morphology was not replicated into the product particles; products were fine powders resulting from the disintegration of the growing polymer particles during polymerization. Forte and Coutinho (1996) also found that catalyst prepared without an internal electron donor usually resulted in poor morphologies and lower activities than those prepared with DBP. Small increases in bulk density were observed with increasing DBP/MgCl₂ mole ratios >0.03 for both slurry and gas-phase operation. The bulk density reached maximum of about 0.40 g/cm³ for gas-phase operation and 0.34 g/cm³ for slurry operation at DBP/MgCl₂ ratio between 0.06 and 0.07. The maximum DBP/MgCl₂ ratio in this study was 0.12, because above this value, significant amount of undissolved DBP/TiCl₄ complex precipitated during catalyst preparation. The bulk density of the polyethylenes made in the gas phase were consistently higher than those made in slurry; this is due to swelling of the polymer by the heptane during slurry operation.

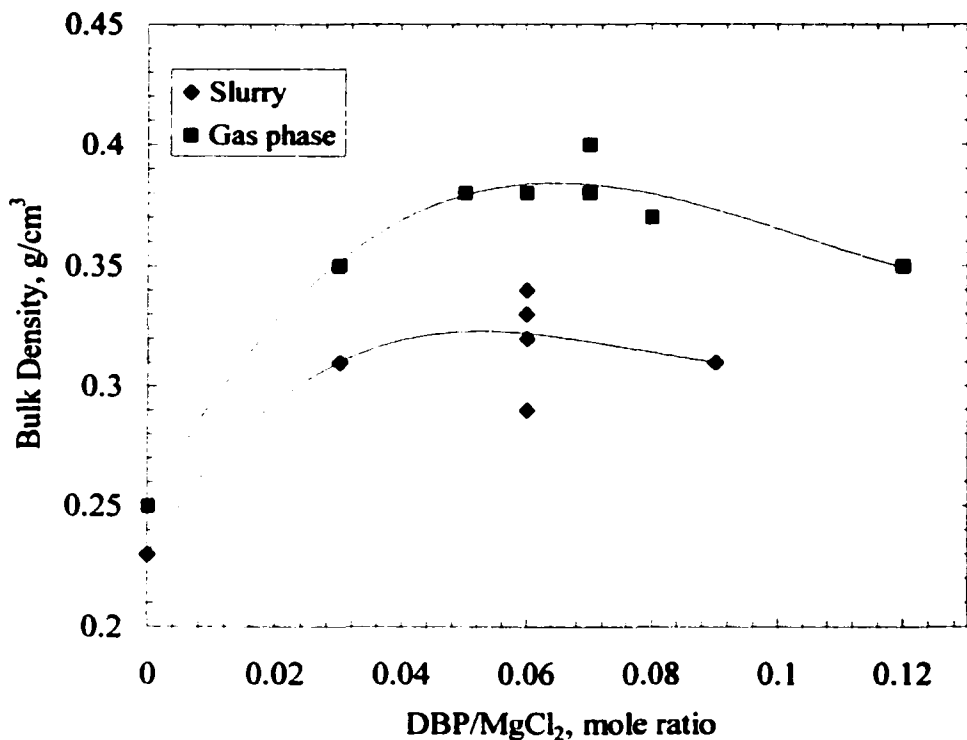


Figure 4.11 Relationship between DBP/MgCl₂ and bulk density.

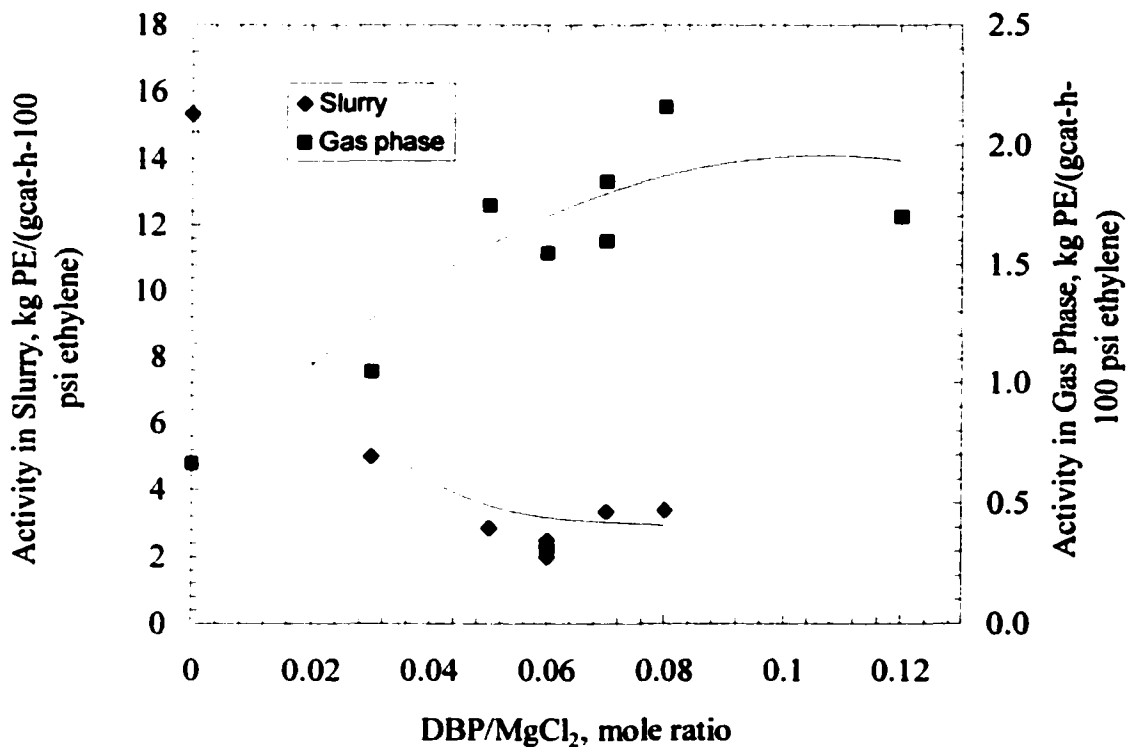


Figure 4.12 Dependence of average homopolymerization rate on DBP/MgCl₂.

The possible reasons for DBP influence on morphology are (1) DBP stabilizes the MgCl_2 crystallites by coordination, forms a stronger matrix on which the living polymer grows up; and/or (2) by inhibiting the formation of some sites, the DBP makes the polymerization happen evenly everywhere inside the catalyst, and thus prevents the non-uniform stress breaking up the particle into irregular shapes.

Contradictory findings on the electron donor influence on propylene polymerization are reported in the literature; some researchers (Hu and Chien, 1988; Kang et al., 1990) suggested that electron donor increase catalytic activity while others (Park and Lee, 1992; Xu et al., 1998) argued that they reduce activity. The effect of DBP on the activity observed in this study, shown in Figure 4.12, was unexpected, i.e. higher DBP concentrations resulted in higher activities for gas-phase polymerization and lower activities for slurry operation. A similar behavior was only found in Skomorokhov's work (Skomorokhov et al. 1996); they reported that ED (electron donor) increased the reactivity of ethylene polymerization for MgCl_2 -supported Ti catalysts.

The above observations imply that DBP has different affects on the types or relative amounts of different catalytic sites present in supported Ziegler-Natta catalysts. It was observed that DBP reacts with TiCl_4 to form a yellow complex; similar to the results reported by others (e.g. Dusseault and Hsu, 1993a). It is generally believed that the TiCl_4 and EB complex is inactive for polymerization if it is not fixed to the MgCl_2 support (Keii et al., 1982; Sergeev et al., 1983; Keszler and Simon, 1982; Dusseault and Hsu, 1993a). The complex becomes active if deposited on MgCl_2 (Kashiwa, 1980; Keszler et al., 1982). In slurry operation, some of the DBP/ TiCl_4 complex may dissolve in the liquid and become inactive, resulting in a decrease in activity. For gas-phase operation, ED may increase the catalyst activity by increasing the propagation rate (Kang et al., 1990; Huang and Rempel, 1995) although it blocks some the atactic centres. However, if ED amount is above some level, the effect of reducing reaction centres can offset the effect of increasing propagation rate and result in decreased activity.

4.2.4 Effects of Dibutyl Phthalate on Copolymerization

The above discussion showed that DBP had significant influence on ethylene homopolymerization; its effect on copolymerization is the main subject in this section. Experimental results are summarized in Table 4.2 and these results show that, unlike homopolymerization, DBP content had little effect on copolymerization activity. It was also found that the catalyst with highest DBP content (Cat-2) produced copolymer with the best spherical morphology. This leads to the conclusion that DBP plays an important role in polyethylene morphology control.

Table 4-2. Summary of Copolymerization Activities for Catalysts with Different DBP Contents.

Catalyst name	DBP/MgCl ₂ Mole ratio	Morphology	Activity ¹ kg PE/(gcat-h)	Activity ² kg PE/(gcat-h)
Cat-7	0	Broken particles	2.3 (GasCo7)	2.7 (GasCo10)
Cat-1	0.03	Broken particles	1.7 (GasCo6)	--
Cat-3	0.05	Broken particles	2.0 (GasCo5)	4.5 (GasCo4)
Cat-4	0.07	Broken particles	1.9 (GasCo3)	3.5 (GasCo9)
Cat-2	0.12	Spheres	--	3.2 (GasCo8)

¹Reaction conditions were $P_{C_2H_4}=200$ psi, $P_{H_2}=50$ psi, $P_{N_2}=14$ psi, $P_{C_6H_{12}}=14\sim 15$ psi, 200 g salt as seedbed, 70°C gas phase, 2 h run. Comonomer added once at the beginning of reaction after hydrogen was introduced, no comonomer was added during the runs.

²Reaction conditions were kept the same as previous conditions except that hydrogen was introduced after 1-hexene.

It is surprising to see the sequence of hydrogen addition has a significant effect on the total polymerization rate. Adding hydrogen after rather than before 1-hexene changed the average polymerization rate by as much as 125% (see Cat-3 results in Table 4.2).

The compositions of copolymers made with Cat-4 were further measured by ¹³C-NMR. Analysis results show that both polymers had similar chemical compositions; 1-hexene content was 3.0 mol% for GasCo3 and 2.8 mol% for GasCo9.

Hydrogen could affect the active site structure, either by changing Ti oxidation state (Chien and Nozaki, 1991; Kissin, 1989a), by forming more active sites (Soares and Hamielec, 1996a) or by other reversible reactions (Keii, 1988). Hydrogen could reduce ethylene reaction rate (Keii, 1988; Kioka and Kashiwa, 1991; Salajka et al., 1993; Huang et al., 1995) but increase α -olefin polymerization rate (Keii, 1988; Kioka and Kashiwa, 1991; Soares and Hamielec, 1996a). The hydrogen/1-hexene addition sequence could also affect the catalyst's site or their distributions. If this was the cause, then the ratio of ethylene/1-hexene rate should also be affected and the product would have different comonomer composition. This was not the case since the 1-hexene contents in the polymers made from different hydrogen/1-hexene addition sequence were very similar.

According to the above discussion, the interaction of hydrogen with the prepolymerized catalyst appears to result in sites which are harder to activate than sites onto which monomers are coordinated. However, the initial presence of the hydrogen does not appear to affect the nature of the catalytic site once it is activated.

Some of the polymers (GasCo8, 9 10) produced when hydrogen was added after the 1-hexene were further analyzed to study DBP effects on 1-hexene incorporation ability. The results were plotted in Figure 4.13. It can be seen that DBP shows negative effects on 1-hexene incorporation in polymer. With the increase of DBP content in catalyst, both the 1-hexene reaction rate and the 1-hexene content in copolymer decrease. (Since different catalysts have different reaction activity, higher comonomer content in polymer does not necessarily mean the higher comonomer reaction rate.) Contrary to the effect on average copolymerization reaction rate, electron donor DBP showed significant influence on 1-hexene incorporation ability.

Many scientists (Soga et al., 1982; Kashiwa and Yoshitake, 1984; Murachev et al., 1989) believed that in Ziegler-Natta catalyst, the Ti^{+2} reaction site only produces polyethylene at lower rate and shows no activity for higher α -olefins while Ti^{+3} centre can react with both ethylene and other α -olefins. As a result, the 1-hexene incorporation ability is

determined by Ti^{+3} centres. Furthermore, Ti^{+3} ions exist in two states: isospecific states and nonspecific states (Chien and Hu, 1989); both of them have the ability to react with 1-hexene. As was reviewed in Chapter 2, internal donors such as DBP and EB can poison the non-stereospecific sites selectively (Galli et al., 1984; Chien and Bres, 1986; Park and Lee, 1992; Dusseault and Hsu, 1993a). As the amount DBP increases, more nonspecific sites are blocked and the total 1-hexene reactive sites decreases, which results in the lower 1-hexene reaction rate as shown in Figure 4.13. However, Ti^{+3} sites are only a small fraction of the total sites; 80% are Ti^{+2} after contact with TEA according to Kashiwa and Yoshitake (1984). Hence, the ethylene rates should not be affected as much by the ED content as the 1-hexene rates.

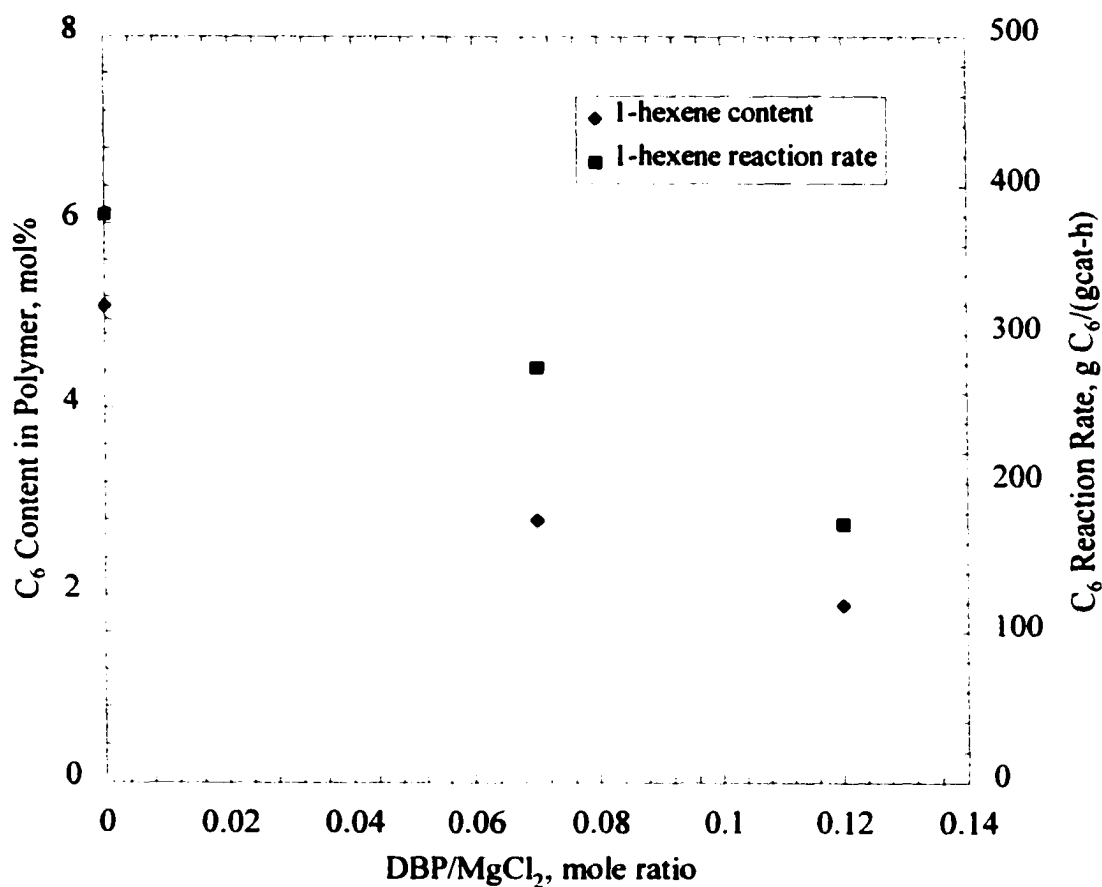


Figure 4.13 Effects of DBP content on 1-hexene incorporation ability.

CHAPTER 5. PREPOLYMER STUDIES

Prepolymerization is used to control polymerization with very active catalysts to produce nascent polymer with good morphology and to avoid overheating during the initial stages of polymerization. Heat transfer resistances are a main concern for high activity catalysts and prepolymerization done at mild conditions reduces the severity of heat transfer effects. It has been found that prepolymerization can increase catalyst activity (Yano et al., 1986; Xu et al., 1990; Wu et al., 1996; Czaja and Krol, 1998); this rate enhancement is mainly due to more active sites becoming exposed to monomer which is associated with more even fragmentation under mild conditions. Prepolymerization has no effects on the nature of active sites (Yano et al., 1986; Soares and Hamielec, 1996a; Czaja and Krol, 1998) and has no impact on the basic properties of the polymer product, such as molar mass and its distribution, crystallinity, melting point, and isotacticity (Czaja and Krol, 1998). Thus, in this study, we employed prepolymerization to produce the catalyst (i.e. the prepolymer) to study kinetics of copolymerization in the gas phase. The use of the prepolymer as catalyst avoids the influence of transfer problem and results in product with good morphology.

There is a lack of experimental observation regarding the early stages of particle growth. SEM and x-ray microanalysis method were used to probe the initial stages of polymerization under mild reaction conditions. The results are reported in Section 5.1. In Section 5.2, the effects of prepolymer particle size on reaction rate and product characteristics are presented.

5.1 Polymer Growth on the Catalysts

Polymer growth under mild reaction conditions was observed by SEM and EDAX on a series of samples with different yields (from 1 g PE/gcat to 16 g PE/gcat). Slow reaction rates make it easy to control prepolymer yields at low value. A typical prepolymerization profile and reaction conditions are shown in Figure 5.1. Temperature was kept around 30°C, ethylene pressure was 8 psi, and hydrogen pressure was 11 psi. The reaction rate increased continuously during the 3-hour run.

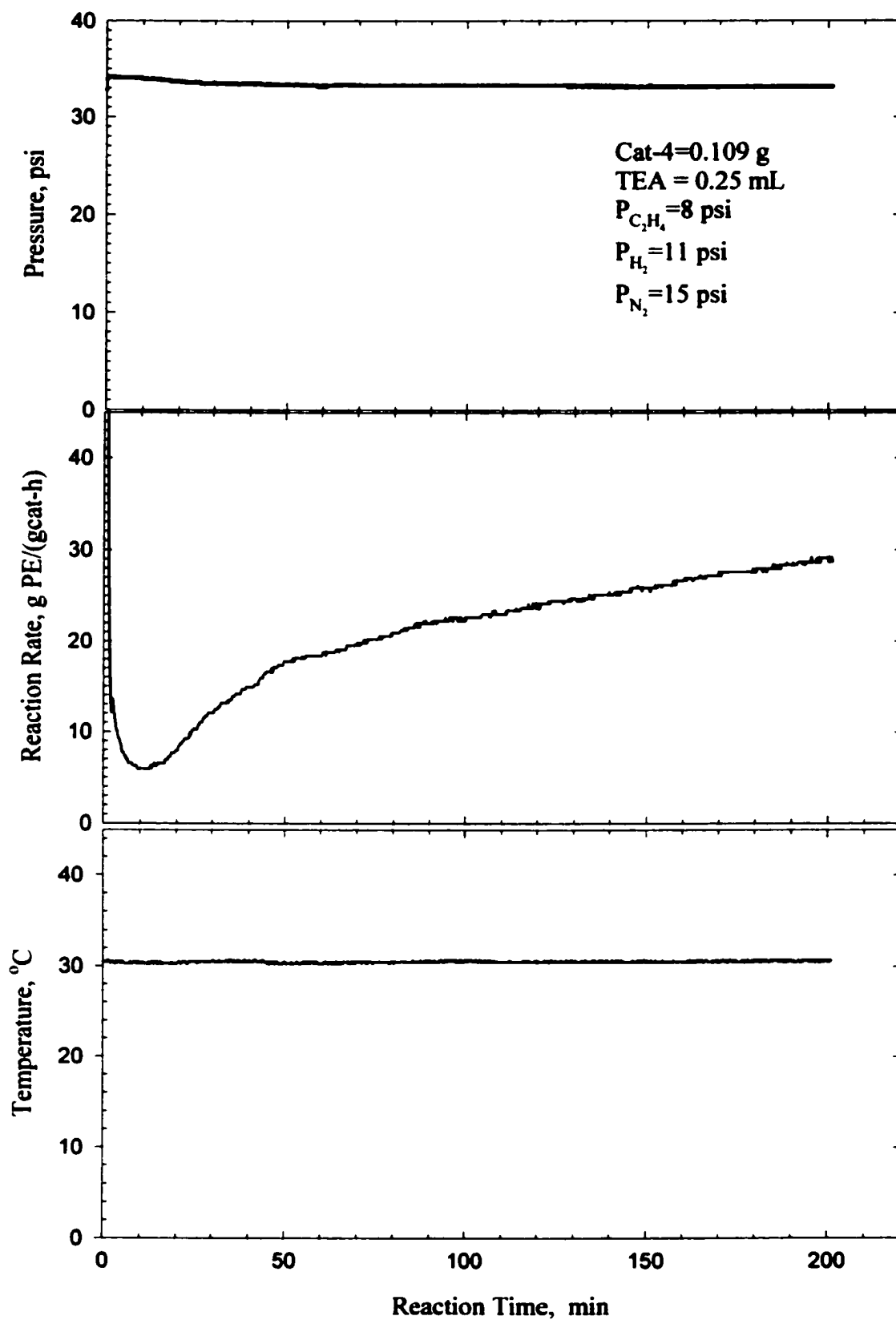
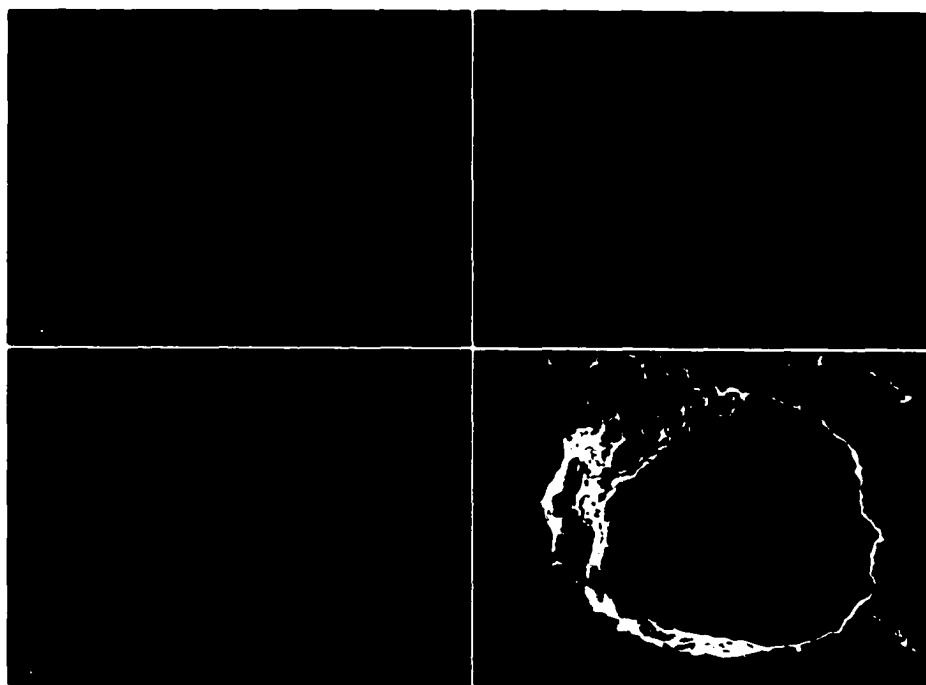


Figure 5.1 Typical reaction profile of prepolymerization run.

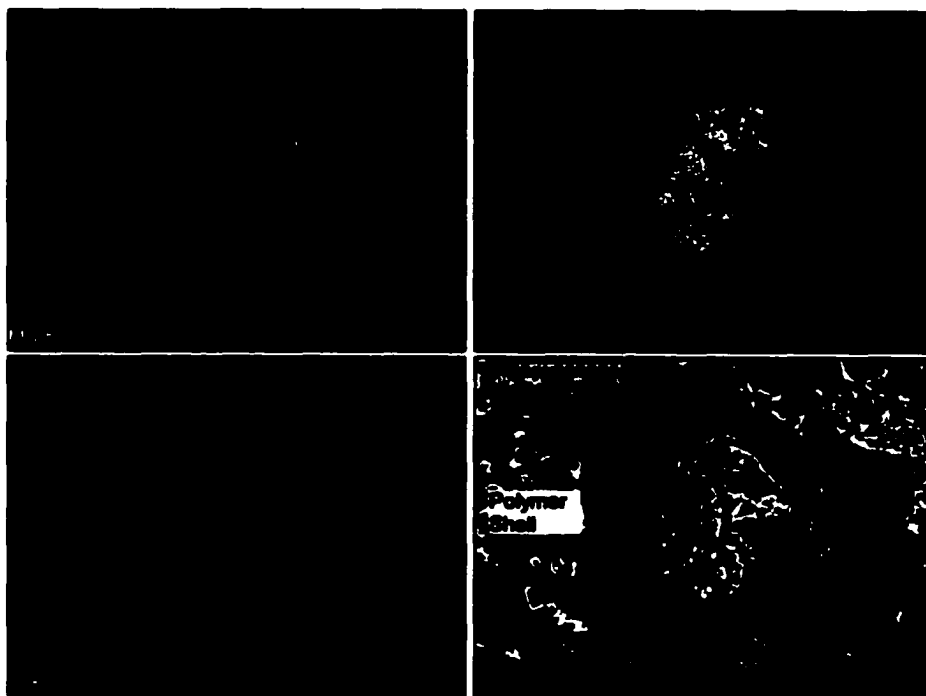
In another run, with similar reaction conditions as shown in Figure 5.1, prepolymer was withdrawn from the reactor at different reaction time (from 3 min to 65 min), dried by nitrogen flow and stored in the glove box. The yields of prepolymers were estimated from the rate profile shown in Figure 5.1. The prepolymer samples with different yields were then imbedded in epoxy and microtomed before SEM analyses.

Figure 5.2 (a) to (e) are the cross section images and x-ray dot mappings of active elements Cl, Mg and Ti for catalyst and prepolymer particles with different polymerization degrees. For catalyst Cat-4 (Figure 5.2 (a)), the distribution of active element Ti is uniform throughout the whole particle. Figure 5.2 (b) is the prepolymer (Pre-1) image after 3 min reaction (1 g PE/gcat). Two different textures can be clearly distinguished in the growing particle (Pre-1). At the outer layer, a 10-30 μm thick polymer shell is forming. X-ray mapping pictures illustrate that the signals of catalyst elements Ti, Mg and Cl are strong at the centre area and fade out at the edge of particle. It can also be seen that long fissures appeared around the centre of the particle and the catalyst begins to break up. This result suggests that catalyst particles do not fracture immediately after polymerization begins, at least not under mild reaction conditions. Furthermore, it can be concluded from this observation that significant external film mass transfer resistance may be present at this stage of polymerization in the slurry. This observation directly confirms Floyd's simulation (Floyd et al., 1986b) and is different from Hutchinson's assumption (Hutchinson et al., 1992) that no mass transfer limitations existed during the prepolymerization stage.

Figure 5.2 (c) is the polymer (Pre-2) image after 30 min polymerization (4.6 g PE/gcat). The growing particle continued to break up. Large pores are found at the centre of the particle. The appearance of this hollow feature is the consequence of uneven particle growth. Faster accumulation of polymer at the surface of the particle strains the surrounding structure and results in fragmentation to relieve this stress created by uneven growth.

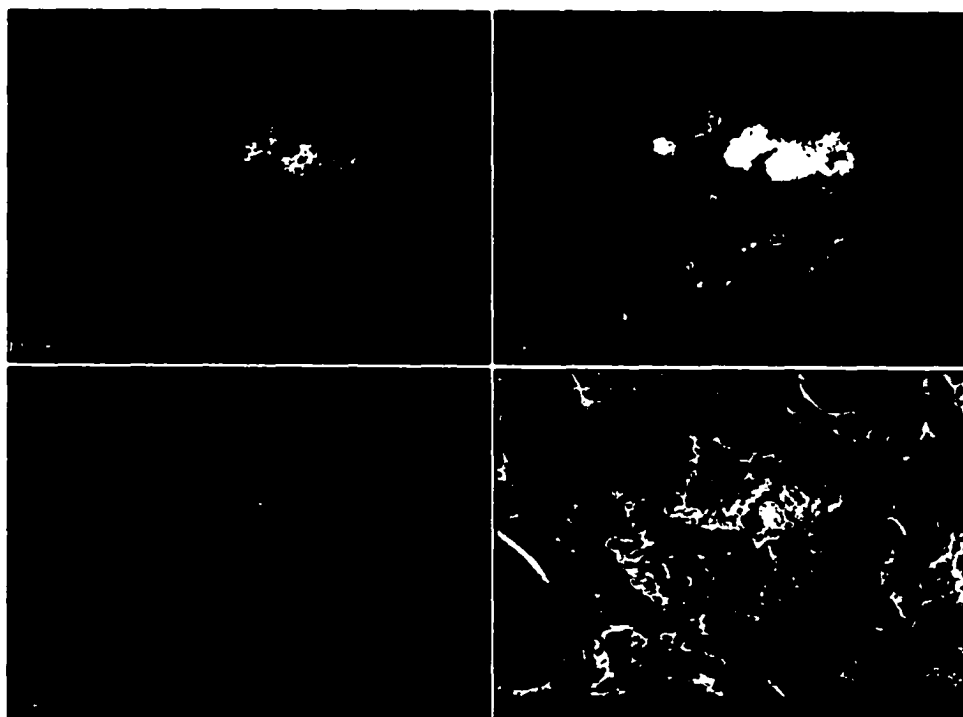


(a) Catalyst

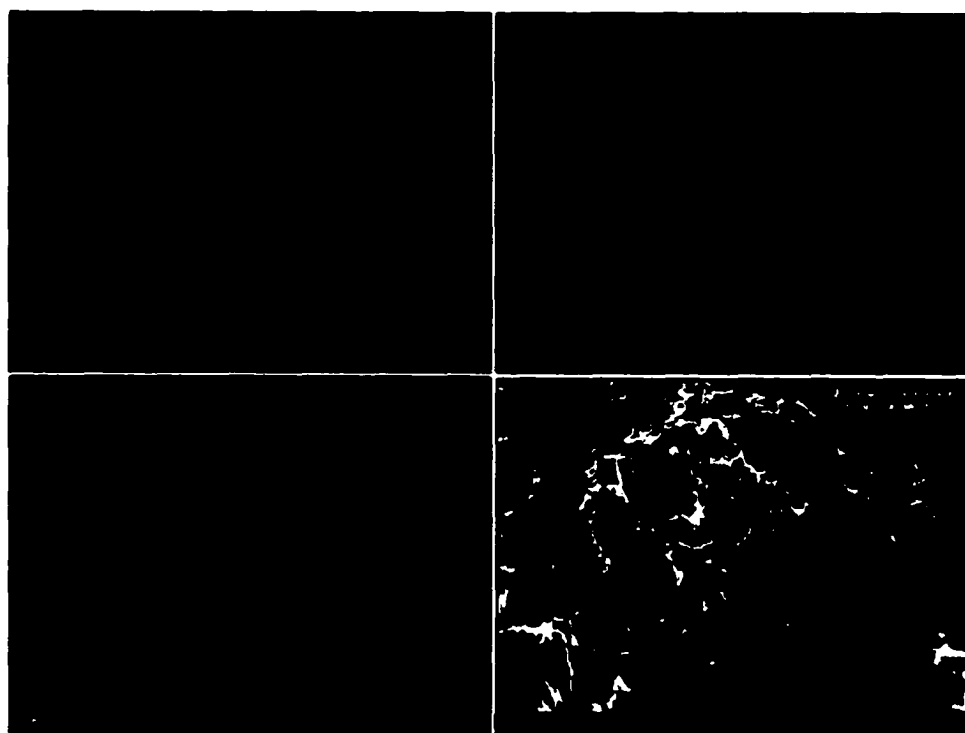


(b) 3 min prepolymerization, yield=1 g PE/gcat.

Figure 5.2 Particle growth observation. Color pictures are x-ray dot mappings of elements Mg (blue), Cl (red) and Ti (yellow). Black/white pictures are SEM micrographs of catalyst and prepolymers.

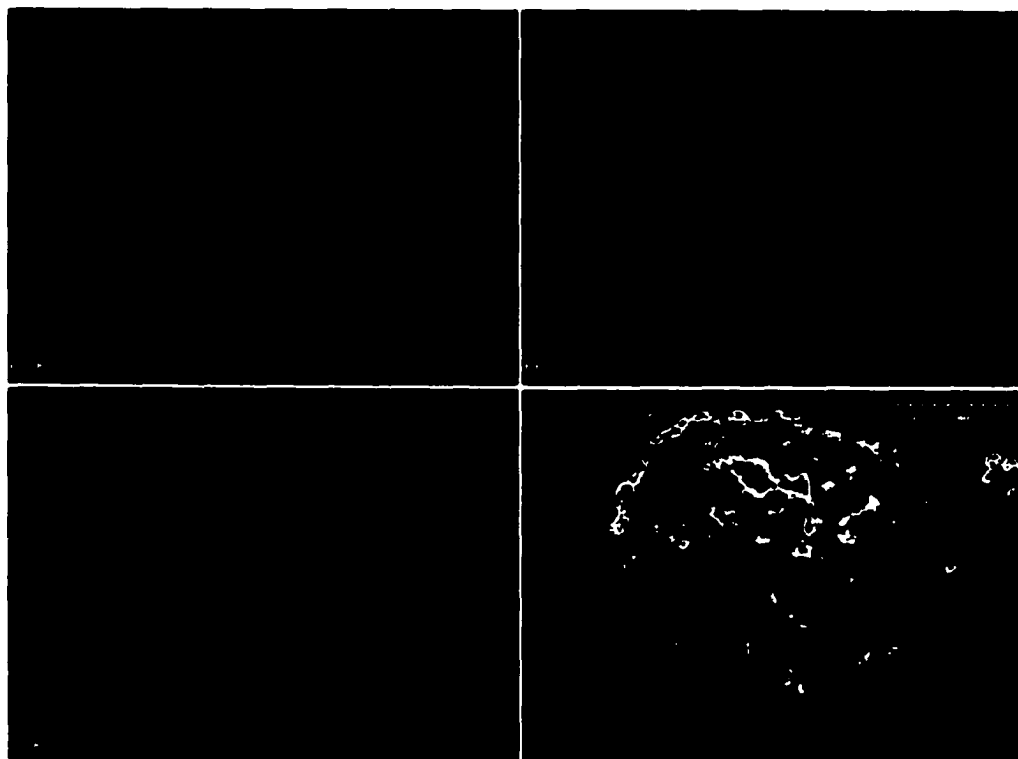


(c) 30 min prepolymerization, yield=4.65 g PE/gcat.



(d) 45 min prepolymerization, yield =9.3 g PE/gcat.

Figure 5.2 Particle growth observation (continued).



(e) 65 min prepolymerization, yield=16 g PE/gcat.

Figure 5.2 Particle growing observation (continued).

Since large pores appear at this stage, monomer can access the inner part of the particle without difficulty and polymer begins to form at the centre. The bright part shown in the x-ray mapping picture in Figure 5.2 (c) is the catalyst-rich part that has not completely broken up. Although the macro shape of catalyst particle is still spherical, internal structure changed a lot, at least at this stage of polymerization.

As polymerization continues (Figure 5.2 (d), 45 min polymerization, and (e), 65 min polymerization), the signal intensities of catalyst elements become weaker and weaker and it is not easy to distinguish Ti signals from the background noise. This is because the catalyst fragments are surrounded by more produced polymer. At this stage, polymer grows faster inside and fills up the voids because of the higher concentration of catalyst fragments in the particle centre. Finally, catalyst fragments are evenly dispersed throughout the whole polymer matrix.

To further determine spatial variation in composition of the prepolymer particles, x-ray quantitative analysis was carried out on the cross section of particles. The examination results are reported in Table 5.1. As an example of Pre-1 (3 min polymerization), the amount of Cl, Mg and Ti at the centre of particle are 32 wt%, 7.0 wt%, and 1.6 wt% respectively, but the composition values are much lower at the edge of the particle, they were 6.5 wt%, 1.4 wt%, and 0.4 wt%. It should be noted that the values from x-ray microanalysis are not very accurate. The thickness of carbon coat on the surface of specimen, the flatness and selection of specific observation area, and the disturbance of background noise all affect the accuracy of measurement. However, the results in Table 5.1 show the general trends of element distribution with respect to position, reaction time or yield.

Table 5.1 X-ray Quantitative Analyses of Catalyst and Prepolymers with Different Yield.

	Time yield		Concentration at the			Concentration at			Overall		
	min	g PE/gcat	particle centre wt%			the edge wt%			Concentration wt%		
			Cl	Mg	Ti	Cl	Mg	Ti	Cl	Mg	Ti
Cat-4	0	0	43	15	3.1	44	17	2.8	43	16	2.9
Pre-1	3	1.0	32	7.0	1.6	6.5	1.4	0.4	21	5.2	1.0
Pre-2	30	4.6	10	2.1	0.8	1.7	0.4	0.1	3.7	0.8	0.2
Pre-3	45	9.3	3.3	0.7	0.2	1.0	0.2	-0.04	2.6	0.6	0.1
Pre-4	65	16	1.7	0.5	0.1	0.5	0.2	-0.04	1.0	0.3	0.1

The differences in Cl, Mg and Ti contents between inner and outer part of the growing particle on the reaction yields is further plotted in Figure 5.3 using the values from Table 5.1. For the catalyst (Cat-4), the elements are almost evenly distributed through whole particle (mole ratios of Cl, Mg and Ti concentrations at the centre to their concentrations at the exterior of the particle are almost equal to one). At the onset of reaction, ethylene polymerizes immediately, the reaction rate is much faster at the surface of particle than at the centre. The differences in the concentrations of catalyst's elements between outer layer and centre increase and reach the maximum at polymer yield of 4.6 g PE/gcat. As reaction continues, the uneven expansion of the particle results in an open structure in the

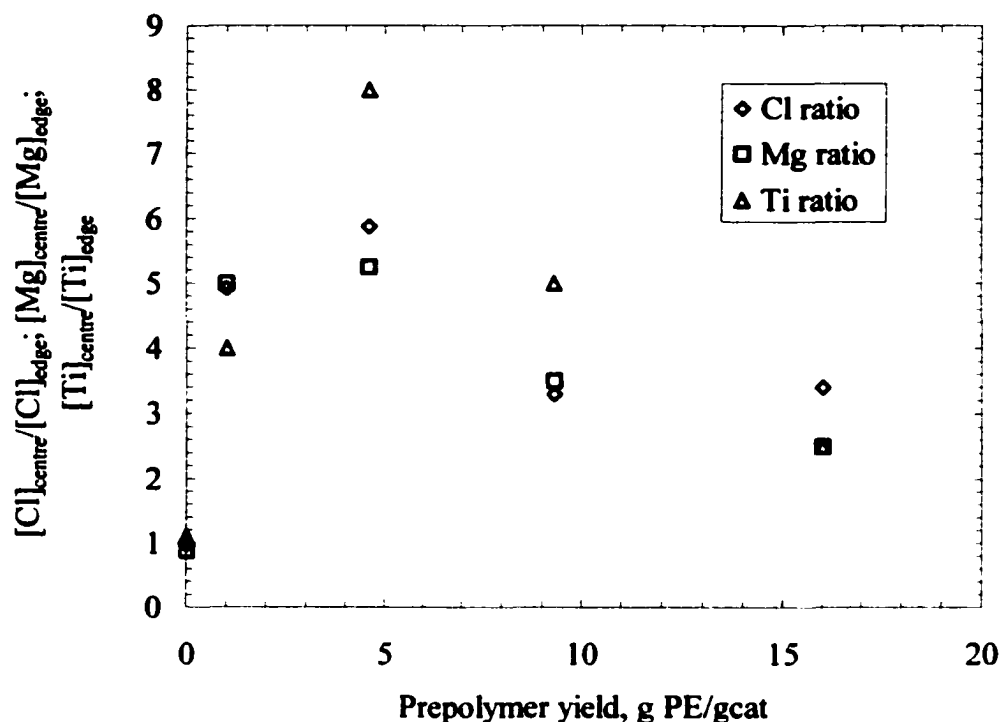


Figure 5.3 Concentration differences of Cl, Mg and Ti between outer layer and inner part.

growing particle and monomer transfer rates increases. At this stage polymer grows faster inside the particle than at the surface because of higher concentration of catalyst fragment in the centre area. As polymer continues forming and particle grows more uniformly, the average catalyst concentration decreases and the difference of the catalyst concentration between outside and inner area becomes less significant. After 65 min of reaction, the concentration ratios of all species between particle centre and edge further reduced.

Noristi et al (1994) observed the polypropylene growth over spherical MgCl_2 -supported TiCl_4 catalyst under mild reaction conditions (60°C , $P_{\text{C}_3}=0.2$ MPa, 2-h slurry) by SEM, TEM and EDAX microanalysis. They found that the polymer grew uniformly throughout the catalyst particle from the onset of polymerization. The catalyst broke up very early into fragments and these fragments were uniformly distributed in the polymer particle throughout the whole growth process. No mass and heat transfer occurred under this mild condition. These conclusions are different from our findings: catalyst particles did not evenly grow at the beginning of reaction in our study. Faster growth in the outer shell results in the open structure of the particle. With the increase of void fraction, the transfer

coefficient increases, polymer grows faster at the inside of the particle and the voids are gradually filled with polymer.

According to the above discussion, a general particle growth model is presented below:

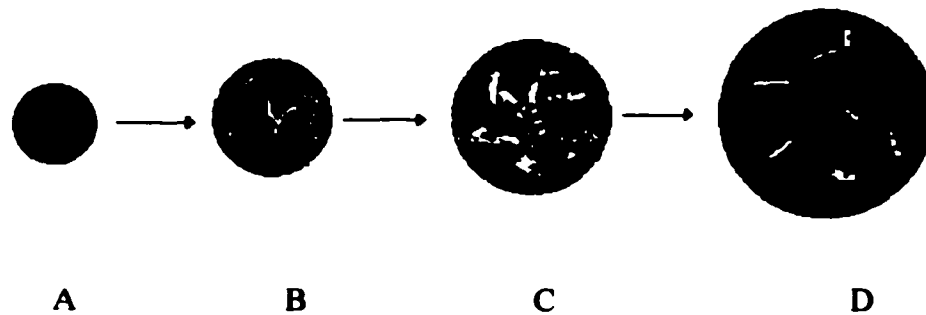


Figure 5.4 Particle growth model under mild reaction conditions.

In Figure 5.4, the dark areas represent catalyst fragments; grey areas are polymer-rich regions; light grey areas are for catalyst-polymer transitional regions; and white areas are voids. The model reflects the main stages during particle growth: Particle A is the aggregate of basic catalyst particles. At the beginning of reaction, polymer first forms at the surface of Particle B while the centre part is a catalyst-rich region with the appearance of cracks due to non-uniform expansion across the particle. As polymerization continues, the cracks in the central area increase in number and become larger. This open structure facilitates monomer transfer, i.e. polymer grows faster inside the particle and fills the voids. As the yield increases, catalyst fragments are gradually diluted and finally disperse more uniformly throughout the whole polymer (Particle D).

The current experiments and model suggest that uneven growth in the particle during prepolymerization does not necessarily lead to poor morphology; this conclusion is different from previous researchers' conclusions (Hutchinson and Ray, 1991; Hutchinson et al., 1992; Ferrero et al., 1992; Mkrtychyan et al., 1986). In the present interpretation, controlling initial polymerization rate is the key for obtaining good morphology. According to Wu (1999), mass transfer limitation of monomer causes a polymer crust to form at the surface of catalyst (e.g. outer layer of Particle B). This crust would prevent the catalyst from breaking apart totally and thus the crust keeps the spherical morphology

of the catalyst. If the initial reaction rate is too fast, rapid expansion will rupture the crust, and catalyst fragmentation will result in a relatively loose agglomeration which subsequently disintegrates into fines and irregular shaped particles.

5.2 Prepolymer Size Effects

Results on the effects of prepolymer particle size are presented in this section. Catalyst Cat-5 was first prepolymerized under mild conditions as described in the previous section. The prepolymer (Pre13, see Appendix D) was then separated into different sizes by sieving. This process was done in the glove box. In the next step, a series of slurry polymerization runs were carried out, using prepolymers with different size as catalysts, under similar reaction conditions: $P_{C_2H_4} = 140$ psi, $P_{H_2} = 40$ psi, $P_{N_2} = 20$ psi, $T = 70^\circ\text{C}$, run length = 2.5 h. After reaction, the nascent polymer was screened to obtain the mass fraction (w_i) as a function of size. The average size of polymer particles was then calculated as the weight average size:

$$\bar{d} = \sum w_i d_i \quad (5.1)$$

The polymerization profiles with prepolymers of different size are compared in Figure 5.5. From Figure 5.5, it can be seen that all the reaction rate profiles are similar at the beginning: reaction rates start at the lowest points, then increase. For large prepolymer size (particle size >0.25 mm), reaction rate increases continuously during 2.5 h reaction period. For prepolymer with sizes between 0.21-0.25 mm, the rate essentially becomes constant at its maximum value. For small particles (<0.21 mm), the polymerization rate decays after reaching a maximum.

At first glance, these differences in rate profiles may be attributed to mass transfer effects (Floyd et al., 1986a, 1986b, 1987; Hutchinson et al., 1992; McKenna et al., 1996), i.e. as mass transfer problem becomes more severe, the rate profile changes from decay type to acceleration type. For large particle size, increased catalyst volume results in a large increase in monomer consumption rate relative to the rate of diffusion, creating concentration gradients. As polymer grows, pore volume increases and monomer can

diffuse into the particle faster, resulting in an increasing type profile. However, this mass transfer limitation will lead to a lower production rate: the acceleration or hybrid type of reaction will never be reached the maximum rate and their activities should be lower than the decay type (less mass transfer controlled). However, this is not the case in this study (see Figure 5.5). The smallest particles (0.16~0.21mm), which are supposed to be less affected by transfer resistance, have the slowest reaction rate and show decay type of rate profile (line 5 in Figure 5.5). Thus, the differences between rate shapes are not only due to mass transfer resistances. This conclusion is confirmed by product characterization and will be discussed later in this section. The decay in activity for the smallest prepolymer particle is probably due to deactivation by impurities since the larger surface to volume ratio of the smaller particles makes themselves more vulnerable to poisoning.

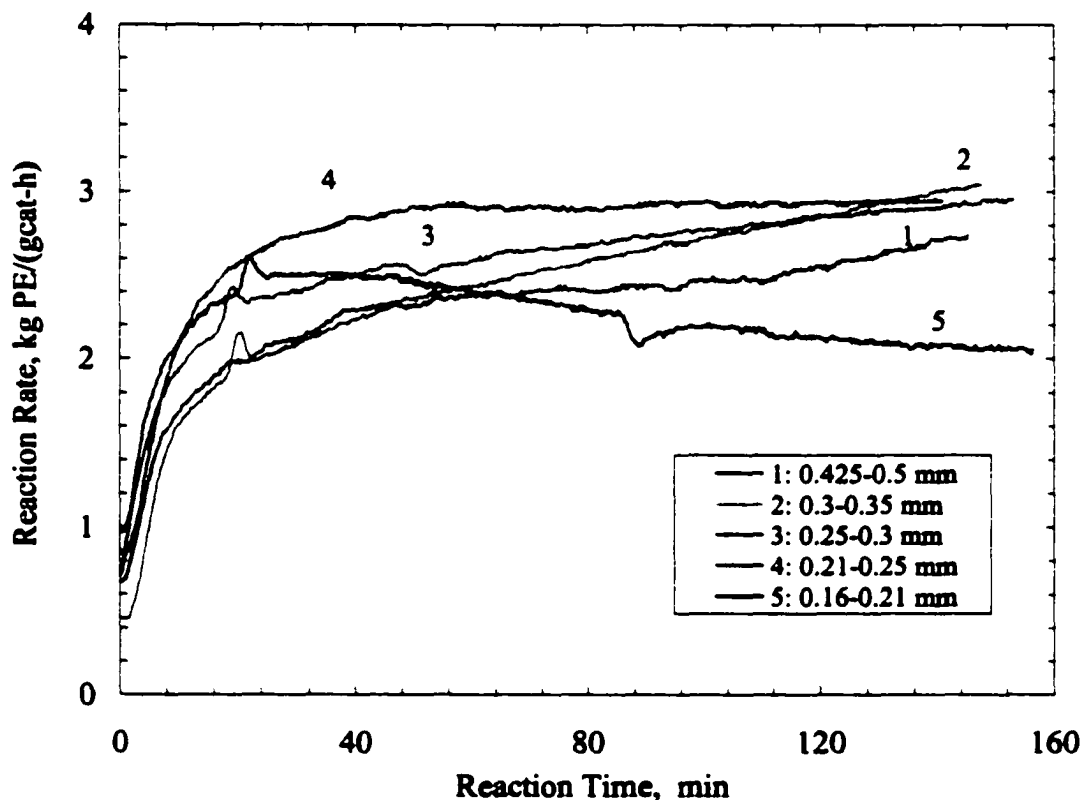


Figure 5.5 Polymerization profiles of prepolymers with different particle size under same reaction conditions.

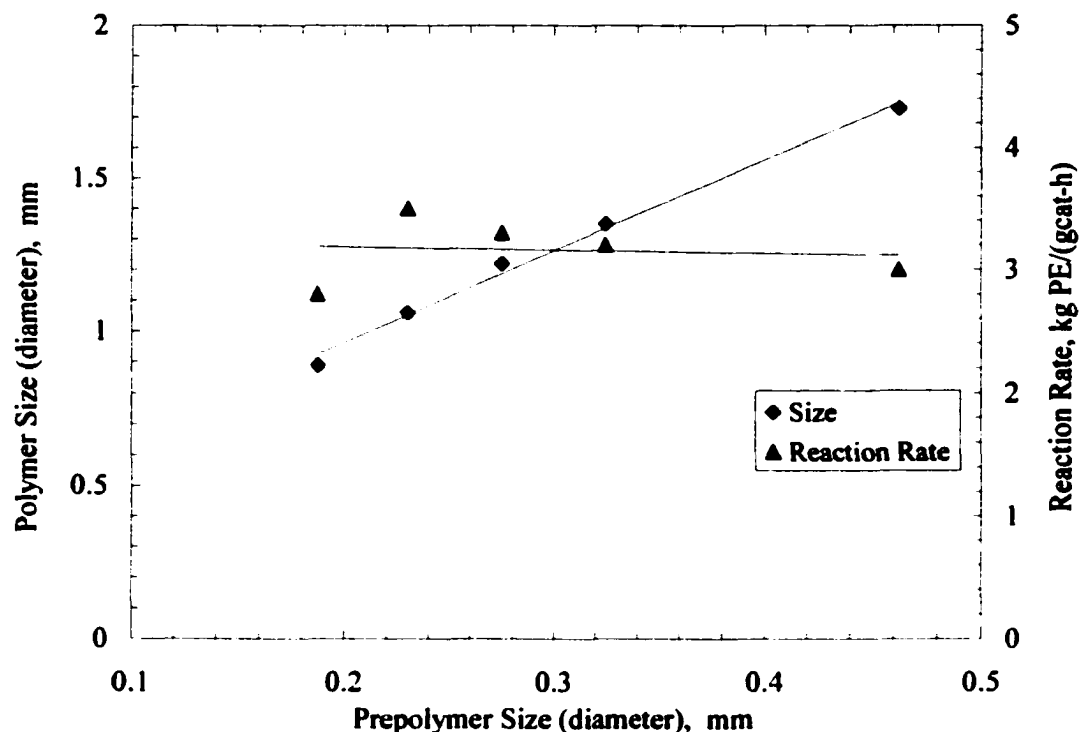


Figure 5.6 Polymer particle size and average polymerization rate as functions of prepolymer particle size.

The effects of prepolymer size on polymer product size and polymerization activity are plotted in Figure 5.6. Average polymer size is a linear function of prepolymer size, i.e. the specific activity is independent of prepolymer size. These results imply that the concentration of active sites is not a function of catalyst particle size.

Figure 5.7 and Figure 5.8 illustrate the relationship between particle size and molar mass and polydispersity. Prepolymer molar mass varies significantly with prepolymer size (see Figure 5.7). For prepolymer smaller than 0.3 mm, M_w decreases as size increases. This is a typical mass transfer control case. Monomer has difficulty in transporting from solvent into the inside of the catalyst fragments while hydrogen is generally regarded unaffected by transfer limitations. The chain length for molecules at the centre of particle will be shorter than that at the surface of particle.

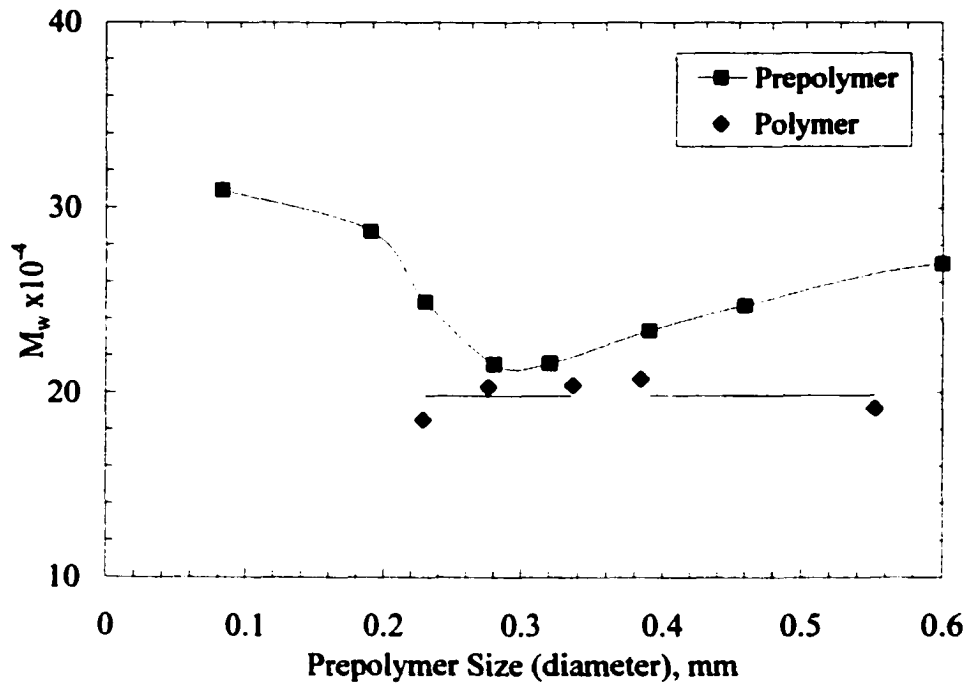


Figure 5.7 Dependence of M_w on prepolymer size.

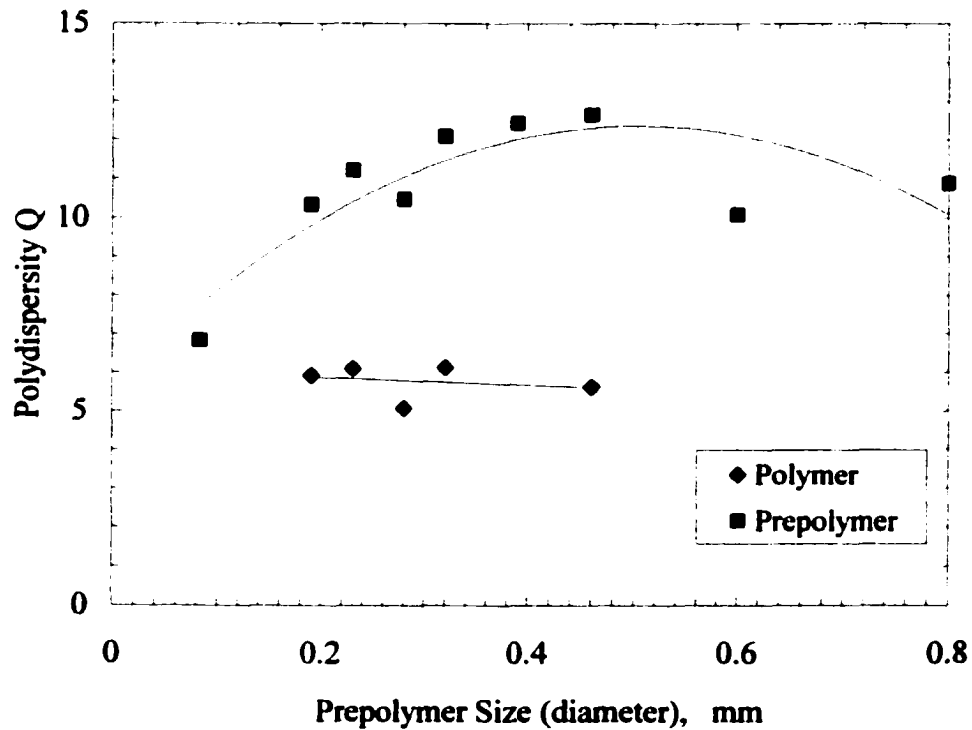


Figure 5.8 Dependence of polydispersity Q on prepolymer size.

Equation 5.1 gives the expression of average chain length

$$X_n = \frac{k_p[M]}{k_M[M] + k_S + k_A[A] + k_H[H]} \quad (5.1)$$

where X_n is the number average chain length; k_p is the propagation rate constant; k_M is the rate constant for chain transfer to monomer, k_S is the rate constant for spontaneous intramolecular transfer; k_A is the rate constant for chain transfer to cocatalyst; and k_H is the rate constant for chain transfer to hydrogen. Among these chain transfer reactions, transfer to hydrogen is dominant. According to Equation 5.1, if monomer concentration $[M]$ decreases due to mass transfer difficulties but hydrogen concentration $[H]$ does not change, the polymer molar mass decreases. This conclusion is in agreement with other researchers' suggestions that mass transfer limitations would reduce molar masses (Floyd et al., 1987; Hutchinson et al., 1992; Wu, 1999).

For prepolymer particle size larger than 0.3 mm, M_w , unexpectedly increases with increasing particle size. Previous experiments (Wu, 1999) also showed similar results. This phenomenon is contrary to the explanation for mass transfer limitation. The possible explanation is that the inside structure of large particles is different from those of small ones: large particles may have higher void fraction or macro cracks, which result in reduced mass transfer limitations.

Although the molar mass of prepolymers varied with prepolymer particle size, the molar mass of the corresponding polymer was not affected by prepolymer size (see Figure 5.7). Prepolymers with different sizes and molar masses produce polymers with similar M_w . This result suggests that transfer effects are not significant during polymerization.

The effects of prepolymer size on polydispersity Q were also studied and the results are shown in Figure 5.8. For prepolymers, Q changes significantly as prepolymer particle size increases. Mass transfer limitation alone do not provide a reasonable explanation.

Polymer polydispersity is not affected by prepolymer size, which also suggests the lack of monomer transfer resistance during polymerization.

CHAPTER 6. KINETICS OF ETHYLENE/1-HEXENE COPOLYMERIZATION

The study of olefin copolymerization kinetics is an especially challenging problem. The difficulties stem from the combination of two factors (Kissin, 1995): first, an intrinsic difficulty of studying copolymerization kinetics; second, difficulties related to the fact that different active centres in heterogeneous catalysts have different stabilities, possess different copolymerization abilities and produce macromolecules with different sizes. Most previous laboratory copolymerization studies were conducted in the slurry phase; very few studies were found for gas-phase copolymerization (see Chapter 2). In the current study, ethylene/1-hexene copolymerization rates in the gas phase over prepolymerized Ziegler-Natta catalysts were observed to change with time under conditions of constant temperature and constant pressure. The rate profile usually exhibits a maximum close the beginning of polymerization reactions followed by rate decay to a relatively steady-state level of activity. The reproducibility of gas-phase operations presents problems (Bu et al., 1995; Wu, 1999). Hence, the reproducibility will be first examined in Section 6.1 to establish confidence in the subsequent discussions on polymerization kinetics. The effects of Al/Ti ratio are discussed in Section 6.2; monomer/comonomer concentration effects are discussed in Section 6.3; the effects of hydrogen are presented in Section 6.4; Section 6.5 deals with the effects of temperature; in Section 6.6 reaction time effects are examined; and finally, Section 6.7 focuses on the comparison of homopolymerization and copolymerization in slurry and gas phases.

6.1 Reproducibility of Copolymerization Experiments

The reproducibility of rate profiles is one of the most problematic areas of Ziegler-Natta olefin polymerization because Ziegler-Natta catalysts are very sensitive to impurities and operational procedures, e.g., the time a catalyst spending in the reactor before monomer is charged can lead to observable differences in kinetic behavior. Detailed discussions of irreproducibility have already been given by previous investigations (Bu et al., 1995; McKenna et al., 1996; Han-Adebekun et al., 1997a; Wu, 1999) and will not be repeated here. In this study, single batches of prepolymerized catalysts were used for studying the

effects of various parameters on gas-phase copolymerization profiles. This reduces irreproducibility associated with catalyst preparation and prepolymerized catalyst preparation.

Comparison of the rate behavior of two runs, which were commonly done for each 1-hexene concentration to determine the effect of concentration of monomers on rate, gave an indication of the reproducibility. In the first run of the pair, 1-hexene was only added at the beginning of the run and in the second run 1-hexene was added intermittently throughout the run to maintain a constant gas-phase concentration of 1-hexene. These pairs of runs, which were carried out within a day or two of each other, are a measure of the reproducibility of the procedures and the resulting rates. Results for such a pair of runs (GasCo14 and GasCo15) are summarized in Table 6.1. The difference between the resulting average rates is within 7%; this is good reproducibility if one keeps in mind the 1-hexene concentrations were not quite the same in both runs. The variations in 1-hexene/ethylene ratios with time for the two runs are shown in Figure 6.1. The rate profiles for these two runs, as measured by the rate of addition of ethylene to the reactor, are also shown in Figure 6.1. The rate profiles are fairly similar with the exception of the fluctuation at low polymerization times. The sharp variations in the rate of ethylene addition at low reaction times are due to the introduction relatively large amounts of 1-hexene into the reactor at these times; such variations in the ethylene addition rate occur in all runs in which 1-hexene was added intermittently; the magnitude of the fluctuations depends on the total reactor pressure and the amount of 1-hexene added. These fluctuations are not changes in polymerization rate but only changes in ethylene addition rate. The polymerization rate is essentially the ethylene addition rate with the removal of the sharp, short-duration decreases in the ethylene addition rate resulting from the 1-hexene addition. In Figure 6.1 and subsequent figures for runs in which 1-hexene was added during the run, the normalized ethylene addition rate, including the fluctuations, will be referred to as the polymerization rate R_p in kg PE/(gcat-h).

The second type of reproducibility test was to repeat a copolymerization run with the same prepolymer as catalyst and similar operating conditions. The two runs should be

done several weeks apart to determine whether storage has a large effect on the activity of the prepolymer. The results for two such runs (GasCo18 and GasCo40) are also summarized in Table 6.1 and the rate profiles, 1-hexene/ethylene ratios and total pressure as a function of time are shown in Figure 6.2. Run GasCo40 was done about 2 month after Run GasCo18. The average activity for GasCo40 was 13% higher than that for GasCo18. These results indicate that storage of the prepolymer does not cause deactivation. Inaccuracy in the amount of injected catalyst could be responsible for the observed differences in specific activity since the instantaneous rates for GasCo40 are 10 to 17% higher for all reaction times greater than 10 minutes (see Figure 6.2). However, experiments with different amounts of prepolymer showed that the injection was very reproducible (see Section 6.2). The most likely cause for the difference in activity between the two runs is the inability to obtain reproducible 1-hexene/ethylene ratio in the early stages of polymerization; the variations in C_6/C_2 ratios at polymerization times <15 min were more pronounced for Runs GasCo18 and GasCo40 than for GasCo14 and GasCo15. The C_6/C_2 ratios for GasCo18 were higher than those for GasCo40 and increases in C_6/C_2 ratios cause decreases in average activity especially at low ethylene pressures (see Section 6.3).

Table 6.1 Summary of Copolymerization Results for Reproducibility Study.¹

Run No.	Amount	Amount	Partial Pressure		Gas Phase	PE	Average
	of Pre18 g	of TEA mL	Ethylene psi	1-Hexene psi	C_6/C_2 Ratio ²	Yield g	Reaction Rate kg PE/(gcat-h)
GasCo14	0.118	0.25	108	6.7	No control	14.9	5.3
GasCo15	0.120	0.25	107	5.9	0.055	14.1	4.9
GasCo18	0.150	0.27	62	3.7	0.058	8.2	2.3
GasCo40	0.152	0.27	60	3.4	0.056	9.7	2.6

¹ Other conditions: $P_{H_2} = 0$ psi, $P_{N_2} = 14$ psi, $T = 70^\circ\text{C}$, Length of Runs = 2 h.

² C_6/C_2 Ratio based on GC analysis.

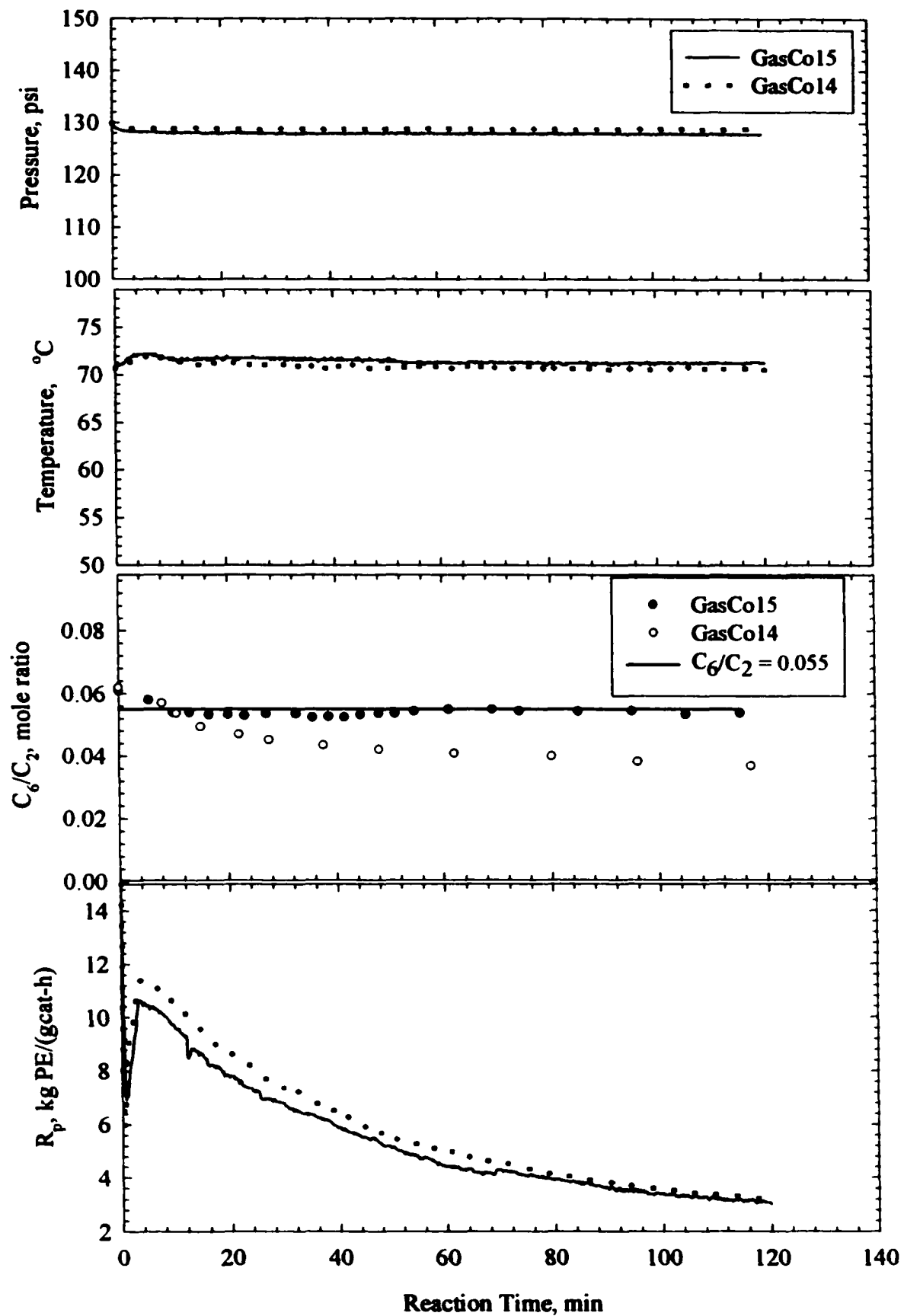


Figure 6.1 Comparison of reaction profiles of two runs with comonomer control (GasCo15) and without control (GasCo14).

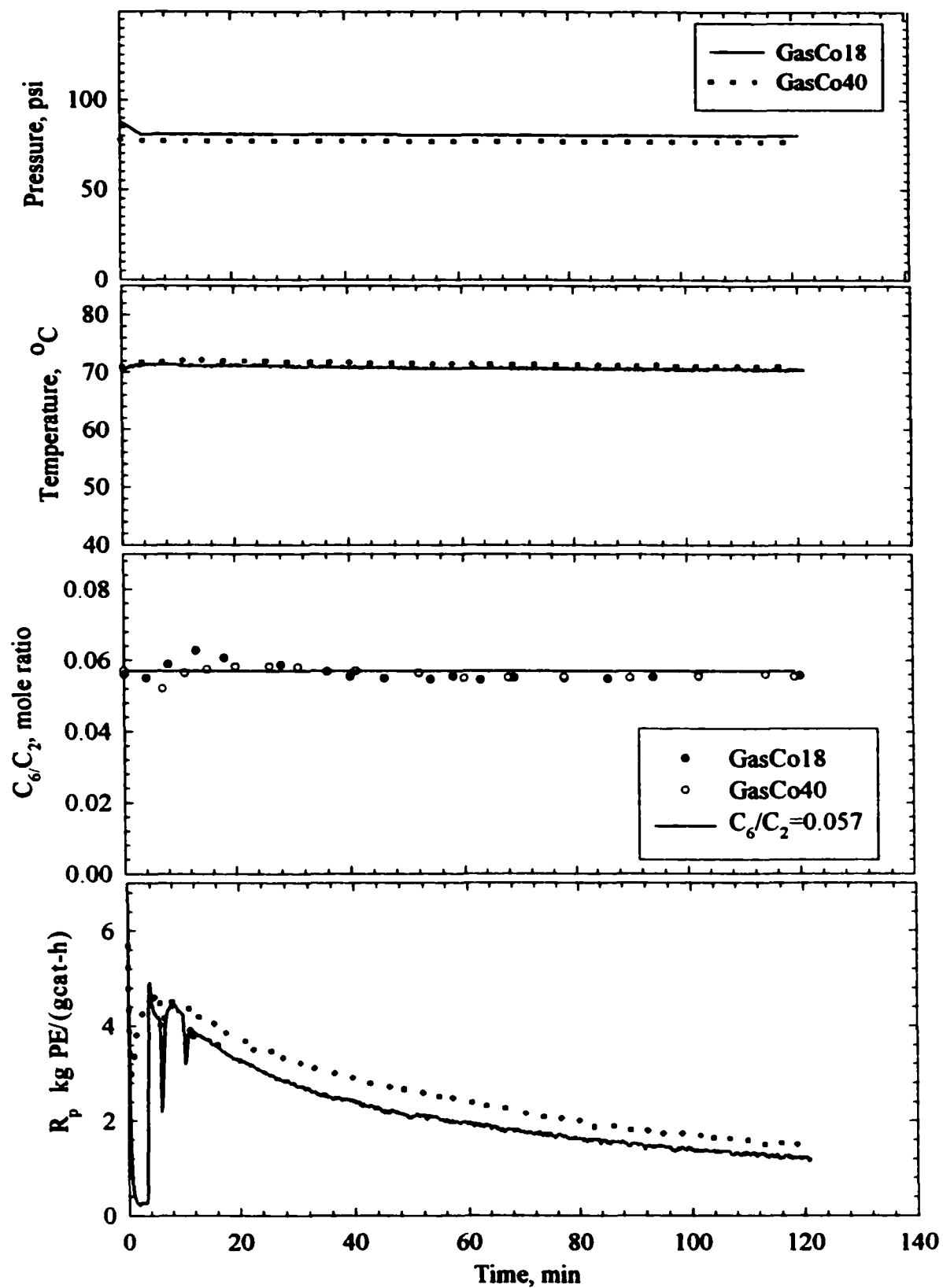


Figure 6.2 Comparison of reaction profiles of two runs (GasCo18 and GasCo40) under similar reaction conditions.

6.2 Effects of Prepolymerized Catalyst Amount

Reaction rates change significantly with changes in ethylene pressure. In order to control reactor temperature, the catalyst amount was adjusted so that the total ethylene consumption rate was usually < 30 g/h; i.e. less catalyst was charged to the reactor at high ethylene pressures. Triethylaluminum (TEA) was used as a scavenger and as a cocatalyst. The influence the Al/Ti ratio was determined by charging different amounts of catalyst to the reactor but the same amounts of TEA with other reaction conditions kept the same. The experimental results were summarized in Table 6.2 and rate profiles are shown in Figure 6.3 and Figure 6.4. For all three runs, 1-hexene was added before ethylene was charged and no 1-hexene was added after the initial addition. It can be seen from the results in Table 6.2 that the average rates for all three runs are very similar (< 5% variation). The ethylene reaction profiles all had similar shapes, but the maximum occurred at different times (see Figure 6.3). The rates of 1-hexene consumption, based on the changes in gas-phase composition with time, were similar for the three runs (Figure 6.4).

Table 6.2 Experimental Results in Studying the Effects of Catalyst Amount on Kinetics.

Run No.	Amount of Pre18 g	Amount of TEA mL	P _{H2} psi	P _{C2} psi	C ₆ mL	Temp °C	PE Yield g	Average Rate kg PE/(gcat-h)
GasCo11	0.081	0.25	0	195	6	70	21.3	11.0
GasCo12	0.039	0.25	0	199	6	70	10.7	11.5
GasCo13	0.130	0.25	0	198	6	70	36.6	11.8

The above results show that the average reaction rates over a 2 h period do not depend on the amount of catalyst or the Al/Ti ratio. However, differences did occur in the initial activation rates. It is not known whether this is attributed to the difference in Al/Ti ratio or other unknown variations in reaction conditions, e.g. variation in injection condition or

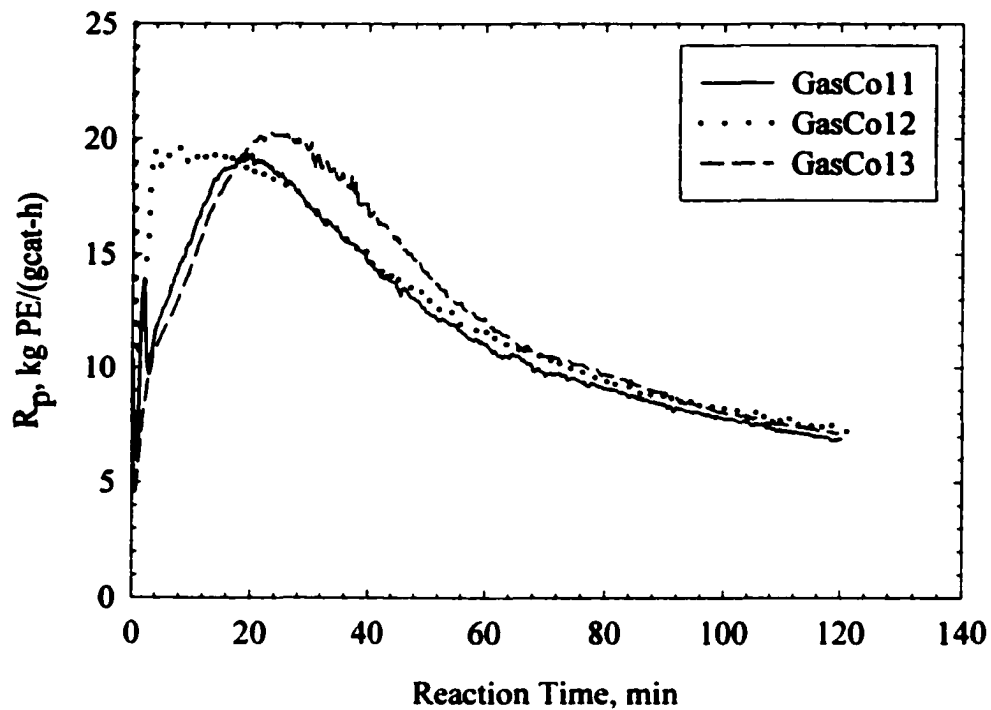


Figure 6.3 Comparison of ethylene reaction profiles for different amounts of catalyst.

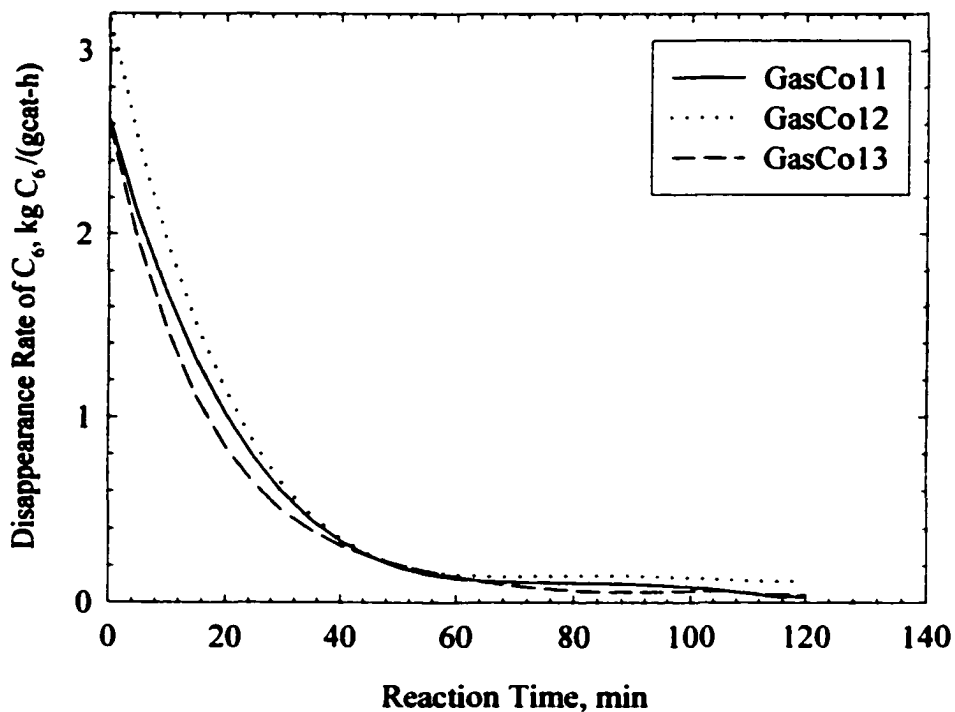


Figure 6.4 Comparison of 1-hexene consumption rates at different Al/Ti ratios based on GC analyses.

local hot spot due to some catalyst agglomeration. It is not possible to reliably measure the Al/Ti ratio during gas-phase experiments because the amount of TEA consumed as a scavenger can vary from run to run.

6.3 Effects of Monomer/Comonomer Concentrations on Kinetics

In this section, kinetic results on the effects of monomer/comonomer ratios are presented. Copolymerization was carried out at 70°C, $P_{N_2}=15$ psi, TEA=0.25-0.27 mL, and without hydrogen. At 70°C, the 1-hexene saturation vapor pressure is 18 psi according to Antoine equation calculation (see Appendix B). In this study, 1-hexene pressures of 3 to 14 psi were used. In order to study gas-phase kinetics at high 1-hexene/ ethylene ratios, low ethylene pressures must be used; ethylene pressures of 60 psi to 250 psi were selected in the current study. The reaction rate was low at low ethylene concentration, sometimes <700 g PE/(gcat-h) at 60 psi ethylene pressure. No hydrogen was added in these runs since hydrogen would have reduced the rate even further. However, in the absence of hydrogen, the molar masses of the polymer were high, leading to difficulties in product characterization, especially by GPC and ^{13}C -NMR.

The conditions for 1-hexene/ethylene copolymerization runs, for which 1-hexene was added intermittent to maintain constant gas-phase concentration of 1-hexene, are listed in Table 6.3. The results are divided into the following categories for analysis and discussion:

1. Constant ethylene pressure with varying 1-hexene pressures.
2. Constant 1-hexene: ethylene ratio in gas phase.
3. Constant 1-hexene pressure with varying ethylene pressures.

6.3.1 Constant Ethylene Pressure

The rate profiles for varying concentrations of 1-hexene at a constant ethylene pressure of 60, 150 and 250 psi are shown in Figures 6.5, 6.6 and 6.7 (the sharp drops in 'rate' are due to the addition of 1-hexene; see Section 6.1). The absolute rates are strong function of ethylene pressure as well as being very sensitive to 1-hexene pressure. The activation-deactivation phenomena have a strong dependence on 1-hexene pressure. It can be seen

Table 6.3 Copolymerization Results at Different Ethylene and 1-Hexene Pressures.¹

Run No.	Amount of Pre18 g	Amount of TEA mL	Partial Pressures		C ₆ /C ₂ Ratio ²	PE Yield g	1-Hexene Consumption ³ g
			Ethylene psi	1-hexene psi			
GasCo18	0.150	0.27	62	3.7	0.058	8.2	0.49
GasCo34	0.159	0.27	60	6.3	0.105	4.5	0.57
GasCo35	0.144	0.27	60	5.1	0.085	4.5	0.42
GasCo36	0.157	0.27	62	9.3	0.151	2.6	0.67
GasCo37	0.157	0.27	62	8.4	0.136	2.4	0.60
GasCo38	0.192	0.27	65	11.5	0.180	3.3	1.13
GasCo39	0.156	0.27	60	7.5	0.125	2.3	0.55
GasCo40	0.152	0.27	60	3.4	0.056	9.7	0.44
GasCo15	0.120	0.25	107	5.9	0.055	14.1	0.60
GasCo53	0.126	0.27	105	14.0	0.134	6.5	1.38
GasCo20	0.085	0.25	151	8.3	0.055	15.0	0.66
GasCo42	0.097	0.25	150	12.5	0.083	14.1	1.58
GasCo44	0.069	0.25	150	6.2	0.042	15.2	0.39
GasCo45	0.070	0.25	150	3.2	0.022	16.4	0.54
GasCo46	0.076	0.25	150	14.0	0.093	8.4	1.22
GasCo24	0.048	0.25	200	11.5	0.057	10.7	0.27
GasCo26	0.053	0.25	250	13.8	0.055	17.4	0.80
GasCo48	0.053	0.24	250	8.1	0.032	20.3	1.01
GasCo50	0.053	0.24	250	14.1	0.057	16.4	0.79
GasCo51	0.049	0.24	250	6.3	0.025	20.2	0.69
GasCo52	0.057	0.24	250	11.7	0.047	19.7	0.84

¹ Other Conditions: P_{N2} = 14 psi; P_{H2} = 0; T = 70°C; Length of Runs = 2 h.

² C₆/C₂ Ratio based on GC analysis.

³ 1-Hexene consumption based on the actual addition amount of 1-hexene during the runs with the deduction of 1-hexene loss in sampling flow and 1-hexene composition increase in gas phase after reactions.

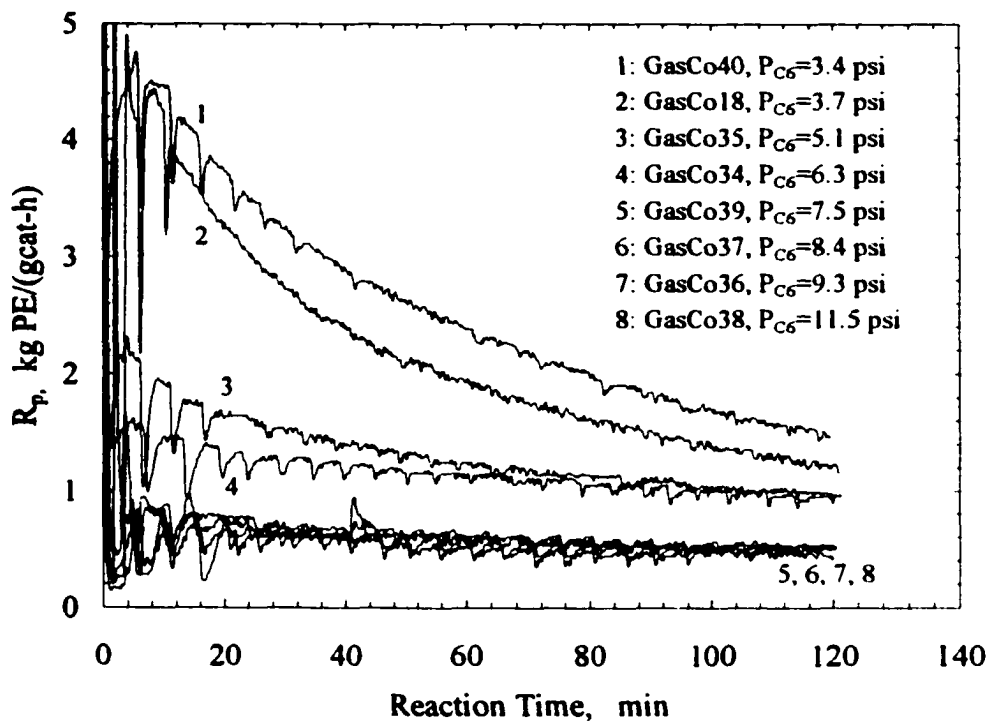


Figure 6.5 Ethylene rate profiles at P_{C_2} =60 psi and different 1-hexene pressures.

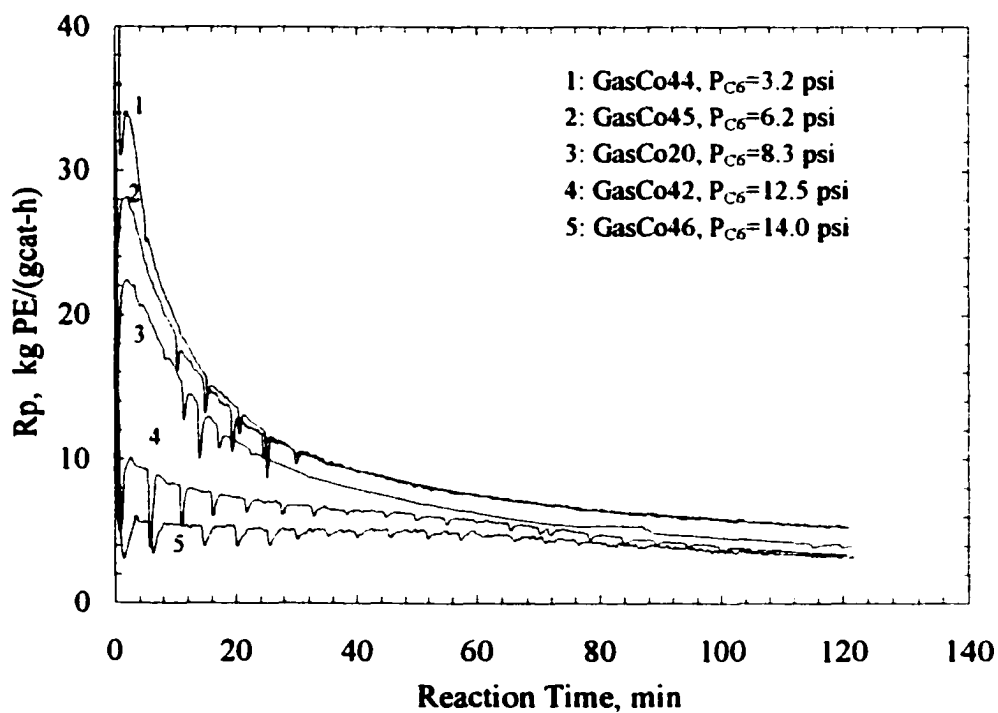


Figure 6.6 Ethylene rate profiles at P_{C_2} =150 psi and different 1-hexene pressures.

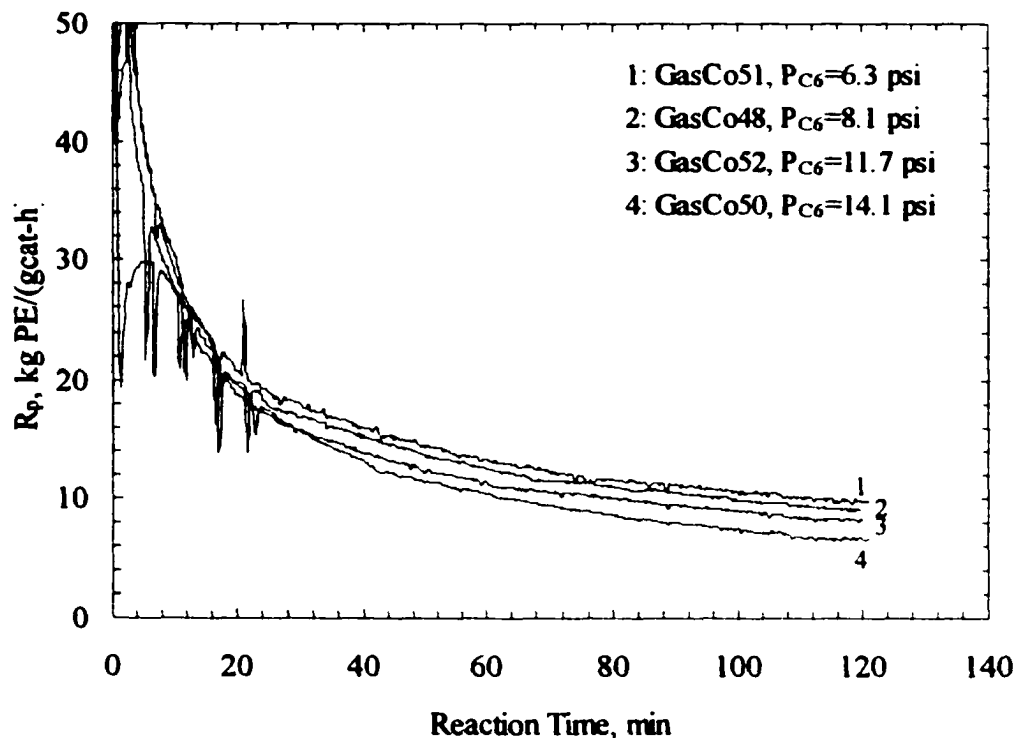


Figure 6.7, Ethylene rate profiles at $P_{C_2}=250$ psi and different 1-hexene pressures.

from Figures 6.5, 6.6 and 6.7 that with the increase of 1-hexene pressure, both the activation rate and the decay rate are reduced.

The variation in average rate of PE production as function of ethylene and 1-hexene pressure is shown in Figure 6.8. The observed decrease in average rate shows the inhibiting effect of 1-hexene for ethylene/1-hexene copolymerization kinetics. Two possibilities may explain this trend. The first explanation is that the introduction of 1-hexene reduces ethylene concentration near the reactive sites, i.e. lower ethylene solubility in polymer phase in the presence of 1-hexene. However, previous experiments (Moore and Wanke, 2000) showed that the ethylene co-sorption amount in the ethylene/1-hexene mixture could be much higher than the amount sorbed by the polymer sample when exposed to pure ethylene. Thus, this solubility study rules out the first explanation. The second explanation is that ethylene and 1-hexene compete with each other for occupying the active sites. Since 1-hexene shows very low reactivity for Ziegler-Natta catalytic system (Dange et al., 1986), the polymerization rate will decrease

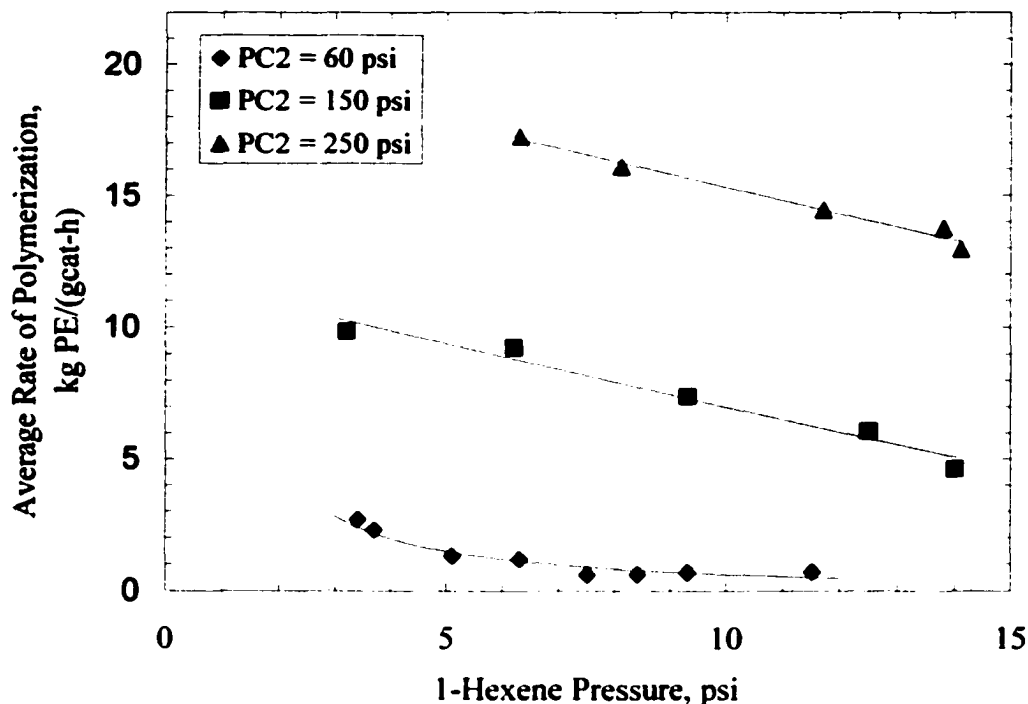


Figure 6.8 Dependence of average rate of PE production on ethylene and 1-hexene pressures.

if the active sites are occupied by 1-hexene. According to this explanation, a Langmuir-Hinshelwood adsorption theory may be suitable for kinetic modeling (see Chapter 8).

Figure 6.9 is a plot of average 1-hexene consumption rate (includes 1-hexene incorporation rate and 1-hexene sorption rate) from GC analyses as a function of 1-hexene pressure at 60, 150 and 250 psi of ethylene. For all cases, 1-hexene consumption rates increased with the increase of 1-hexene pressure.

Figure 6.9 also shows that at the same 1-hexene pressure, an increase in ethylene concentration led to an increase in the amount of 1-hexene consumed. An explanation for this observation is that the presence of ethylene results in more rapid activation of sites which also incorporate with 1-hexene. An explanation of this role of ethylene was given by Kissin (Kissin et al., 1999a, 1999d) and was briefly reviewed in Chapter 2.

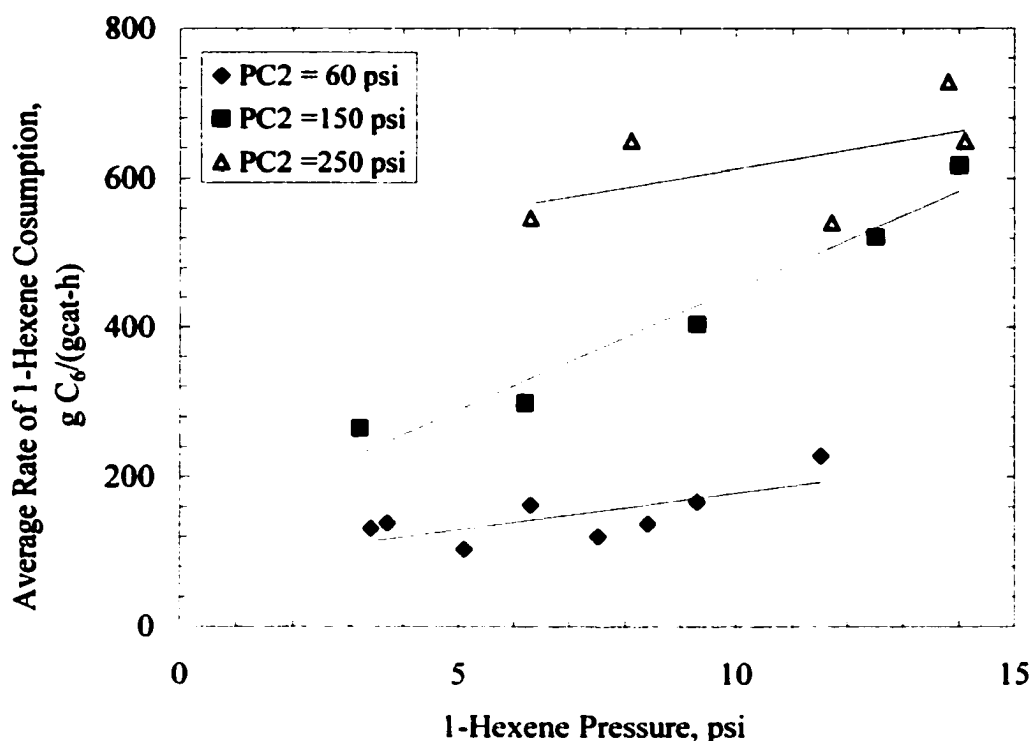


Figure 6.9 Dependence of 1-hexene consumption rate on ethylene and 1-hexene pressures.

6.3.2 Constant 1-Hexene/Ethylene Ratios

Rate profiles at constant 1-hexene/ethylene ratio of about 0.055 for various ethylene and 1-hexene pressures are shown in Figure 6.10. The summary of these experiments was already given in Table 6.3. The results show that the ethylene reaction rates increased as ethylene pressure increased at constant 1-hexene/ethylene ratio. From the discussion in Section 6.3.1, it is known that at the same ethylene pressure, the average rate of PE production decreased with the increase of 1-hexene pressure. The results shown in Figure 6.10 suggest that the reaction rates are mainly determined by ethylene pressure, not 1-hexene concentration. It can also be seen in Figure 6.10 that the rate maxima were strong functions of ethylene pressure; the activities at later times were weaker functions. This dependence on ethylene is further demonstrated in Figure 6.11. (This phenomenon can also be seen in Figures 6.5, 6.6 and 6.7, but some of the maximum rates are not easily determined at high 1-hexene pressure or at very high ethylene pressure in those figures.)

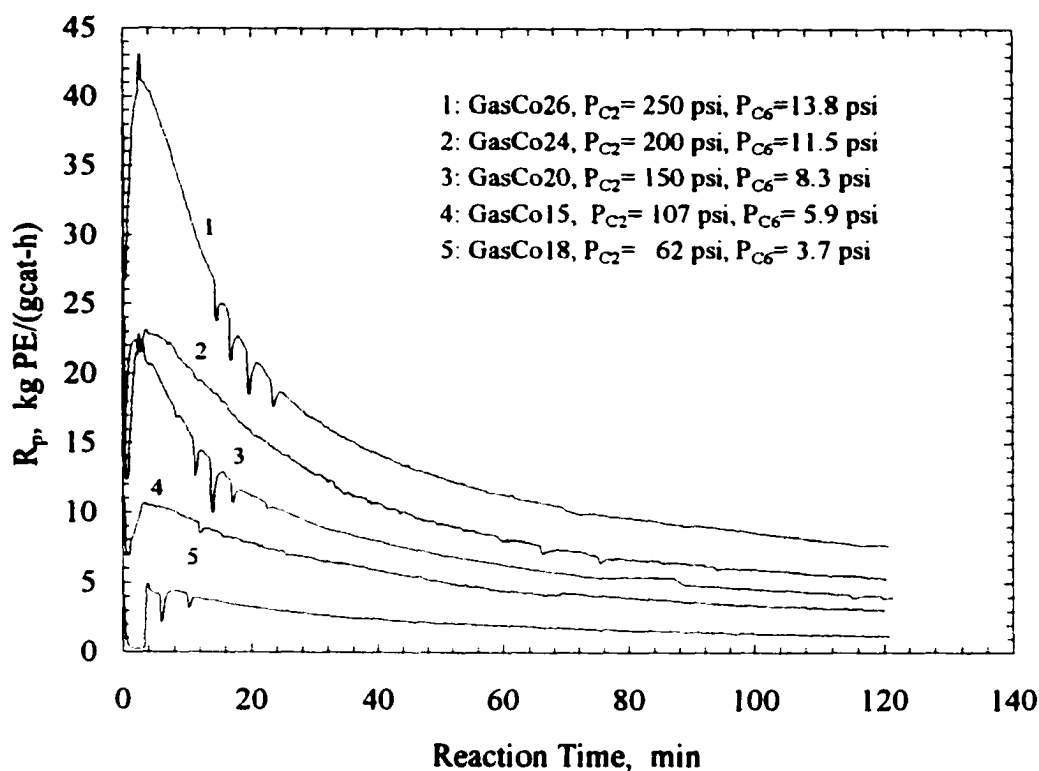


Figure 6.10 Ethylene rate profiles at constant C_6/C_2 ratio.

The relationships of the maximum rates and rates after two hours as a function of ethylene pressure at constant C_6/C_2 ratio are plotted in Figure 6.11. Fitting these rates with a power-law rate function shows that the maximum rate varies with P_{C_2} to the 1.54 power, while the order respect to ethylene was essentially unity after 2 h. This time dependence of the reaction order is probable due to the interaction between the rates of site activation and deactivation properties (Wu et al., 1999).

The average 1-hexene consumption as a function of 1-hexene pressure at constant C_6/C_2 ratio is shown in Figure 6.12. The order with respect to 1-hexene pressure appeared to be greater than unity. This can be due to the same reason as given for the larger than unity order for ethylene. However, the increase in 1-hexene solubility in PE with higher comonomer concentration could also contribute to the greater than unity apparent reaction order.

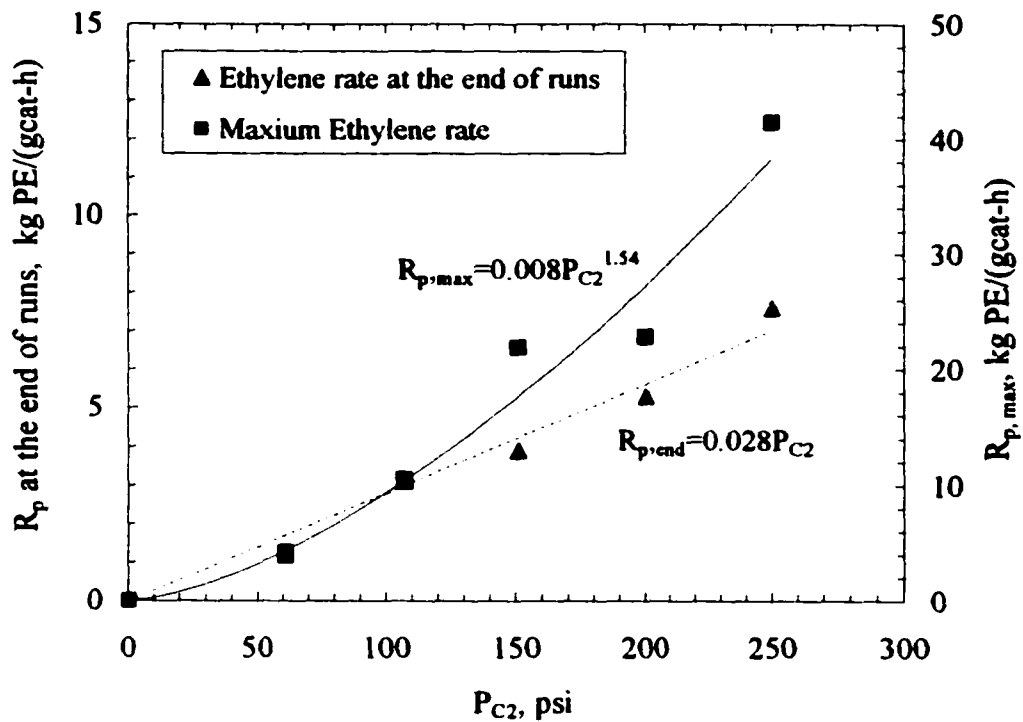


Figure 6.11 Dependence of ethylene reaction rates in the early stage and in the end of runs on ethylene partial pressure with $C_6/C_2 = 0.055$.

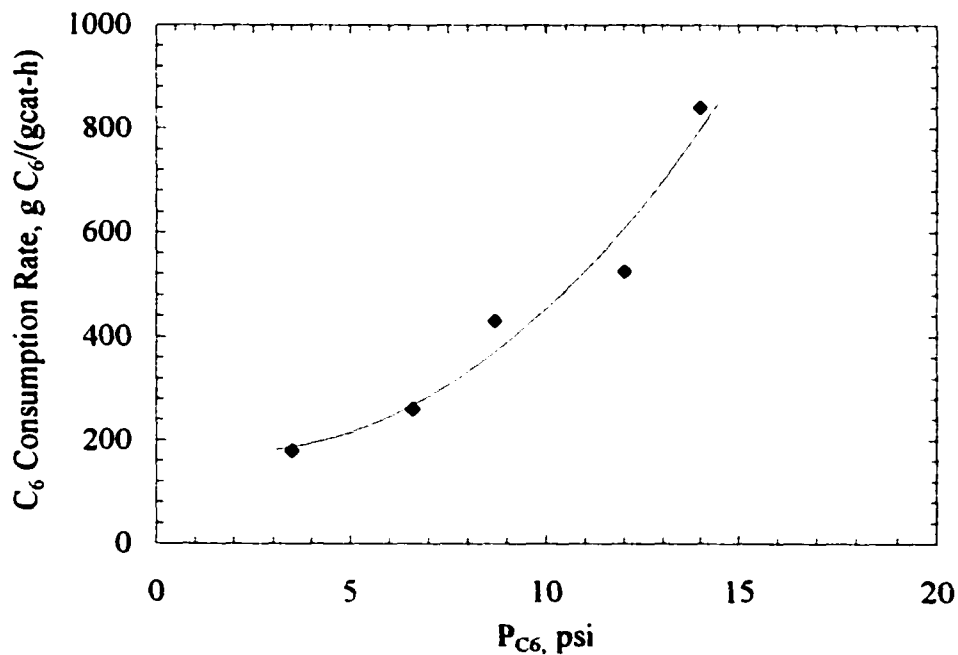


Figure 6.12 Dependence of overall 1-hexene consumption rate on 1-hexene pressure with $C_6/C_2 = 0.055$.

6.3.3 Constant 1-Hexene Pressure

In this section, the relationship between ethylene pressure and average rate of PE production at same 1-hexene partial pressures is explored. The results are shown in Figure 6.13. (Experimental conditions are given in Table 6.3). At similar 1-hexene pressures, average reaction rates increased as ethylene pressure increased. However, the power-law orders with respect to ethylene pressure were quite different at different 1-hexene pressures. At low 1-hexene pressure (6.4 psi), the reaction rate was proportional to ethylene pressure (first order). With the increase of 1-hexene concentration, the power-law order n increased to 1.2 at $P_{C_6} = 8.1$ psi and to 2.0 at $P_{C_6} = 14$ psi.

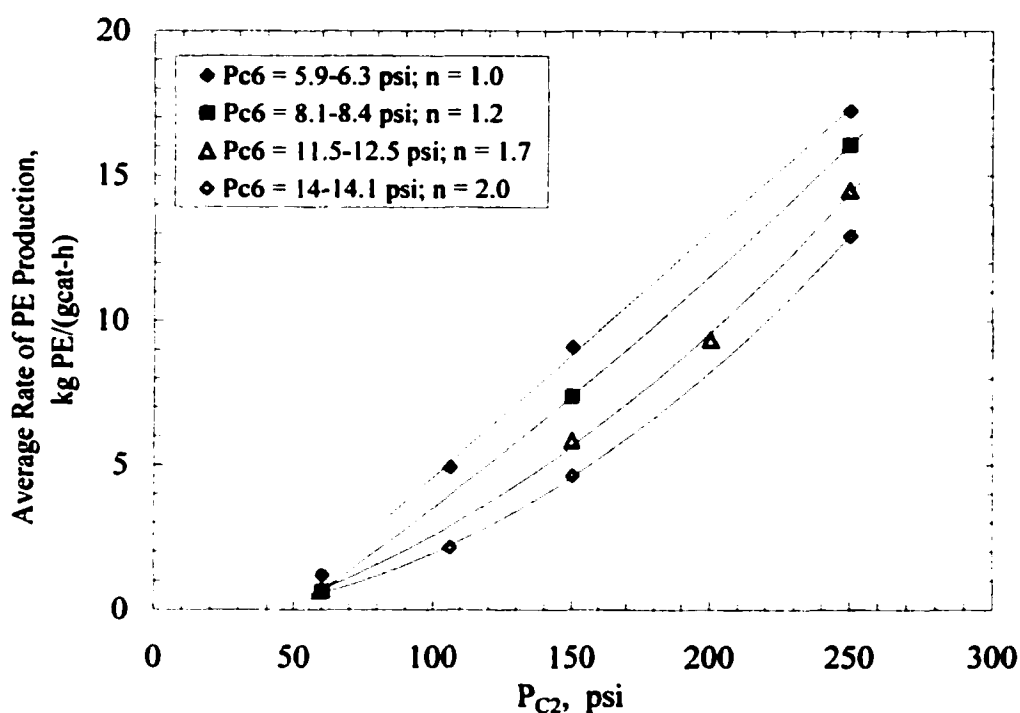


Figure 6.13 The power order relations between ethylene pressure and average reaction activity at constant 1-hexene pressures.

Some researchers (Karol et al., 1993) found that both ethylene homopolymerization and ethylene/1-hexene copolymerization over Ti based Ziegler-Natta catalysts showed second-order dependency of activity on the ethylene partial pressure either in gas-phase or in slurry-phase reactions. Our experimental results show that the overall (apparent)

order based on ethylene bulk concentration is not constant. Solubility studies (see Chapter 7) showed that the solubility of 1-hexene in PE is not linearly related to its pressure; the amount of sorption was much higher at high 1-hexene pressure. The changes in solubilities may be part of the reason for the behavior.

The dependence of 1-hexene consumption rates on ethylene pressure at constant 1-hexene pressures is shown in Figure 6.14. At low 1-hexene pressure ($P_{C6} = 6.4, 8.3$ psi), higher ethylene pressure led to higher 1-hexene consumption rates. However, at high 1-hexene pressure ($P_{C6} = 11.5$ and 14 psi), no clear trend was evident between 1-hexene consumption rate and ethylene concentrations.

6.4 Effects of Hydrogen

Hydrogen effects on olefin polymerization are complex; hydrogen can either decrease ethylene polymerization rate, increase propylene polymerization rate or have no effect on olefin polymerization rate. The current experimental results of copolymerization in the presence of hydrogen are summarized in Table 6.4. All reaction runs were carried out at $P_{C2}=150$ psi and 1-hexene/ethylene mole ratio of about 0.08. Figure 6.15 is the plot of ethylene polymerization rate profiles at different hydrogen pressures (0-30 psi). It can be seen from this figure that hydrogen reduced the polymerization rate. Unlike the reduction feature of 1-hexene, where 1-hexene decreased the reaction rate more significantly at the beginning of runs (see Figures 6.5, 6.6 and 6.10), hydrogen reduced the rate throughout the runs. Kissin et al. (1999a) studied the effects of hydrogen on kinetics of ethylene/1-hexene slurry copolymerization over $MgCl_2$ -supported $TiCl_4$ catalysts. They found that hydrogen did not reduce the maximum reaction rate at the beginning but accelerated the catalyst decay. The difference between Kissin's findings and current experimental results may be attributed to the different hydrogen effects on prepolymerized catalysts and catalysts, or to the difference between slurry and gas-phase operations.

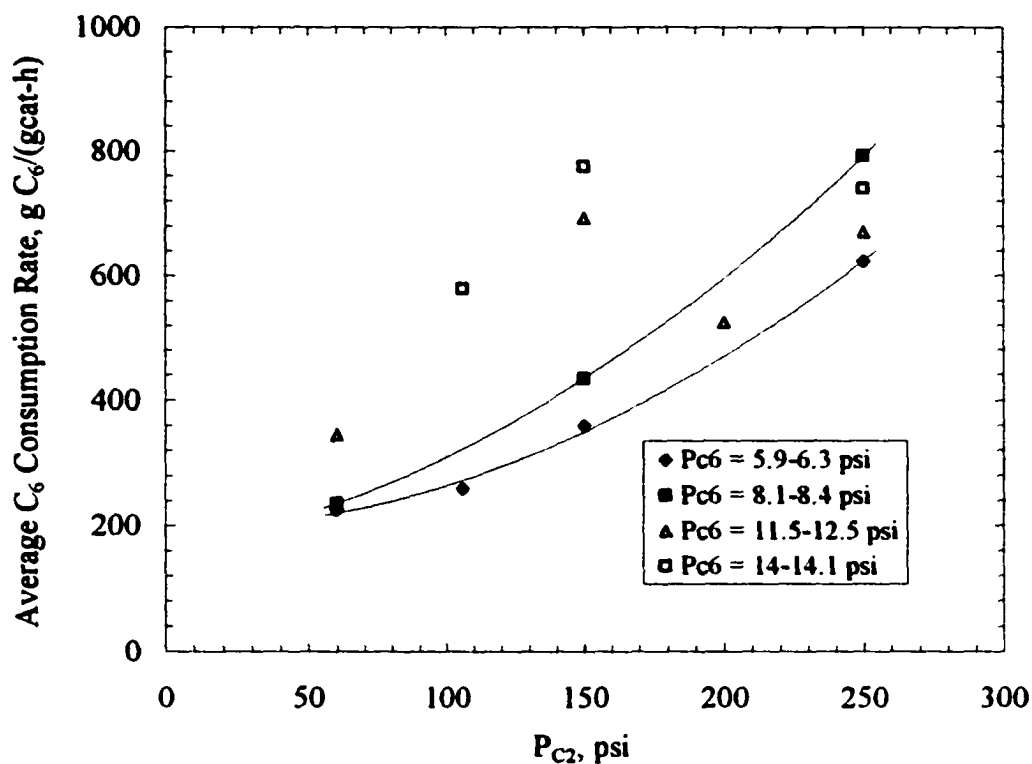


Figure 6.14 Dependence of average 1-hexene consumption rate on ethylene pressure at constant 1-hexene pressures.

Table 6-4 Summary of Polymerization Runs at Different Hydrogen Pressures.¹

Run No.	Amount of Pre18 g	Amount of TEA mL	Partial Pressures			C_6/C_2 Ratio	PE Yield g	C_6 Consumption ² g	C_6 Content in Polymer ³ mol %
			H_2 psi	C_2 psi	C_6 psi				
GasCo42	0.097	0.25	0	150	12.5	0.083	14.1	1.6	1.1
GasCo61	0.104	0.25	6	150	12.0	0.080	7.0	1.6	4.3
GasCo60	0.106	0.25	12	150	12.0	0.080	4.5	1.4	3.8
GasCo59	0.116	0.25	30	150	11.9	0.079	3.9	1.3	3.6

¹ Other conditions: $P_{N_2} = 14$ psi; $T=70^\circ C$; Length of Runs = 2 h; hydrogen was added after 1-hexene.

² C_6 consumption based on the actual addition amount of 1-hexene during the runs.

³ C_6 Content in Polymer based on ^{13}C -NMR measurement.

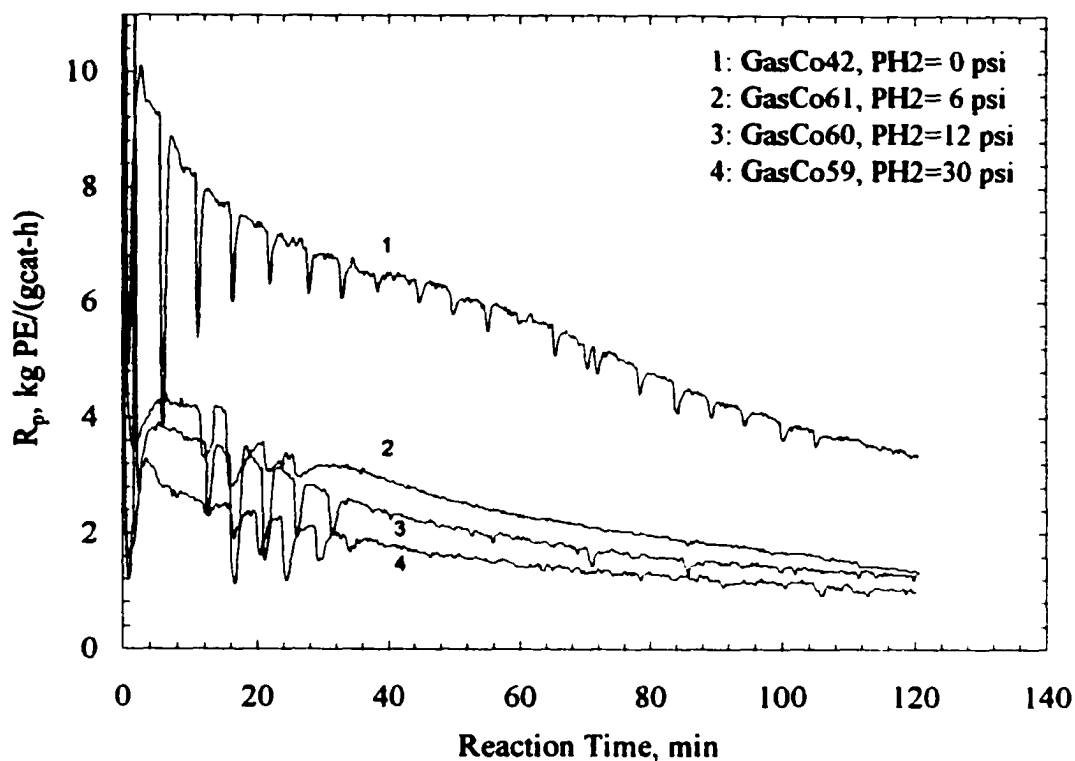


Figure 6.15 Rate profiles of copolymerization at different hydrogen concentrations.

The average reaction rates of ethylene and 1-hexene can be estimated if the mass of polymer produced and the comonomer content in copolymer are known. Figure 6.16 shows the effects of hydrogen on ethylene and 1-hexene incorporation rates based on the data shown in Table 6.4. It can be seen from the figure that average ethylene reaction rate was very sensitive to hydrogen; introduction of small quantity hydrogen reduced the reaction rate sharply. Further increase in hydrogen amount did not have a significant effect. This phenomenon suggests that hydrogen has significant influence on ethylene polymerization and interacts strongly with the reaction sites at low hydrogen pressure (i.e. high coverage at low pressure). The hydrogen effect on comonomer incorporation is complex. If the data point at 6 psi hydrogen is neglected, then it seems that hydrogen caused a slight decrease in 1-hexene incorporation. But the decrease is less than the decrease in the ethylene polymerization rates. However, the 1-hexene rate at 6 psi is probably correct since the ratio of 1-hexene to ethylene rates (shown in Figure 6.17) at 6 psi is the same as the ratios at 12 and 30 psi of hydrogen. The R_{C6}/R_{C6} ratio at all these

pressures is about 3 to 4 times higher in the presence of hydrogen than in the absence of hydrogen (see ^{13}C -NMR results in Table 6.4).

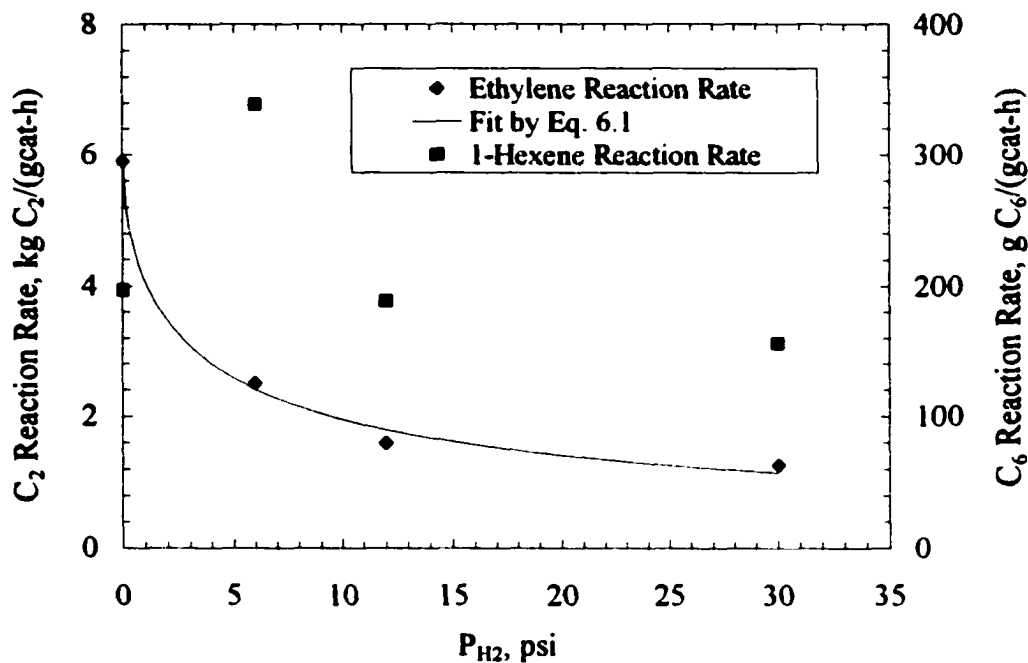


Figure 6.16 Hydrogen effects on ethylene and 1-hexene reaction rates.

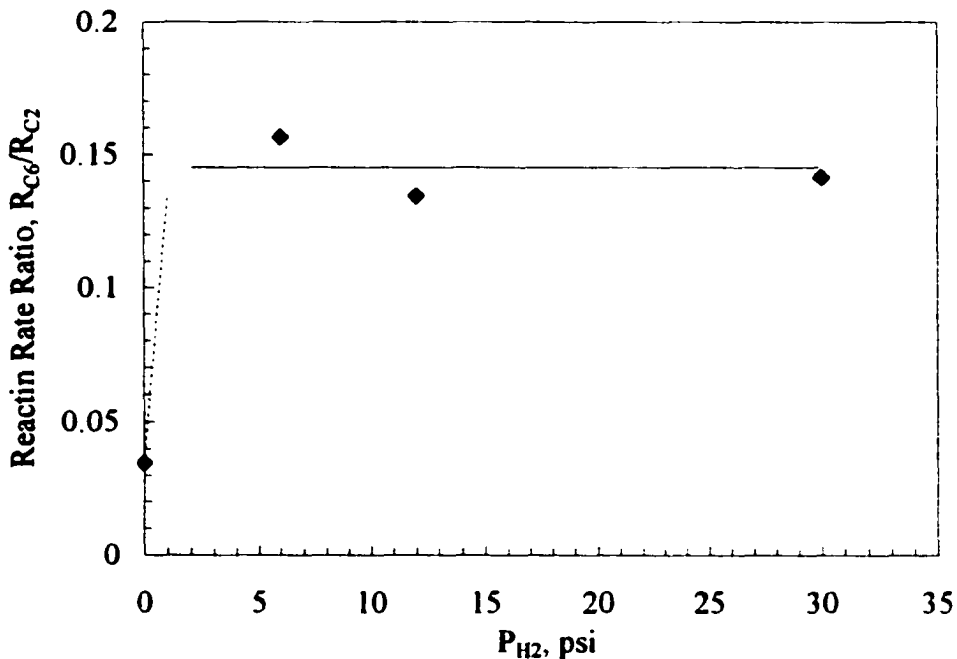


Figure 6.17 Hydrogen effect on reaction rate ratio of 1-hexene/ethylene

This increased in relative 1-hexene incorporation rates can be explained by Kissin's theory (Kissin et al., 1999a to 1999d) that in the presence of hydrogen, the number of non-reactive sites with β -agostic coordination state (see Chapter 2) increases, leading to the reduction of ethylene polymerization rate. When an α -olefin is present, it inserts into the Ti-H bond with an immediate formation of Ti-polymer bond, bypassing the non-reactive β -agostic coordination state. As a result, 1-hexene reaction rate is affected less by hydrogen than the ethylene rate.

Using a Langmuir-Hinshelwood expression to fit the average ethylene reaction rate as a function of hydrogen pressure yields

$$R_p = \frac{R_{p0}}{1 + 0.447 P_{H_2}^{0.657}} \quad (6.1)$$

where R_{p0} is the ethylene polymerization rate in the absence of hydrogen. The fit is shown in Figure 6.16. This result is in agreement with other researchers (Huang et al., 1997; Keii, 1980), who observed that Langmuir-Hinshelwood expression with orders of 0.5 to 1 with respect to hydrogen described the effect of hydrogen on ethylene polymerization rates.

6.5 Effects of Temperature

Results on the effects of temperature effects on copolymerization kinetics are summarized in Table 6.5. Since the 1-hexene vapor pressure is very low at room temperature, copolymerization was carried out at relative high temperatures (60 to 90°C) so that a relatively high 1-hexene pressure could be used. Hydrogen was kept between 12 and 14 psi and 1-hexene/ethylene ratio in gas phase was controlled about 0.08. The ethylene reaction rate profiles at different temperatures are shown in Figure 6.18. As temperature increased, both the activation rate and the deactivation rate decreased.

The reaction rates of 1-hexene can be calculated from the ^{13}C -NMR measurements shown in Table 6.5. The dependence of average 1-hexene and ethylene reaction rates on temperature are shown Figure 6.19. The decrease in reaction rates with increasing

temperature shows that the deactivation processes are more temperature sensitive than the activation processes.

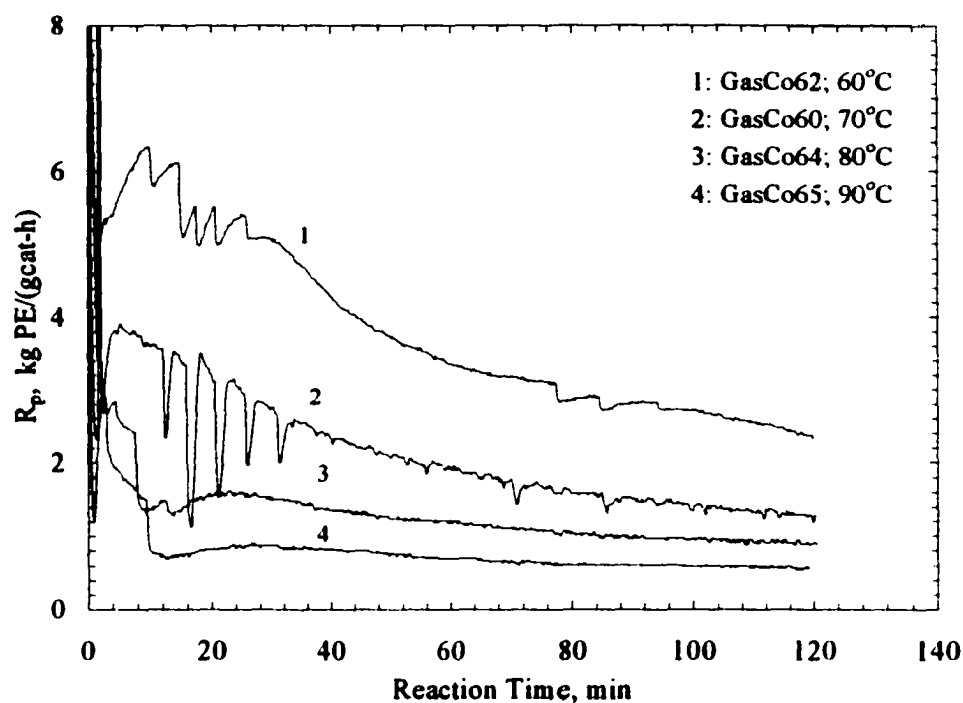


Figure 6.18 Rate profiles of copolymerization at different reaction temperatures.

Table 6.5 Experimental Results of Copolymerization under Different Temperatures.¹

Run No.	Amount of Pre18 g	Temp °C	Partial Pressures			C_6/C_2 Ratio	PE Yield g	C_6 Consumption ² g	C_6 Content in Polymer ³ mol%
			H_2 psi	C_2 psi	C_6 psi				
GasCo62	0.129	60	15	150	11.8	0.078	11.2	2.8	4.4
GasCo60	0.106	70	12	150	12.0	0.080	4.5	1.4	3.8
GasCo64	0.110	80	12	150	12.4	0.083	3.0	1.1	4.0
GasCo65	0.119	90	13	150	12.4	0.083	1.5	0.93	3.2

¹ Other conditions: $P_{N_2} = 14$ psi; TEA = 0.25 mL; Length of Runs = 2 h, hydrogen was added after 1-hexene.

² C_6 Consumption based on the actual addition amount of 1-hexene during the runs.

³ C_6 Content in Polymer based on ^{13}C -NMR measurement.

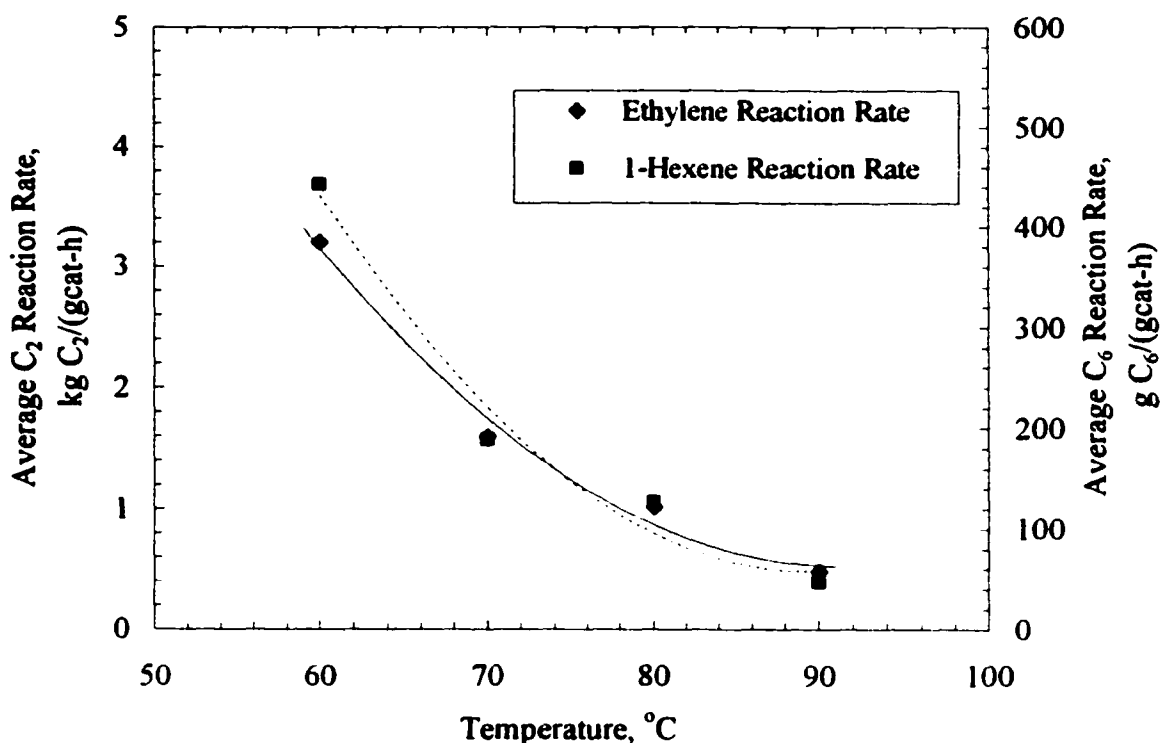


Figure 6.19 Dependence of average reaction rates of 1-hexene and ethylene on reaction temperature.

The effect of temperature on the relative 1-hexene/ethylene reaction rate ratio is shown in Figure 6.20. Increase in temperature resulted in a slight decrease in the R_{C_6}/R_{C_2} ratio. This implies that the deactivation of 1-hexene reactive site is more sensitive to temperature than 1-hexene less reactive site.

An Arrhenius plot of average rate of PE production is shown in Figure 6.21. R_p is the average rate of PE production, $[M]$ is the ethylene gas-phase concentration calculated by ideal gas law. The apparent activation energy from Figure 6.21 is negative, i.e. the average rate decreases with increasing temperature. The decrease in average rate with increasing temperature is due to the sensitivity of the deactivation to temperature, i.e. the activation energy for the deactivation processes is higher than the activation energy for the activation processes.

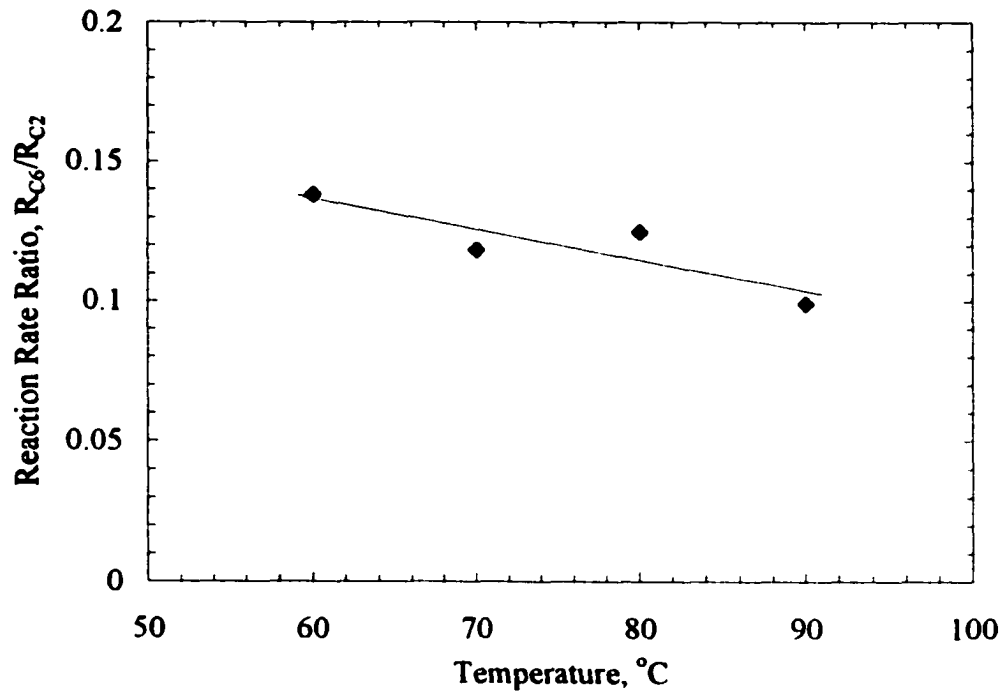


Figure 6.20 Dependence of 1-hexene/ ethylene reaction rate ratio on reaction temperature.

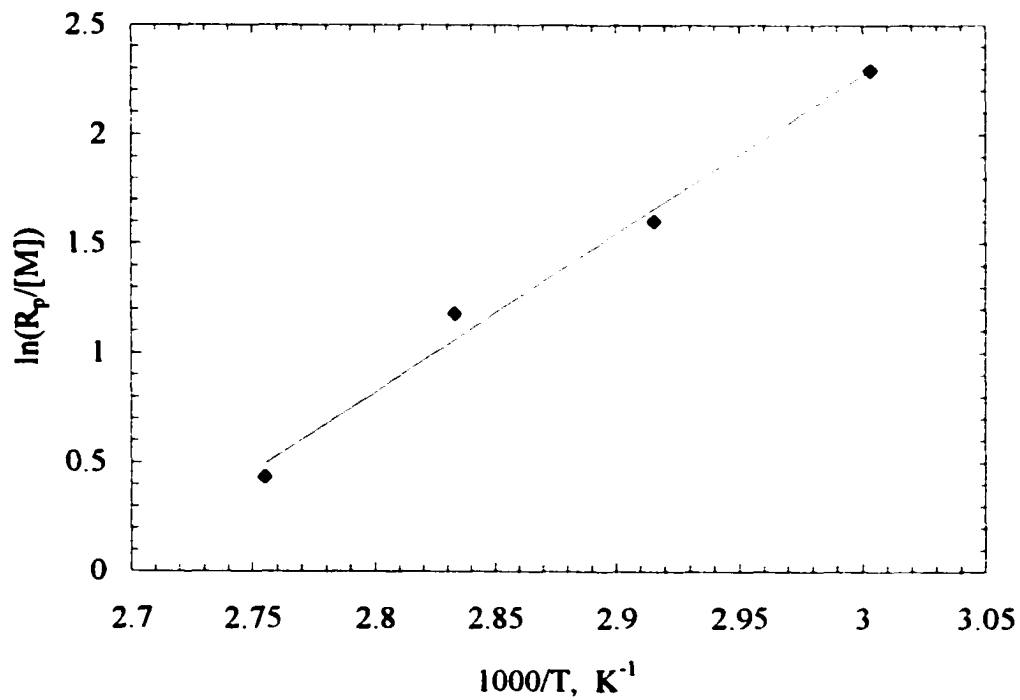


Figure 6.21 Arrhenius plot of the average copolymerization rate.

6.6 Effects of Length of Runs

Runs of different duration were done to determine the effect of polymerization time on 1-hexene consumption. Figure 6.22 shows the rate profiles for the reactions with run lengths from 0.5 to 4 h. All other conditions were constant ($P_{C_2} = 150$ psi, $P_{C_6} = 14$ psi, $P_{H_2} = 0$, $T = 70^\circ\text{C}$). It can be seen from Figure 6.22 that the rate profiles were very reproducible. The changes of copolymer yield and 1-hexene consumption per mass of polymer produced with time are shown in Figure 6.23. The overall 1-hexene consumption per gram of polymer (i.e. sorbed and reacted amount) increased during the first hour of reaction; but after one hour, the average amount of 1-hexene in polymer decreased. This result implies that the active sites responsible for 1-hexene incorporation are active at the early stages of reactions and deactivate more rapidly than the sites for ethylene polymerization.

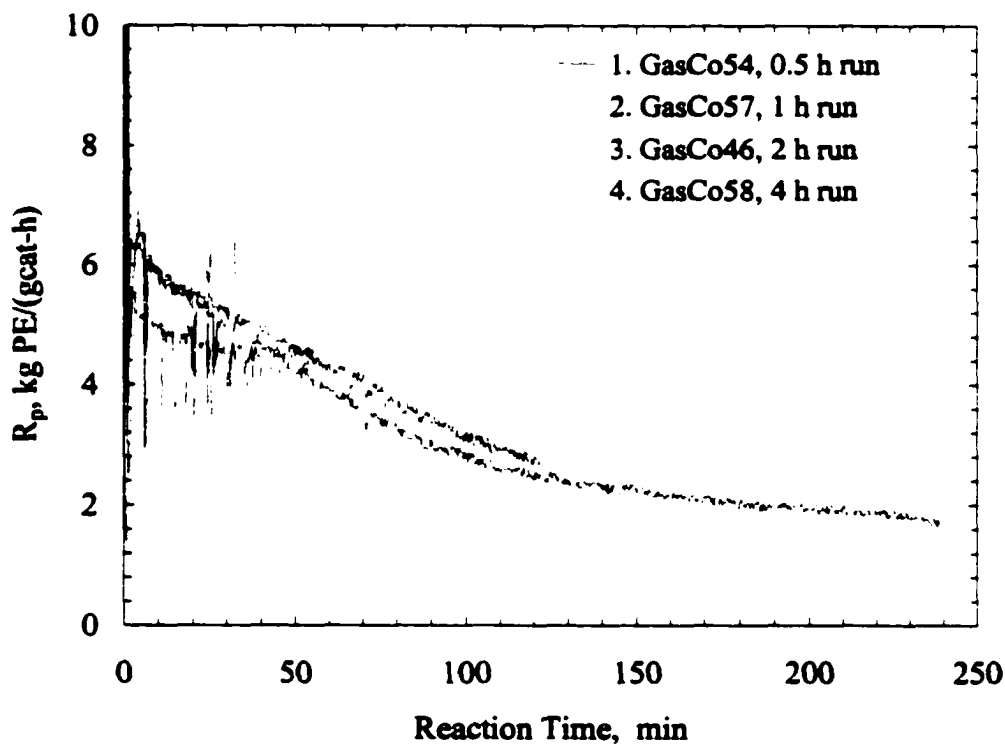


Figure 6.22 Ethylene rate profiles with different lengths of runs. ($P_{C_2}=150$ psi, $P_{C_6}=14$ psi, $T = 70^\circ\text{C}$)

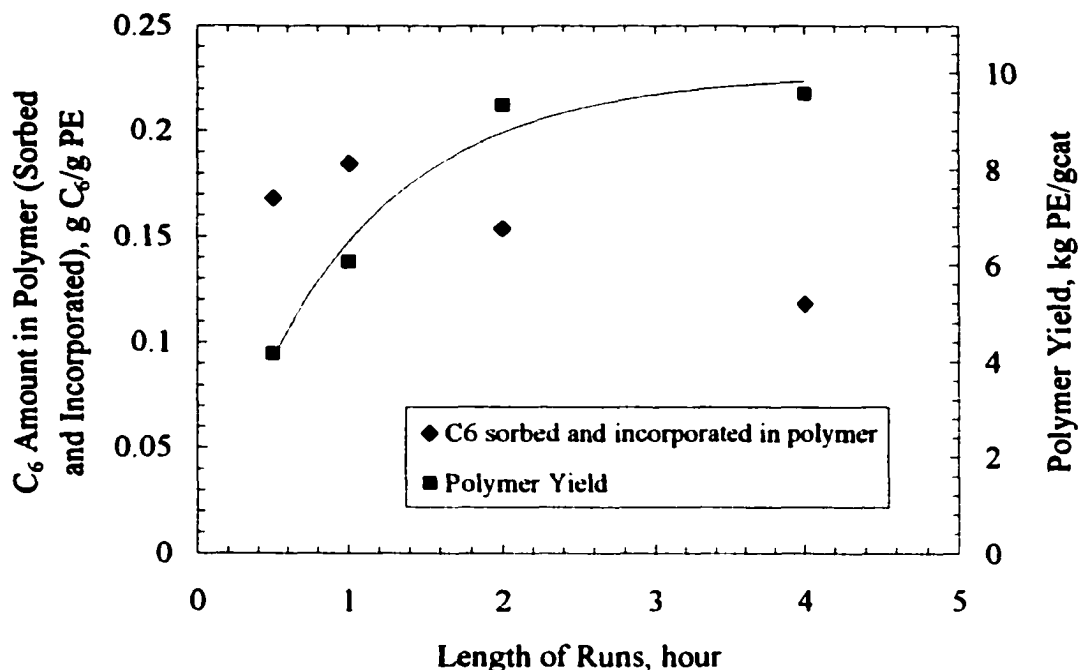


Figure 6.23 Dependence of polymer yield and average 1-hexene amount dissolved and incorporated in polymer on length of runs.

The deactivation part of the profiles shown in Figure 6.22 are described well by a first-order decay expression, i.e.

$$R_p = R_\infty + (R_{\max} - R_\infty) \cdot e^{[-k_d(t-t_{\max})]} \quad (6.2)$$

where t_{\max} is the time at maximum rate R_{\max} and R_∞ is the reaction rate at long times.

The fit for the 4-h copolymerization run is shown in Figure 6.24. It can be seen from the figure that the decay in polymerization rate with time is well represented by the fitted function.

6.7 Comparison of Homopolymerization and Copolymerization in Gas Phase and Slurry Phase

It was observed that the kinetics of homopolymerization and copolymerization in gas phase and slurry are very different. These differences are illustrated in this section. The experimental conditions and results are listed in Table 6.6 and the rate profiles are shown in Figure 6.25.

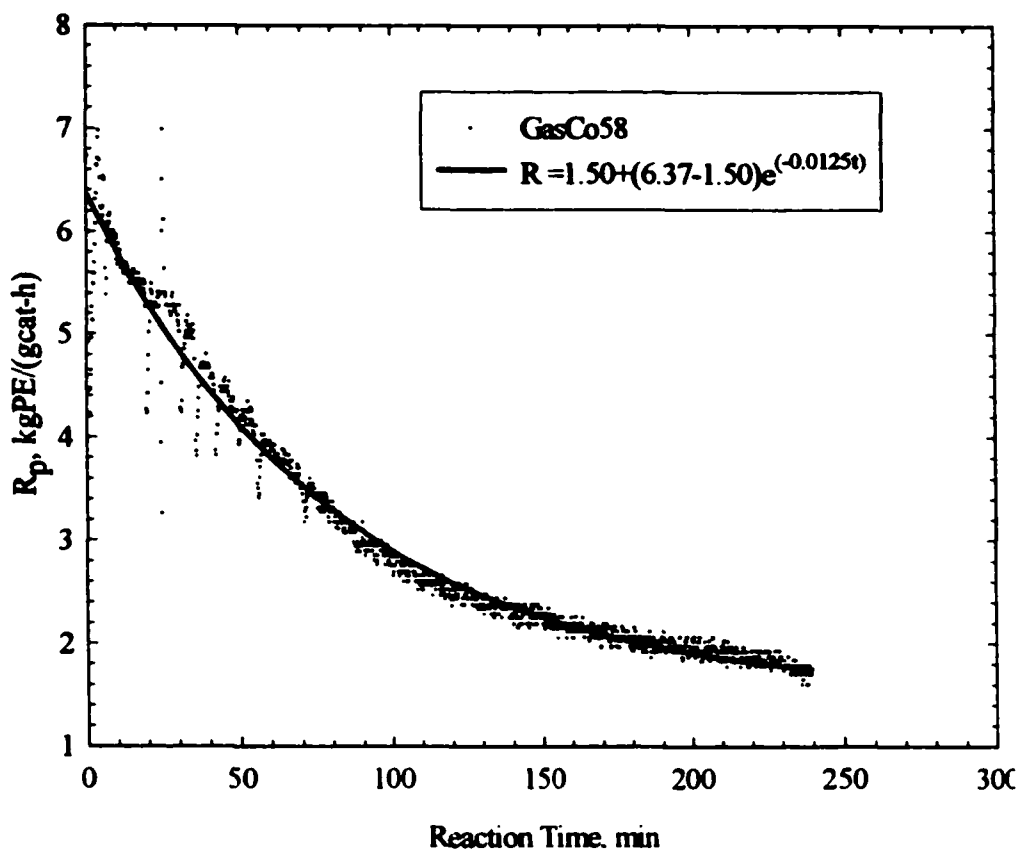


Figure 6.24 Plot of R_p versus time according to first-order decay law, eq. (6.2).

Table 6.6 Experimental Conditions and Results for Homo- and Copolymerization Runs in Slurry phase and Gas Phase.¹

Run No.	Phase	Amount of Pre 18 g	Amount of TEA mL	Partial Pressure		C_6 Amount ² mL	Length of Runs h	PE Yield g/h
				H ₂ psi	C ₂ psi			
Slu-8	slurry	0.111	0.30	40	140	0	2	6.7
Slu-9	slurry	0.118	0.30	40	140	5.0	2	8.3
GasHo7	gas	0.113	0.25	53	199	0	1.8	4.9
GasCo9	gas	0.110	0.25	49	206	6.0	2	4.6

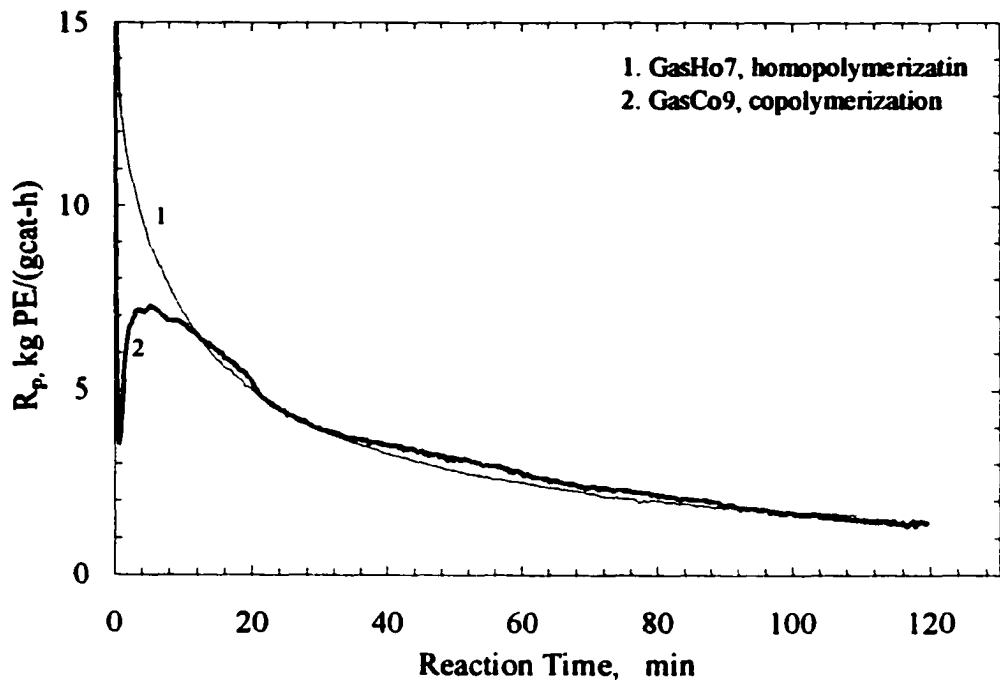
¹ Other conditions: $P_{N_2} = 14$ psi; 70°C.

² 1-Hexene was added once at the beginning.

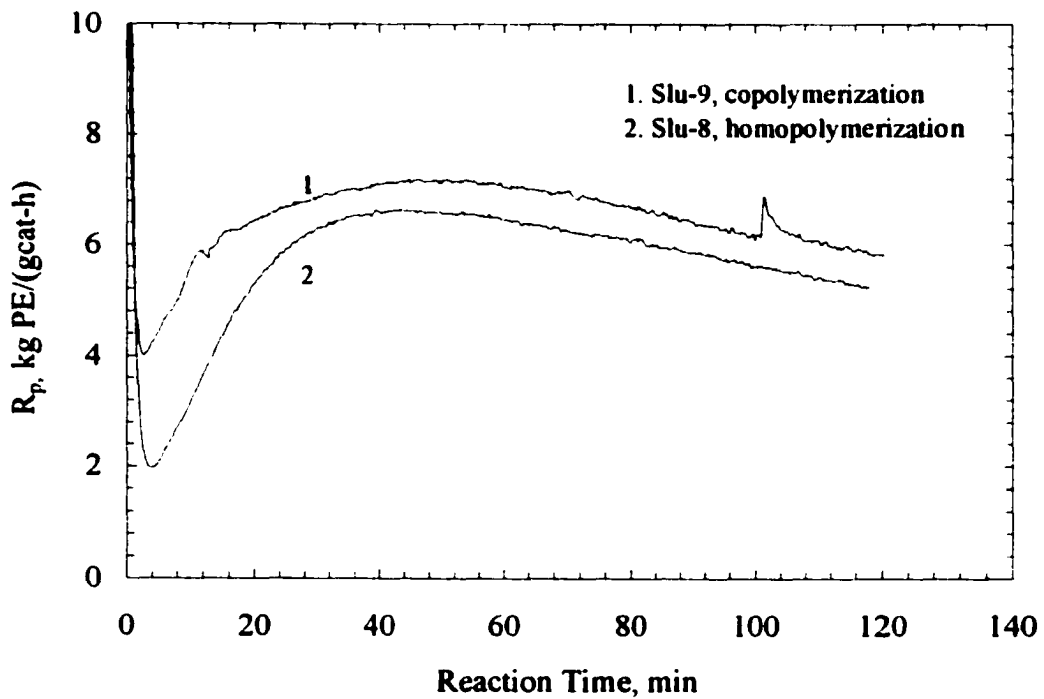
In Figure 6.25 (a), ethylene homo- and co-polymerization rate profiles in the gas phase are compared. For homopolymerization run, the acceleration period was much shorter than could be detected, i.e. only a decay was observed. For copolymerization, the rate of activation was reduced by the presence of 1-hexene and the maximum rate appeared at about 7 min after the run began. The kinetics of these two runs after 20 min of run were very similar. This implies, in agreement with the observation in the previous section, that ethylene homopolymerization dominates in the later stages of polymerization.

Homo- and co-polymerization activity profiles in slurry phase are shown in Figure 6.25 (b). The rate profiles are quite different from the gas-phase polymerization profiles shown in Figure 6.25 (a); the acceleration period is longer and the decay rate is slower. In slurry phase, the copolymerization showed consistently higher rates than the homopolymerization. This comonomer enhancement effect has often been reported by researchers (Munoz-Escalona et al., 1987; Karol et al., 1993; Calabro and Lo, 1988; Han-Aderekun et al., 1997b; Ko et al., 1997). Proposed causes of this enhancement effect (Calabro and Lo, 1988; Chien and Nozaki, 1993; Floyd, et al., 1986; Ko, et al., 1997) include: (1) generation of more active sites by complete fragmentation; (2) increases in propagation rate; (3) changes in the oxidation state of Ti; and (4) higher diffusion coefficients.

In the current study, prepolymerized material was used as the catalyst. The fragmentation should be complete after the prepolymerization; thus increases in the generation of more sites by complete fragmentation is probably not the cause of the enhancement observed in the current study. If changes in Ti oxidation state or increases in propagation rate happen in slurry polymerization, then it is not easy to understand the rate decrease in gas-phase operations.



(a)



(b)

Figure 6.25 Comparison of ethylene homo- and copolymerization rate profiles in gas-phase (a) and slurry-phase (b) operations.

Mass transfer limitations inside growing particle may be a problem for slurry polymerizations but can be neglected in gas-phase reactions (Floyd et al., 1986a, 1986b and 1987). The presence of 1-hexene may change the structure of the polymer and thereby increase mass transfer rate or olefin solubility. Another possible reason for the enhancement by 1-hexene in the slurry is that 1-hexene may increase the solubility of ethylene in liquid. This would lead to higher ethylene concentrations in the liquid and thus increase the polymerization rate. Additional studies are required to elucidate the difference of the 1-hexene effect between gas-phase and slurry operations.

CHAPTER 7. NASCENT COPOLYMER PROPERTIES AND SOLUBILITIES

The effects of polymerization conditions on nascent polymer properties are discussed in this chapter. Several analytical techniques were employed in this study. GPC was used to measure molar mass and polydispersity. Comonomer content and distribution in copolymer were determined by ^{13}C -NMR and TREF methods. Melting point and crystallinity were analyzed by DSC. Solubilities of ethylene and 1-hexene in nascent copolymer were measured and co-solubility of 1-hexene was estimated.

7.1 Molar Mass and Its Distributions

Molar mass distribution (MMD) has a major affect on PE properties. Resins with narrow MMD have good low-temperature impact strength; resins with broad MMD have greater stress cracking resistance and ease of processing (Maraschin, 2001). In this part, molar masses and polydispersities for homopolymerization and copolymerization are examined and the effects of 1-hexene content, hydrogen amount and temperature on molar masses are discussed.

7.1.1. Comparison of Homo- and Copolymerization

Molar masses for homopolymerization and copolymerization (with hydrogen added before and after the 1-hexene addition) are listed in Table 7.1. Comparison shows that under similar reaction conditions, the M_n and M_w of copolymers are lower than that of homopolymer, i.e. 1-hexene acts as a chain transfer agent. The polydispersity (Q) is also larger for copolymers. This is because different chain transfer effects of 1-hexene on different sites broaden the molar mass distributions. The sequence of hydrogen addition (see Chapter 4) affected the rate, but it did not significantly affect M_n and M_w .

7.1.2 Comonomer Effects on Molar Masses

The effect of 1-hexene on molar masses for polymer product at low ethylene pressure (60 psi) is shown in Figure 7.1. It is found that molar masses decreased with increasing 1-hexene pressure because of chain transfer effect. Polydispersities (Q) increased with increasing of 1-hexene pressures. This effect on Q is due to the formations of more low

Table 7.1 Molar Mass and Polydispersity of Homopolymer and Copolymer under Similar Reaction Conditions.¹

Run No.	Average Rate			Q
	kg PE/(gcat-h)	$M_n \times 10^{-4}$	$M_w \times 10^{-4}$	
GasHo6	3.7	3.27	12.8	3.9
GasCo3 ²	1.9	1.28	8.32	6.5
GasCo9 ³	3.5	1.52	8.16	5.4

¹ Conditions: $P_{C_2} = 200$ psi, $P_{H_2} = 50$ psi, $P_{N_2} = 14$ psi, $T = 70^\circ\text{C}$, $C_6 = 6$ mL for copolymerization, Length of Runs = 2 h.

² GasCo3: Hydrogen added before 1-hexene.

³ GasCo9: Hydrogen added after 1-hexene.

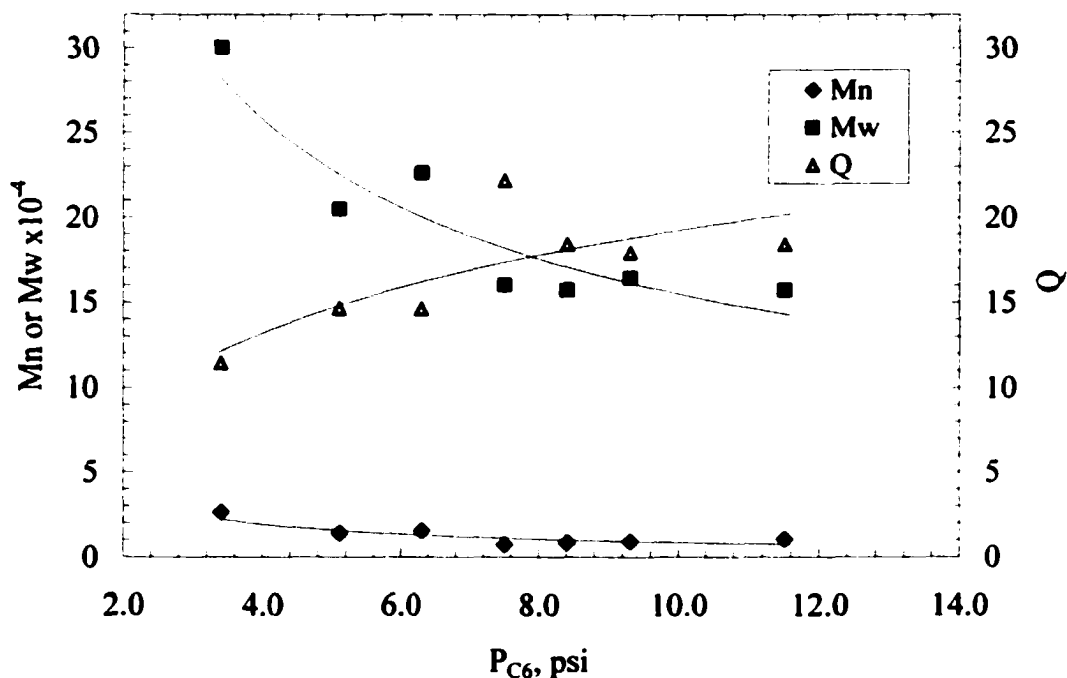


Figure 7.1 Relationship between 1-hexene pressure and molar mass and polydispersity ($P_{C_2}=60$ psi).

molar mass PE containing 1-hexene, i.e. an increase in the copolymer/homopolymer ratio.

7.1.3 Effects of Hydrogen

Figure 7.2 shows the effects of hydrogen on M_n , M_w and Q . Experimental conditions and results for the copolymerization runs are listed in Table 6.4. The introduction of 6 psi hydrogen, caused a sharp decrease in M_n and M_w , but further increase in the amount of hydrogen only resulted in a small decrease in M_n . The dependences of M_n and M_w on $[H_2]$ have been correlated by

$$M_n \text{ (or } M_w) = \frac{1}{a + b[H_2]^n} \quad (7.1)$$

The results shown in Figure 7.2, both M_n and M_w , are well correlated by Equation 7.1 (see lines and equations in Figure 7.1). This dependence on hydrogen process is in agreement with the results of other scientists (e.g. Keii, 1988; Salajka et al., 1993; Huang et al., 1997) who found values of n between 0.5 and 1.0. The polydispersity was independent of hydrogen pressure of a value of about 10.

7.1.4 Effects of Temperature

Molar masses as a function of temperature are shown Figure 7.3. Run conditions were summarized in Table 6.5. It can be seen in Figure 7.3 that both M_w and M_n decreased with increasing temperature while polydispersity Q was a constant at about 10. This result suggests that for each site, temperature accelerates chain transfer reactions and the ratios of activation energies for chain transfer to propagation have similar values for different sites.

7.1.5 Effects of Length of Runs

The effects of run length on kinetics were discussed in Chapter 6; the influences of run length on molar masses are shown in Figure 7.4. It can be seen that both M_n and M_w increased significantly during the first hour of reaction. After one hour, M_n and M_w continued to increase but slowly. Polydispersity Q decreased with the increase of run length in the first hour of run. After one hour, Q was independent of reaction time. The dependence of M_n , M_w and Q on reaction time strongly supported the postulate that different types of active sites predominate at different times during the life of a $TiCl_4/MgCl_2$ catalyst.

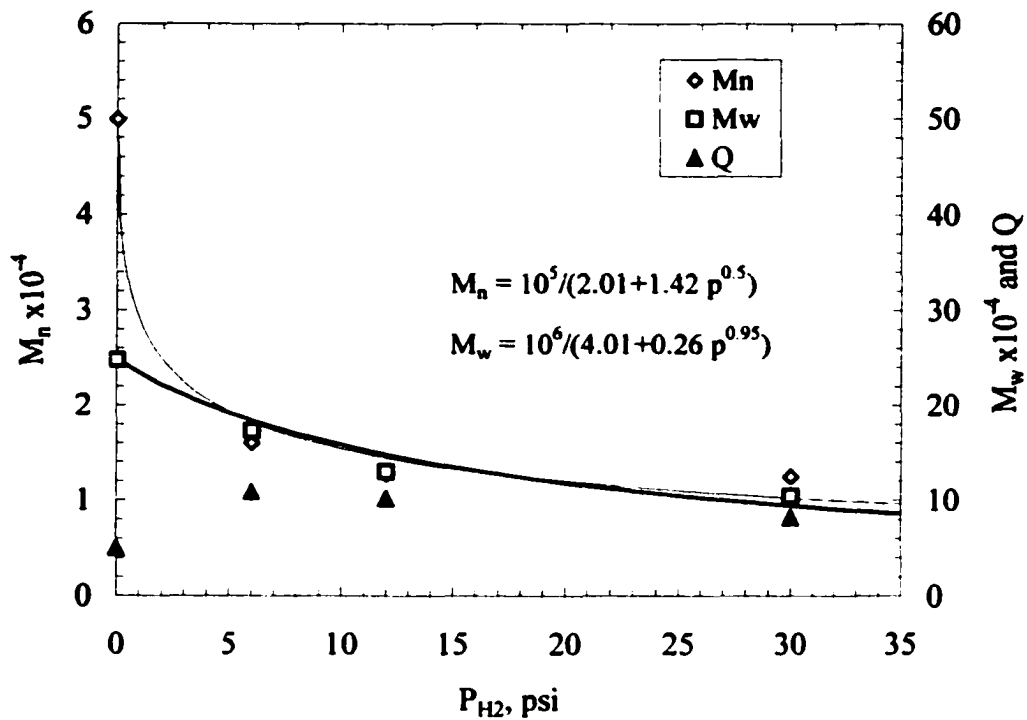


Figure 7.2 Effects of hydrogen on molar mass and polydispersity (Runs Gas42, 59 60 and 61).

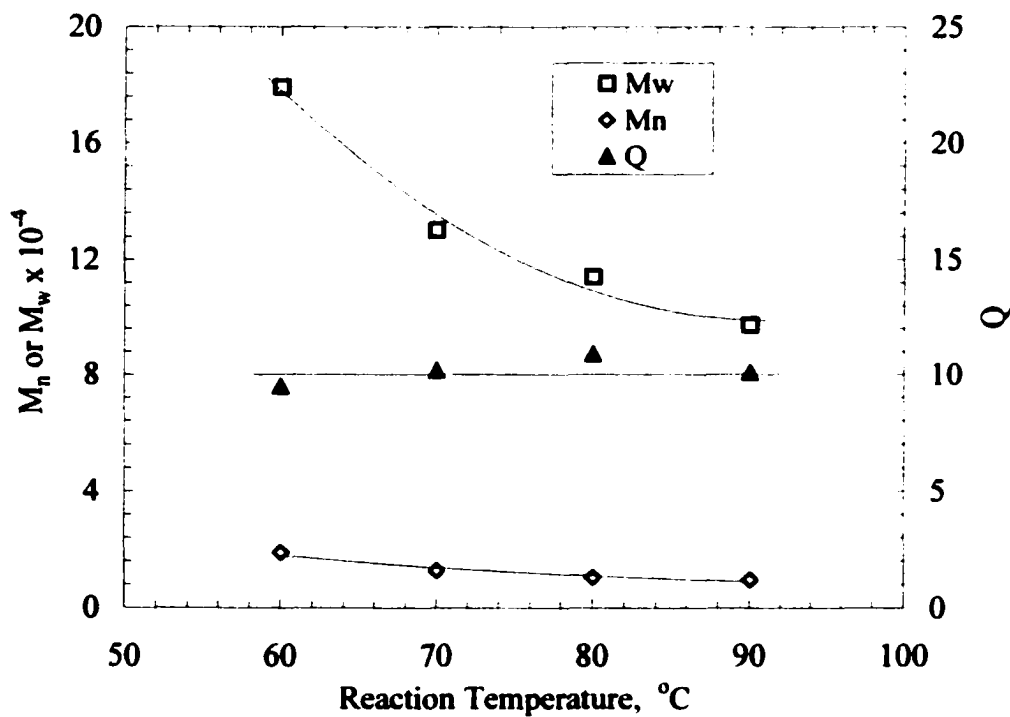


Figure 7.3 Effects of temperature on molar mass and polydispersity. (Runs GasCo60, 62, 64, and 65).

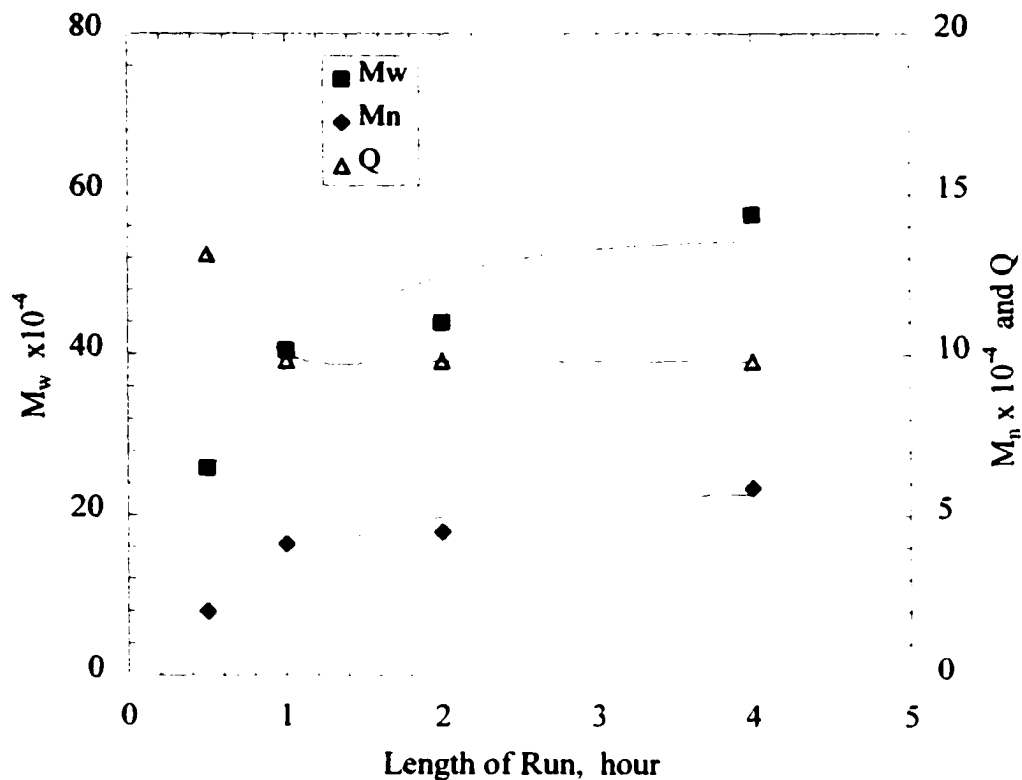


Figure 7.4 Effects of run lengths on M_n , M_w and polydispersity. (Runs GasCo54, 0.5 h; GasCo57, 1 h; GasCo46, 2 h; GasCo58, 4h).

7.2 Chemical Composition of LLDPE

Chemical composition, e.g. comonomer content and its distribution, is very important feature for LLDPE. The 1-hexene was measured by ^{13}C -NMR and TREF was used to examine the comonomer distribution in copolymer.

7.2.1 Results from ^{13}C -NMR Measurement

The average 1-hexene content in polymer as a function of 1-hexene pressure during polymerization is plotted in Figure 7.5. The results in Figure 7.5 show that at high ethylene pressures (e.g. 150 psi), the 1-hexene incorporation rate is proportional to the 1-hexene pressure. However, at low ethylene pressure (e.g. 60 psi), the 1-hexene incorporation rate is a more complex function of 1-hexene pressure. A power law function with an order of 1.48 provides a reasonable fit for the behavior at 60 psi ethylene (see Figure 7.5).

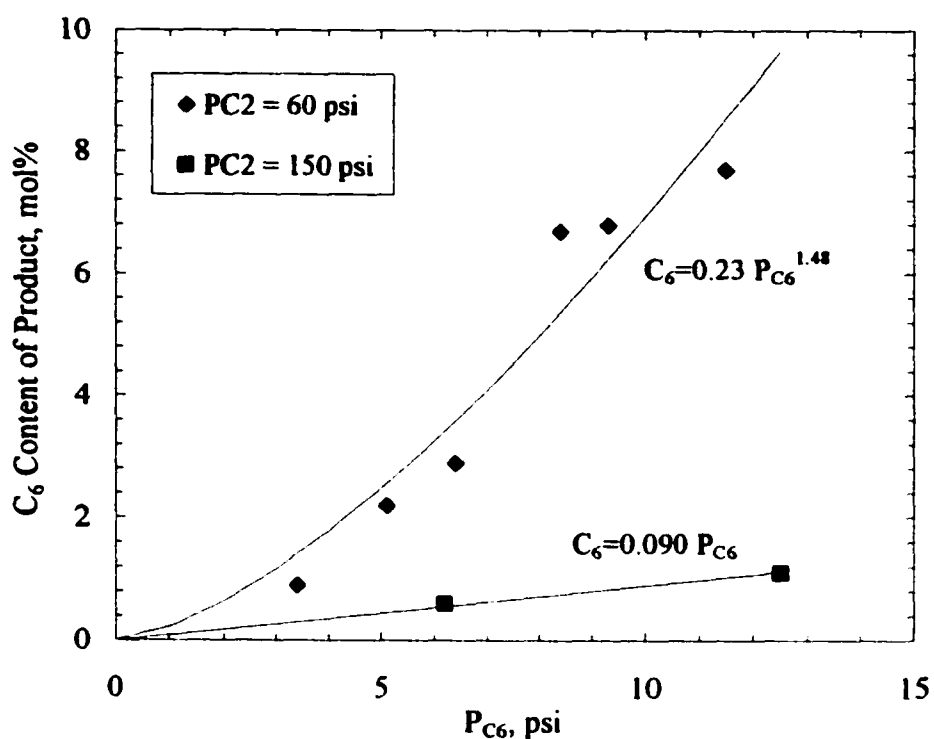


Figure 7.5 1-Hexene content of the product as a function of 1-hexene pressure in the reactor.

The effect of hydrogen on 1-hexene content in the polymer is shown in Figure 7.6. Introduction of hydrogen led to a sharp increase of 1-hexene incorporation into the copolymer. However, increases in the concentration of hydrogen did not affect the content of 1-hexene in the copolymer. The reason why the presence of hydrogen increase the 1-hexene incorporation rate relative to the ethylene polymerization rate is given in Chapter 6.

The relationship between 1-hexene content and temperature is shown in Figure 7.7. Increases in temperature resulted in decreases in the 1-hexene content in the polymer. This implies that the activation energy for 1-hexene propagation is less than the activation energy for ethylene propagation (see Figure 6.20).

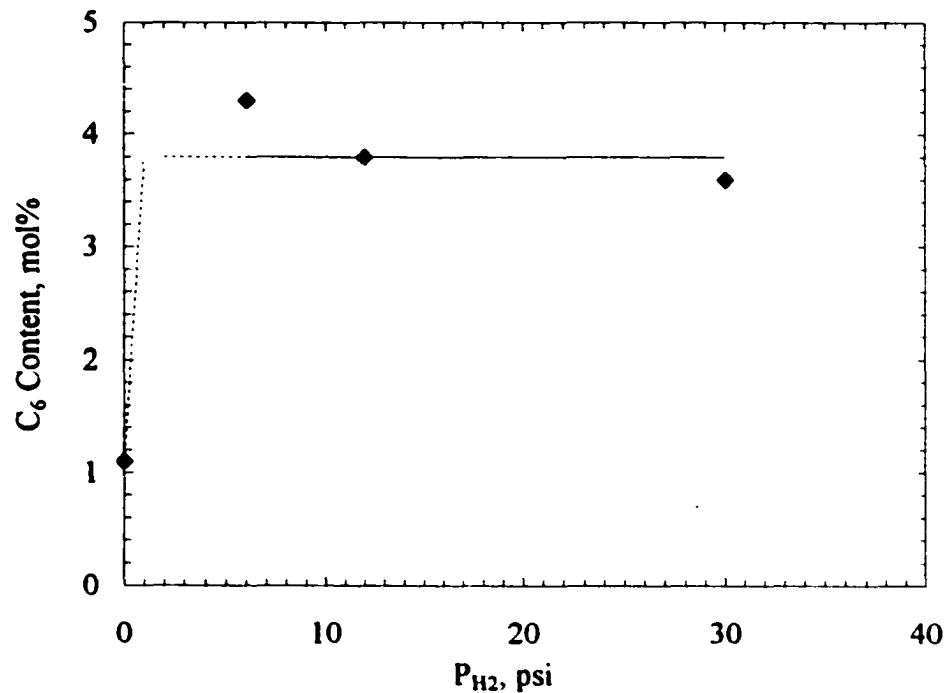


Figure 7.6 1-Hexene content in the copolymer as a function of hydrogen pressure.

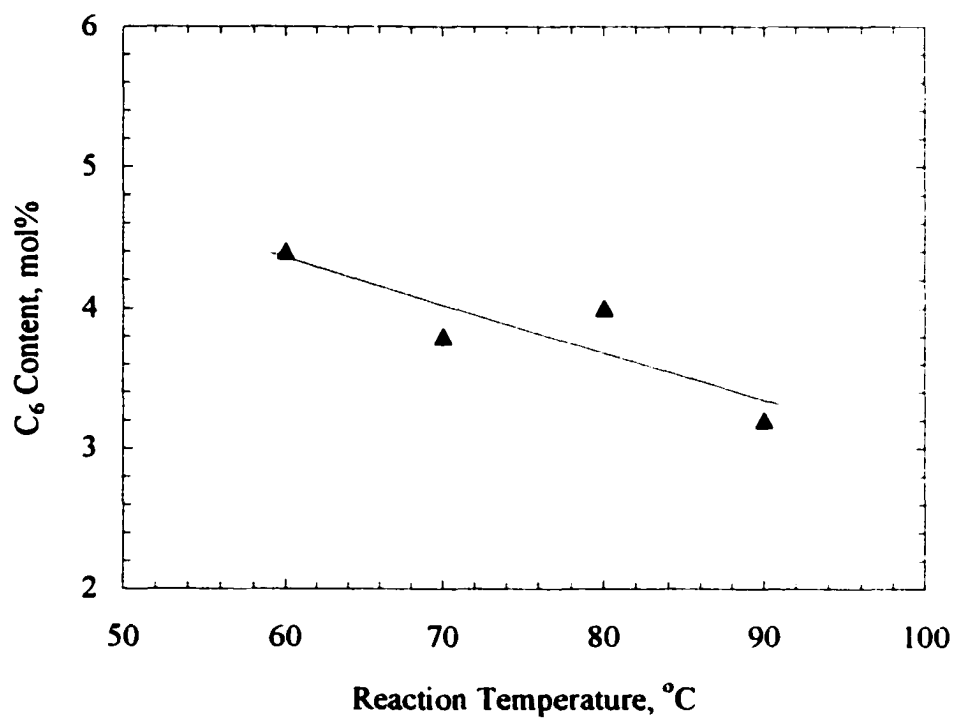


Figure 7.7 1-Hexene content in the copolymer as a function of reaction temperature.

7.2.2 1-Hexene Distribution in Polymer from TREF Analyses

TREF was used to measure comonomer composition distribution of some copolymers produced at 60 psi of ethylene pressure. The results are shown in Figure 7.8. In Figure 7.8, all profiles are characterized by a very distinctive sharp peak at homopolymer range together with a very weak, high branching tail toward lower elution temperature. Compared with TREF results of Ziegler-Natta LLDPEs by other researchers (Zhang et al., 2000; Usami et al., 1986; Glockner, 1990), the lack of the copolymer peak in the current TREF profiles indicates the low incorporation of 1-hexene into the copolymer.

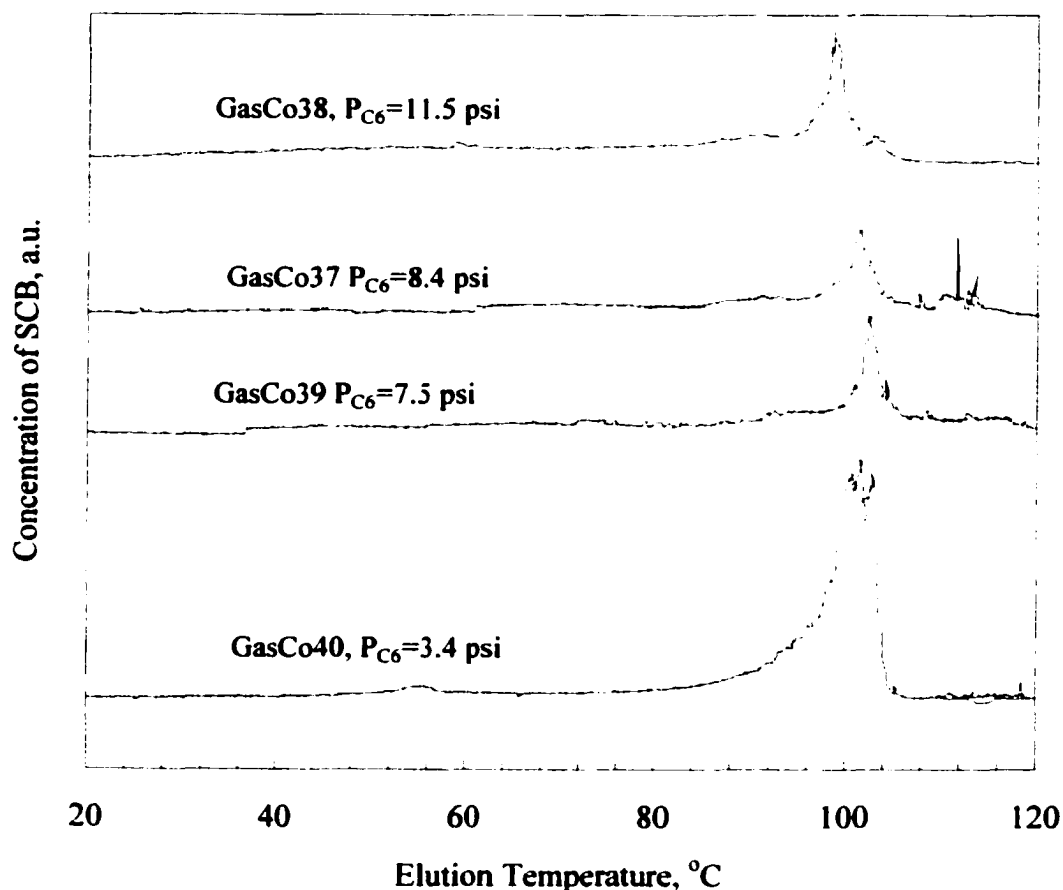


Figure 7.8 Short chain branch distribution (SCBD) of copolymers produced under ethylene pressure of 60 psi and different 1-hexene pressures

The samples analyzed by TREF were also measured by ^{13}C -NMR and the results are compared in Figure 7.9. The calculation of average SCB content followed the method

described by Zhang (1999). It can be seen from this figure that at low 1-hexene content (i.e. low SCB content), the results for TREF and NMR were comparable. At high SCB content, the values from ^{13}C -NMR measurement were much larger than those from TREF. The probable reason for the difference in ^{13}C -NMR and TREF results is that a large amount of the 1-hexene is present in a small fraction of the PE and this results in a high branch concentration for this fraction. If the 1-hexene content is very high, larger than 50 methyls per 1000 carbon atoms (Wild, et al., 1982) or as high as 20 mole percent (70 $\text{CH}_3/1000\text{C}$, Woo et al., 2000), then molecules will not be crystallized and thus are not detected by TREF. It was found that about one-third of PE sample made at 70°C , 9.3 psi of 1-hexene at 62 psi ethylene (GasCo36) was soluble in 1,2,4-trichlorobenzene at room temperature. The soluble fraction contained 30 mol% 1-hexene. More detailed analysis of this sample are described in Section 8.1. The comonomer content of PE can also be underestimated by TREF if the intramolecular branch distribution is very heterogeneous since TREF separates polymer molecules according to their longest unbranched sequences and not according to the average branch content.

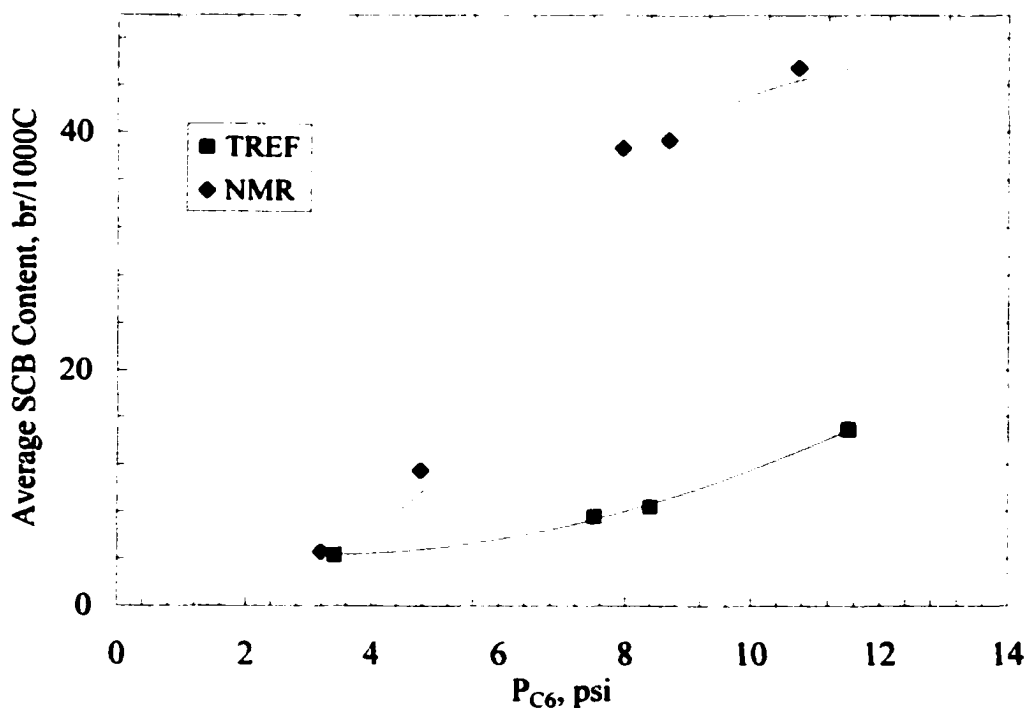


Figure 7.9 Comparison of average SCB contents measured by ^{13}C -NMR and TREF.

7.3 Crystallinity

Crystallinity is an important LLDPE property. The modulus of ethylene/ α -olefin copolymers has been found not to be determined by the branch distribution and branch type but by the crystallinity (Sehanobish et al., 1994). For most studies of crystallinity, the samples have been prepared using careful conditions, such as slow crystallization from solutions or annealing of melt-crystallized specimens. Study of nascent polyethylene have attracted little attention (Parker et al., 1996). In the current study, the crystallinity of nascent polymer was examined by DSC in order to study the effect of various reaction conditions on the crystallinity of nascent polymer. The analysis procedure and calculation of crystallinity are described in Section 3.4.5.

7.3.1 General Features of DSC Curve

The reaction conditions used to produce nascent LLDPE samples used for DSC studies were summarized in Table 7.2. The melting points of the samples shown in Table 7.2 (128-136°C) are generally higher than those (120-125°C) reported by other researchers for LLDPE (Shanks and Amarasinghe, 2000).

Figure 7.10 shows typical DSC endotherms for the nascent polymers obtained in this study. All curves show a very broad peak from 50°C to 145°C. These broad peaks suggest broad distributions of 1-hexene in the polymers. It is interesting to see that all curves have a single-peak at high temperature. Some investigations have reported bimodal or multi-modal DSC patterns from Ziegler-Natta LLDPEs (Wild et al., 1990; Zhang, 1999; Shanks and Amarasinghe, 2000), which suggested the crystal size or lamella thickness consist of two or more overlapping distributions. The single peak feature is probably due to the low sensitivity of DSC measurement for the sample without thermal treatment before analysis (Zhang, 1999) or the fact that very high 1-hexene content molecules exist only in amorphous phase, as discussed in Section 7.1, which dealt with TREF analyses.

It can be seen in Figure 7.10 that the copolymer with higher 1-hexene content (GasCo38) had a lower melting point than the sample with a lower 1-hexene content (GasCo40).

This is because at higher 1-hexene content, the lamella dimension becomes smaller or crystalline regularity is destroyed due to high branch content. GasCo40 and GasCo42 had similar 1-hexene contents and molar masses while GasCo42 was produced at higher ethylene pressure (150 psi) and GasCo40 was under low ethylene pressure (60 psi). However, the melting point of GasCo42 is higher than GasCo40 but showed lower crystallinity. This result suggests that other unknown factors may also influence the melting point and crystallinity. Introduction of hydrogen (GasCo59) largely reduce the melting point and crystallinity (compared to GasCo42). These reductions are mainly due to higher comonomer content.

Table 7.2 Summary of Reaction Conditions and DSC Analysis Results.*

Run No.	Partial pressures			Reaction Temperature °C	C ₆ Content in Polymer Mol%	melting Point °C	Crystallinity wt%
	P _{H₂} psi	P _{C₂} psi	P _{C₆} psi				
GasCo35	0	60	5.1	70	2.2	132	43.6
GasCo36	0	62	9.3	70	6.8	131	28.6
GasCo37	0	62	8.4	70	6.7	131	35.8
GasCo38	0	65	11.5	70	7.7	131	30.4
GasCo40	0	60	3.5	70	0.9	135	58.0
GasCo42	0	150	12.5	70	1.1	136	53.4
GasCo44	0	150	6.2	70	0.6	139	58.9
GasCo59	30	150	12.0	70	4.0	129	43.2
GasCo60	12	150	12.0	70	3.8	130	43.3
GasCo61	6	150	12.0	70	4.3	130	43.6
GasCo62	15	150	11.8	60	4.4	129	41.7
GasCo64	12	150	12.4	80	4.0	128	43.2
GasCo65	13	150	12.4	90	3.2	129	40.0

* Other conditions: TEA = 0.25-0.27 mL, Length of runs = 2 h.

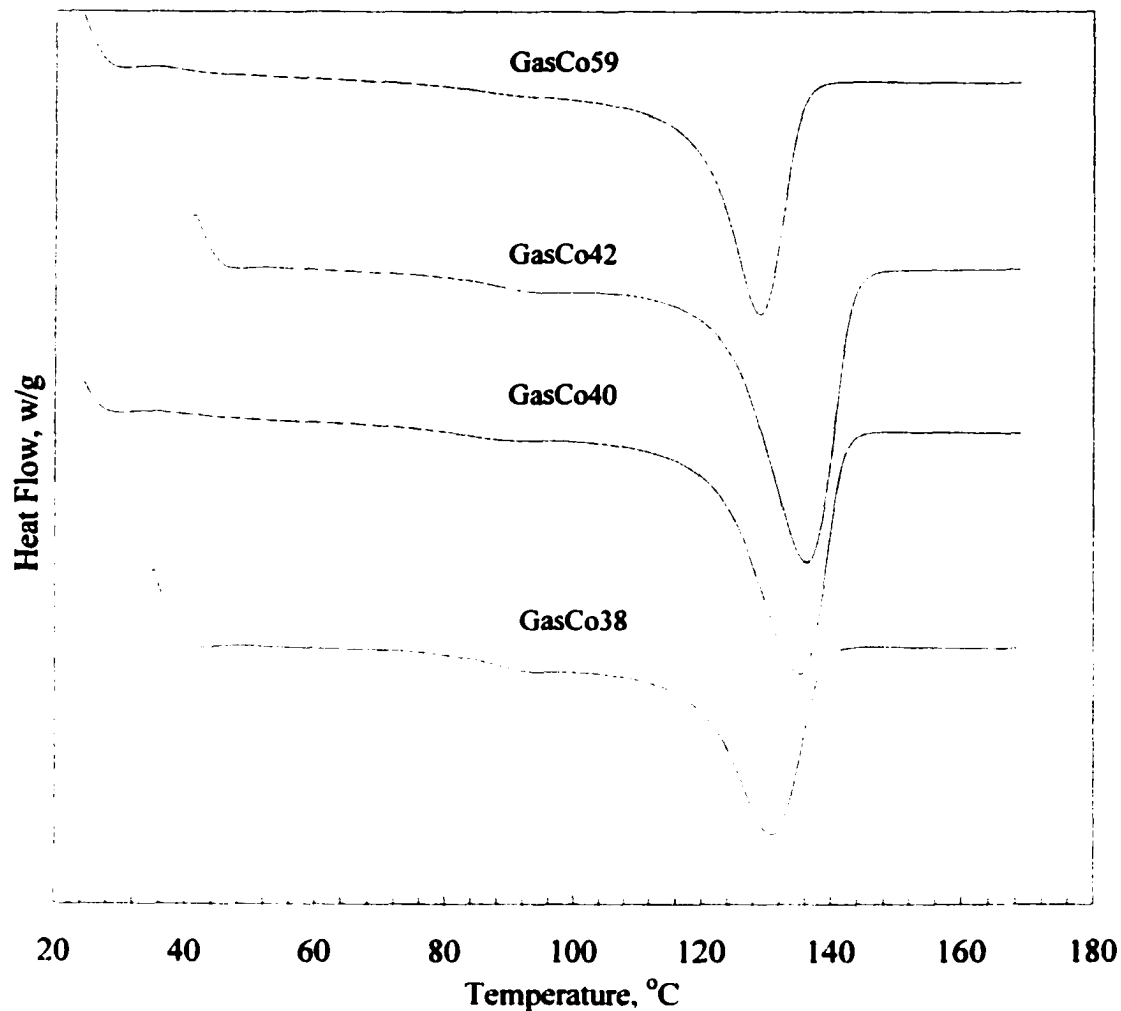


Figure 7.10 DSC endotherms of nascent LLDPE samples.

7.3.2 Effects of Comonomer Concentration

The relationship between comonomer concentration in copolymer and crystallinity χ_c is discussed in this section. The results are shown in Figure 7.11. All samples examined were polymerized under ethylene pressure of 60 psi but at different 1-hexene pressures. It can be seen in Figure 7.11 that crystallinity was lower at high 1-hexene contents.

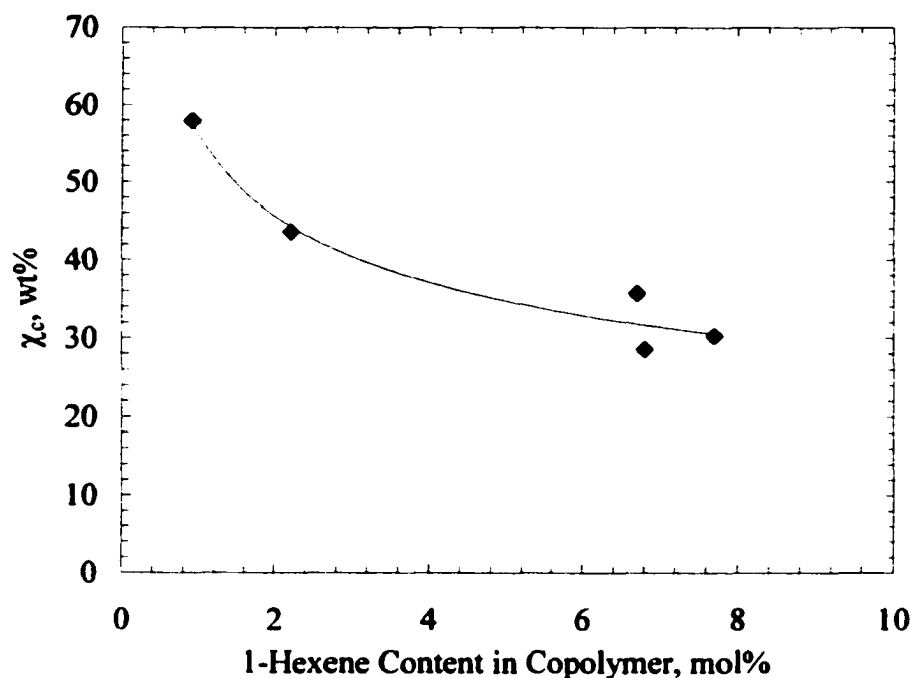


Figure 7.11 Dependence of crystallinity on 1-hexene content in polymer.

7.3.3 Effects of Hydrogen

Hydrogen has been found to have significant effects on molar mass and comonomer content in polymer. Its influence on copolymer crystallinity is shown in Figure 7.12. Copolymer crystallinity decreased with the introduction of hydrogen, but the crystallinity is not a function of hydrogen concentration. This is because the introduction of hydrogen increased comonomer incorporation in copolymer, reduces crystallinity of copolymer. Since the 1-hexene content in copolymer was not a function of hydrogen concentration as discussed in previous section, the crystallinity is also independent of hydrogen concentration.

7.3.4 Effects of Temperature

It is known from Figure 7.7 that the 1-hexene content in copolymer decreased with the increase of reaction temperature. DSC analyses however, showed that the polymer crystallinity was independent of reaction temperature (see Figure 7.13). This result suggests that besides the content of comonomer in the polymer, reaction condition is also an important factor in affecting nascent polymer crystallinity.

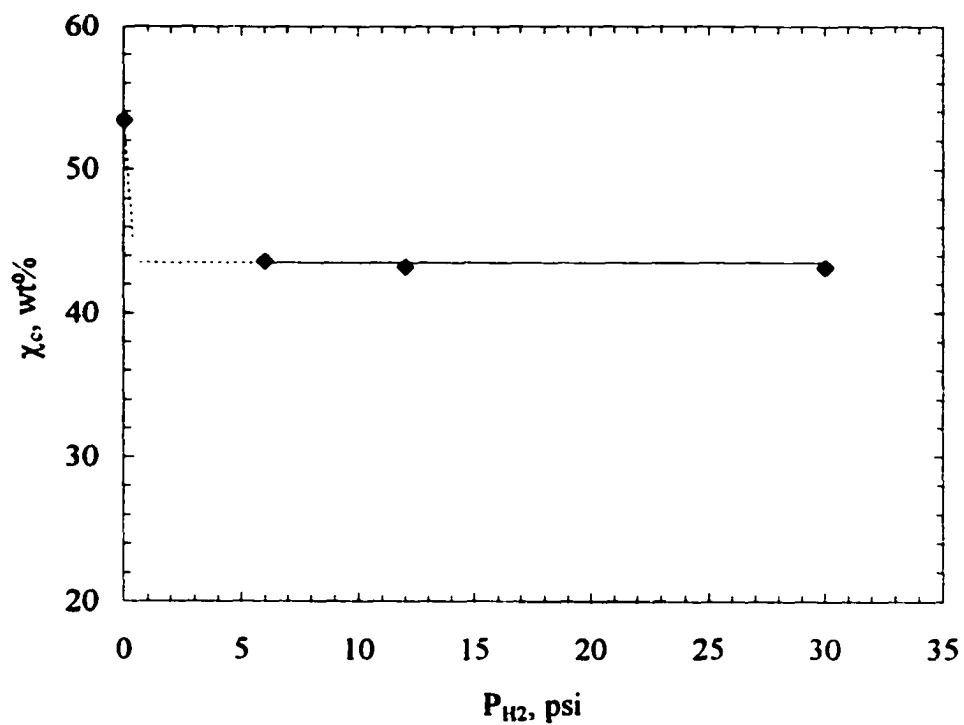


Figure 7.12 Dependence of crystallinity on hydrogen.

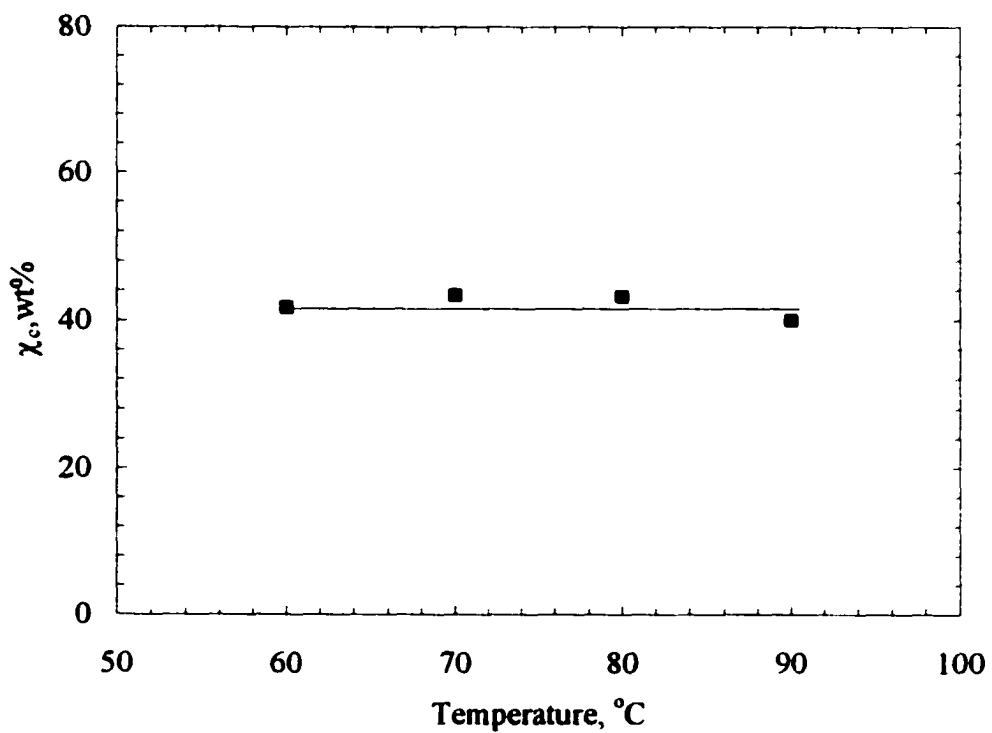


Figure 7.13 Dependence of crystallinity on reaction temperature.

7.4 Solubility

Reactants (ethylene and 1-hexene) have to dissolve in the polymer phase before they interact with catalytic sites and participate reactions. As a result, the concentrations of monomer/comonomer in polymer phase are very important in the describing copolymerization kinetics. In the current study, solubilities of ethylene and 1-hexene were measured, the non-linear behavior of 1-hexene sorption was modeled, and co-sorption of ethylene/1-hexene mixtures were estimated.

7.4.1 Solubilities of Ethylene and 1-Hexene in Nascent Polymer

The solubilities of pure hexene and ethylene were measured in nascent polymer from run GasCo38. The solubility of ethylene in GasCo38 as a function of temperature and pressure is shown in Figure 7.14. It is seen that the solubility of ethylene has linear relationship with ethylene pressure (Henry's law) and the solubility at higher temperature is consistently lower than the solubility at lower temperature.

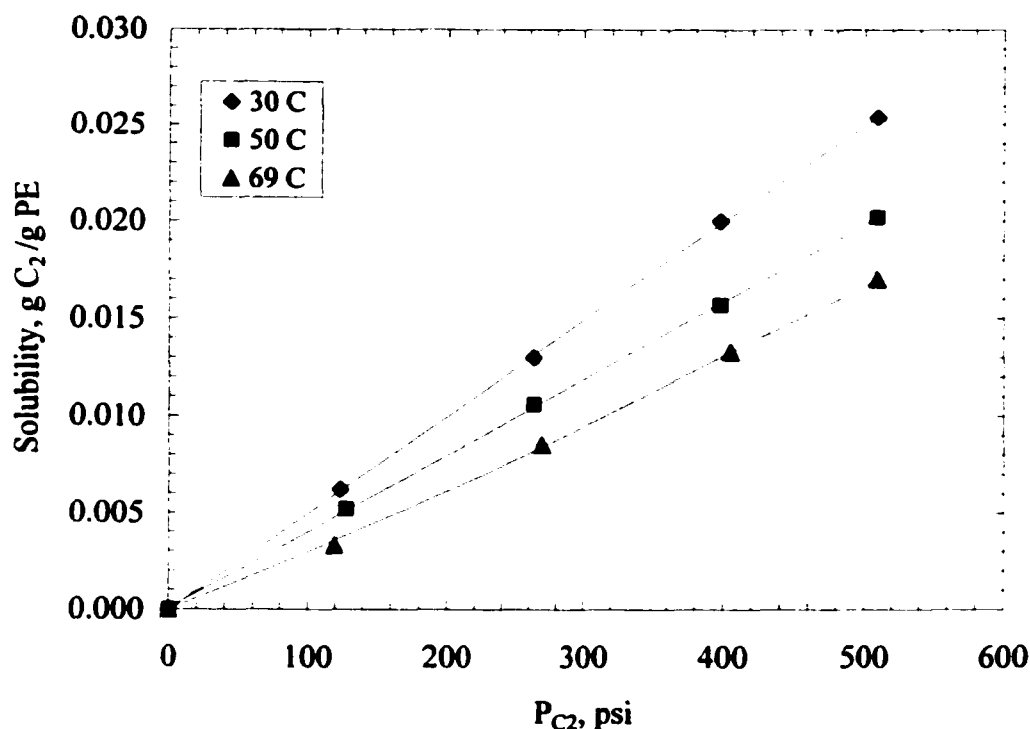


Figure 7.14 Solubility of ethylene in GasCo38 as a function of ethylene pressure at different temperatures.

Figure 7.15 shows the solubility of 1-hexene in the GasCo38 polymer; the behavior of 1-hexene was quite different than that of ethylene. The solubility of 1-hexene increased sharply at high 1-hexene pressure; this observation is consistent with previous results (Moore and Wanke, 2001). This phenomenon is probably due to the non-ideal behavior of 1-hexene in PE as the 1-hexene pressure approaches its vapor pressure.

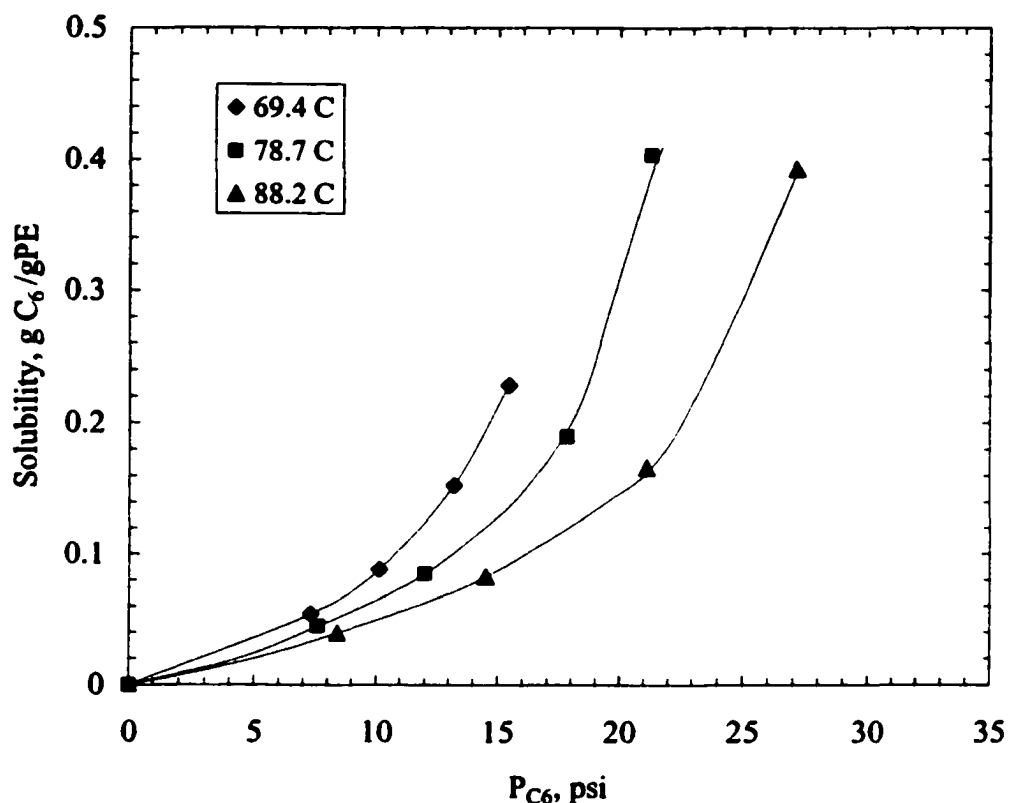


Figure 7.15 Solubility of 1-hexene in GasCo38 as a function of 1-hexene pressure at different temperatures.

It is usually assumed that the solubility of monomers only occurred in the amorphous part of polymer (Micheals and Bixer, 1961; Hutchinson and Ray, 1990). Previous work done by Moore (Moore, 2000; Moore and Wanke, 2001) clearly showed that the solubilities of ethylene and 1-hexene do not only depend on the amorphous content of polymers, but also are dependent on other factors such as polymer type (e.g. HDPE, LDPE and LLDPE). Hence, the unit of solubility used in the current study is the total 1-hexene amount adsorbed per unity mass of polymer. The solubilities of 1-hexene in GasCo38 and

other commercial polyethylenes at 69°C are compared in Figure 7.16. The solubility for GasCo38 was similar to 1-butene LLDPE made with Ziegler-Natta catalysts and much lower than that of 1-hexene LLDPE made with metallocene catalysts.

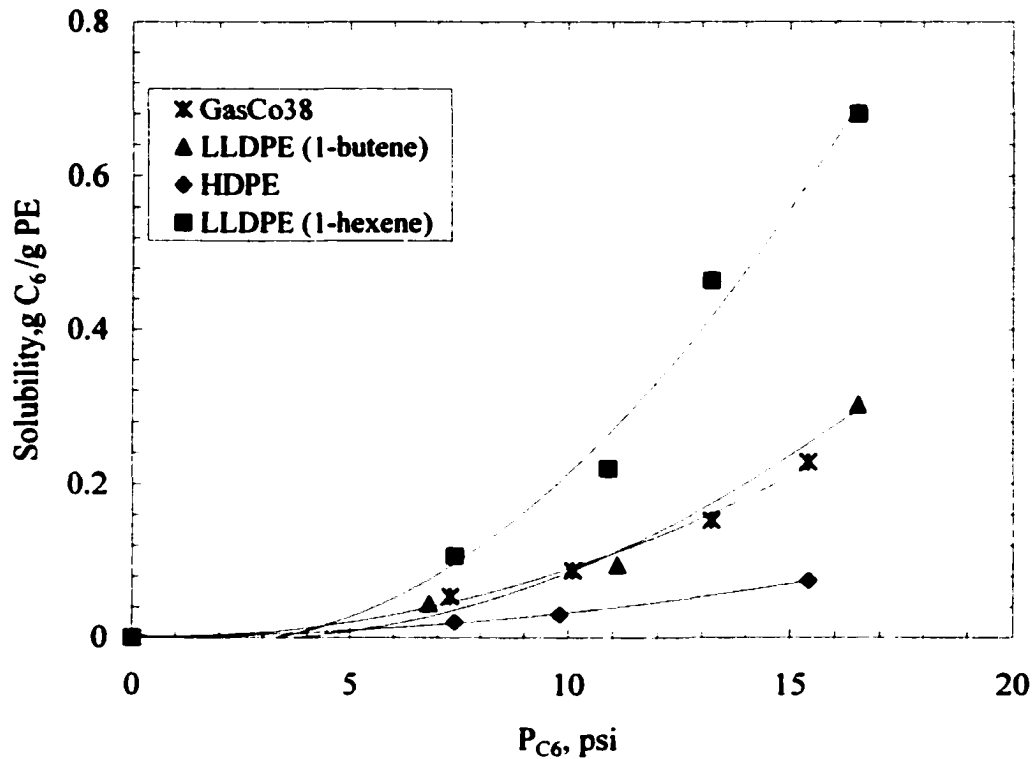


Figure 7.16 Comparison of the 1-hexene solubilities of commercial polyethylenes and GasCo38 at 69°C. The data of commercial polyethylene are obtained from Moore (2000).

7.4.2 Modeling of Ethylene and 1-Hexene Concentration in Polymer

The validity of Henry's law to the sorption of ethylene in polyethylenes has been confirmed by many researchers (Michaels and Bixler, 1961; Beret and Hager, 1979; Huchinson and Ray, 1990; Moore and Wanke, 2001). The reason for measuring the ethylene solubility in this study was to determine Henry's constant for a nascent polymer since the constant determined by other researchers may not be suitable for the polymer synthesized in this work.

As shown by the result in Figure 7.16, Henry's law is not applicable for heavier hydrocarbons at high pressures. In this case, Flory-Huggins theory can be applied. In this study, solubility is regarded independent of molar mass because, according to Michaels and Bixler (1961), solubility is independent of molar mass if $M_n > 6000$.

The Consistency of Henry's Law and Flory-Huggins Theory for Ethylene Solubility Study

The Henry's law can be written as

$$S = k^* P \quad (7.2)$$

where S (g C₂/g PE) is the solubility of ethylene, k^* is Henry's constant and P is the ethylene partial pressure. Fitting the data at 69°C in Figure 7.14, yields $k^* = 3.31 \times 10^{-5}$ g C₂/(g PE-psi).

Henry's law can be treated as a simplified form from Flory-Huggins theory. The general Flory-Huggins equation has the form (Flory, 1953)

$$\ln a = \ln \left(\frac{f}{f^0} \right) = \ln \phi + (1 - \phi) + \chi(1 - \phi)^2 \quad (7.3)$$

where a is the activity of the penetrant, f^0 is the fugacity at standard state, ϕ is the volume fraction of the penetrant in the polymer and χ is the Flory-Huggins interaction parameter for solvent. Ethylene, at the conditions of the current studies, behaves as an ideal gas (i.e. $a = P/P^0$) and the amount of ethylene sorbed is small ($\phi \ll 1$). Under these conditions, Equation 7.3 becomes

$$\ln \frac{P}{P^0} = \ln \phi + 1 + \chi \quad (7.4)$$

which is equal to

$$\phi = \frac{P}{P^0 \cdot e^{(1+\chi)}} = k^* P \quad (7.5)$$

P^0 is the pressure at standard state and usually is chosen as 1 bar. Equation 7.5 is Henry's law since $P^0 e^{(1+\chi)}$ is a constant if χ is constant.

Modeling of 1-Hexene Solubility by Flory-Huggins Theory and Peng-Robinson Equation of State

The Florry-Huggins equation and the Peng-Robinson Equation of State were used to model sorption results of 1-hexene shown in Figure 7.15. The Equation of State is used to calculated thermodynamic properties in the gas phase (e.g. fugacity) but cannot be used in the polymer phase because 1-hexene dissolved in LLDPE is not a liquid mixture. The fugacity f of 1-hexene in the gas phase according to the Peng-Robinson Equation (Peng and Robinson, 1976) is given by:

$$\ln \frac{f}{P} = Z - 1 - \ln(Z - B) - \frac{A}{2\sqrt{2}B} \ln\left(\frac{Z + 2.414B}{Z - 0.414B}\right) \quad (7.6)$$

$$A = \frac{aP}{R^2T^2}$$

$$B = \frac{bP}{RT}$$

$$Z = \frac{Pv}{RT}$$

$$\alpha = 0.45724 \frac{R^2T_c^2}{P_c} \left[1 + (0.37464 + 1.54226\omega - 0.2699\omega^2) \cdot (1 - T_r^{0.5}) \right]^2$$

$$b = 0.0778 \frac{RT_c}{P_c}$$

Where $T_c = 508.5\text{K}$ and $P_c = 3160 \text{ kPa}$ are the critical properties of 1-hexene. The acentric factor ω for 1-hexene given by Yaws (1992) is 0.285. The molar volume v is estimated by another expression of P-R equation, i.e.

$$P = \frac{RT}{v - b} - \frac{\alpha}{v(v + b) + b(v - b)} \quad (7.7)$$

The volume fraction occupied by sorbed 1-hexene in polymer containing sorbed 1-hexene, ϕ , is defined as

$$\phi = \frac{V_{C_6}}{V_{PE} + V_{C_6}} = \frac{V_{C_6}}{V_{Total}} \quad (7.8)$$

where V_{C6} and V_{PE} are the volumes of sorbed 1-hexene and the volume of the polymer. Moore (2000) measured the volume changes for the sorption of 1-hexene in various polyethylenes. The results from Moore for a polyethylene made with Ziegler-Natta catalyst, which had similar sorption behavior to as the GasCo38 sample from the current work (see Figure 7.16), showed that the relationship between amount of 1-hexene sorbed and total volume is well described by

$$V_{Total} = V_o (1+S) = V_{PE} (1+S) \quad (7.9)$$

where S is the solubility of 1-hexene in the polymer in (g of 1-hexene)/(g of polymer) and V_o is the initial volume of the polymer, i.e. V_{PE} . Replacing V_{C6} by $(V_{Total} - V_{PE})$ and substituting for V_{PE} from Equation 7.9 yields

$$\phi = \frac{S}{1+S} \quad (7.10)$$

i.e. the specific volumes per unit mass of 1-hexene and polyethylene are essentially equal.

Substituting Equation 7.10 into Equation 7.3 yields

$$\ln a = \ln \frac{f}{P^o} = \ln\left(\frac{S}{1+S}\right) + \frac{1}{1+S} + \chi \left(\frac{1}{1+S}\right)^2 \quad (7.11)$$

Equation 7.11 is a relationship between fugacity of the 1-hexene in the gas phase, which can be estimated from Equation 7.6, the solubility of 1-hexene in the polymer and the interaction coefficient of sorbed 1-hexene and the polymer, χ . The reference pressure, P^o , is taken as the saturation pressure of 1-hexene at the temperature at which the solubility was measured.

The solubility results shown in Figure 7.15, were used to calculate the interaction parameter, χ , as a function of adsorption conditions (1-hexene pressure and temperatures). The results are plotted in Figure 7.17. These results show that χ is essentially independent of temperature, but decreases linearly with increasing 1-hexene pressure.

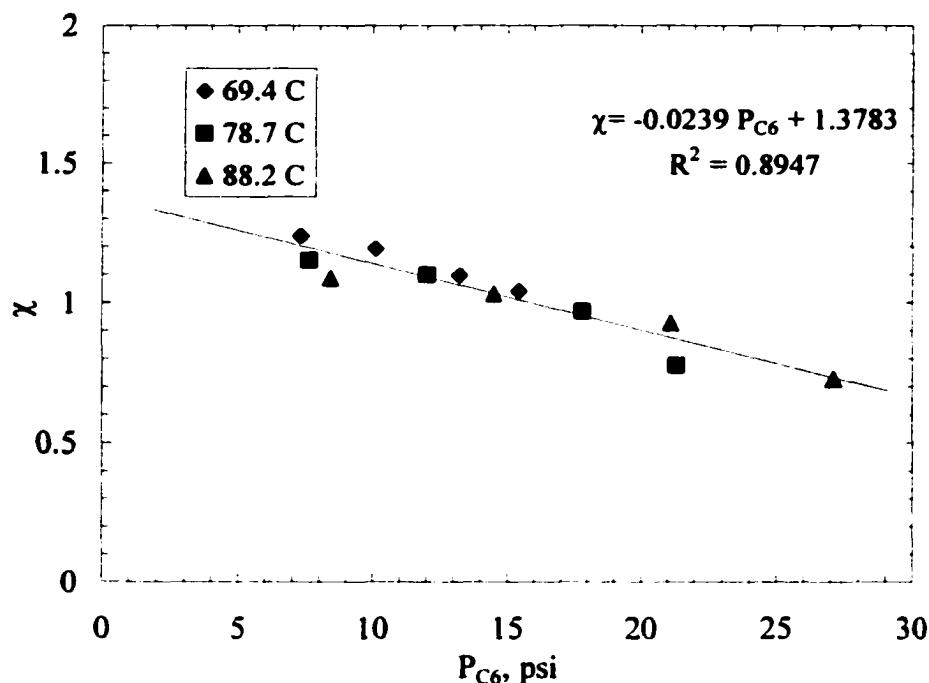


Figure 7.17 Flory-Huggins interaction parameter as a function of 1-hexene pressure.

The solubility of 1-hexene as a function of 1-hexene pressure can now be calculated using Equation 7.11, the Peng-Robinson equation and the fitted dependence of χ on 1-hexene pressure. The results of this fit by the combination of the Flory-Huggins and Peng-Robinson equations are shown in Figure 7.18; the fit is excellent.

7.4.3 Co-solubility Estimation

Previous study (Moore and Wanke, 2001) showed that the co-sorption behavior of ethylene /1-hexene mixture in the polymer sample was significant and quite different from the solubilities measured under pure ethylene or 1-hexene conditions. However, the quantitative measurement of co-solubility was not done by Moore and Wanke. In this study, the co-solubility was indirectly estimated from the data gathered during the kinetic experiments and the ^{13}C -NMR analyses of the products.

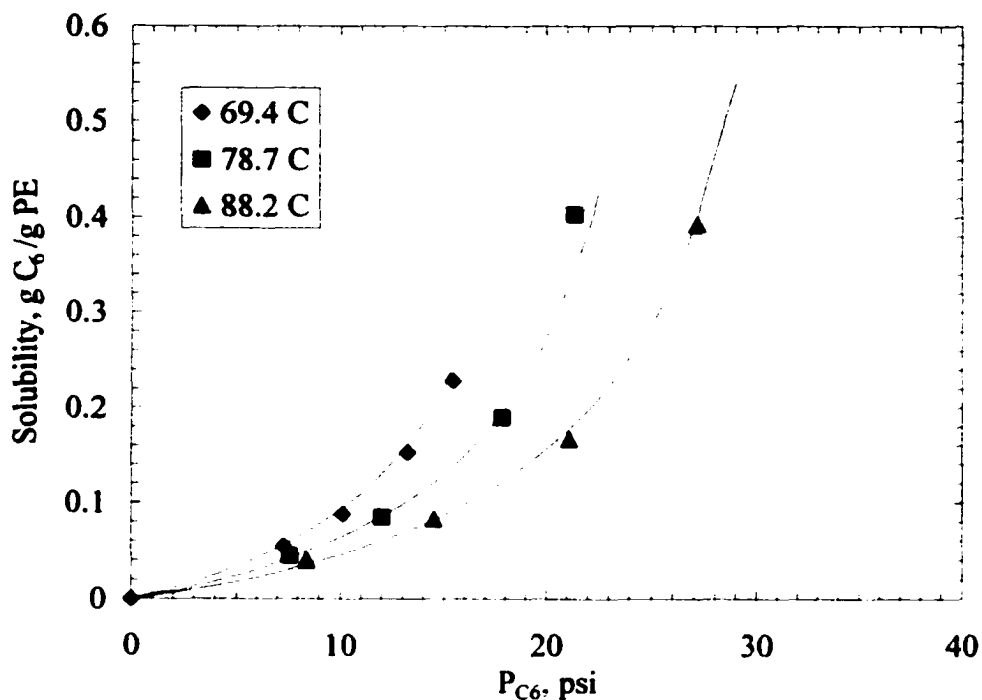


Figure 7.18 Experimental results and Florry-Huggins/Peng-Robinson simulations for 1-hexene solubility at different pressures and temperatures for GasCo38.

The amount of 1-hexene sorbed in the polymer in the reactor can be estimated from the measured amount of 1-hexene added during an experiment, the measured 1-hexene content of the product (as obtained by ¹³C-NMR), the change in the amount of 1-hexene in the gas phase between the beginning and the end of the run, and the amount of 1-hexene removed from the reactor in the GC sample stream. The procedure for these calculations is illustrated in Appendix C. The calculated amounts of 1-hexene sorbed in the products made at different 1-hexene and ethylene pressures are plotted in Figure 7.19; the measured solubilities for pure 1-hexene vapor by the product from run GasCo38 is included for comparison. The higher solubilities of 1-hexene in the products made at 60 psi ethylene compared to those for products made at 150 psi ethylene pressure is understandable since the crystalline of the products made 150 psi is higher than those made at 60 psi ethylene. However, the reason for the higher solubility of 1-hexene in the presence of 60 psi ethylene compared to the solubility without the presence of ethylene is not known. Separate experiments, using nascent polymer in the absence of reaction,

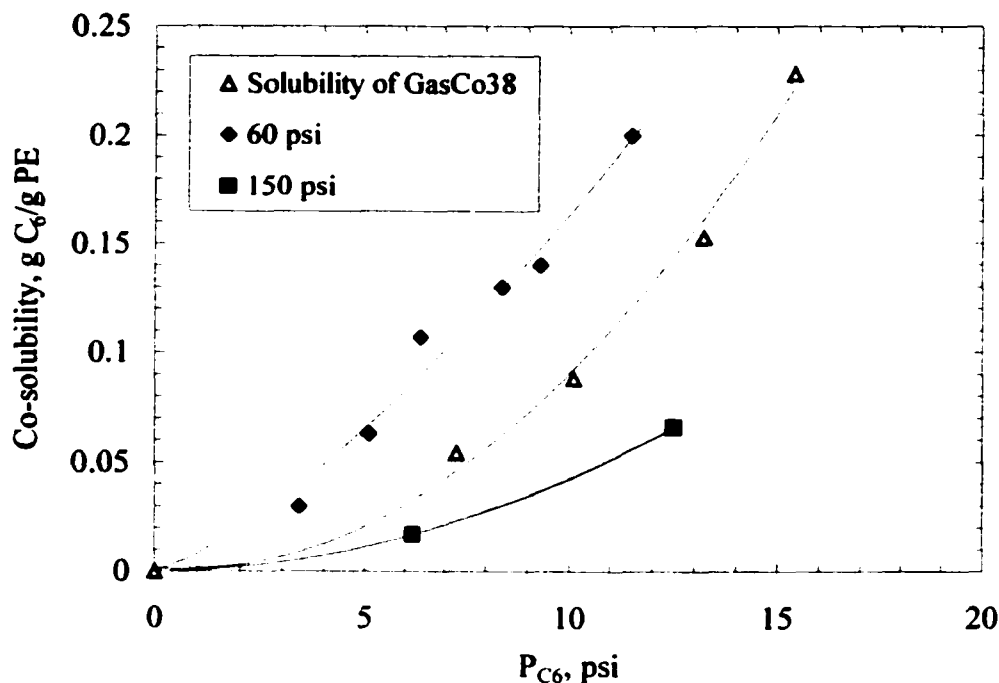


Figure 7.19 Comparison of calculated co-solubility of 1-hexene in polymers and the measurement solubility of 1-hexene in GasCo38.

should be done to verify or refute that indirect estimates of the high 1-hexene solubility in the presence of ethylene.

The solubilities in Figure 7.19 are plotted as a function of P_{C_6}/P_{C_2} ratio in Figure 7.20 rather than as a function of 1-hexene pressure. It is interesting to find that the results for the two ethylene pressures fell on the same line. This implies that the solubility of 1-hexene in the copolymer during the runs depends on the 1-hexene/ethylene ratio in gas phase and not on 1-hexene pressure. This observation is used in the modeling presented in Chapter 8.

The solubility of 1-hexene in the presence of hydrogen and ethylene is shown in Figure 7.21. The 1-hexene solubility increased with the presence of hydrogen because the increase in 1-hexene content reduces crystallinity of polymer (see Figures 7.6 and 7.12). The 1-hexene solubility increased with increasing of hydrogen concentration in the reactor. The reason for this is not clear since the 1-hexene content and crystallinity of the

polymer did not increase with increases in hydrogen pressure from 6 to 30 psi (see Figures 7.6, 7.12).

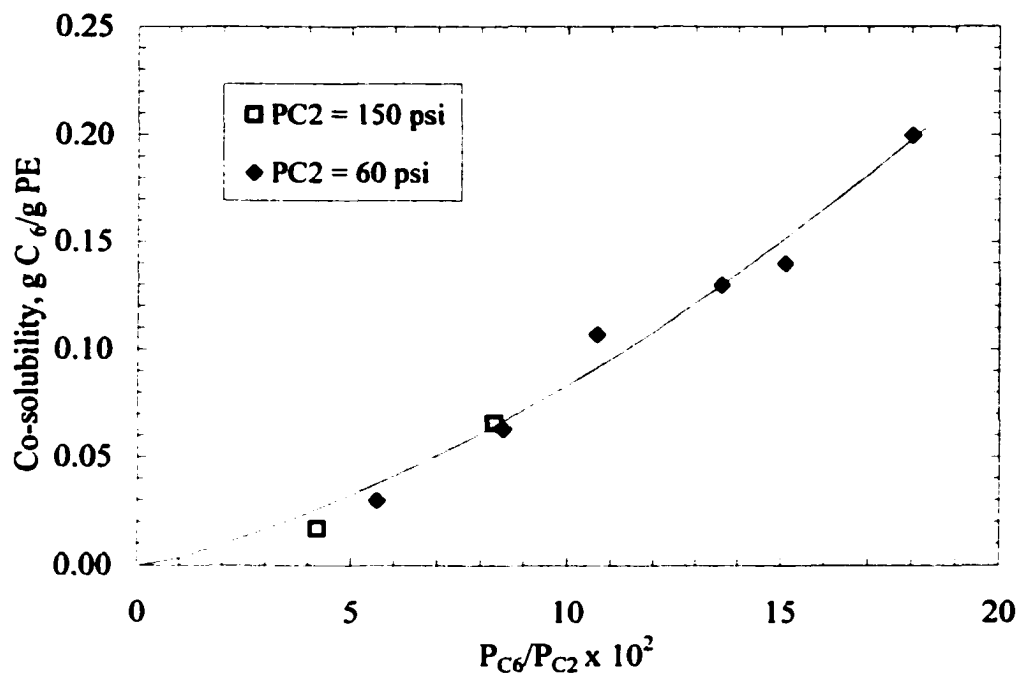


Figure 7.20 Co-solubility of 1-hexene in the product based on 1-hexene/ethylene ratio.

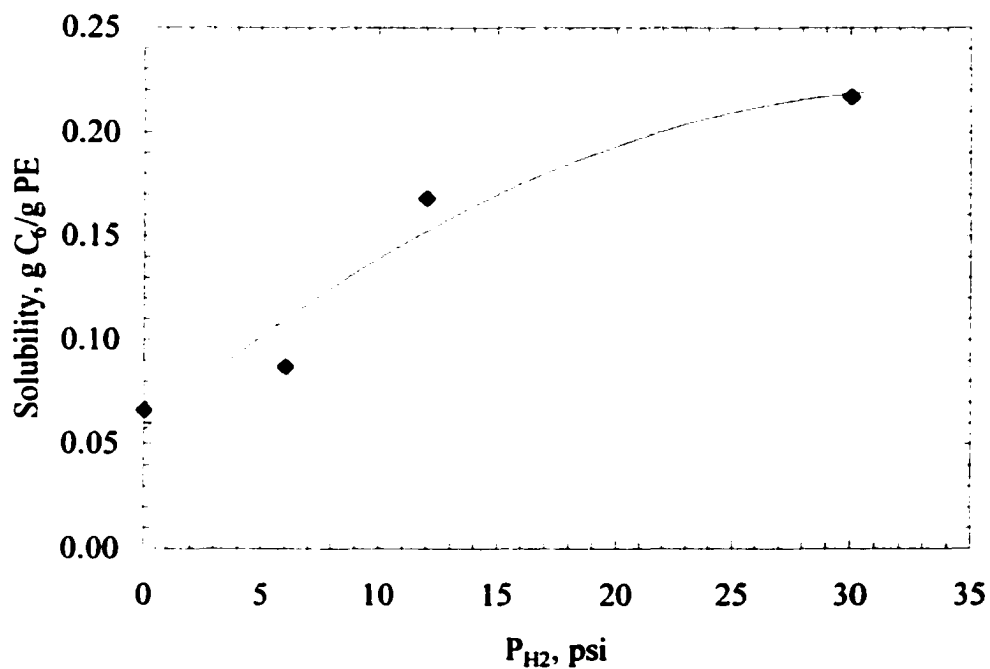


Figure 7.21 Co-solubility of 1-hexene in the presence of hydrogen.

Increases in temperature resulted in increases in the calculated co-solubility of 1-hexene (see Figure 7.22). The co-solubility increased with the increase of temperature even though the polymers produced at high temperature had lower 1-hexene incorporation in polymer (see Figure 7.7). This trend is also contrary to the measured 1-hexene solubilities in the absence of ethylene (see Figure 7.15). These observations again emphasize the need for “measured” rather than “inferred” solubilities of olefins from gas mixtures.

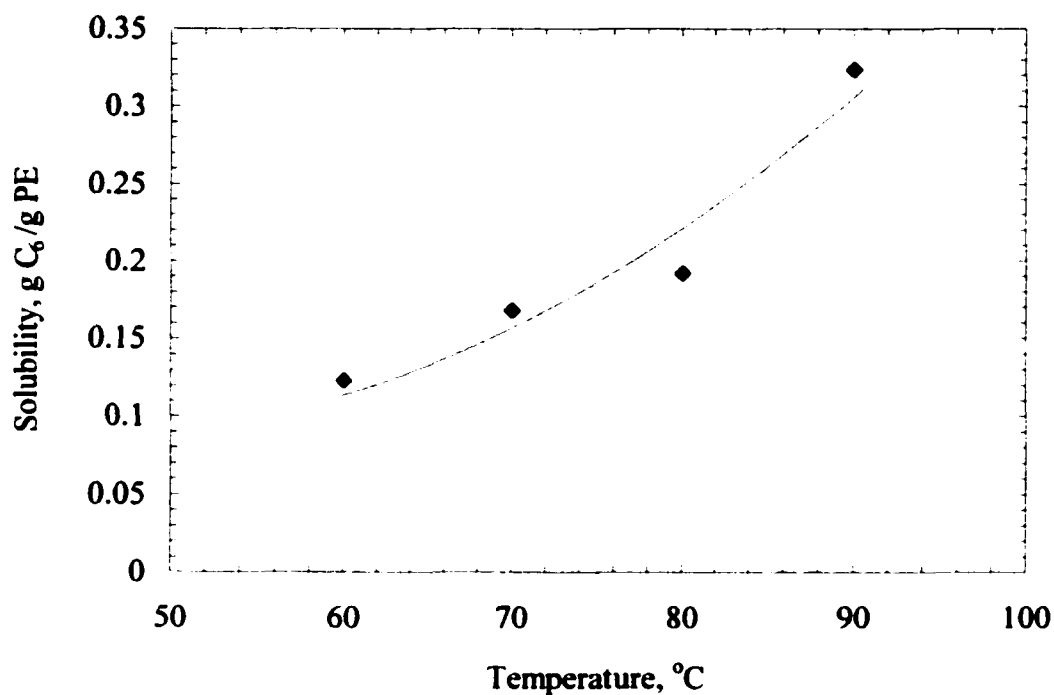


Figure 7.22 Co-solubility of 1-hexene at different reaction temperatures.

CHAPTER 8. KINETIC INTERPRETATION OF ETHYLENE/ 1-HEXENE COPOLYMERIZATION

Kinetic modeling is useful in understanding reaction behaviors and optimizing industrial operation conditions. Numerous kinetic models have been proposed for Ziegler-Natta polymerizations (see Chapter 2); the emphasis in these models has been on the kinetic behaviors for slurry copolymerization. The multi-site model, common used for supported Ziegler-Natta catalysts, will also be used in the current study.

In Section 8.1, a discussion about multi-site nature of catalysts is given. Reaction schemes and mathematical model are presented in Section 8.2. In Section 8.3 the model fitting process, the obtained kinetic parameters and the simulation results are presented. In the final section, some comments on the model are given.

8.1 Multiple Site Nature

The multiple-site nature of Ziegler-Natta catalysts has usually not been based on kinetic measurements but has been based on broad molar mass distribution and bimodal characteristics in TREF profiles. In this study, the multiple-site nature of catalysts is based on the measured ethylene and 1-hexene polymerization rates. The usual broad and multi-peak molar mass distributions were also observed in the product.

Figure 8.1 shows an 8-hour homopolymerization rate profile, the reaction rate reached a maximum almost immediately after ethylene was introduced at the beginning of the reaction; this was followed by a decrease in activity for about 2.5 hours, and then the rate increased again. A second maxima in rate appeared after 6 hours of polymerization. This phenomenon suggests at least two sites exist in the catalyst; one is activated rapidly and one is activated very slowly. This experimental finding is consistent with the observation of previous work in our group (Wu et al., 1999).

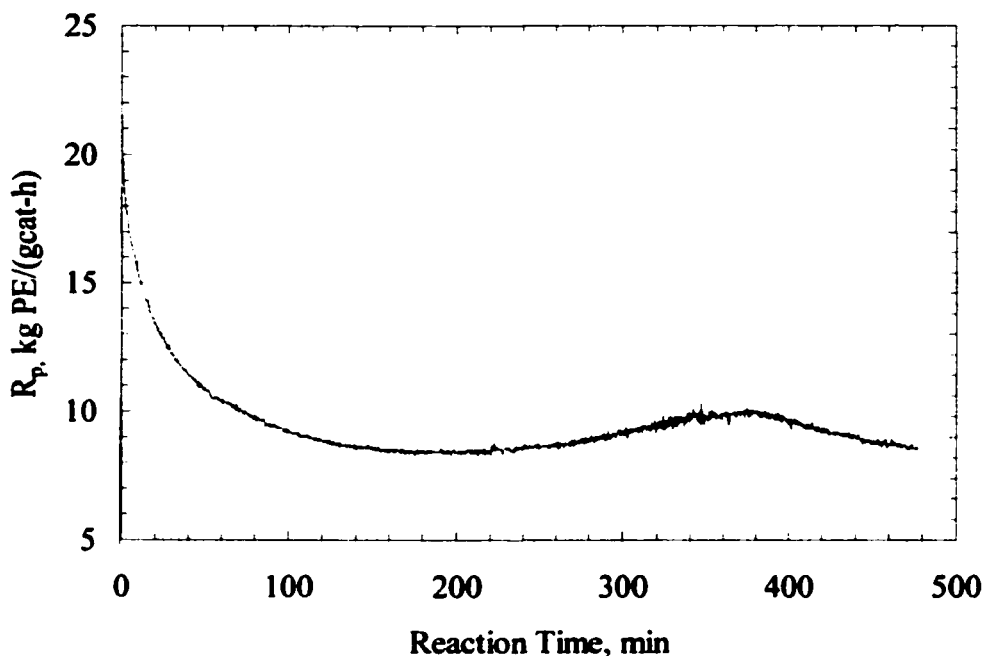


Figure 8.1 Long homopolymerization run (GasHo13).

Carbon13-NMR characterization of the product also showed the multiple-site nature of the catalyst sites. One copolymer product (GasCo36) was placed into 1,2,4-trichlorobenzene (TCB) at room temperature for 2.5 hours. The liquid phase was analyzed by ^{13}C -NMR, which yielded a 1-hexene content for the dissolved polymer of 30.3 mol%. A polymer with such high 1-hexene content does not crystallize from solution. This is the possible reason that the analysis results by ^{13}C -NMR yielded much higher 1-hexene content than TREF analyses (see Chapter 7).

The dissolved polymer, non-dissolved polymer and whole sample were further analyzed by GPC. The results are shown in Figure 8.2. Line 1 in Figure 8.2 represents the polymer dissolved in TCB at room temperature. This polymer had the lowest molar mass ($M_n=2,450$, $M_w=19,000$) and a long tail at low molar masses. Line 2 is the GPC curve for the undissolved part of the sample. It had the highest molar mass ($M_n=20,000$, $M_w=303,000$) and a shoulder on the high molar mass side. Line 3 is the analysis of the whole sample ($M_n=10,600$, $M_w=287,000$). It can be clearly seen that Line 3 has two shoulders, one on each side of its main peak; the left shoulder results from the copolymer

which had highest 1-hexene content and dissolved in the TCB at room temperature. Hence GPC results show that the copolymer sample contained three different structures.

The amount of the dissolved polymer fraction were obtained from the GPC analysis. The GPC analysis showed that 29.6% of the sample was soluble in the TCB at room temperature. Mass balance calculation showed that more than 90% of the 1-hexene in the whole polymer was contained in the dissolved fraction.

The observed homopolymerization rate profile (Figure 8.1) and the ^{13}C -NMR and GPC results clearly show that the $\text{TiCl}_4/\text{MgCl}_2$ catalysts in the current work contained at least 3 different types of catalytic sites. The solubility experiment suggests that two of the sites are homopolymerization sites.

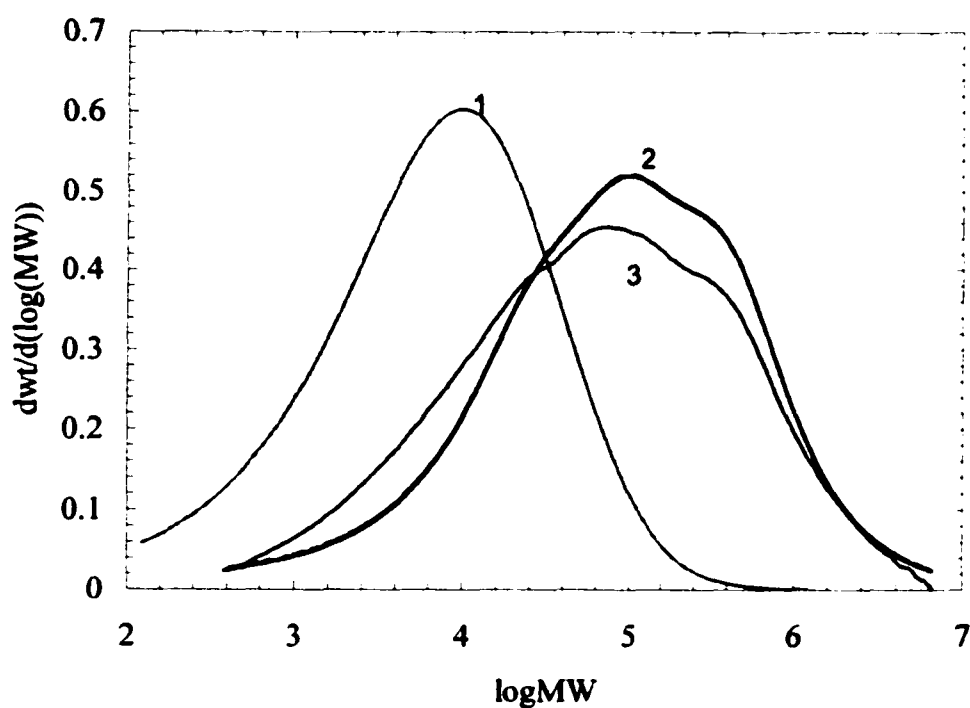


Figure 8.2 Multiple-site nature of catalyst observed from molar mass distribution curve. (1: dissolved polymer; 2: non-dissolved part; 3 whole sample.)

The GPC curve for the whole sample of GasCo36 was further deconvoluted by Peakfit software, a three-Flory peak generally described the three peak trend (see Figure 8.3). At

least one additional peak is needed in order to obtain better simulation result at the large molar mass end.

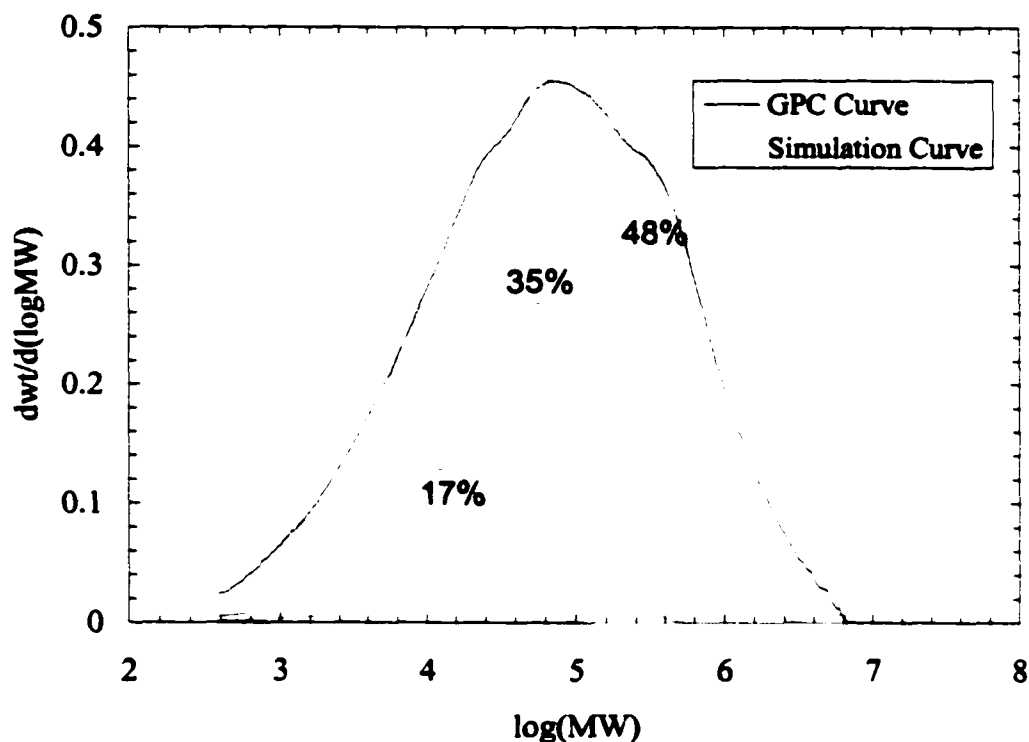


Figure 8.3 Deconvolution result of GPC curve of sample GasCo36 ($P_{C2}=60$ psi, $P_{C6}=9.3$ psi) by three Flory peaks. The numbers in the Figure are the area percentages for each peak.

8.2 Modeling of Copolymerization

A three-site model was assumed on the basis of the material presented in Section 8.1. Kissin and co-workers (Kissin, 1993, 1995, Kissin et al., 1999a, 1999b, 1999c, 1999d) used a five-site model to describe the copolymerization of 1-hexene and ethylene in the slurry phase. They based their model on GPC analysis of PE from runs of different duration. In their model, two of the sites deactivated very rapidly. In the current study, prepolymerized catalysts were used and these rapidly deactivating sites may already be partially deactivated during the prepolymerization. Hence, the proposed three-site model in the current study is probably very similar to that proposed by Kissin and co-workers.

The details of the model should be such that it reflects the following general experimental observations:

1. The ethylene polymerization rate increases rapidly in the first few minutes and then decays to a relatively constant activity over the next 60 to 90 minutes (see activity profiles in Section 6.3).
2. The 1-hexene addition required to maintain constant concentrations in the gas phase were high at reaction times less than 20 min and usually decreased to about zero in the following 40 min of polymerization.
3. Increasing 1-hexene concentrations at constant ethylene pressure resulted in decreases in ethylene polymerization rates; the decrease in ethylene polymerization rates was more pronounced at the beginning than at the end of the runs (see Figures. 6.5 to 6.7 and 6.10).
4. Increases in ethylene pressure at constant 1-hexene concentration or constant 1-hexene/ethylene ratios increased polymerization rates (see Figures. 6.8, 6.9 and 6.10).
5. The apparent reaction order with respect to ethylene pressure is significantly above unity at the beginning of the polymerizations and decreases to about unity after 2 h of polymerization (see Figure 6.11).
6. Increasing 1-hexene concentrations did not necessarily increase the rate of 1-hexene incorporation, but the 1-hexene content of the polymer always increased with increasing 1-hexene concentration because this increase of 1-hexene concentration resulted in a decrease in ethylene polymerization rate (see Observation 3 above).

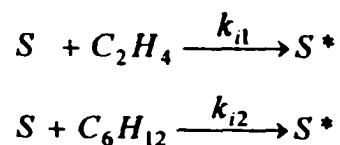
The above observations as well as GPC results in Section 8.1, and observations by other investigators with similar catalyst systems led to following model assumptions and model properties:

1. Catalyst has three types of catalytic sites.
2. The three types of catalytic sites have the following properties: Site 1 incorporates 1-hexene and is activated rapidly and deactivates rapidly (Observation 2); Sites 2 and 3 are homopolymerization sites; Site 3 activates and deactivates slowly and the activation – deactivation rates for Site 2 are intermediate to the rates of Sites 1 and 3.

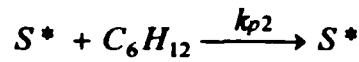
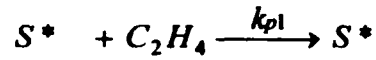
3. All three types of sites are activated and deactivated independent of each other and one type of site is not converted to another type of site.
4. Ethylene concentration in the polymer is related to the ethylene pressure by Henry's law (see Figure 7.14). (It is assumed that the concentration of dissolved ethylene is only a function of ethylene pressure and temperature and not a function of type of polymer and 1-hexene concentration).
5. The dissolved 1-hexene concentration in the polymer is calculated from the co-solubility results described in Chapter 7 (see Figure 7.20)
6. The interaction of the dissolved olefins with the active sites described by Langmuir-Hinshelwood adsorption functions.
7. A lumped polymerization propagation rate constant is used for each site and each monomer.
8. Two types of deactivation processes are assumed to occur, one is simultaneous deactivation without the participation of either monomer or comonomer (Keii, 1982; Han-Adebekun and Ray, 1997), and the other one involves participation of ethylene since it was observed that deactivation rates increased with increasing ethylene pressures (Figure 6.10).
9. Effects of co-catalyst are not included in the model since it was found that the rates were affected by the catalyst to co-catalyst ratio (See Section 6.2).
10. Heat and mass transfer effects are assumed to be negligible (see Wu, 1999; Wu et al. 1999).

According to the above statements, the following reaction steps, in the absence of hydrogen, are proposed for each type of site except that the propagation rate for 1-hexene is zero for Sites 2 and 3:

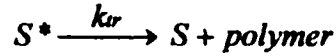
Site Initiation:



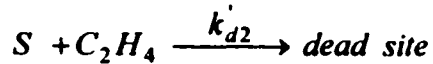
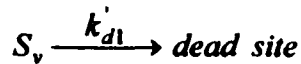
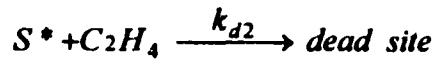
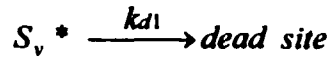
Propagation Reactions:



Chain Transfer:



Site Deactivation



where S is a potential active site; S^* is the active site; S_v and S_v^* are sites without associated with monomer; subscripts 1 and 2 denote reactions with ethylene and 1-hexene; k_{i1} and k_{i2} are rate constants for initiation reactions; k_{p1} and k_{p2} are propagation reaction constants; k_{d1} and k'_{d1} are the spontaneous deactivation rate constants for potential and active sites, and k_{d2} and k'_{d2} are ethylene-assisted deactivation constants for potential and active sites; k_{tr} is the spontaneous chain transfer reaction constant. Other chain transfer reactions (e.g. chain transfer to monomer or to comonomer) are not included because they do not change the concentration of S^* .

Based on the above proposed reaction schemes, the time dependence of the active site and the potential site concentrations are given by the Equations 8.1 and 8.2.

$$\frac{d[S^*]}{dt} = (k_{i1}\theta_1 + k_{i2}\theta_2)[S] - (k_{tr} + k_{d1}(1 - \theta_1 - \theta_2) + k_{d2}\theta_1)[S^*] \quad (8.1)$$

$$\frac{d[S]}{dt} = -(k_{i1}\theta_1 + k_{i2}\theta_2 + k'_{d1}(1 - \theta_1 - \theta_2) + k'_{d2})[S] + k_{tr}[S^*] \quad (8.2)$$

where $[S]$ is the concentration of potentially active sites and $[S^*]$ is the concentration of active sites for each site; θ_1 and θ_2 represent the fraction of sites occupied by ethylene

and 1-hexene respectively, and $(1-\theta_1-\theta_2)$ is the fraction of sites on which neither ethylene or 1-hexene is adsorbed. It is assumed that θ_1 and θ_2 have the same value for S and S^* . The coverage θ_1 and θ_2 can be described by Langmuir-Hinshelwood equations, i.e.

$$\theta_1 = \frac{K_1[M_1]}{1 + K_1[M_1] + K_2[M_2]} \quad (8.3)$$

$$\theta_2 = \frac{K_2[M_2]}{1 + K_1[M_1] + K_2[M_2]} \quad (8.4)$$

where K_1 and K_2 are the Langmuir-type adsorption equilibrium constants for ethylene and 1-hexene, $[M_1]$ and $[M_2]$ are the ethylene and 1-hexene concentrations (mol/g PE) dissolved in the polymer. For a given experiment at constant ethylene and 1-hexene concentrations, the values of θ_1 and θ_2 are assumed to be constant.

To reduce the number of adjustable parameters, it is assumed that $k_{d1}=k_{d1}'$ and $k_{d2}=k_{d2}'$. The initial conditions are $[S]=S_0$ and $[S^*]=0$, Constant S_0 is the number of potential sites per unit mass of catalyst before polymerization. Equations 8.1 and 8.2 can be solved analytically and the resulting expression for the concentrations of active sites as a function of time is

$$[S^*] = \frac{S_0 \cdot (k_{i1}\theta_1 + k_{i2}\theta_2)}{k_{i1}\theta_1 + k_{i2}\theta_2 + k_r} e^{-E_1 t} \left(1 - e^{-E_2 t} \right) \quad (8.5)$$

$$E_1 = k_{d1}(1 - \theta_1 - \theta_2) + k_{d2}\theta_1$$

$$E_2 = k_{i1}\theta_1 + k_{i2}\theta_2 + k_r$$

The propagation rates for ethylene and 1-hexene R_{p1} and R_{p2} are given as

$$R_{p1} = k_{p1}[S^*]\theta_1 \quad (8.6)$$

$$R_{p2} = k_{p2}[S^*]\theta_2 \quad (8.7)$$

where $[S^*]\theta_1$ is the fraction of active sites occupied by ethylene and $[S^*]\theta_2$ is the fraction occupied by 1-hexene.

Substituting Equation 8.5 into 8.6 and 8.7 yields

$$R_{p1} = \frac{k_{p1}}{k_{tr}} \cdot S_0 \frac{(k_{i1}\theta_1 + k_{i2}\theta_2) \cdot \theta_1}{\frac{k_{i1}\theta_1}{k_{tr}} + \frac{k_{i2}\theta_2}{k_{tr}} + 1} \cdot e^{-E_1 t} \cdot [1 - e^{-E_2 t}] \quad (8.8)$$

$$R_{p2} = \frac{k_{p2}}{k_{tr}} \cdot S_0 \frac{(k_{i1}\theta_1 + k_{i2}\theta_2) \cdot \theta_2}{\frac{k_{i1}\theta_1}{k_{tr}} + \frac{k_{i2}\theta_2}{k_{tr}} + 1} \cdot e^{-E_1 t} \cdot [1 - e^{-E_2 t}] \quad (8.9)$$

Limiting forms of Equations 8.8 and 8.9 result in the observed dependence of ethylene and 1-hexene rate (Observations 3 to 6), for example,

$$\text{if } 1 \gg \left[\frac{k_{i1}\theta_1}{k_{tr}} + \frac{k_{i2}\theta_2}{k_{tr}} \right] \quad \text{and} \quad k_{i1} \gg k_{i2}$$

then the rate of ethylene polymerization is directly proportional to θ_1^2 , and the order of the ethylene pressure dependence of θ_1 is between 0 and 1, i.e. the order with respect to ethylene concentration from 0 to 2. (see Eq. 8.3 and recall that according to Henry's law, $[M_1]$ is directly proportional to the ethylene pressure). When $k_{i1}\theta_1 \gg k_{i2}\theta_2$, then Equation 8.9 predicts that the rate of 1-hexene incorporation varies as $k_{i1}\theta_1\theta_2/[1+k_{i1}\theta_1]$, i.e. increases in ethylene pressure, which result in increases in θ_1 , result in increase in 1-hexene incorporation rate at constant values of θ_2 . This behavior is in agreement with the experimental observations.

The overall ethylene polymerization rate, R_{p1} , is the summation of polymerization rates for Sites 1, 2 and 3, i.e.

$$R_{p1} = \sum_{n=1}^3 R_{p1,n} \quad (8.10)$$

where n refers to the different type of catalytic sites.

The rate of 1-hexene polymerization is

$$R_{p2} = R_{p2,1}$$

Since $k_{p2,2} = k_{p2,3} = 0$.

It has to be stressed that the above reaction model is a phenomenological model which attempts to capture the experimental general observations. Various rate models were examined; the above simple model provided a reasonable description of the observed kinetic behavior.

8.3 Model Fitting Procedure and Results

For estimation of parameters, Equations 8.8 and 8.9 were simplified to Equations 8.11 and 8.12 since for a single isothermal run, θ_1 , θ_2 and other kinetic parameters (i.e. k_p , k_i , k_d) are constants. There are only four unknown parameters in Equations 8.11 and 8.12 (A_1 , A_2 , E_1 and E_2).

$$R_{p1} = A_1 \cdot e^{-E_1 t} \cdot (1 - e^{-E_2 t}) \quad (8.11)$$

$$R_{p2} = A_2 \cdot e^{-E_1 t} \cdot (1 - e^{-E_2 t}) \quad (8.12)$$

This estimation of parameters requires rates of 1-hexene and ethylene polymerization as a function of time. Ethylene polymerization rates are measured directly by the ethylene flow to the reactor. Rate of 1-hexene polymerization profiles were obtained from the measured rate of 1-hexene addition and the known total 1-hexene content of the product as determined by ^{13}C -NMR. Detailed description of the calculational procedure and a set of sample calculations of how the 1-hexene addition rates were converted to 1-hexene activity profiles is given in Appendix C. A sample of a 1-hexene activity profile based on this procedure is shown in Figure 8.4 for run GasCo40. Similar profiles will be shown for other runs at the end of the section where model results are compared with experimental measurements.

Values of A_2 , E_1 and E_2 for Site-1 were estimated by fitting 1-hexene rates, of the type shown in Figure 8.4, with Equation 8.12. If values of θ_1 and θ_2 are known as a function of ethylene and 1-hexene pressures, then parameters for Site-1 can be estimated from the values of A_2 , E_1 and E_2 .

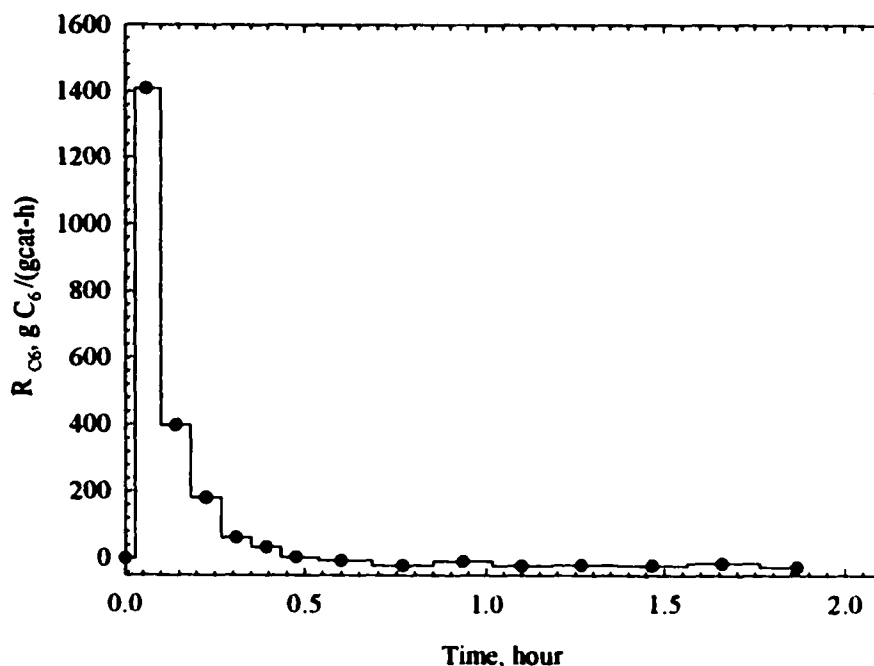


Figure 8.4 1-Hexene average reaction rate for run GasCo40 ($P_{C_2} = 60$ psi, $P_{C_6} = 3.4$ psi).

The values of K_1 and K_2 , which are needed to calculate θ_1 and θ_2 , were estimated from the ^{13}C -NMR analysis of the polymer from GasCo36 (see Section 8.1). Most of the 1-hexene content in the polymer was contained in the fraction solved in TCB at room temperature. The fraction constituted 29.6% of the total polymer and had a 1-hexene content of 30.3 mol%. The relative rates of ethylene and 1-hexene polymerization can be obtained by combining Equations 8.3, 8.4, 8.8 and 8.9, i.e.

$$\frac{R_{p1,1}}{R_{p2}} = \frac{k_{p1,1}K_1[M_1]}{k_{p2,1}K_2[M_2]} \quad (8.13)$$

The values of $[M_1]$ and $[M_2]$ can be calculated according to solubility and co-solubility studies (see Chapter 7). If the ratio of propagation rate was chosen arbitrarily as 70; a range of 45 to 140 was obtained by Kissin et al. (1999a and 1999b) for propagation rate ratios. With the above values, a K_1/K_2 ratio of 1/3.2 is obtained.

A value of $1000 \text{ g PE} \cdot \text{mol}^{-1}$ was chosen for K_1 , since $K_1[M_1]$ should be much less than unity to obtain first order polymerization kinetics with respect to ethylene (Keii, 1982;

Burfield et al., 1972). The value of K_2 is $3,200 \text{ g PE}\cdot\text{mol}^{-1}$ using the assumed value from K_1 .

With the above values of K_1 and K_2 , and the estimation of A_2 , E_1 , and E_2 based on the 1-hexene rate of disappearance, all the other kinetic parameters except $k_p S_0$ can be estimated for Site 1. Values of the parameters for Sites 2 and 3, which are assumed only involve ethylene polymerization were estimated by trial and error.

Sigma Plot and Excel Solver software were used in the trial and error estimation of the parameters. The set of parameters which provided a reasonable fit for copolymerization results are listed in Table 8.1. In the choice of parameters, emphasis was given to reproduce the general shapes of profiles and the location of rate maxima even if the fit of the absolute rate suffered. The kinetic parameters listed in Table 8.1 are the values which provide a reasonable description of the rate behavior at reaction conditions of 70°C in the absence of hydrogen for different ethylene and 1-hexene pressures. Total ethylene polymerization rates obtained from the model are compared with experimentally measured in Figures 8.5 to Figure 8.10. This simple model reproduces all the major experimentally-observed trends in the ethylene rate profiles. The general trends in ethylene activity profiles are mimicked by the model over a wide range of ethylene pressures (60 to 250 psi) and large range of ethylene to 1-hexene ratios of 6 to 40 (see results in Figures 8.5 to 8.9). These variations in operating conditions resulted in a 30 fold variation in average rates (cf. Runs GasCo39 and GasCo51, Table 6.3) and a 90-fold variation in the maximum rates of ethylene polymerization for these runs [see Figures 8.5(f) and 8.9 (a)].

The ability of the model to reproduce the experimental rates of 1-hexene incorporation are shown in Figure 8.10. Only 6 runs are shown in Figures 8.10(a) to 8.10(e) because the ^{13}C -NMR analyses were only available for these runs. Nevertheless, the model reproduces the trends observed in the 1-hexene rate behavior, such as increases in 1-hexene pressure at constant ethylene pressure resulting in lower maximum 1-hexene rates [cf. Figures 8.10 (c) and (d)], and observed increases in 1-hexene rates with increasing

ethylene pressure at constant 1-hexene pressure [cf. Figures 8.10 (a) and (e)]. Some of the disagreement between the model and the experimental 1-hexene rates are probably due to the incorrectness of the assumption that the 1-hexene solubility per unit mass of produced PE is constant. The polymer produced during the initial stages of polymerization has a higher 1-hexene content than polymer produced in the later stages (see Section 6.7). Hence, the solubility of the 1-hexene should be higher for the polymer formed initially. Neglecting this effect results in the calculated 1-hexene rates which frequently had negative values during the later stages of polymerization (see Figure 8.10). Considerably more detailed understanding of the solubility of 1-hexene and ethylene as a function of LLDPE composition is required to refine this aspect of the data analysis and parameter estimations in the model.

Table 8.1 Complete Parameters Used for Multi-Site Model Simulations

	Site-1	Site-2	Site-3	Unit	Explanation
K_1	1000	1000	1000	$\text{g PE} \cdot \text{mol}^{-1}$	Equilibrium adsorption constant for ethylene in copolymer (arbitrarily chosen)
K_2	3200	3200	3200	$\text{g PE} \cdot \text{mol}^{-1}$	Equilibrium adsorption constant for 1-hexene in copolymer
k_{i1}	100	80	15	h^{-1}	Initiation rate constant by ethylene
k_{i2}	0.1	0.5	0	h^{-1}	Initiation rate constant by 1-hexene
k_{tr}	40	3	0.001	h^{-1}	Chain transfer rate constant
k_{d1}	17	2	0.03	h^{-1}	Growing site spontaneous deactivation constant
k_{d2}	7	1.2	0.03	h^{-1}	Growing site ethylene-assisted deactivation constant
k_{d1}'	17	2	0.03	h^{-1}	Potential active site spontaneous deactivation constant
k_{d2}'	7	1.2	0.03	h^{-1}	Potential active site ethylene-assisted deactivation constant
$k_{p1}S_0$	2400	180	52	$\text{kg PE} \cdot (\text{g cat})^{-1} \cdot \text{h}^{-1}$	Lumped propagation rate constant for ethylene
$k_{p2}S_0$	28	0	0	$\text{kg PE} \cdot (\text{g cat})^{-1} \cdot \text{h}^{-1}$	Lumped propagation rate constant for 1-hexene

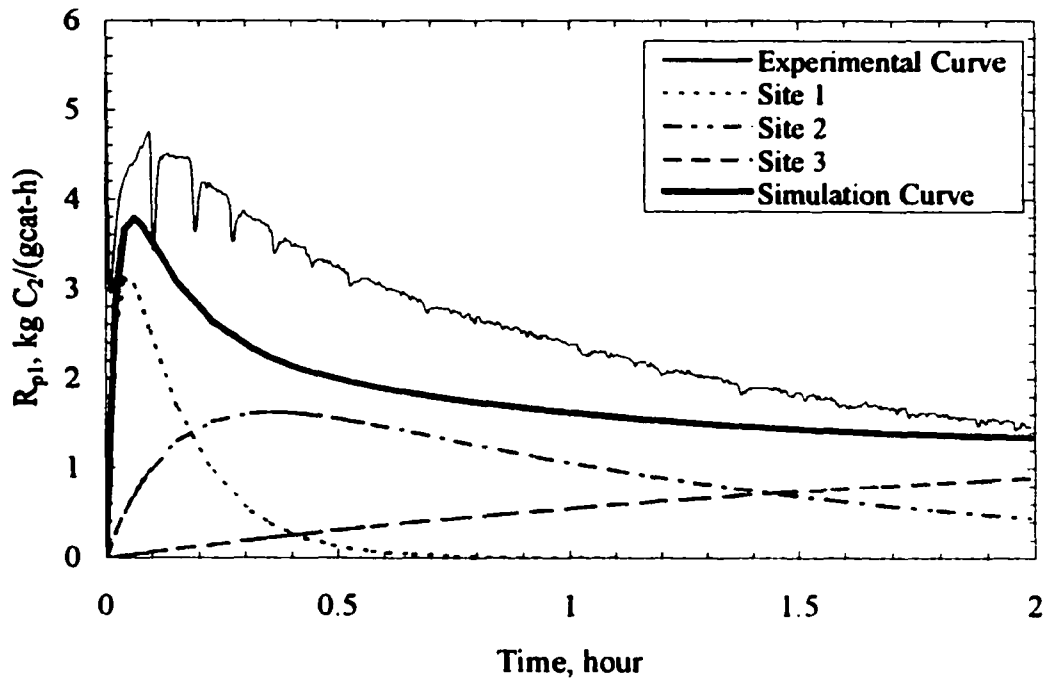


Figure 8.5 (a) Comparison of ethylene reaction profile and model prediction for run GasCo40 ($P_{C_6}=3.5$ psi, $P_{C_2}=60$ psi).

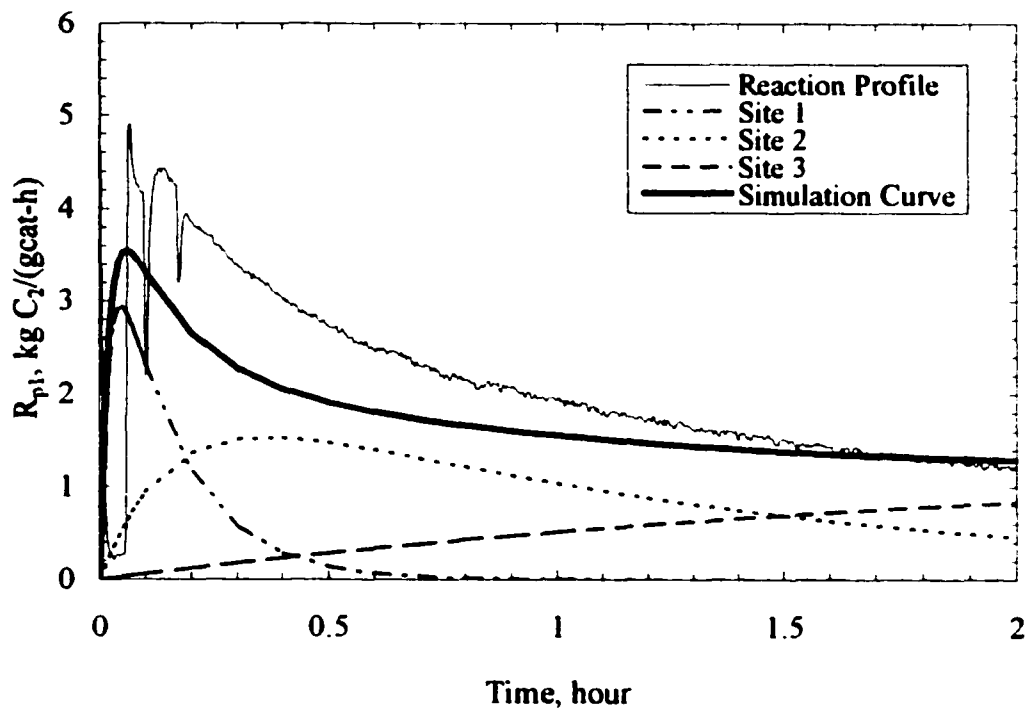


Figure 8.5 (b) Comparison of experimental ethylene reaction profile and model prediction for run GasCo18 ($P_{C_6}=3.7$ psi, $P_{C_2}=60$ psi).

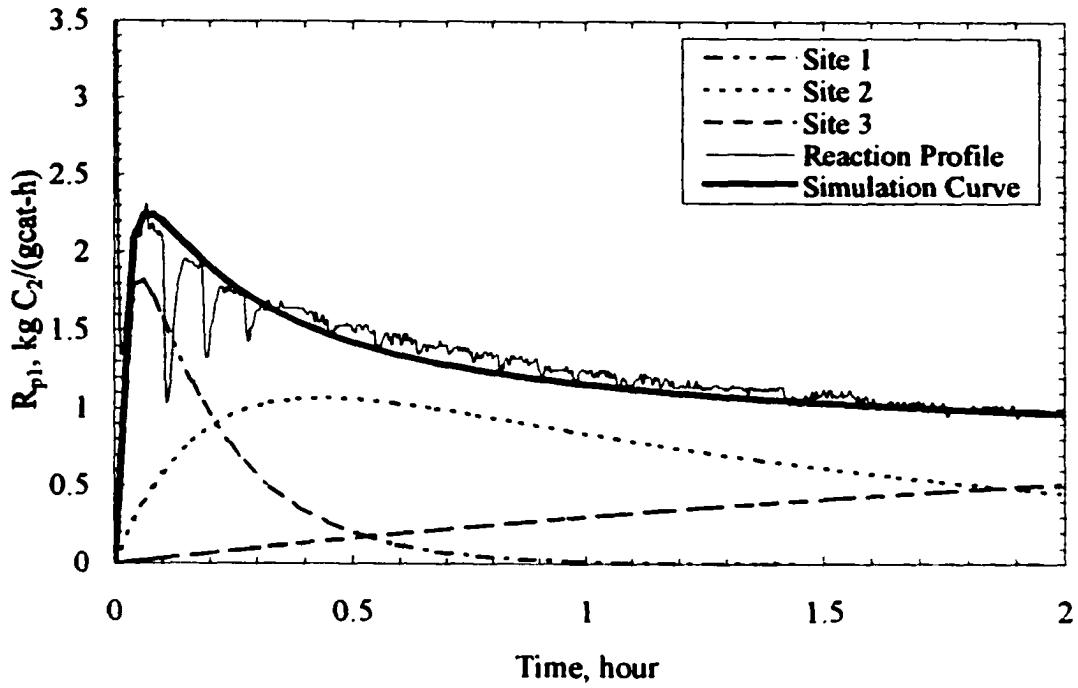


Figure 8.5 (c) Comparison of ethylene reaction profile and model prediction for run GasCo35 ($P_{C_6}=5.1$ psi, $P_{C_2}=60$ psi).

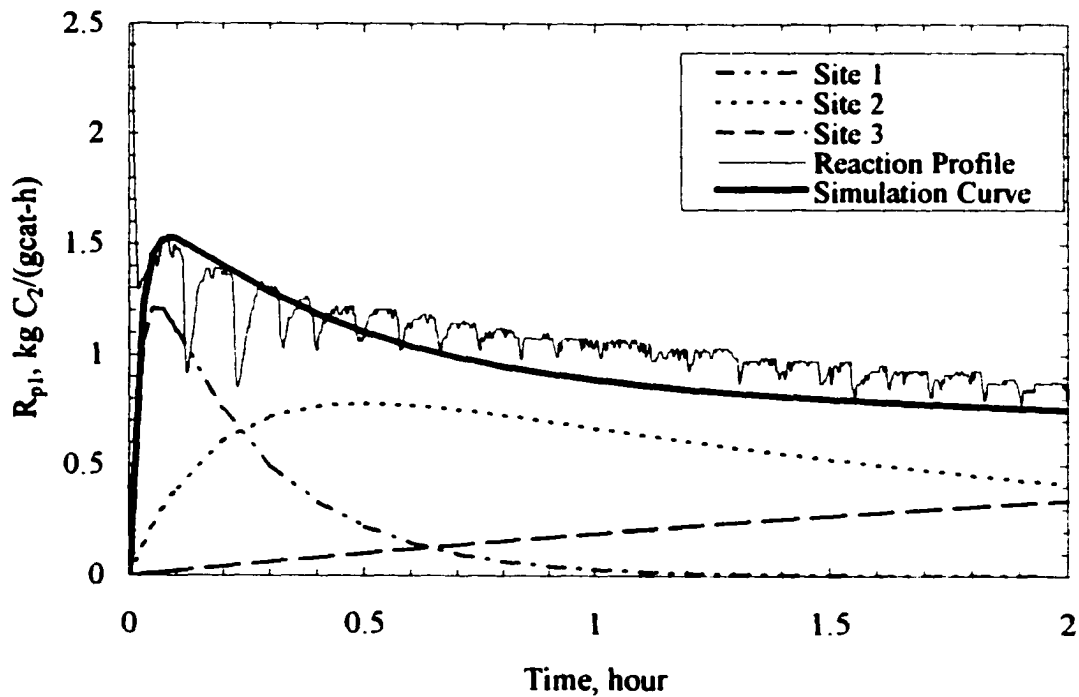


Figure 8.5 (d) Comparison of experimental ethylene reaction profile and model prediction for run GasCo34 ($P_{C_6}=6.4$ psi, $P_{C_2}=60$ psi).

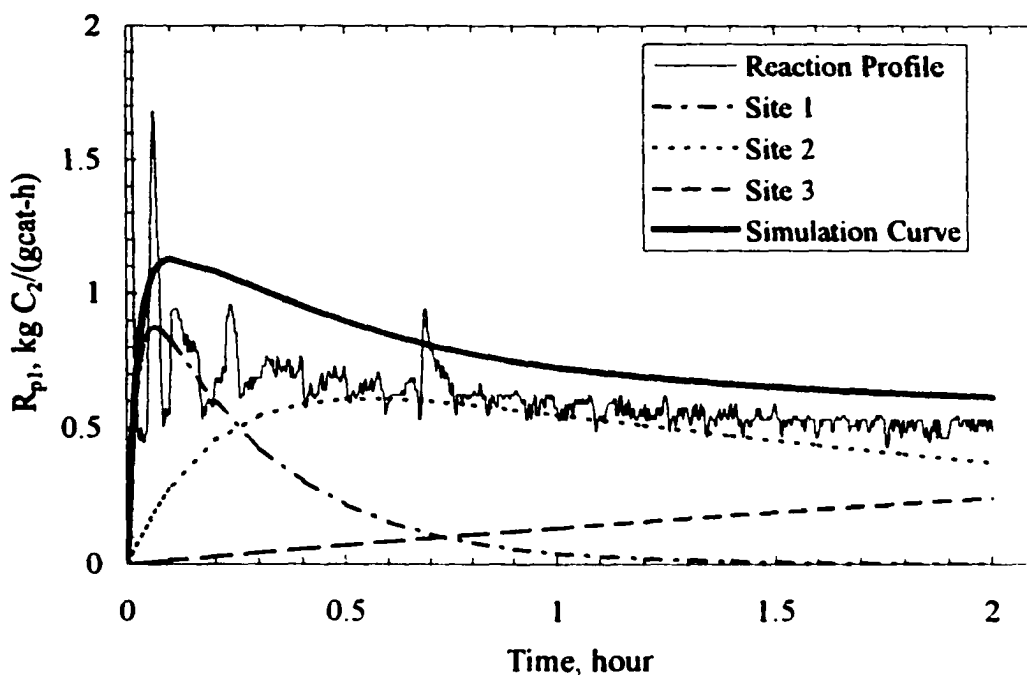


Figure 8.5 (e) Comparison of experimental ethylene reaction profile and model prediction for run GasCo39 ($P_{C6}=7.5$ psi, $P_{C2}=60$ psi).

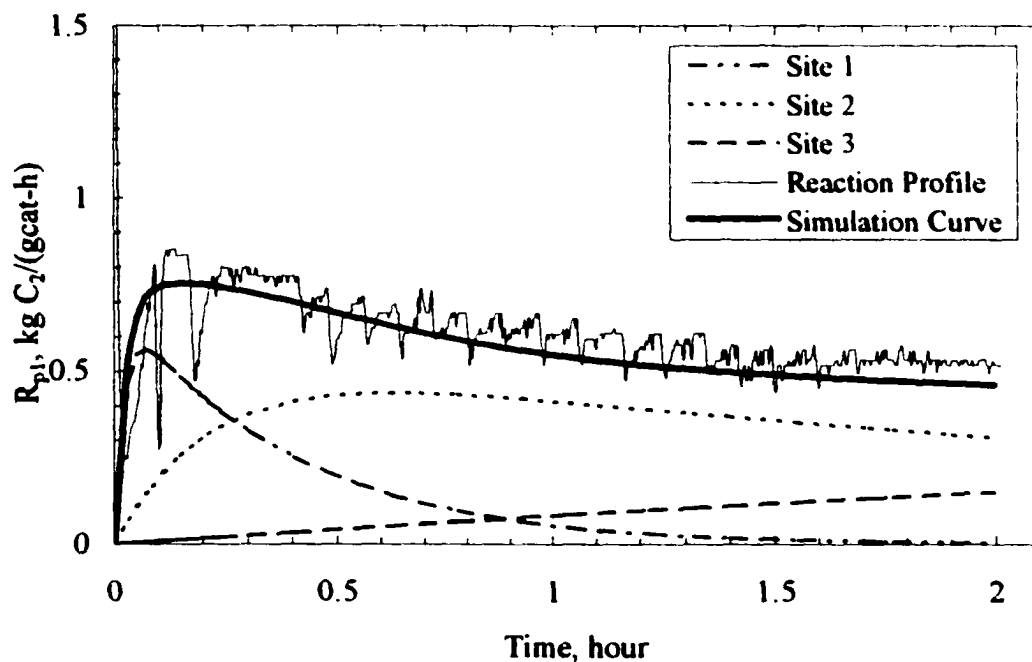


Figure 8.5 (f) Comparison of experimental ethylene reaction profile and model prediction for run GasCo36 ($P_{C6}=9.3$ psi, $P_{C2}=60$ psi).

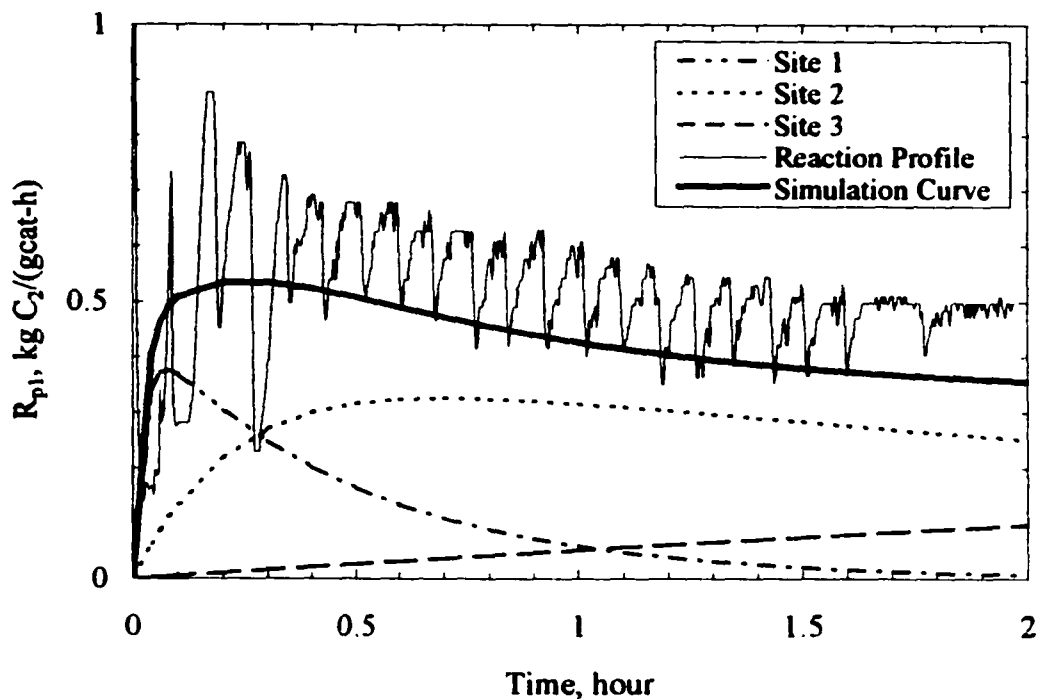


Figure 8.5 (g) Comparison of ethylene reaction profile and model prediction for run GasCo38 ($P_{C6}=11.5$ psi, $P_{C2}=60$ psi).

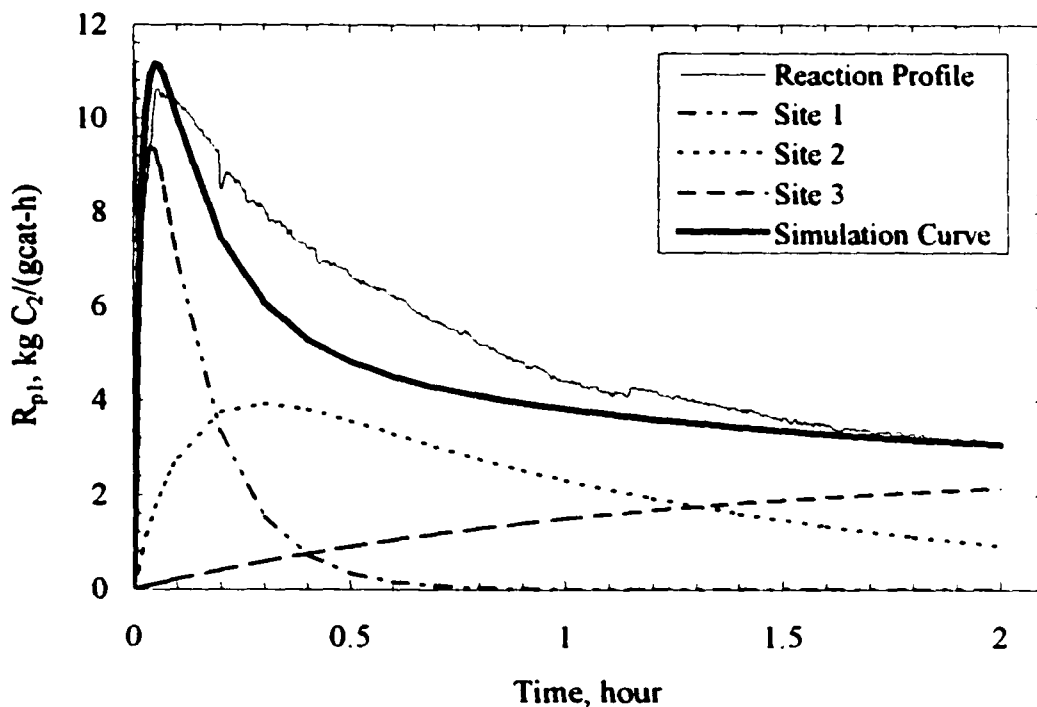


Figure 8.6 (a) Comparison of experimental ethylene reaction profile and model prediction for run GasCo15 ($P_{C6}=5.9$ psi, $P_{C2}=107$ psi).

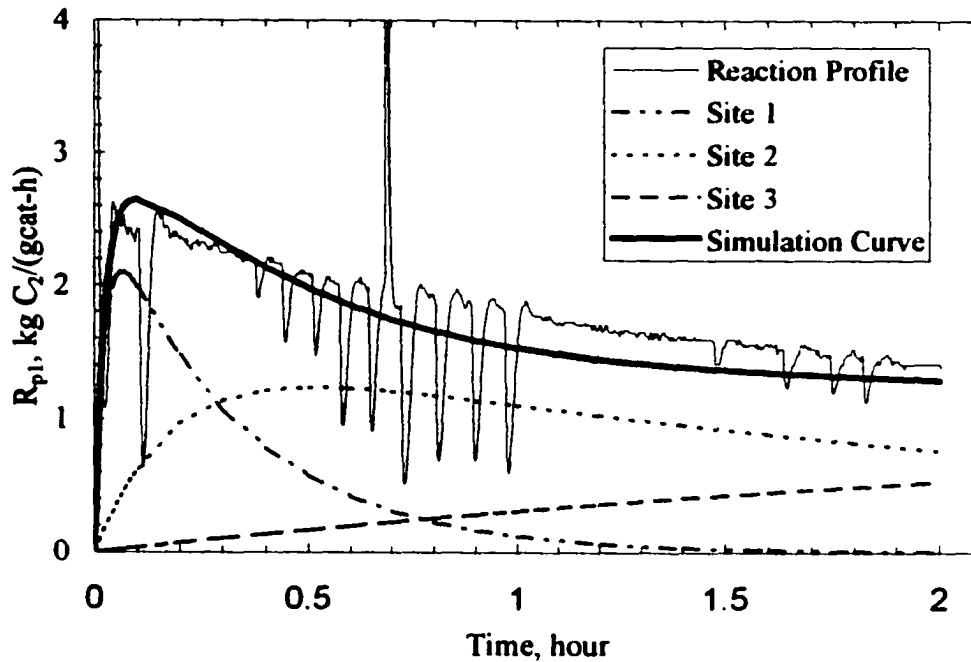


Figure 8.6 (b) Comparison of experimental ethylene reaction profile and model prediction for run GasCo53 ($P_{C_6}=14$ psi, $P_{C_2}=105$ psi).

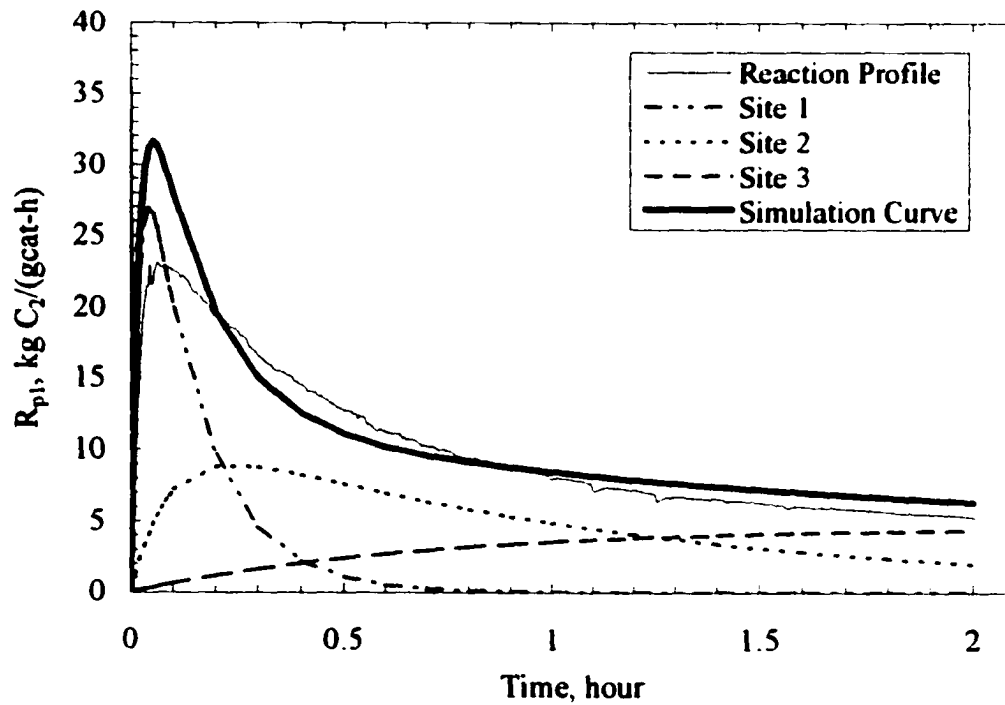


Figure 8.7 Comparison of experimental ethylene reaction profile and model prediction for run GasCo24 ($P_{C_6}=11.5$ psi, $P_{C_2}=200$ psi).

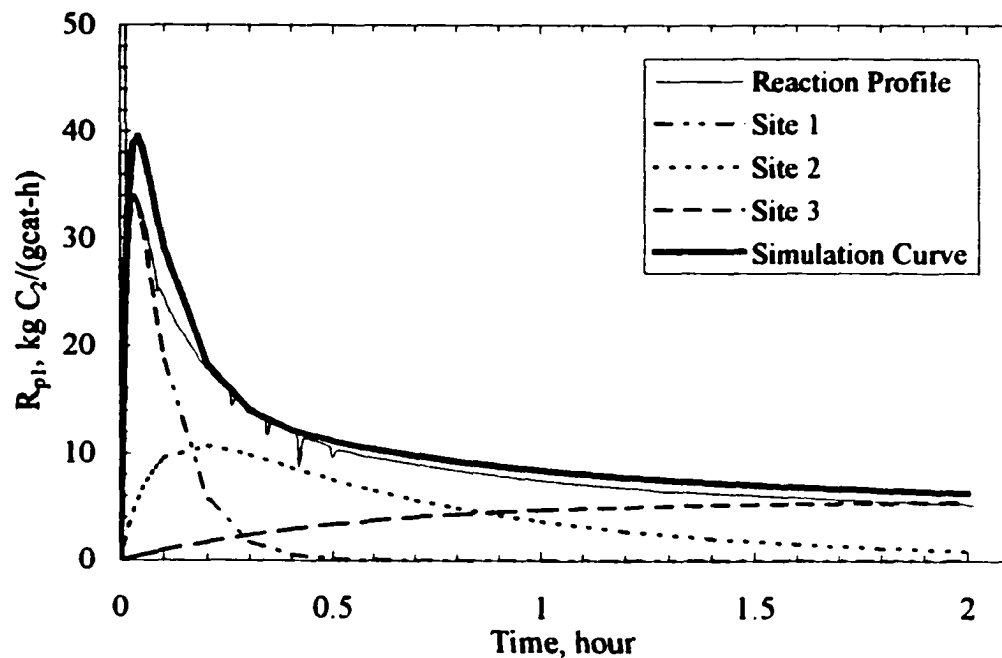


Figure 8.8 (a) Comparison of experimental ethylene reaction profile and model prediction for run GasCo45 ($P_{C6}=3.2$ psi, $P_{C2}=150$ psi).

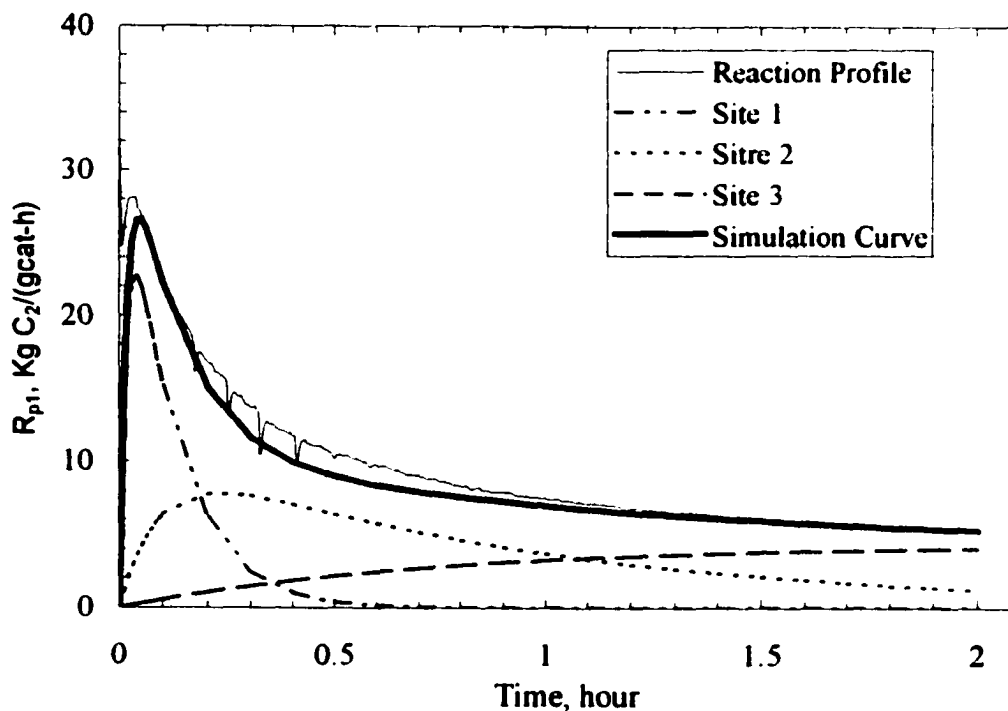


Figure 8.8 (b) Comparison of ethylene reaction profile and model prediction for run GasCo44 ($P_{C6}=6.4$ psi, $P_{C2}=150$ psi).

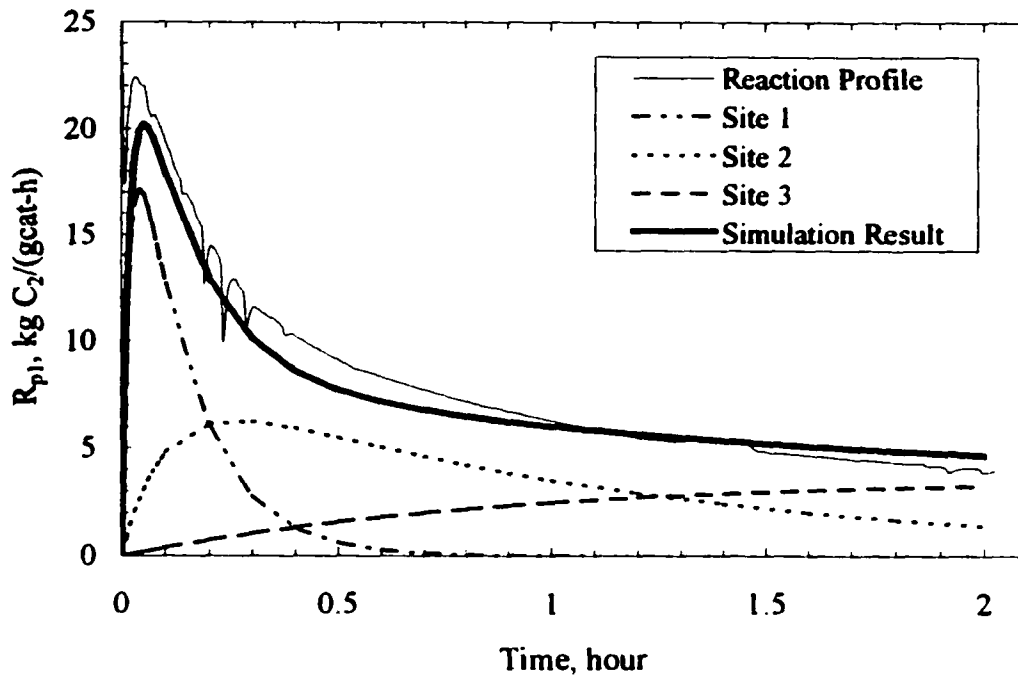


Figure 8.8 (c) Comparison of ethylene reaction profile and model prediction for run GasCo20 ($P_{C_6}=8.3$ psi, $P_{C_2}=150$ psi).

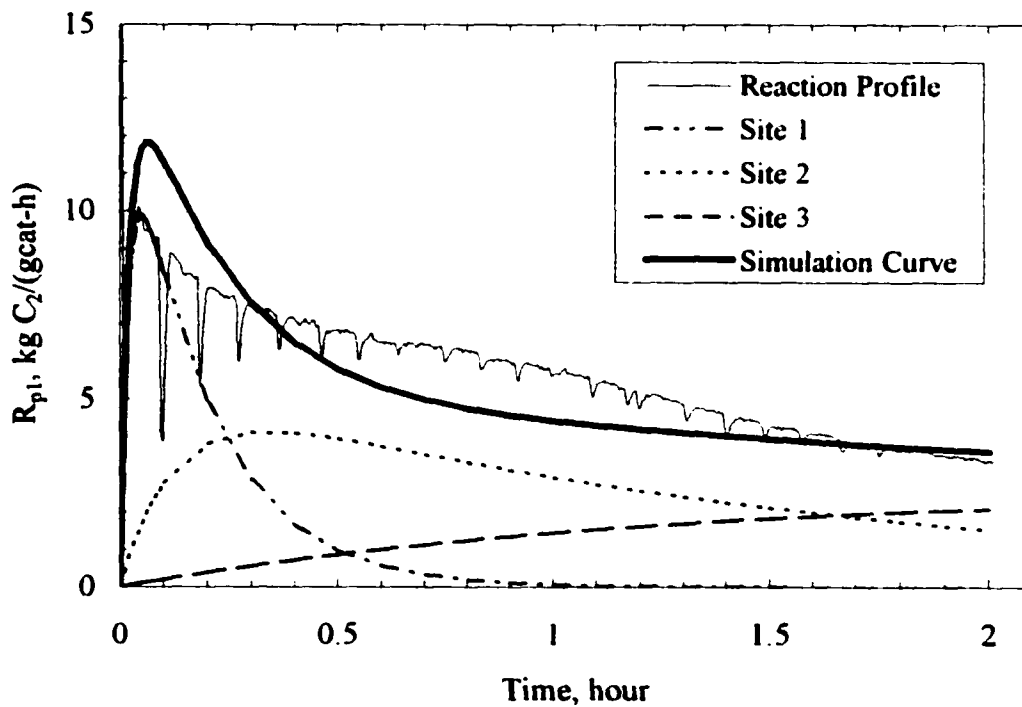


Figure 8.8 (d) Comparison of experimental ethylene reaction profile and model prediction for run GasCo42 ($P_{C_6}=12.5$ psi, $P_{C_2}=150$ psi).

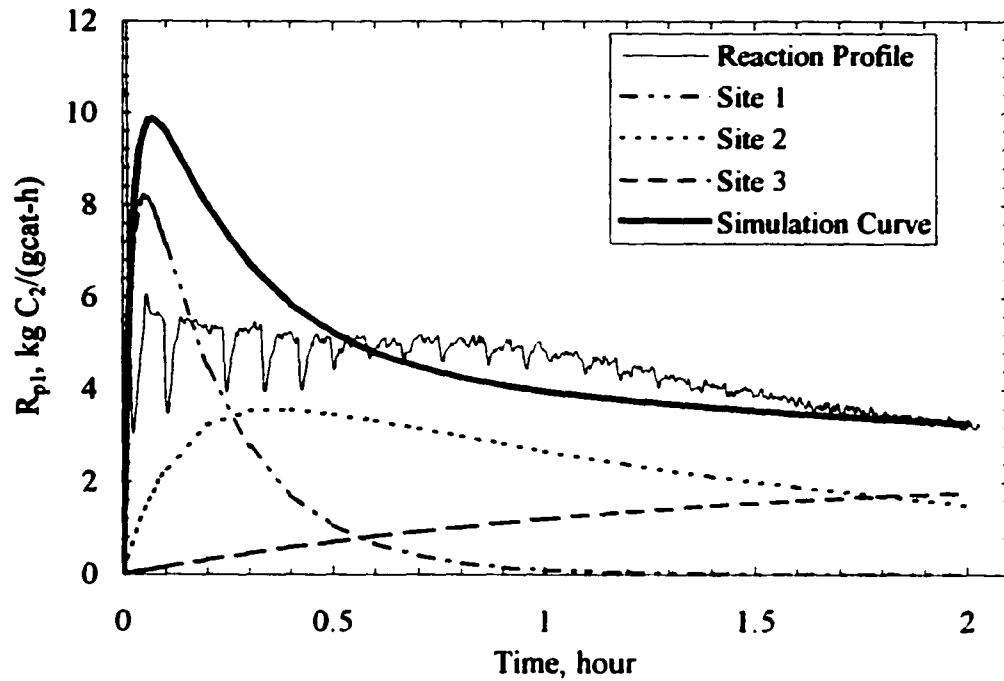


Figure 8.8 (e) Comparison of experimental ethylene reaction profile and model prediction for run GasCo46 ($P_{C6}=14$ psi, $P_{C2}=150$ psi).

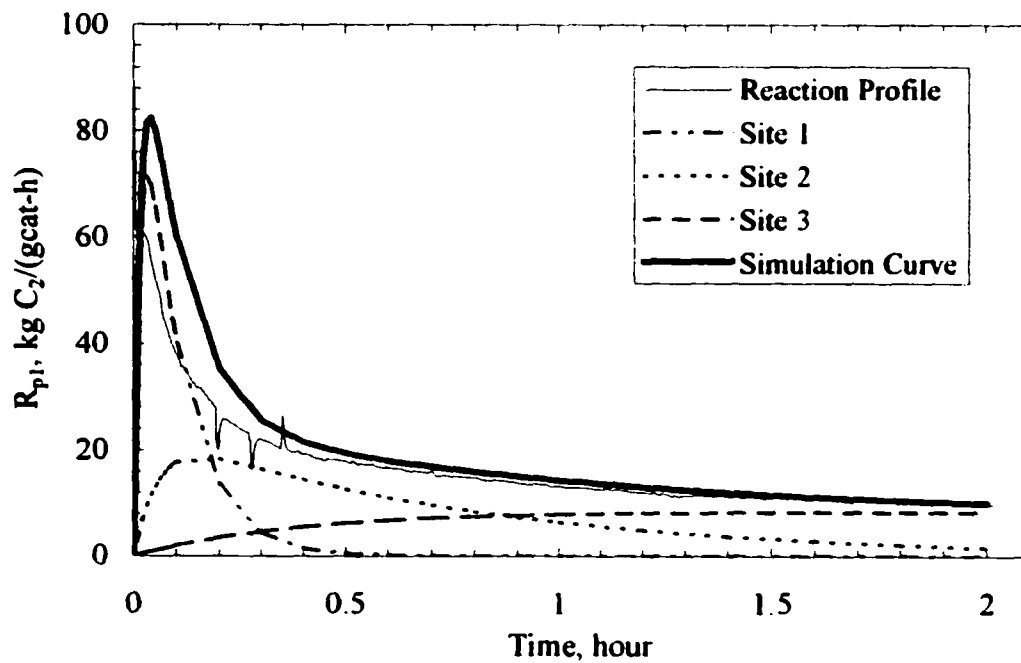


Figure 8.8 (a) Comparison of experimental ethylene reaction profile and model prediction for run GasCo51 ($P_{C6}=6.3$ psi, $P_{C2}=250$ psi).

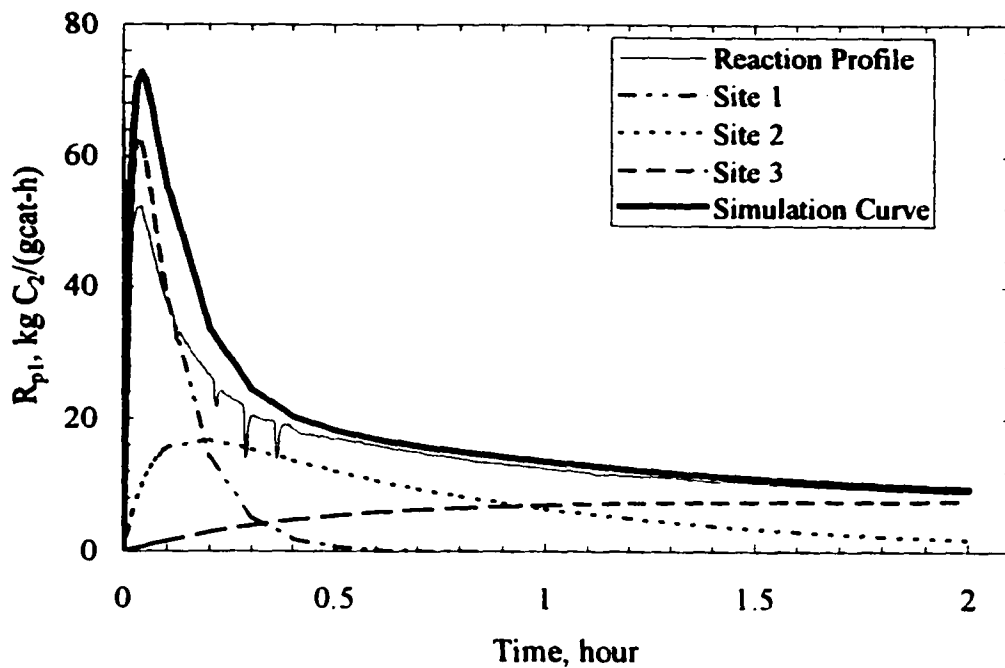


Figure 8.9 (b) Comparison of experimental ethylene reaction profile and model prediction for run GasCo48 ($P_{C6}=8.1$ psi, $P_{C2}=250$ psi).

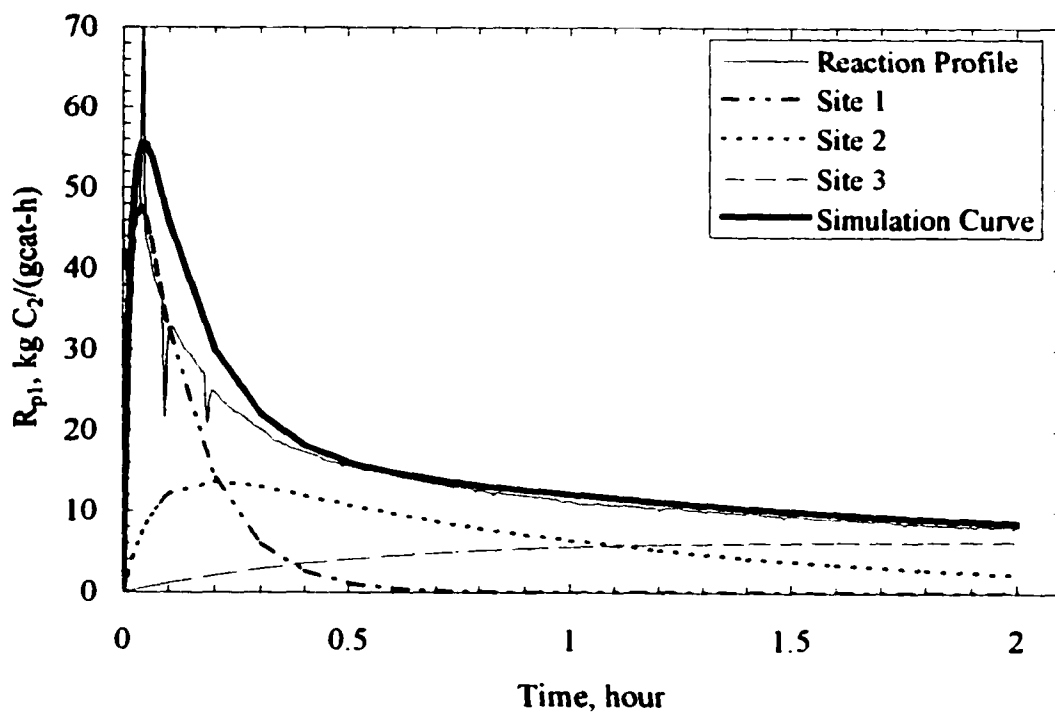


Figure 8.9 (c) Comparison of experimental ethylene reaction profile and model prediction for run GasCo52 ($P_{C6}=11.7$ psi, $P_{C2}=250$ psi).

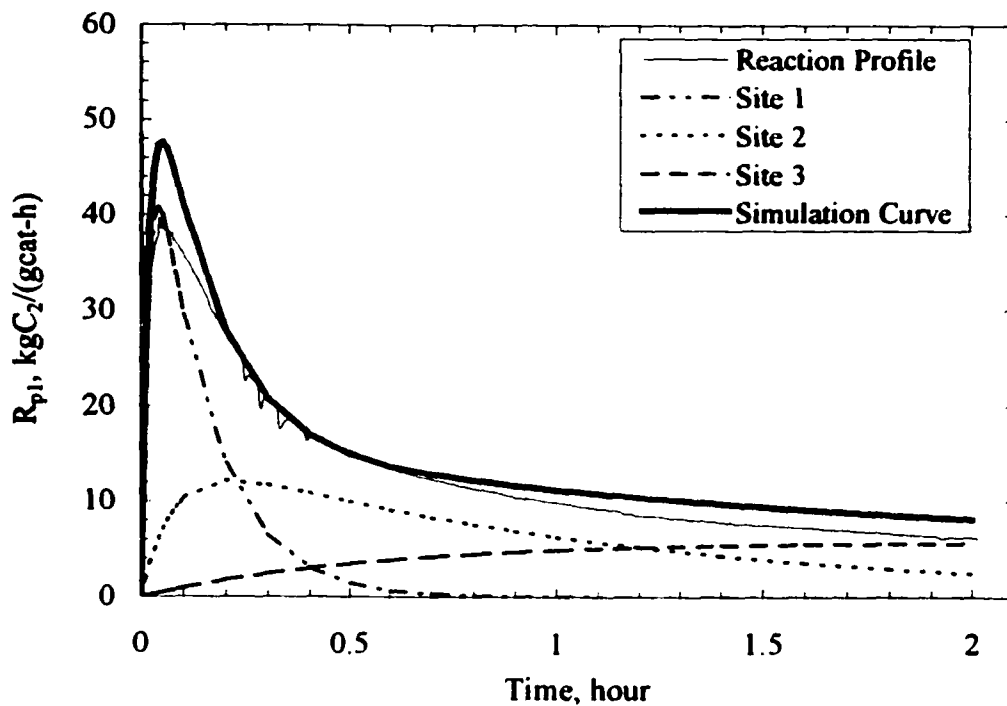


Figure 8.9 (d) Comparison of experimental ethylene reaction profile and model prediction for run GasCo26 ($P_{C6}=13.8$ psi, $P_{C2}=250$ psi).

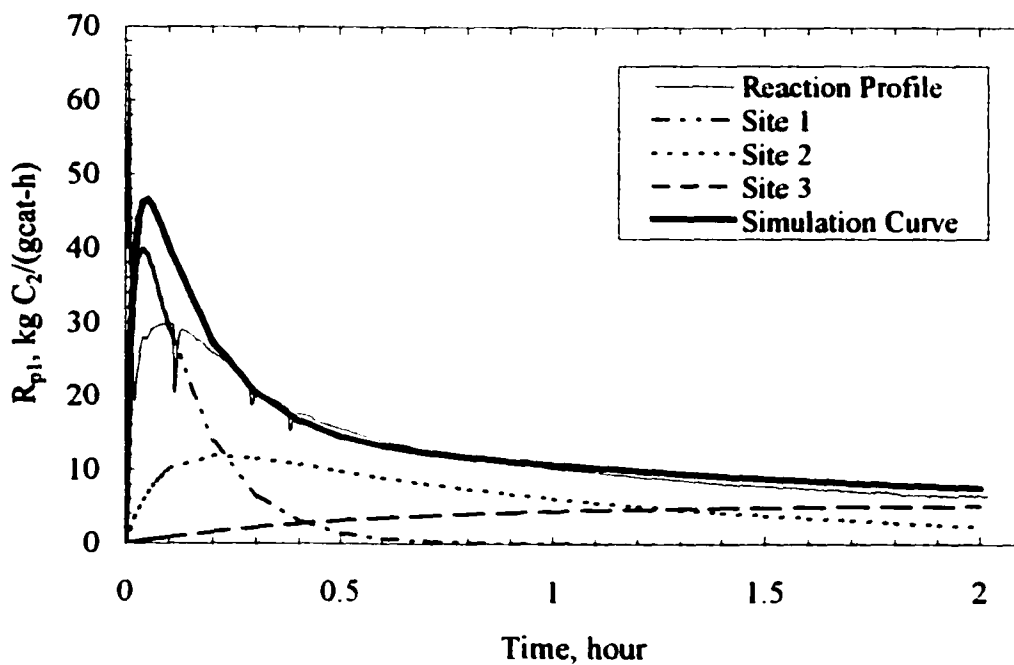


Figure 8.9 (e) Comparison of experimental ethylene reaction profile and model prediction for run GasCo50 ($P_{C6}=14.1$ psi, $P_{C2}=250$ psi).

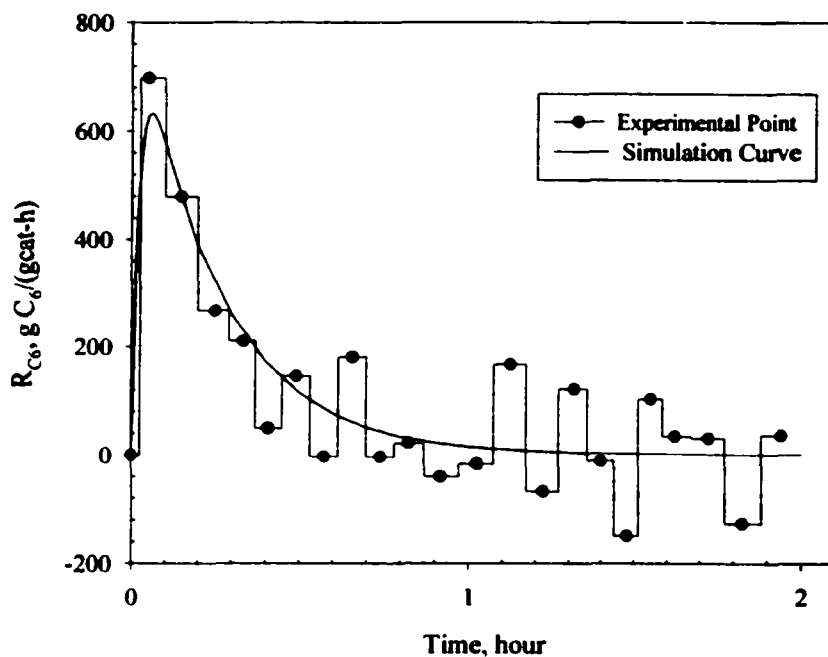


Figure 8.10 (a) 1-Hexene reaction rate and the simulation curve for run GasCo34 ($P_{C_2}=60$ psi, $P_{C_6}=6.4$ psi).

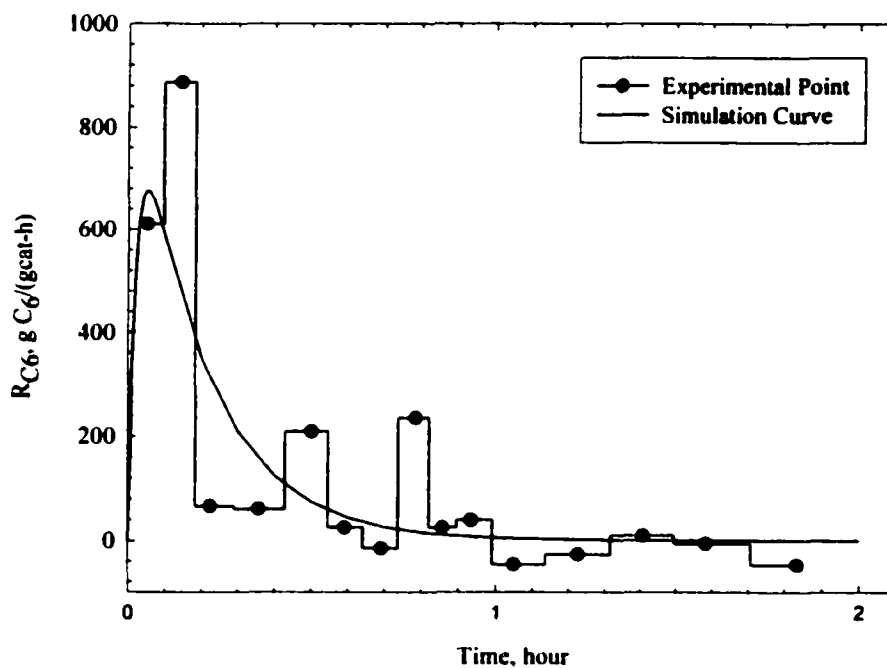


Figure 8.10 (b) 1-Hexene reaction rate and the simulation curve for run GasCo35 ($P_{C_2}=60$ psi, $P_{C_6}=5.1$ psi).

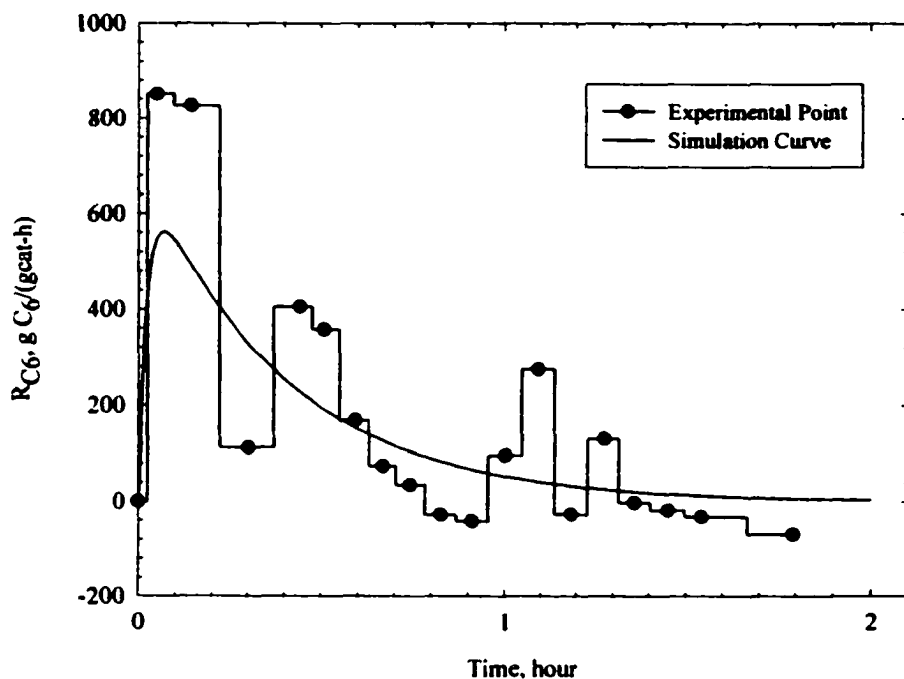


Figure 8.10 (c) 1-Hexene reaction rate and the simulation curve for run GasCo36 ($P_{C_2}=60$ psi, $P_{C_6}=9.3$ psi).

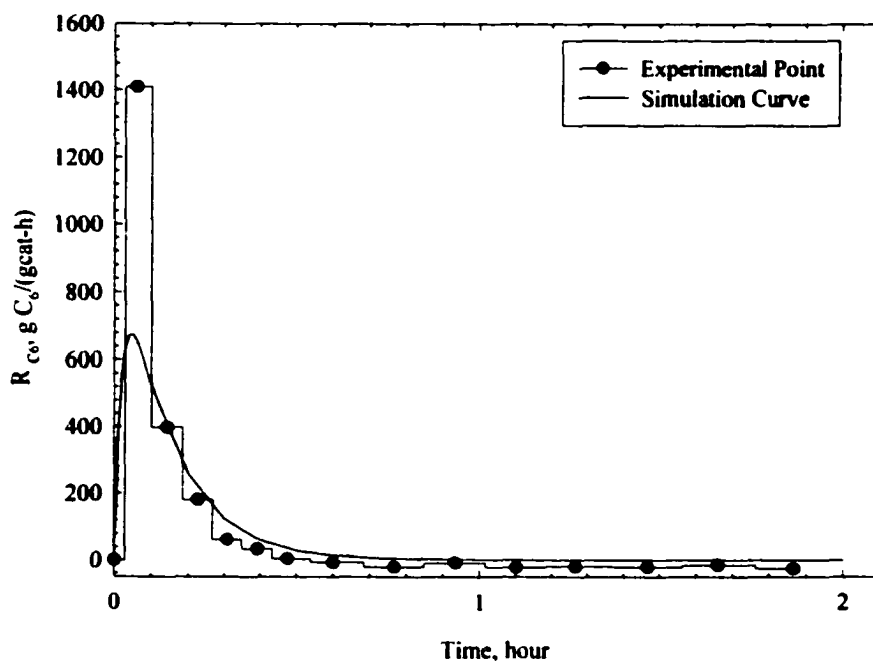


Figure 8.10 (d) 1-Hexene reaction rate and the simulation curve for run GasCo40 ($P_{C_2}=60$ psi, $P_{C_6}=3.4$ psi).

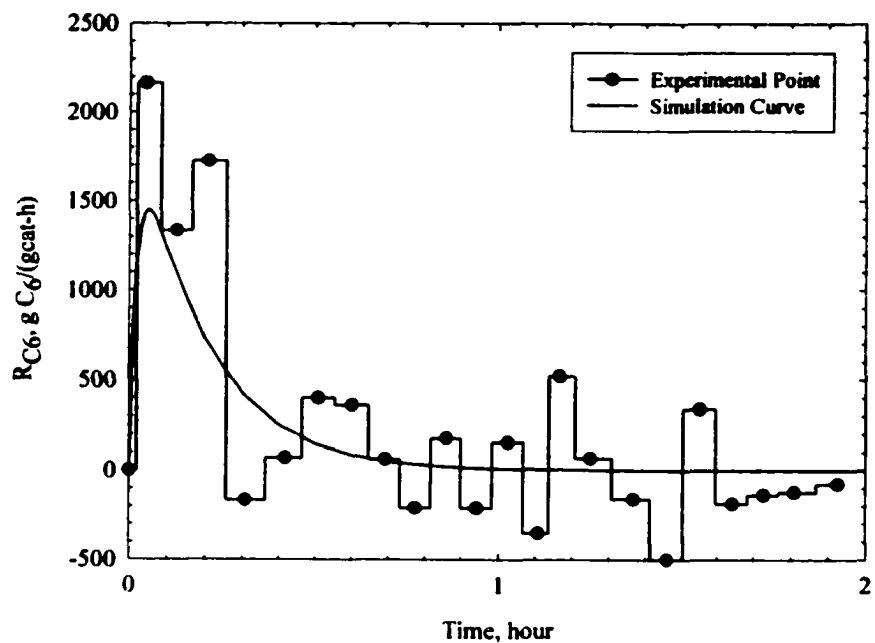


Figure 8.10 (e) 1-Hexene reaction rate and the simulation curve for run GasCo42 ($P_{C_2}=150$ psi, $P_{C_6}=12.5$ psi).

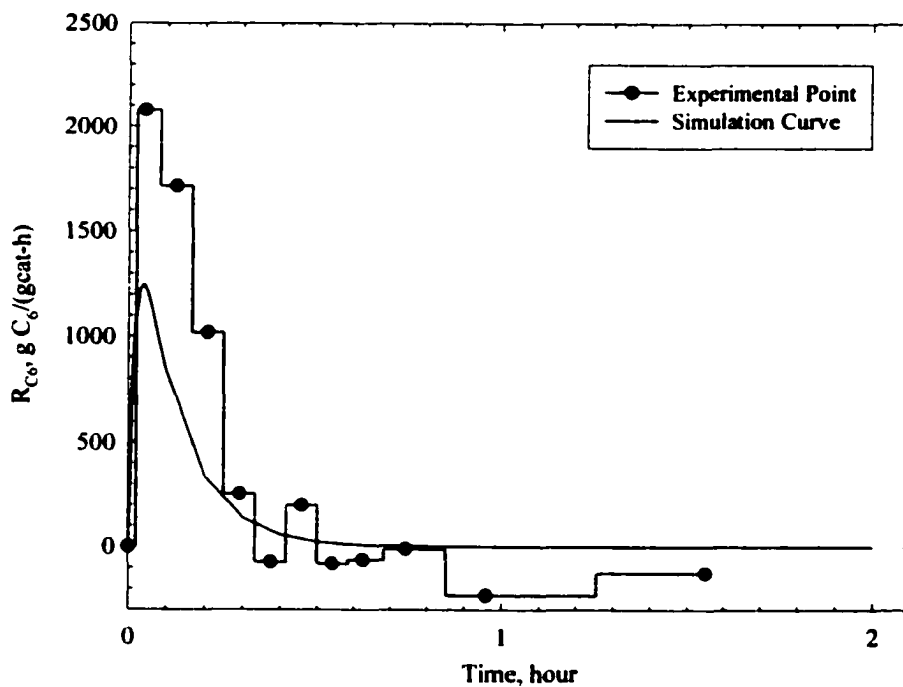


Figure 8.10 (e) 1-Hexene reaction rate and the simulation curve for run GasCo44 ($P_{C_2}=150$ psi, $P_{C_6}=6.2$ psi).

8.4 Comments on Model

8.4.1 Model Improvements

The 3-site model presented in the previous sections provide a fairly good description of the observed 1-hexene/ethylene copolymerization. However, various changes in the model should improve the model-data agreement. Possible improvements are:

1. Fine-tuning of parameters. A considerable amount of trial and error was done to estimate some of the parameter values, but other parameters, such as K_1 and K_2 were estimated from limited data and not varied during the fitting process and others, such as k_{d1} and k_{d1}' , were set equal to each other. Expanding the trial and error search to all parameters will result in improvements.
2. Adding 1-hexene incorporation ability in Site 2. This will increase the number of parameters but this increase will greatly improve the model capability to fit 1-hexene rate profiles.
3. Using better 1-hexene solubility models. More detailed knowledge about the relationship between 1-hexene sorption and polymer structure could result in significant model improvements.
4. Including temperature effects in the model. In the current study, care was taken to exclude macroscopic temperature gradient, but it is possible that temperature gradients are present inside the growing particles during the initial high activity stages of polymerization. Higher temperatures could significantly increase the deactivation rates.

There is little to be gained in understanding the processes occurring during copolymerization by fine-tuning the parameters or adding parameters to including 1-hexene incorporation for Site 2. Improved understanding of solubility properties during copolymerization and quantification of temperature effects would be worthwhile additions to the understanding as well as improvements to modeling of copolymerization. Improved experimental procedures, which would provide improved reliability of experimental rate profiles, would allow the model to be refined and more precise parameters to be estimated. The most significant improvement in experimental

procedures would be to devise better protocols for the intermittent 1-hexene addition which better reflects the 1-hexene consumption.

8.4.2 Additional Comparison of Model and Experimental Results

Two more comparisons of the model with experiments are presented in this section. The relationship between 1-hexene content of the product and 1-hexene partial pressure was shown in Figure 7.5. These experimentally determined values of 1-hexene content are compared with the model predictions in Figure 8.11. It can be seen that experimental results are very well reflected in the model predictions. This provides evidence that the general structure of the model incorporates the significant process of the copolymerization.

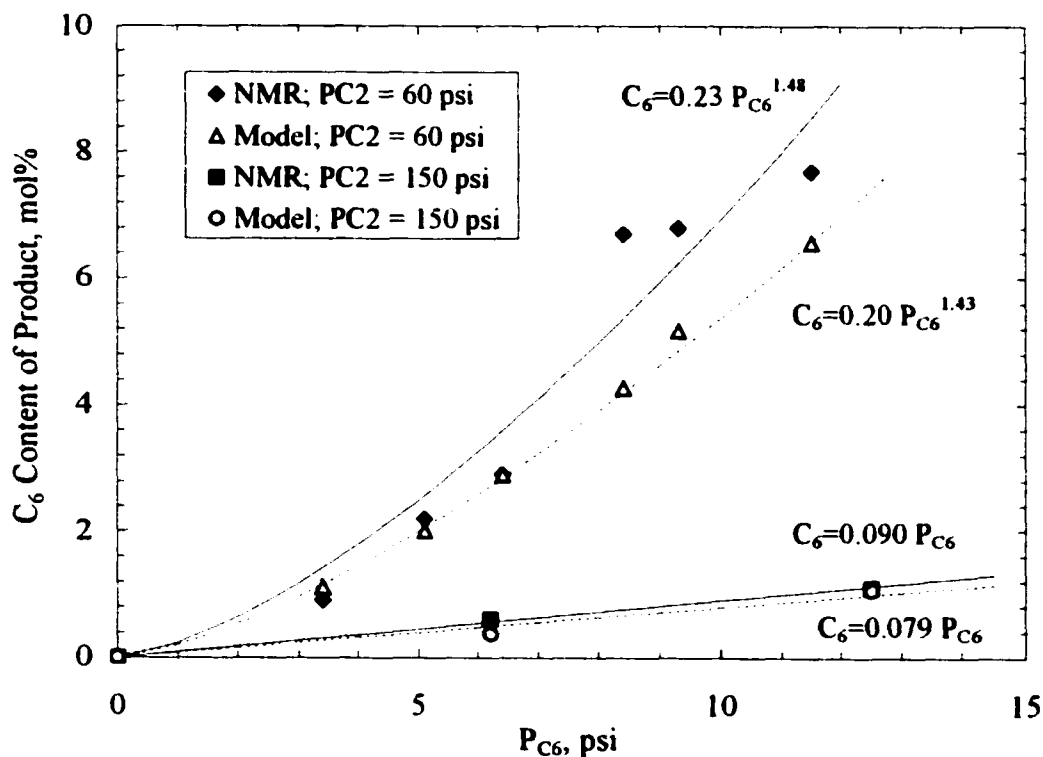


Figure 8.11 Comparison of 1-hexene content measured from ^{13}C -NMR and model predictions.

The ability of the model to predict the homopolymerization activity profile for the 8-h run shown in Figure 8.1 (run GasHo13) was a final test of the model. The comparison of the model prediction and experimental results are shown in Figure 8.12. The initial rates predicted by the model are much higher than those observed, but the results after two hours agree very well with the observed rates; however, the second rate maximum at about 6 h is not predicted by the model. The initial lower than predicted rates are probably due to high temperatures internal particle temperature caused by high initial rates; recall that a 30°C temperature change caused an over 10-fold decrease in average polymerization rate (see Figure 6.19). An additional type of catalytic site is probably required to model the second maxima. The important part of the model prediction is that it predicts that the maximum in the rate occurs at very short times for homopolymerization. This is in agreement with experimental observations. It should be pointed out that no homopolymerization results were used in obtaining the model parameters.

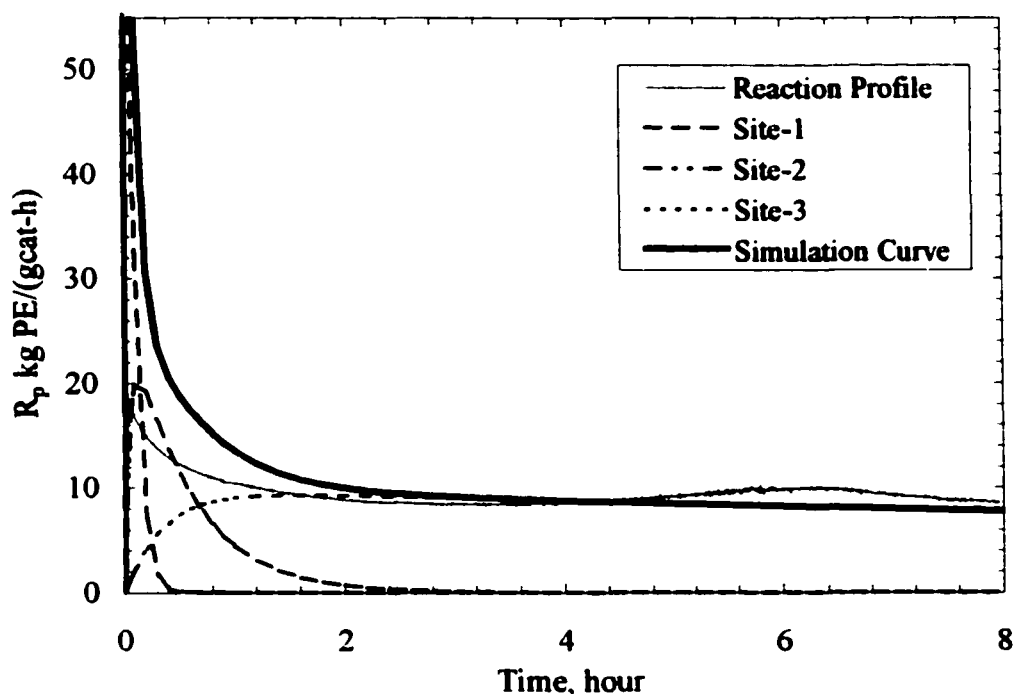


Figure 8.11. Comparison of experimental profile and simulation results of homopolymerization GasHo13 ($P_{C_2}=200$ psi, $P_{C_6}=0$ psi) by applying kinetic parameters listed in Table 8.1.

In summary, the model appears to include the key processes and phenomena which occur during the copolymerization of 1-hexene and ethylene over $\text{TiCl}_4/\text{MgCl}_2$ catalysts. Little can be gained by refining the parameters in the model. It is believed that better understanding and modeling of the olefin solubility in polymers and the interaction of the dissolved polymers with active sites are the key to improved models for copolymerization.

CHAPTER 9 CONCLUSIONS AND RECOMMENDATIONS

9.1 Conclusions and Observations

The conclusions and observations for the current work in the areas of catalyst preparation, prepolymerization, monomer solubility, copolymerization behavior and modeling of 1-hexene/ethylene copolymerization over $\text{TiCl}_4/\text{MgCl}_2$ catalysts are summarized below.

The results of studies with various support and catalyst preparation methods led to the following conclusions:

1. The sphericity of support particles is strongly influenced by the following factors:
 - a) The $\text{C}_2\text{H}_5\text{OH} : \text{MgCl}_2$ ratio in the initial emulsion (it should be about 3 for good supports).
 - b) The stirring time (it should be >20 minutes to establish steady state for the emulsion).
 - c) The particle size could be controlled by the stirring speed and temperature of the emulsion (increases in stirring speed and increases in temperature resulted in smaller particles).
2. The performance of the catalysts was affected significantly by the following:
 - a) The support should be dealcoholated to a $\text{C}_2\text{H}_5\text{OH} : \text{MgCl}_2$ ratio of about 1.5 to 2 in order to obtain catalyst with high activity.
 - b) The rate of TiCl_4 addition should be slow and started at low temperature; drop-wise addition starting at 0°C retained spherical particle shapes in the final polymer products.
 - c) Treatment with excess TiCl_4 and multiple washings with hot heptane removed fines and small particles.
 - d) Addition of dibutylphthalate increased rates of ethylene homopolymerization in the gas phase, decreased 1-hexene incorporation rates, increased bulk densities and improved product morphology;
 - e) The activity of the catalysts was not correlated with the Ti content for catalyst containing 2 to 6.5 mass% Ti.

The observation of the structure of the prepolymer at various stages in the prepolymerization led to the following conclusions:

1. The catalyst particles did not fragment evenly; cracks and voids appeared early in the prepolymerization.
2. A crust on the external surface of the prepolymer resulted in the retention of the spherical shapes in spite of internal cracks and voids.
3. In later stages of prepolymerization, the inside structure of the prepolymer particles became more homogeneous.
4. The Ti was evenly distributed in the catalyst particles, but during the initial stages of prepolymerization, Ti concentration gradients developed in the prepolymer particles; the Ti concentration was lower in the outer layers of the particles than in the interior.
5. The specific activity of prepolymer particles was independent of prepolymer particle size, i.e. the concentration of active sites was not a function of prepolymer size.

The measured ethylene and 1-hexene solubilities in nascent polymer particles and the inferred solubilities for material balance calculations led to the following conclusions:

1. Ethylene solubility in nascent 1-hexene/ethylene copolymers produced in this study is well described by Henry's law.
2. 1-Hexene solubility in nascent 1-hexene/ethylene copolymers produced in this study is well described by the Flory-Huggins equation with activities estimated from the Peng-Robinson equation; the interaction parameter was found to be a linear function of 1-hexene pressure.
3. The solubility of 1-hexene in the presence of ethylene, based on material balance calculations of kinetics runs, was found to be dependent only on the 1-hexene/ethylene ratio at 70°C and ethylene pressures of 60 and 150 psi.

The following effects of operating conditions on activity and activity profiles were observed:

1. The activity profiles for 1-hexene/ethylene copolymerization had a short period of increasing activity, followed by a deactivation to a relatively constant level of activity after 1 to 2 h.
2. Increasing of 1-hexene pressure at constant ethylene pressure resulted in a decrease in total polymerization rate but in an increase in the 1-hexene content of the product.
3. At constant 1-hexene pressure, the 1-hexene consumption rate increased with increasing ethylene pressure.
4. The dependence of rate on ethylene pressure at constant 1-hexene/ethylene ratio was time dependent; at 70°C, the apparent order with respect to ethylene pressure was 1.54 at the maximum rate and 1.0 after two hours.
5. The presence of hydrogen resulted in a large decrease in overall polymerization activity, but in a significant increase in the 1-hexene content of the product. This increase of 1-hexene content in the polymer was not a function of hydrogen concentration.
6. Increasing reaction temperature from 60 to 90°C, the average reaction rates for ethylene and 1-hexene both decreased.
7. The 1-hexene consumption rate was very time dependent and most of the 1-hexene was incorporated into the polymer in the first 20 minutes of polymerization.

The heterogeneity of the polymer product was observed from TREF and DSC analyses, which showed homopolymer signals, and ^{13}C -NMR measurement, which showed very high 1-hexene content in some fractions of the nascent polymer samples.

A three-site kinetic model based on experimental observations was proposed; this model and the parameters estimated from the kinetics and solubility calculations described the observed trend well (hydrogen was not included in the model). The ability of the model to mimic the general experimental trends over wide ranges of conditions suggests that the basic steps in the model are correct.

9.2 Recommendations

This study explored a broad range of variables in the gas-phase copolymerization of 1-hexene and ethylene over $\text{TiCl}_4/\text{MgCl}_2$ catalysts. More detailed studies are required to confirm some of the observations and conclusions of the current work. The result that at isothermal conditions the 1-hexene solubility is only a function of 1-hexene/ethylene ratio must be confirmed by independent solubility measurements on nascent polymers in the absence of reaction. It is also important that the ethylene solubility be determined in the presence of 1-hexene. The effect of hydrogen on olefin solubility should also be measured. I believe that an accurate quantitative description of the solubility of olefins at reaction conditions is required before significant improvements in kinetic models of copolymerization are possible. Hence, it is recommended that detailed studies of olefin sorption by well-characterized nascent polymers be measured.

Other factors which require additional investigation include:

1. The effect of initial exposure of catalysts to 1-hexene should be studied in more detail. Experiments should be done in which the prepolymerized catalysts are initially exposed to premixed 1-hexene/ethylene mixtures of different compositions, i.e. without being exposed to pure 1-hexene.
2. The effects of hydrogen on polymerization rate and 1-hexene incorporation should be studied in more detail. The marked effect of hydrogen on 1-hexene polymer content, but the lack of this dependence on hydrogen pressure should be verified.
3. More detailed studies of the effects of temperature are suggested since most of the experiments in the current work were done at a reaction temperature of 70°C .
4. More detailed distribution measurements of Ti in the catalysts, prepolymer and nascent polymer particles should be done with techniques more sensitive than EDAX, e.g. scanning Auger spectroscopy.
5. Additional ^{13}C -NMR analyses should be done on polymers made in this study; the results of these measurements can be used to test to proposed model.

In addition to the above studies, improvements in the procedure and equipment for the kinetic measurements should be made; these include:

- 1. Development of a better, more reproducible method for the addition of 1-hexene during the experiments. A continuous addition method would be optimum if a rapid analysis method for the 1-hexene/ethylene ratio, such as mass spectroscopy, is added to the system. An automatic control system could then be used to maintain a constant gas phase composition.**
- 2. An improved gas sampling system, which ensures that no condensation occurs in the sampling line, should be installed. Such a sampling system should sample the gas in the reactor directly without any appreciable hold-up, e.g. a zero-volume valve.**
- 3. A reactor with improved temperature control would improve the reproducibility since large amounts of catalyst could be used. It is recommended that a larger reactor, e.g. 2 litres, with improved heat transfer be constructed. Such a reactor should also make it easier to control the 1-hexene/ethylene ratio due to the larger amounts of reactants in the reactor.**

REFERENCES

- Akar, A., Billingham, N.C. and Calvert, P. D., The Morphology of Polyethylenes Produced by Alumina-Supported Transition Metal Alkyls. *Transition Metal Catalyzed Polymerizations Alkenes and Dienes, Part B*, MMI Press, New York, 779-797 (1981).
- Alamo, R., Domszy, R. and Mandelkern, L., Thermodynamic and Structural Properties of Copolymers of Ethylene. *Journal of Physical Chemistry*, **88**, 6587-6595 (1984).
- Al-Sammerrai, D. and Al-Nidawy, N., Polyethylene Synthesis, Properties and Uses. *Handbook of Polymer Science and Technology*, **2**, 341 (1989).
- Bajgur, C. and Sivaram, S., The Evolution of New Generation 'Single-Site' Ziegler-Natta Catalysts. *Current Science*, **78**, 1325-1335 (2000).
- Baker, R. T. K., Harris, P. S., Waite, R. J. and Roper, A. N., Continuous Electron Microscopic Observation of the Behavior of Ziegler-Natta Catalysts. *Polymer Letters Edition*, **11**, 45-53 (1973).
- Barbe, P. C., Noristi, L., Baruzzi, G. and Marchetti, E., Microscopic Analysis of Polyolefin Initial Formation on $\text{TiCl}_4/\text{MgCl}_2$ Supported Catalysts. *Die Makromolekulare Chemie, Rapid Communication*, **4**, 249-252 (1983).
- Barbe, P., Cecchin, G. and Noristi, L., Catalytical and Radical Polymerization. *Advances in Polymer Science*, **81**, 1-81 (1987).
- Barbe, P., Noristi, L., Baruzzi, G. and Marchetti, E., Microscopic analysis of polyolefin initial formation on MgCl_2 -Supported TiCl_4 Catalysts. *Die Makromolekulare Chemie, Rapid Communications*, **4**, 249-252 (1983).
- Baulin, A., Novikova, Y., Maksimov, V., Vyshinskaya, L. and Ivanchev, S., Relation between the Reduction of Titanium in Ziegler Catalysts and Catalytic Activity in Polymerization of Ethylene. *Polymer Science USSR*, **22**, 205-214 (1980).
- Baumhardt-Neto, R., Galland, G. B., Mauler, R. S. and Quijada, R., Optimization of Olefin Copolymerization: Effects of Reaction Parameters on Catalytic Activity and Properties. *Polymer Bulletin*, **40**, 103-109 (1998).
- Beach, D. L. and Kissin, Y. V. High Density Polyethylene. *Encyclopedia of Polymer Science and Engineering*, **6**, 454-490 (1986).
- Beret, S. and Hager, S. L., Ethylene Solubility and Diffusion in Low Density Polyethylene and Ethylene Copolymers. *Journal of Applied Polymer Science*, **24**, 1787-1796 (1979).

- Bialek, M. and Czaja, K., The Effect of the Comonomer on the Copolymerization of Ethylene with Long Chain α -Olefins Using Ziegler-Natta Catalysts Supported on $\text{MgCl}_2(\text{THF})_2$. *Polymer*, **41**, 7899-7904 (2000).
- Blitz, J. P. and McFaddin, D. C., The Characterization of Short Chain Branching in Polyethylene Using Fourier Transform Infrared Spectroscopy. *Journal of Applied Polymer Science*, **51**, 13-20 (1994).
- Böhm, L. L., Ethylene Polymerization Process with a Highly Active Ziegler-Natta Catalyst: 2. Molecular Weight Regulation. *Polymer*, **19**, 562-566 (1978).
- Böhm, L. L., Ethylene Polymerization Process with a Highly Active Ziegler-Natta Catalyst: 1. Kinetics. *Polymer*, **19**, 553-561 (1978a).
- Böhm, L. L., Reaction Model for Ziegler-Natta Polymerization Process. *Polymer*, **19**, 545-552 (1978b).
- Bonini, F., Storti, G., Morbidelli, M. and Carra, S., Modeling of Ziegler-Natta Olefin Polymerization. *Gazzetta Chimica Italiana*, **126**, 75-84 (1996).
- Boor, J., Jr., *Ziegler-Natta Catalysts and Polymerizations*. Academic Press, New York (1979).
- Bosowska, K. and Nowakowska, M. The Role for a Lewis Base and MgCl_2 in Third-Generation Ziegler-Natta Catalysts. *Journal of Applied Polymer Science*, **69**, 1005-1011 (1998).
- Bremner, T. and Rudin, A., Melt Flow Index Values and Molecular Weight Distributions of Commercial Thermoplastics. *Journal of Applied Polymer Science*, **41**, 1617-1627 (1990).
- Brown, R., PE Makers Face Near-Term Pressures. *Chemical Market Reporter*, **257**, 3-24 (2000).
- Bu, N., Lynch, D. and Wanke, S., Kinetics of Catalytic Gas-Phase Homopolymerization of Ethylene over $\text{SiO}_2/\text{MgCl}_2$ -Supported TiCl_4 Catalysts. *Polymer Reaction Engineering*, **3**, 1-22 (1995).
- Buckalew, L. and Schumacher, J. W., Linear Low-Density Polyethylene (LLDPE) Resins, *Chemical Industries Newsletter*, **3**, 2-4 (2000).
- Budzien, J. L., McCoy, J. D., Weihkauf, D. J., LaViolette, R. A. and Peterson, E. S., Solubility of Gases in Amorphous Polyethylene. *Macromolecules*, **31**, 3368-3371 (1998a).

Budzien, J. L., McCoy, J. D., Curro, J. G., LaViolette, R. A. and Peterson, E. S., The Solubility of Gases in Polyethylene: Integral Equation Study of Standard Molecular Models. *Macromolecules*, **31**, 6669-6675 (1998b).

Bukatov, G. D., Yechevskaya, L. G. and Zakharov, V. A., Copolymerization of Ethylene with α -Olefins by Highly Active Supported Catalysts of Various Composition. *Transition Metals and Organometallics as Catalysts for Olefin Polymerization*, Springer-Verlag Press, Berlin, 101-108 (1988).

Burfield, D., Ziegler-Natta Catalysis. A General Kinetic Scheme. *Polymer*, **13**, 302-306 (1972).

Busico, V., Corradini, P., Martino, L. Proto, A. and Savino, V., Polymerization of Propene in the Presence of $MgCl_2$ -Supported Ziegler-Natta Catalysts. I. The Role of Ethyl Benzoate as Internal and External Base. *Die Makromolekulare Chemie*, **186**, 1279-1288 (1985).

Calabro, D. C. and Lo, F. Y., A Comparison of the Reaction Kinetics for the Homo- and Copolymerization of Ethylene and Hexene with a Heterogeneous Ziegler Catalyst. *Transition Metal Catalyzed Polymerizations: Ziegler-Natta and Metathesis Polymerizations*, edited by R. P. Quirk, Cambridge University Press, New York, 729-739 (1988).

Cavallo, L., Guerra, G. and Corradini, P., Mechanism of Propagation and Termination Reactions in Classical Heterogeneous Ziegler-Natta Catalytic Systems: A Nonlocal Density Functional Study. *Journal of the American Chemistry Society*, **120**, 2428-2436 (1998).

Chen, M. P., Gas Phase Olefin Copolymerization with Ziegler-Natta Catalysts. *Ph.D. thesis*, University of Wisconsin (1993).

Cheng, H. N., Automated Approaches for the ^{13}C NMR Characterization of Polyolefins. *Transition Metal Catalyzed Polymerizations Alkenes and Dienes, Part B.*, MMI press, New York, 617-637 (1982).

Chien, J. C. W., Wu, J. and Kuo, C., Magnesium Chloride Supported High-Mileage Catalysts for Olefin Polymerization. I. Chemical Composition and Oxidation States of Titanium. *Journal of Polymer Science: Part A: Polymer Chemistry*, **20**, 2019-2032 (1982).

Chien, J. C. W. and Kuo, C. I., Magnesium Chloride Supported High-Mileage Catalysts for Olefin Polymerization. X. Effect of Hydrogen and Catalytic Site Deactivation. *Journal of Polymer Science: Part A: Polymer Chemistry*, **24**, 2707-2727 (1986).

Chien, J. C. W. and Bres, P., Magnesium Chloride Supported High Mileage Catalysts for Olefin Polymerization. XIII. Effect of External Lewis Base on Ethylene Polymerization. *Journal of Polymer Science: Part A: Polymer Chemistry*, **24**, 1976-1988 (1986).

Chien, J. C. W. and Hu, Y., Magnesium Chloride Supported High-Mileage Catalysts for Olefin Polymerization. XVII. Effect of Lewis Base on Propylene Polymerization. *Journal of Polymer Science: Part A: Polymer Chemistry*, **25**, 2847-2870 (1987).

Chien, J. C. W. and Hu, Y., Superactive and Stereospecific Catalysts. III. Definitive Identification of Active Sites by Electron Paramagnetic Resonance. *Journal of Polymer Science: Part A: Polymer Chemistry*, **27**, 897-913 (1989).

Chien, J. C. W., Weber, S. and Hu, Y., Magnesium Chloride Supported Catalysts for Olefin Polymerization. XIX. Titanium Oxidation States, Catalyst Deactivation, and Active Site Structure. *Journal of Polymer Science: Part A: Polymer Chemistry*, **27**, 1499-1514 (1989).

Chien, J. C. W. and NozaKi, T., High Activity Magnesium Chloride Supported Catalysts for Olefin Polymerization. XXIX. Molecular Basis of Hydrogen Activation of Magnesium Chloride Supported Ziegler-Natta Catalysts. *Journal of Polymer Science: Part A: Polymer Chemistry*, **29**, 505-514 (1991).

Chien, J. C. W. and Nozaki, T., Ethylene-Hexene Copolymerization by Heterogeneous and Homogeneous Ziegler-Natta Catalysts and the Comonomer Effect. *Journal of Polymer Science: Part A: Polymer Chemistry*, **31**, 227-237 (1993).

Chinh, J.C. and Dumain, A. Process for Gas Phase Polymerization of Olefins in a Fluidized Bed Reactor. *US 5028670* (1991).

Cho, H., Chung, J., Han J., Ko Y. and Lee, W., Polymerization of Ethylene and Ethylene/1-Hexene over Ziegler-Natta/Metallocene Hybrid Catalysts Supported on $MgCl_2$ Prepared by a Recrystallization Method. *Journal of Applied Polymer Science*, **70**, 1707-1715 (1998).

Choi, H. K., Kim, J. H., Ko, Y. S. and Woo, S. I., Prediction of the Molecular Weight of Polyethylene Produced in a Semibatch Slurry Reactor by Computer Simulation. *Industrial and Engineering Chemistry Research*, **36**, 1337-1342 (1997).

Choi, J. H., Chung, J.S., Shin, H. W., Song, I. K. and Lee, W. Y., The Effect of Alcohol Treatment in the Preparation of $MgCl_2$ Support by a Recrystallization Method on the Catalytic Activity and Isotactic Index for Propylene Polymerization. *European Polymer Journal*, **32**, 405-410 (1996).

Choi, K. Y. and Ray, W. H., Recent Development in Transition Metal Catalyzed Olefin Polymerization, A Survey. II Propylene Polymerization. *Macromolecular Chemistry and Physics*, **25** 57-97 (1985).

Choi, K. Y., Tang, S. and Sirohi, A., Estimation of Kinetic Parameters in Transition-Metal-Catalyzed Gas-Phase Olefin Copolymerization Processes. *Industrial and Engineering Chemistry Research*, **36**, 1095-1102 (1997).

Chu, K. J. and Park, T. H., Side Chain Effects on the Thermal Properties of Ethylene Copolymers Prepared over Metallocene Catalyst. *Materials Letters*, **31**, 11-14 (1997).

Chu, K. J., Ha, J. W. and Park, T.H., Physical Properties of the Nascent Polyethylenes Prepared with Different Kinds of Catalysts. *Materials Letters*, **30**, 115-118 (1997).

Chu, K. J., Soares, J. B. P., Penlidis and Ihm, S. K., The Influence of the Ti^{3+} Species on the Microstructure of Ethylene/1-Hexene Copolymers. *Macromolecular Chemistry and Physics*, **200**, 1298-1305 (1999).

Chu, K. J., Soares, J. B. P., Penlidis, A. and Ihm S. K., Effect of Prepolymerization and Hydrogen Pressure on the Microstructure of Ethylene/1-Hexene Copolymers Made with $MgCl_2$ -Supported $TiCl_3$ Catalysts. *European Polymer Journal*, **36**, 3-11 (2000).

Chung, J., Han, H., Cho, H., Lee, W. and Park, H., The Effects of Desolvation Methods of the Recrystallized $MgCl_2$ -Alcohol Adduct on Catalyst Characteristics and the Bulk Density of Polyethylene. *Die Angewandte Makromolekulare Chemie*, **253**, 17-25 (1996).

Ciardelli, F., Altomare, A., Arribas, G., Conti, G. and Colle, R., Election Transfer Mechanism in Olefin Polymerization. *Polymer for Advanced Technologies*, **6**, 159-167 (1994).

Cossee, P., Ziegler-Natta Catalysis I. Mechanism of Polymerization of α -Olefins with Ziegler-Natta Catalysts. *Journal of Catalysis*, **3**, 80-88 (1964).

Cruz, V. L., Escalona, A. M. and Martinez-Salazar, J. M., A Theoretical Study of the Comonomer Effect in the Ethylene Polymerization with Zirconocene Catalytic System. *Journal of Polymer Science: Part A: Polymer Chemistry*, **36**, 1157-1167 (1998).

Cunningham, M. F., Dusseault, J. A., Dumas, C. and Hsu, C.C., Kinetics of Propylene Polymerization over $MgCl_2$ Supported Catalysts in a Slurry Reactor. *Transition Metal Catalyzed Polymerizations: Ziegler-Natta and Metathesis Polymerizations*, Cambridge University Press, 136-150 (1988).

Czaja, K. and Krol B., Two-Step Polymerization of Propylene over $MgCl_2$ -Supported Titanium Catalyst. *Macromolecular Chemistry and Physics*, **199**, 451-455 (1998).

Czaja, K. and Krol, B., Nature of Activating Effect of Two-Step Polymerization of Propylene. *Journal of Applied Polymer Science*, **71**, 353-359 (1999).

Czaja, K., Ludmila, A. and Novakshonova, N. K., Deactivation of Oxide-Supported Titanium Catalysts in the Ethylene Polymerization Process. *Macromolecular Chemistry and Physics*, **200**, 983-988 (1999).

Dall'Occo, T., Zucchini, U. and Cuffiani, I., Industrial Aspects of the Production of Catalysts for Ethylene Polymerization. *Transition Metals and Organometallics as Catalysts for Olefin Polymerization*, edited by W. Kaminsky and H. Sinn, Spring-Verlag, Berlin (1988).

Dange, D. K., Heller, J. P. and Wilson, K. V., Poly-1-Hexene, Synthesis and Solubility in Dense Carbon Dioxide. *Journal of Applied Polymer Science*, **32**, 3775-3781 (1986).

De Carvalho, A. B., Gloor, P. E. and Hamielec, A. E., A Kinetic Mathematical Model for Heterogeneous Ziegler-Natta Copolymerization. *Polymer*, **30**, 280-296 (1989).

De Pooter, M., Smith, P. B., Dohrer, K. K., Bennett, K. F., Meadows, M. D., Smith, C. G., Schouwenaars, H. P. and Geerards, R.A., Determination of Composition of Common Linear Low Density Polyethylene Copolymer by ^{13}C -NMR Spectroscopy. *Journal of Applied Polymer Science*, **42**, 399-408 (1991).

Di Nota, V. and Bresadola, S., New Synthesis of a Highly Active δ - MgCl_2 for $\text{MgCl}_2/\text{TiCl}_4/\text{AlEt}_3$ Catalytic Systems. *Macromolecular Chemistry and Physics*, **197**, 3827-3835 (1996).

Doi, Y., Suzuki, E. and Keii, T., Transition Metal Catalyzed Polymerizations: Alkenes, Dienes, Part A., MMI Press, **4**, 47-82 (1983).

Dumas, C. and Hsu, C.C., Propylene Polymerization in a Semibatch Slurry Reactor over Supported $\text{TiCl}_4/\text{MgCl}_2$ /Ethyl Benzoate/Triethyl Aluminum Catalyst. II. A Kinetic Study Based on a Multisite Model. *Journal of Applied Polymer Science*, **37**, 1625-1644 (1989).

Dupuy, J. and Spitz, R., Modification of Ziegler-Natta Catalysts by Cyclopentadienyl-Type Ligands: Activation of Titanium-Based Catalysts. *Journal of Applied Polymer Science*, **65**, 2281-2288 (1997).

Dusseault, J. J. A. and Hsu, C. C., MgCl_2 -Supported Ziegler-Natta Catalysts for Olefin Polymerization: Basic Structures, Mechanism, and Kinetic Behavior. *Macromolecular Chemistry and Physics*, **33**, 103-145 (1993a).

Dusseault, J. J. A. and Hsu, C. C., Gas Phase Polymerization of Ethylene Using MgCl_2 /Ethyl Benzoate/ TiCl_4 + Triethylaluminum Catalyst: Effects of Triethylaluminum and Temperature. *Journal of Applied Polymer Science*, **50**, 431-447 (1993b).

Dyer, G., Manuel L. and Robinson, D., The SCLAIR Story. *Canadian Chemical News*, **49**, 24-25 (1997).

Ferraris, M., Rosati, R., Parodi, S., Giannetti, E. and Albizzati, E., Catalyst Components and Catalysts for the Polymerization of Alpha-Olefins, *US Patent 4,339,054* (1983).

Ferrero, M. A., Koffl, E., Sommer, R., and Conner, W. C., Characterization of the Changes in the Initial Morphology for MgCl₂-Supported Ziegler-Natta Polymerization Catalysts. *Journal of Polymer Science: Part A: Polymer Chemistry*, **30**, 2131-2141 (1994).

Fisa, B., Revol, J. F. and Marchessault, R. H., Crystalline During Polymerization of Ethylene: Successive Events. *Journal of Polymer Science: Polymer Physics Edition*, **12**, 2309-2317 (1974).

Flory, P. J., Molecular Size Distribution in Ethylene Oxide Polymers. *Journal of the American Chemistry Society*, **62**, 1561-1565 (1940).

Flory, P. J., *Principles of Polymer Chemistry*, Cornell University, Ithaca (1953).

Floyd, S., Choi, K. Y., Taylor, T. W. and Ray, W. H., Polymerization of Olefins through Heterogeneous Catalysis. III. Polymer Particle Modeling with an Analysis of Intraparticle Heat and Mass Transfer Effects. *Journal of Applied Polymer Science*, **32**, 2935-2960 (1986a).

Floyd, S., Choi, K. Y., Taylor, T. W. and Ray, W. H., Polymerization of Olefins through Heterogeneous Catalysis. IV. Modeling of Heat and Mass Transfer Resistance in the Polymer Particle Boundary Layer. *Journal of Applied Polymer Science*, **31**, 2231-2265 (1986b).

Floyd, S., Heiskanen, T., Taylor, T. W. and Ray, W. H., Polymerization of Olefins through Heterogeneous Catalysis. VI. Effect of Particle Heat and Mass Transfer on Polymerization Behavior and Polymer Properties. *Journal of Applied Polymer Science*, **33**, 1021-1065 (1987).

Forte, M. C. and Coutinho, F. M. B., Highly Active Magnesium Chloride Supported Ziegler-Natta Catalysts with Controlled Morphology. *European Polymer Journal*, **32**, 223-231 (1996).

Frederick, Y., Nowlin, T. and Shinomoto, R., A Process for Forming a Carrier Material. **WO 9414856**, 1994.

Galli, P., Barbe, P., Guidetti, G., Zannetti, R., Martorana, A., Marigo, A., Bergozza, M. and Fichera, A., The Activation of MgCl₂-supported Ziegler-Natta Catalysts: A Structural Investigation. *European Polymer Journal*, **19**, 19-24 (1983).

Galli, P., Barbe, P. and Noristi, L., High Yield Catalysts in Olefin Polymerization, General Outlook on Theoretical Aspects and Industrial Uses. *Die Angewandte Makromolekulare Chemie*, **120**, 73-90 (1984).

Gerbasì, R., Marigo, A., Martorana, A., Zannetti, R., Guidetti, G. P. and Baruzzi, G., The Activation of MgCl_2 -supported Ziegler-Natta Catalysts-II. *European Polymer Journal*, **20**, 967-970 (1984).

Giannini, U., Polymerization of Olefins with High Activity Catalysts. *Die Makromolekular Chemie: Supplement*, **5**, 216-229 (1981).

Glockner, G., Temperature Rising Elution Fractionation: A Review. *Journal of Applied Polymer Science: Applied Polymer Symposium*, **45**, 1-24 (1990).

Goodall, B. L., Super High Activity Supported Catalysts for the Stereospecific Polymerization of α -Olefins: History, Development, Mechanistic Aspects, and Characterization. *Transition Metal Catalyzed Polymerizations: Alkenes, Dienes, Part A*, edited by R. P. Quirk, Cambridge University Press, New York, 355-378 (1983).

Graff, R. J. L., Kortleve, G. and Vonk, C. G., On the Size of the Primary Particles in Ziegler Catalysts. *Polymer Letters*, **8**, 735-739 (1970).

Guo, M., Cheng, S., Quirk, R. P., Variable Temperature, Solid-State ^{13}C -NMR Study of Linear Low Density Polyethylene. *Olefin Polymerization, Emerging Frontiers, ACS Symposium Series*, **749**, 163-176 (2000).

Gupta, V. K., Advances in Polyolefins Synthesis Using Transition Metal Catalyst Systems. *Journal of Polymer Materials*, **16**, 97-111 (1999).

Guyot, A., Bobichon, C. and Spitz, R., Activation and Stereospecific Control in Propylene Polymerization with MgCl_2 Supported Ziegler-Natta Catalysts. *Transition Metals and Organometallics as Catalysts for Olefin Polymerization*, edited by W. Kamminsky and H. Sinn, Springer-Verlag, Berlin, 13-20 (1988).

Guyot, A., Spitz, Roger, Dassaud, J. P. and Gomez, C., Mechanism of Deactivation and Reaction of Ziegler-Natta Catalysts for Propene Polymerization. *Journal of Molecular Catalysis*, **82**, 29-36 (1993).

Han-Aderekun, G. C., Debling, J. A. and Ray, W. H., Polymerization of Olefins Through Heterogeneous Catalysis. XVI. Design and Control of a Laboratory Stirred Bed Copolymerization Reactor. *Journal of Applied Polymer Science*, **64**, 373-382 (1997a).

Han-Aderekun, G. C., Hamba, M. and Ray, W. H., Kinetic Study of Gas Phase Olefin Polymerization with a $\text{TiCl}_4/\text{MgCl}_2$ Catalyst I. Effect of Polymerization Conditions. *Journal of Polymer Science: Part A: Polymer Chemistry*, **35**, 2063-2074 (1997b).

Hasebe, K., Mori, H. and Terano M., X-Ray Photoelectron Spectroscopy Analysis for Oxidation States of Titanium Chloride on the Surface of Ziegler-Natta Catalysts. *Journal of Molecular Catalysis A: Chemical*, **124**, L1-L3 (1997a).

- Hasebe, K. Mori, H. Keii, T. and Terano M., Titanium Distribution on the Surface of Ziegler-Natta Catalysts Observed by Scanning Auger Electron Microscopy. *Journal of Molecular Catalysis A: Chemical*, **115**, 259-263 (1997b).
- Hindryckx, F., Dubois, Ph., Jerome, R. and Marti, M. G., Ethylene Polymerization by a High Activity $MgCl_2$ Supported Ti catalyst in the Presence of Hydrogen and/or 1-Octene. *Polymer*, **39**, 621-629 (1998).
- Hogan, J. P. and Banks, R. L., Polymers and Production Thereof. *US patent 2,825, 721* (1958).
- Hu, Y. and Chien J., Superactive and Stereospecific Catalysts. I. Structures and Productivity. *Journal of Polymer Science: Part A: Polymer Chemistry*, **26**, 2003-2018 (1988).
- Huang, J. and Rempel G., Ziegler-Natta Catalysts for Olefin Polymerization. *Progress in Polymer Science*, **20**, 459-526 (1995).
- Huang, J. C. K., Lacombe, Y., Lynch, D. T. and Wanke, S. E., Effects of Hydrogen and 1-Butene Concentrations on the Molecular Properties of Polyethylene Produced by Catalytic Gas-Phase Polymerization. *Industrial and Engineering Chemistry Research*, **36**, 1136-1143 (1997).
- Hutchinson, R. A. and Ray, W. H., Polymerization of Olefins Through Heterogeneous Catalysis. VII. Particle Ignition and Extinction Phenomena. *Journal of Applied Polymer Science*, **34**, 657-676 (1987).
- Hutchinson, R. A. and Ray, W. H., Polymerization of Olefins Through Heterogeneous Catalysis. VIII. Monomer Sorption Effects. *Journal of Applied Polymer Science*, **41**, 51-81 (1990).
- Hutchinson, R. A. and Ray, W. H., Polymerization of Olefins Through Heterogeneous Catalysis. IX: Experimental Study of Propylene Polymerization over a High Activity $MgCl_2$ -Supported Ti Catalyst. *Journal of Applied Polymer Science*, **43**, 1271-1285 (1991).
- Hutchinson, R. A. and Ray, W. H., Polymerization of Olefins Through Heterogeneous Catalysis. X: Modeling of Particle Growth and Morphology. *Journal of Applied Polymer Science*, **44**, 1389-1414 (1992).
- Jaber, I. A. and Fink, G., Active Sites Concentration in Ethylene Homo and Copolymerization with 1-Hexene using the Highly Active $TiCl_4/MgH_2-AtEt_3$ Catalyst system. *Journal of Molecular Catalysis A: Chemical*, **98**, 135-141 (1995).

Jaber, I.A. and Ray, W. H., Polymerization of Olefin through Heterogeneous Catalysis. XIII. The Influence of Comonomer in the Solution Copolymerization of Ethylene. *Journal of Applied Polymer Science*, **49**, 1709-1724 (1993).

James, D., E. Linear Low Density Polyethylene. *Encyclopedia of Polymer Science and Engineering*, **6**, 429-454 (1986).

Jejelowo, M. O., Lynch, D. T. and Wanke, S. E., Comparison of Ethylene Polymerization in Gas-Phase and Slurry Reactors. *Macromolecules*, **24**, 1755-1761 (1991).

Jenny, C. and Maddox, P., Supported Polyolefin Catalysts. *Current Opinion in Solid State & Materials Science*, **3**, 94-103 (1998).

Jones, P. and Oldman R., The Application of X-Ray Absorption Spectroscopy to Study the Titanium Environment on MgCl₂-Supported Ziegler-Natta Catalysts. *Transition Metals and Organometallics as Catalysts for Olefin Polymerization*, edited by W. Kamminsky and H. Sinn, Springer-Verlag, Berlin, 223-229 (1988).

Kageyama, K., Tamazawa, J. and Aida, T., Extrusion Polymerization: Catalyzed Synthesis of Crystalline Linear Polyethylene Nanofibers within a Mesoporous Silica. *Science*, **285**, 2113-2115 (1999).

Kakugo, M., Sadatoshi, H., Yokoyama, M. and Kojima, K., Transmission Electron Microscopic Observation of Nascent Polypropylene Particles Using a New Staining Method. *Macromolecules*, **22**, 547-551 (1989a).

Kakugo, M., Sadatoshi, H., Sakai, J. and Yokoyama, M., Growth of Polypropylene Particles in Heterogeneous Ziegler-Natta Polymerization. *Macromolecules*, **22**, 3172-3177 (1989b).

Kang, K., Ok, M. and Ihm, S., Effect of Internal Lewis Base on Recrystallized MgCl₂-TiCl₄ Catalysts for Polypropylene. *Journal of Applied Polymer Science*, **40**, 1303-1411 (1990).

Karbashewski, E., Kale, L., Rudin, A., Tchir, W. J., Cook, D. G. and Pronovost, J. O., Characterization of Linear Low Density Polyethylene by Temperature Rising Elution Fraction and by Differential Scanning Calorimetry. *Journal of Applied Polymer Science*, **44**, 425-434 (1992).

Karbashewski, E., Rudin, A., Kale, L., Tchir, W. J. and Schreiber, S., Effects of Polymer Structure on the Onset of Processing Defects in Linear Low Density Polyethylenes. *Polymer Engineering and Science*, **31**, 1581-1589 (1999).

Karol, F. J., Catalysis and the UNIPOL Process in the 1990s. *Macromolecular Symposium*, **89**, 563-575 (1995).

Karol, F. J., Kao, S, and Cann, K. J., Comonomer Effects with High-Activity Titanium- and Vanadium-Based Catalysts for Ethylene Polymerization. *Journal of Polymer Science: Part A: Polymer Chemistry*, **31**, 2541-2553 (1993).

Karol, F., Cann, K. and Wagner, B., Developments with High-Activity Titanium, Vanadium and Chromium Catalysts in Ethylene Polymerization. *Transition Metals and Organometallics as Catalysts for Olefin Polymerization*, edited by W. Kamminsky and H. Sinn, Springer-Verlag, Berlin, 149-161 (1988).

Kashiwa, N., Super Active Catalyst for Olefin Polymerization. *Polymer Journal*, **12**, 603-608 (1980).

Kashiwa, N. and Yoshitake, J., The Influence of the Valence State of Titanium in MgCl₂ Supported Catalysts on Olefin Polymerization. *Die Makromolekulare Chemie*, **185**, 1133-1138 (1984).

Keii, T., *Kinetics of Ziegler-Natta Polymerization*, Kodansha Ltd., Tokyo and Chapman & Hall Limited, London (1972).

Keii, T., Propene Polymerization with a Magnesium Chloride-Supported Ziegler-Natta Catalyst, 1. Principal Kinetics. *Die Makromolekulare Chemie*, **183**, 2285-2304 (1982).

Keii, T., Doi, Y., Suzuki, E., Tamura, M., Murata, M. and Soga K., Propene Polymerization with a Magnesium Chloride-Supported Ziegler Catalyst, 2. Molecular Weight Distribution. *Die Makromolekulare Chemie*, **185**, 1537-1557 (1984).

Keii, T., Mechanistic Studies on Ziegler-Natta Catalysis. A Methodological Reconsideration. *Studies in Surface Science and Catalysis*, **25**, 1-25 (1986).

Keii, T., Fundamental Aspects of Effects of Hydrogen on Ziegler-Natta Polymerization. *Transition Metal Catalyzed Polymerization*, Harwood Press, New York, 84-104 (1988).

Keszler, B., Bodor, G. and Simon, A., Studies on Highly Active Coordination Catalysts for Polymerization of α -Olefins: 1. X-Ray Diffraction Investigations of the Catalyst Supports. *Polymer*, **21**, 1037-1040 (1980).

Kim, S. H. and Somorjai, G. A., Polymer Growth Mode on the Heterogeneous Ziegler-Natta Catalyst: Active Sites at the Bottom of the Growing Polymer Layer. *Catalysis Letters*, **68**, 7-11 (2000).

Kioka, M. and Kashiwa, N., Study of the Activity Enhancement Caused by the Addition of Hydrogen in Olefin Polymerization. *Journal of Macromolecular Science-Chemical*, **28**, 865-873 (1991).

Kissin, Y. V., *Isospecific Polymerization of Olefins*, Springer-Verlag, New York (1985).

- Kissin, Y. V. and Beach, D. L., Dual Functional Catalysis for Ethylene Polymerization to Branched Polyethylene. II. Kinetics of Ethylene Polymerization with a Mixed Homogeneous-Heterogeneous Ziegler-Natta Catalyst System. *Journal of Polymer Science: Part A: Polymer Chemistry*, **24**, 1069-1084 (1986).
- Kissin, Y. V., Homogeneous Interpretation of Ethylene Polymerization Kinetics with Supported Ziegler-Natta Catalysts. *Journal of Molecular Catalysis*, **56**, 220-236 (1989a).
- Kissin, Y. V., Principles of Polymerizations with Ziegler-Natta Catalysts. *Handbook of Polymer Science and Technology*, **1**, 103-131 (1989b).
- Kissin, Y. V., Ethylene Polymerization Kinetics with Heterogeneous Ziegler-Natta Catalysts. *Die Makromolekulare Chemie, Macromolecular Symposium*, **66** 83-94 (1993).
- Kissin, Y. V., Kinetics of Olefin Copolymerization with Heterogeneous Ziegler-Natta Catalysts. *Die Makromolekulare Chemie, Macromolecular Symposium*, **89**, 113-123 (1995).
- Kissin, Y. V., Mink, R. I. and Nowlin T. E., Ethylene Polymerization Reactions with Ziegler-Natta Catalysts. I. Ethylene Polymerization Kinetics and Kinetic Mechanism. *Journal of Polymer Science: Part A: Polymer Chemistry*, **37**, 4255-4272 (1999a).
- Kissin, Y. V. and Brandolini, A. J., Ethylene Polymerization Reactions with Ziegler-Natta Catalysts. II. Ethylene Polymerization Reactions in the Presence of Deuterium. *Journal of Polymer Science, Part A, Polymer Chemistry*, **37**, 4273-4280 (1999b).
- Kissin, Y. V., Mink, R. I., Nowlin, T. E. and Brandolini, A. J., Ethylene Polymerization Reactions with Ziegler-Natta Catalysts. III. Chain-End Structures and Polymerization Mechanism. *Journal of Polymer Science: Part A: Polymer Chemistry*, **37**, 4281-4294 (1999c).
- Kissin, Y. V., Mink, R. I., Nowlin, T. E. and Brandolini, A. J., Kinetics and Mechanism of Ethylene Homopolymerization and Copolymerization Reactions with Heterogeneous Ti-Based Ziegler-Natta Catalysts. *Topics in Catalysis*, **7**, 69-88 (1999d).
- Kissin, Y.V., Main Kinetic Features of Ethylene Polymerization Reactions with Heterogeneous Ziegler-Natta Catalysts in the Light of a Multicenter Reaction Mechanism, *Journal of Polymer Science: Part A: Polymer Chemistry*, **39**, 1681-1695 (2001).
- Ko, Y. S., Han, T. K., Park, J. W. and Woo, S. I., Copolymerization of Ethylene-1-Hexene over a Thermally Pretreated $MgCl_2/THF/TiCl_4$ Bimetallic Catalyst. *Journal of Polymer Science: Part A: Polymer Chemistry*, **35**, 2769-2776 (1997).

Kohara, T., Shinoyama, M., Doi, Y. and Keii, T., Elimination and Replacement of Organometallic Cocatalysts during Polymerization of Propene with Heterogeneous Ziegler-Natta Catalysts. *Die Makromolekular Chemie*, **180**, 2139-2151 (1979).

Komon, Z., Bu, X. and Bazan, G., Synthesis of Butene-Ethylene and Hexene-Butene-Ethylene Copolymers from Ethylene via Tandem Action of Well-Defined Homogeneous Catalysts. *Journal of the American Chemistry Society*, **122**, 1830-1831 (2000).

Koranyi, T., Magni, E. and Somorjai, G., Surface Science Approach to the Preparation and Characterization of Model Ziegler-Natta Heterogeneous Polymerization Catalysts. *Topics in Catalysis*, **7**, 179-185 (1999).

Kryzhanovskii, A. V., Gapon, I. I. and Ivanchev, S. S., Modification of A Supported $\text{TiCl}_4/\text{MgCl}_2$ Catalyst by SnCl_4 . *Kinetics and Catalysis*, **31**, 90-94 (1990).

Lacombe, Y., TREF and SEC Characterization of Ethylene/1-Butene Copolymers Produced at Various 1-Butene and Hydrogen Pressures. *M. Sc. Thesis, University of Alberta* (1995).

Loos, J., Thune, P.C., Niemantsverdriet, J. W. and Lemstra, P. J., Polymerization and Crystallization of Polyethylene on a Flat Model Catalyst. *Macromolecules*, **32**, 8910-8913 (1999).

Lynch, D.T. and Wanke S.E., Reactor Design and Operation for Gas-Phase Ethylene Polymerization Using Ziegler-Natta Catalysts. *The Canadian Journal of Chemical Engineering*, **69**, 332-339 (1991).

Lynch, D.T., Jejelowo, M. O. and Wanke, S. E., The Influence of Aluminum Alkyls on the Polymerization of Ethylene with $\text{SiO}_2/\text{MgCl}_2$ -Supported TiCl_4 Catalysts. *The Canadian Journal of Chemical Engineering*, **69**, 657-664 (1991).

Malatesta, A., Reactions of Titanium Halides with Organometallic Compounds. *The Canadian Journal of Chemistry*, **37**, 1176-1186 (1959).

Maraschin, N., Polyethylene. *Modern Plastics World Encyclopedia 2001*, B20-B22 (2001).

Marques, M. M. V., Nunes, C. P., Tait, P. J. T. and Dias, A. R., Ethylene Polymerization Process with a Highly Active Ziegler-Natta Catalyst- Kinetic Studies. *Transition Metals and Organometallics as Catalysts for Olefin Polymerization*, Springer-Verlag press. Berlin, 129-134 (1988).

Marques, M. M. V., Nunes, C. P., Tait, P. J. T. and Dias, A. R., Polymerization of Ethylene Using a High-Activity Ziegler-Natta Catalyst. I. Kinetic Studies. *Journal of Polymer Science: Part A: Polymer Chemistry*, **31**, 209-218 (1993).

Marques, M. M., Tait, T. J. T., Mejzlik, J. and Dias, A. R., Polymerization of Ethylene Using High-Activity Ziegler-Type Catalysts: Active Center Determination. *Journal of Polymer Science: Part A: Polymer Chemistry*, **36**, 573-585 (1998).

Mauler, R. S., Galland, G. B., Scipioni, R. B. and Quijada, R., the Effect of the Ethylene Pressure on its Reaction with 1-Hexene, 1-Octene and 4-Methyl-1-Pentene. *Polymer Bulletin*, **37**, 469-474 (1996).

McKenna, T. F., Barbotin, F. and Spitz R. Modeling of Transfer Phenomena on Heterogeneous Ziegler-Natta Catalysts. II. Experimental Investigation of Intraparticle Mass Transfer Resistance during the Polymerization of Ethylene in Slurry. *Journal of Applied Polymer Science*, **62**, 1835-1841 (1996).

McKenna, T. F., Solubility and Crystallinity Data for Ethylene/Polyethylene Systems. *European Polymer Journal*, **34**, 1255-1260 (1998).

McKenna, T. F. and Soares J. B. P., Single Particle Modeling for Olefin Polymerization on Supported Catalysts: A Review and Proposals for Future Developments. *Chemical Engineering Science*, **56**, 3931-3949 (2001).

Mejzlik, J., Vozka, P., Kratochvila, J. and Lesna M., Recent Developments in the Determination of Active Centers in Olefin Polymerization. *Transition Metals and Organometallics as Catalysts for Olefin Polymerization*, edited by W. Kamminsky and H. Sinn, Springer-Verlag, Berlin, 79-90 (1988).

Mingozi, L. and Nascetti, S., Chemical Composition Distribution and Molecular Weight Distribution Determination of Ethylene, 1-Butene LLDPE. *International Journal of Polymer Analysis & Characterization*, **3**, 59-73 (1996).

Mkrtchyan, S. A., Uvarov, B. A., Tsvetkova, V. I. and Tovmasyan, Y. M., Formation and Growth of Polypropylene and Polyethylene Particles During the Polymerization of Olefins on Deposited Catalysts. *Polymer Science U. S. S. R.*, **28**, 2343-2350 (1986).

Monrabal, B., Crystallization Analysis Fractionation: A New Technique for the Analysis of Branching Distribution in Polyolefins. *Journal of Applied Polymer Science*, **52**, 491-499 (1994).

Moore, S. J., Solubility of α -Olefins in Polyethylenes. *M.Sc. Thesis*, University of Alberta (2000).

- Moore, S. J., Wanke, S. E., Solubility of Ethylene, 1-Butene and 1-Hexene in Polyethylenes, *Chemical Engineering Science*, **56**, 4121-4129 (2001).
- Mori, H., Tashino, K. and Terano, M., Study of the Chain Transfer Reaction by Hydrogen in the Initial Stage of Propene Polymerization. *Macromolecules, Rapid Communication*, **16**, 651-657 (1995).
- Morse, P.M., New Catalysts Renew Polyolefins. *Chemical and Engineering News*. 11-16, July 6, 1998.
- Munoz-Escalona, A. and Parada, A., Factors Affecting the Nascent Structure and Morphology of Polyethylene Obtained by Heterogeneous Ziegler-Natta Catalyst. *Journal of Crystal Growth*, **48**, 250-258 (1980).
- Munoz-Escalona, A., Garcia, H. and Alborno, A., Homo-Copolymerization of Ethylene with Highly Active Catalysts Based on $TiCl_4$ and Grignard Compounds. *Journal of Applied Polymer Science*, **34**, 977-988 (1987).
- Murachev, V. B., Terganova, M. V., Makarov, I. G., Shashkina, Y. F., Kazakova, V. M. and Aksenov, V. I., Study of the Deactivation of a Titanium Catalytic System. *Polymer Science U.S.S.R.*, **31**, 560-565 (1989).
- Natta, G., Pino, P., Corradini, P., Danusso, F., Mantica, E., Mazzanti, G. and Moraglio, G., Crystalline High Polymers of α -olefins. *Journal of the American Chemical Society*, **77**, 1708-1710 (1955).
- Neves, C. J., Monteiro, E. and Habert, A. C., Characterization of Fractionated LLDPE by DSC, FTIR, and SEC. *Journal of Applied Polymer Science*, **50**, 817-824 (1993).
- Noristi, L., Marchetti, E., Baruzzi, G. and Sgarzi, P., Investigation on the Particle Growth Mechanism in Propylene Polymerization with $MgCl_2$ -Supported Ziegler-Natta Catalysts. *Journal of Polymer Science: Part A: Polymer Chemistry*, **32**, 3047-3059 (1994).
- Nowlin, T. E., Kissin, Y. V. and Wagner, K. P., High Activity Ziegler-Natta Catalysts for the Preparation of Ethylene Copolymers. *Journal of Polymer Science: Part A: Polymer Chemistry*, **26**, 755-764 (1988).
- Nowlin, T. E., Low Pressure Manufacture of Polyethylene, *Progress in Polymer Science*, **11**, 29-55 (1985).
- Parada, A., Rajmankina, T. and Chirinos J., Study of the $MgCl_2$ Recrystallization Conditions on Ziegler-Natta Catalyst Properties, *Polymer Bulletin*, **43**, 231-238 (1999).
- Park, H. and Lee W. The Effect of Triethylaluminium Treatment on A Ziegler-Natta Catalyst Supported on Magnesium Chloride Prepared by a Recrystallization Method. *European Polymer Journal*, **28**, 1417-1422 (1992).

- Parker, S. F., Maddams, W.F., Vickers, M. E., Williams, K. P. J. and Downs, G. W., Order in Nascent Polyethylene. *Polymer*, **37**, 2755-2757 (1996).
- Peng, D. Y. and Robinson, D.B., A New Two-Constant Equation of State, *Industrial and Engineering Chemistry Fundamentals*, **15**, 59-65 (1976).
- Perez, E., Benavente, R., Bello, A. and Perena, J. M., Effect of Crystallization Conditions on the Morphological Structure of Ethylene-1-Butene Copolymers Obtained by Different Ziegler-Natta Catalyst Systems. *Polymer Engineering and Science*, **31**, 1189-1193 (1991).
- Pino, P., Rotzinger, B. and Von Achenbach, E., The Role of Some Bases in the Stereospecific Polymerization of Propylene with Titanium Catalysts Supported on Magnesium Chloride, *Makromolekulare Chemie, Supplements*, **13**, 105-122 (1985).
- Platzer N., Branched Polyethylene: LDPE and LLDPE. *Industrial and Engineering Chemistry: Production and Research Development*, **22**, 158-160 (1983).
- Puhakka, E., Pakkanen, T. and Pakkanen T., Theoretical Investigations on Ziegler-Natta Catalysis. *Surface Science*, **334**, 289-294 (1995).
- Pullukat, T. and Hoff, R., Silica-Based Ziegler-Natta Catalysts: A Patent Review. *Catalyst Review*, **41**, 389-428 (1999).
- Putanov, P., Kis, E., Fekete, L. and Dingova, E., The Effects of the Architecture of the Ziegler-Natta Catalyst on the Morphology of Polypropylene. *Polyhedron*, **8**, 1867-1869 (1989).
- Ray, W. H., Practical Benefits from Modeling Olefin Polymerization Reactors. *Transition Metal Catalyzed Polymerization*, Harwood Press, New York, 653-590 (1988).
- Revol, J. F., Luk, W. and Marchessault, R. H., Electron Microscope Investigation on Nascent Polyethylene. *Journal of Crystal Growth*, **48**, 240-249 (1980).
- Russell, C. personal communication, (2000).
- Robinson, S. Breaking the Mould, *Chemistry & Industry*, **12**, 377-378 (2001).
- Sacchetti, M. F., Govoni, G. R. and Clarrocchi, A. F., Component and Catalysts for the Polymerization of Olefins. *U.S. Patent*, 5,221,651 (1993).
- Sacchi, M., Forlini, F., Tritto, I. and Locatelli, P., Polymerization Stereochemistry with Ziegler-Natta Catalysts Containing Dialkylpropane Diethers: A Tool for Understanding Internal/External Donor Relationships. *Macromolecules*, **29**, 3341-3345 (1996).

Salajka, Z., Kratochvila, J., Hudec, P and Vecorek, P., One-Phase Supported Titanium-Based Catalysts for Polymerization of Ethylene II. Effect of Hydrogen. *Journal of Polymer Science: Part A: Polymer Chemistry*, **31**, 1493-1498 (1993).

Schmeal, W. R. and Street, J. R. Polymerization in Catalyst Particles: Calculation of Molecular Weight Distribution. *Journal of Polymer Science: Part B: Polymer Physics*, **10**, 2173-2187 (1972).

Sehanobish, K., Patel, R. M., Croft, B. A., Chum, S. P. and Kao, C. I., Effect of Chain Microstructure on Modulus of Ethylene- α -Olefin Copolymers. *Journal of Applied Polymer Science*, **51**, 887-894 (1994).

Seppala, J. V., Copolymers of Ethylene with Butene-1 and Long Chain α -Olefins. I. Decene-1 as Long Chain α -Olefin. *Journal of Applied Polymer Science*, **30**, 3545-3556 (1985).

Sergeev, S. A., Bukatov, G. D., Zakharov, V. A. and Moroz, E., Propylene Polymerization on Titanium-Magnesium Catalysts, 2) Study of Catalyst Formation. *Makromolekular Chemie*, **184**, 2421-2429 (1983)

Shanks, R. A. and Amarasinghe, G., Comonomer Distribution in Polyethylenes Analysed by DSC After Thermal Fractionation. *Journal of Thermal Analysis and Calorimetry*, **59**, 471-482 (2000).

Shariati, A. Hsu, C. C. and Bacon D. W., A Kinetic Model for Ethylene Polymerization with a Polymer Supported Ziegler-Natta Catalyst. *Polymer Reaction Engineering*, **7**, 97-130 (1999).

Shaw, B. M., McAuley, K.B. and Bacon, D. W., Simulation Joint Chain Length and Composition Fractions from Semi-Batch Ethylene Copolymerization Experiments. *Polymer Reaction Engineering*, **6**, 113-142 (1998).

Shin, H. W., Chung, J. S., Song, I. K., Lee, W. Y., Temperature Effect of $TiCl_4$ Impregnation of a Recrystallized $MgCl_2$ Support on Propene Polymerization. *Macromolecular Chemistry and Physics*, **196**, 3765-3770 (1995).

Shirayama, K., Kita, S.I. and Watabe, H., Effects of Branching on Some Properties of Ethylene/ α -Olefin Copolymers. *Die Makromolekulare Chemie*, **151**, 97-120 (1971).

Sindelar, P., Matula, D. and Holecek, J., One Phase Supported Titanium-Based Catalyst for Polymerization of Ethylene IV. Effect of Alkyl Group at Organoaluminium Compound on Catalyst Performance. *Journal of Polymer Science: Part A: Polymer Chemistry*, **34**, 2163-2171 (1996).

Sinn, H. and Kaminsky, W., Ziegler-Natta Catalysis. *Advanced in Organometallic Chemistry*, **18**, 99-149 (1980).

Skomorokhov, V. B., Zakharov, V. A. and Kirillov, V. A., Determination of the Activation Energies of Ethylene Polymerization on Titanium-Magnesium Catalysts: Experiment and Mathematical Modeling. *Kinetics and Catalysis*, **39**, 757-762 (1998).

Skomorokhov, V. B., Zakharov, V. A. and Kirillov, V. A., Investigation of the Kinetics of Ethylene Polymerization with Supported Titanium-Magnesium Catalyst of Various Composition. *Macromolecular Chemistry and Physics*, **197**, 1615-1631 (1996).

Soares, J. B. P. and Hamielec, A. E., General Dynamic Mathematical Modeling of Heterogeneous Ziegler-Natta and Metallocene Catalyzed Copolymerization with Multiple Site Types and Mass and Heat Transfer Resistances. *Polymer Reaction Engineering*, **3**, 261-324 (1995a).

Soares, J. B. P. and Hamielec, A. E., Temperature Rising Elution Fractionation of Linear Polyolefins. *Polymer*, **36**, 1639-1654 (1995b).

Soares, J. B. P., and Hamielec, A. E., Effect of Hydrogen and of Catalyst Prepolymerization with Propylene on the Polymerization Kinetics of Ethylene with a Non-Supported Heterogeneous Ziegler-Natta Catalyst. *Polymer*, **37**, 4599-4605 (1996a).

Soares, J. B. P., and Hamielec, A. E., Kinetics of Propylene Polymerization with a Non-Supported Heterogeneous Ziegler-Natta Catalyst-Effect of Hydrogen on Rate of Polymerization, Stereoregularity, and Molecular Weight Distribution. *Polymer*, **37**, 4607-4614 (1996b).

Soares, J. B. P., Abbott, R. F., Willis, J. N. and Liu X., A New Methodology for Studying Multiple-Site-Type Catalysts for the Copolymerization of Olefins, *Macromolecular Chemistry and Physics*, **197**, 3383-3396 (1996).

Soares, J. B. P., Kime, J. D. and Rempel, G. L., Analysis and Control of the Molecular Weight and Chemical Composition Distributions of Polyolefins Made with Metallocene and Ziegler-Natta Catalysts. *Industrial and Engineering Chemistry Research*, **36**, 1144-1150 (1997).

Soares, J. B. P., A Second Look at Modeling the Multiplicity of Active Site Types of Ziegler-Natta Catalysts with Flory's and Stockmayer's Distribution. *Polymer Reaction Engineering*, **6**, 225-234 (1998).

Soga, K. and Shiono, T., Ziegler-Natta Catalysts for Olefin Productions. *Progress in Polymer Science*, **7**, 1503-1546 (1997).

Soga, K. and Terano, M., Preparation of Highly Active Supported Catalysts for Producing Polypropylene with Less Content of Chloride. *Polymer Bulletin*, **4**, 39-44 (1981).

Soga, K., Chen, S. and Ohnishi, R., Correlation Between the Oxidation States of Titanium and the Polymerization Activities for Higher α -Olefins and Diene Compounds. *Polymer Bulletin*, **8**, 473-478 (1982).

Soga, K., Doi, Y. and Keii, T., The Effect of Magnesium Chloride on the Polymerization of α -Olefins. *8th International Congress on Catalysis, proceedings*, **5**, 349-358 (1984).

Soga, K., Yanagihar, H. and Lee, D. H., Effect of Monomer Diffusion in the Polymerization of Olefins over Ziegler-Natta Catalysts. *Die Makromolekular Chemie*, **190**, 995-1006 (1989).

Starck, P., Studies of the Comonomer Distributions in Low Density Polyethylenes Using Temperature Rising Elution Fractionation and Stepwise Crystallization by DSC. *Polymer International*, **40** 111-122 (1996).

Terano, M. and Kataoka, T., Stopped Flow Polymerization of Propene with Typical $MgCl_2$ -Supported High Yield Catalysts. *Journal of Molecular Catalysis*, **56**, 203-210 (1989).

Usami, T., Gotoh, Y. and Takayama, S., Generation Mechanism of Short Chain Branching Distribution in Linear Low Density Polyethylenes. *Macromolecules*, **19**, 2722-2726 (1986).

Vogel, Al. I., *A Text Book of Quantitative Inorganic Analysis including Elementary Instrumental Analysis*, 3rd Edition, Green and Co. Ltd., London, 788-790 (1961)

Weber, S., Chien, J. C. W. and Hu, Y., Determination of Titanium Oxidation States in a $MgCl_2$ -Supported Ziegler-Natta Catalyst During Aging and Polymerization. *Transition Metals and Organometallics as Catalysts for Olefin Polymerization*, edited by W. Kamminsky and H. Sinn, Springer-Verlag, Berlin, 46-53 (1988).

Weickert, G., Meier, G. B., Pater, J. T. M. and Westerterp, K. R., The Particle as Microreactor: Catalytic Propylene Polymerizations with Supported Metallocene and Ziegler-Natta Catalysts. *Chemical Engineering Science*, **54**, 3291-3296 (1999).

Wignall, G. D., Alamo, R. G., Londono, J. D., Mandelkern, L. and Stehling, F. C., Small Angle Neutron Scattering Investigations of Liquid-Liquid Phase Separation in Heterogeneous Linear Low Density Polyethylene. *Macromolecules*, **29**, 5332-5335 (1996).

Wild, L., Ryle, T. R., Knobeloch, D. C. and Peat, I. R., Determination of Branching Distributions in Polyethylene and Ethylene Copolymers. *Journal of Polymer Science. Polymer Physics Edition*, **20**, 441-455 (1982).

Wild, L., Chang, S. and Shankernarayanan, Improved Method for Compositionnal Analysis of Polyolefins by DSC. *Polymer Preprints of American Chemical Society*, **31**, 270-271 (1990).

Woo, L., Ling, M. T. K., Khare, A.R. and Westphal, S. P., Short Chain Branching Distribution of Amorphous Ethylene Copolymers. *ACS Symposium Seires*, **749**, *Olefin Polymerization, Emerging Frontiers*, Oxford University Press, 2000.

Wu, L., Ethylene Polymerization over Morphology-Controlled Ziegler-Natta Catalysts, *Ph.D. Thesis*, University of Alberta (1999).

Wu, L., Lynch, D. T. and Wanke, S. E., Kinetics of Gas-Phase Ethylene Polymerization with Morphology Controlled MgCl₂-Supported TiCl₄ Catalyst. *Macromolecules*, **32**, 7990-7998 (1999).

Wu, Q., Wang, H. H. and Lin S. A., Homo- and Copolymerization of Ethylene with Prepolymerized Ti/Mg Supported Catalyst. *Die Makromolekulare Chemie, Rapid Communication*, **13** 357-361 (1996).

Xiao, S., Cai, S., Chen, Z. and Liu, H., The Structure Study of Supported Ziegler-Natta Catalysts for the Polymerization of Olefin. *Studies in Surface Science and Catalysis*, **25**, 431-442 (1986).

Xie, T. Y., McAuley, K. B., Hsu, J. C. C. and Bacon, D. W., Modeling Molecular Weight Development of Gas-Phase α -Olefin Copolymerization. *AIChE Journal*, **41**, 1251-1265 (1995).

Xie, T., McAuley, B., Hsu, J.C.C. and Bacon, W., Gas Phase Ethylene Polymerization-Production Process, Polymer Properties and Reactor Modeling. *Industrial and Engineering Chemistry Research*, **33**, 449-479 (1994).

Xu J., Feng, L. and Yang, S., Highly Active Ziegler-Natta Catalyst for Propylene Polymerization. I. The Effect of Internal Electron Donor. *Shi You Hua Gong*, **35**, 172-175 (1998).

Xu, Z., Zhu, Q., Feng, L. X. and Yang S. L., Ethylene/Propene Copolymerization with a TiCl₃ Catalyst: Effects of Prepolymerization. *Die Markromolekulare Chemie, Rapid Communication*, **11** 79-81 (1990).

Yamahiro, M., Mori, H., Nitta, K. and Terano, M., Electron Donor-Induced Improvement of the Microstructure of Polypropene-Block-Poly (Ethene-co-Propene) Synthesized by a Modified Stopped-Flow Polymerization Method and Correlation with Its Crystalline Morphology. *Polymer*, **40**, 5265-5272(1999).

Yano, T., Inoue, T., Ikai, S., Kai, Y. and Tamura, M., Two-Step Polymerization of Propene by Magnesium Supported Catalysts. *Die Makromolekulare Chemie, Rapid Communication*, **7**, 491-495 (1986).

Yaws, C. L., *Thermodynamic and Physical Property Data*, Gulf Publishing Company, Houston (1992).

Yoon, J. S., Yoo, H. S. and Kang, K. S., Solubility of α -Olefins in Linear Low Density Polyethylenes. *European Polymer Journal*, **32**, 1333-1336 (1996).

Younkin, T., Connor, E., Henderson, J., Friedrich, S., Grubbs, R. and Bansleben, D., Neutral, Single-Component Nickel (II) Polyolefin Catalysts That Tolerate Heteroatoms. *Science*, **287**, 460-462 (2000).

Zakharov, V. A., Makhtarulin, S.I., Perkovets, D. V. and Moroz, E. M., Structure, Composition and Activity of Supported Titanium-Magnesium Catalysts for ethylene Polymerization. *Studies in Surface Science and Catalysis*, **25**, 71-89 (1985).

Ziegler, K., Breil, H., Matin, H. and Holzkamp, E., *German Patent 973,626* (1953).

Zhao, L. and Choi, P., Determination of Solvent-Independent Polymer-Polymer Interaction Parameter by an Improved Inverse Gas Chromatographic Approach. *Polymer*, **42**, 1075-1081 (2001).

Zhang, M., Characterization of Commercial Linear Low Density Polyethylenes by TREF, SEC, DSC, and Cross-Fractionation. *M.Sc. Thesis, University of Alberta* (1999).

Zhang, M., Lynch, D. T. and Wanke, S. E., Characterization of Commercial Linear Low Density Polyethylene by TREF-DSC and TREF-SEC Cross-Fractionation. *Journal of Applied Polymer Science*, **75**, 960-967 (2000).

Zlotnikov, L. M., Pnomareva, Ye. L., Khaikin, S. Ya., Korotkov, S. I., Budtov, V. P. and Ivanchev, S. S., Determination of the Concentration of Active Centers and the Propagation Reaction Rate Constants of the Macrochain on Polymerization of Ethylene on Highly Active Catalysts. *Polymer Science U.S.S.R.*, **30**, 16-22 (1988).

APPENDIX A: ANALYSIS OF GAS-PHASE COMPOSITION IN REACTOR BY GAS CHROMATOGRAPHY

A.1 Gas Chromatography System

Gas chromatography (GC) (Hewlett Packard (*hp*) 5890 series II) was used to analyze gas-phase composition in the reactor. The GC column used was a stainless steel column packed with Alltech Porapak Q (80/100) with a length of 85 cm and ID of 0.08 inches.

Teflon tubing was used to connect the reactor to the GC in order to avoid sorption of 1-hexene on the walls of the connecting tubing. Previous observation showed that 1-hexene adsorbed on 316 stainless steel tubing resulting in unreliable analysis. Small diameter Teflon tubing (1/16" O.D. and 0.01" I.D.) was used to minimized the hold-up in the sampling line. The total length of the sampling line connecting the reactor to the GC was about 115 cm.

The GC operation conditions were:

1. Oven temperature $T_{\text{oven}}=175^{\circ}\text{C}$. At higher temperature, the ethylene signal appeared too early and the integration of its area was not complete. At lower temperature, the retention time of 1-hexene peak was long; more time was needed for one analysis cycle.
2. The temperature of FID (flame ionization detector) was 225°C .
3. Pressures for column flow gas and FID gas were $P_{\text{He}}=70$ psi, $P_{\text{H}_2}=20$ psi, $P_{\text{air}}=30$ psi (cylinder regulator pressures).

The integrator used in this study is *hp 3390A* integrator; the parameter settings were:

1. Peak width at half heights (*PK WD*) was 0.01 at the beginning of each run and increased to 0.16 at time 1.30 min.
2. Peak height was attenuated by factor of 4.
3. Chart speed (*CHT SP*) was equal to 1.0 cm/min.
4. Threshold was set to be 3.
5. Stopped plotting at time 2.4 min.

At these conditions, the general retention times for ethylene and 1-hexene were about 0.13 and 1.61 min respectively. The *PK WD* for ethylene and 1-hexene were about 0.012 and 0.193.

A.2 Determination of Response Factors

In GC quantitative analysis, using a FID, the peak area (or strength of signal) is proportional to mole number of the compound. If the sampling volume is constant, then the area is proportional to the concentration of the detected species

$$C = f \cdot A \quad (\text{A.1})$$

where C is the concentration of detected species, A is the integrated area of its GC signal peak and f is the multiplying factor (called response factor in quantitative analysis).

The quantitative analysis of a mixture requires the relative response factor to be known:

$$\frac{C_6}{C_2} = \frac{f_6 \cdot A_6}{f_2 \cdot A_2} = f' \frac{A_6}{A_2} \quad (\text{A.2})$$

Where subscripts 2 and 6 denote ethylene and 1-hexene; f' is the relative response factor.

The experimental results for determining response factors are summarized in Table A.1. The runs were carried out at the same 1-hexene pressure but different ethylene concentrations at 24°C. In these experiments, 1-hexene and ethylene both were added into the reactor once at the beginning. From Table A.1, it can be seen that the response factors are almost constants at different compositions of mixtures.

Table A.1 also suggests that the relative response factors in the experimental range change with the 1-hexene/ethylene mole ratios; f' s varies from 0.31 at low mole ratio of C_6/C_2 to 0.37 at high C_6/C_2 ratio.

Table A.1 Experimental Results of Response Factor Determination.

P_{C_2} psi	P_{C_6} psi	$[C_6]/[C_2]$	$f_2 \times 10^7$	$f_6 \times 10^7$	$f' = f_6/f_2$
Method A: ethylene pressure increasing					
20.3	3.0	0.148	3.86	1.36	0.35
38.2	3.0	0.079	3.8	1.32	0.35
65.4	3.0	0.046	3.77	1.26	0.33
93.5	3.0	0.032	3.75	1.23	0.33
137.4	3.0	0.022	3.73	1.16	0.31
Method B: ethylene pressure decreasing					
135.7	3.0	0.022	1.84	0.57	0.31
100.8	3.0	0.030	1.84	0.6	0.33
77.1	3.0	0.039	1.84	0.62	0.34
43.7	3.0	0.069	1.85	0.65	0.35
23.7	3.0	0.127	1.88	0.69	0.37
22.5	3.0	0.133	1.87	0.67	0.36

The effect of flow rate of sampling gas on the response factor was also examined in this study. The batch experiment was carried out at 70°C, $P_{C_2}=100$ psi, $P_{C_6}=12.1$ psi. The GC sampling valve was adjusted during the experiment in order to obtain different flow rate. The dependence of response factor value on flow rate of sampling gas is given in Figure A.1. It can be seen that the response factor is relatively insensitive to the flow rate of sampling gas.

A.3 Control of 1-Hexene Composition

Two polymerization runs were done to obtain one experiment at constant gas-phase composition. During the first experiment, 1-hexene was added once into the reactor at the beginning of reaction and the 1-hexene content in gas phase was measured by GC during the run. Then a relationship between the change of 1-hexene content and reaction time was calculated and plotted, as shown in Figure 3.4. A non-linear function was used to fit the 1-hexene concentration as a function of time and the rate of 1-hexene disappearance

from the gas phase was obtained by differentiation of this function (see Figure 3.5). In the second experiment, under similar reaction conditions as the first run, 1-hexene was added into the reactor periodically according to the rate of 1-hexene disappearance obtained from the first run. A single 1-hexene addition process lasted 8 to 15 second. Experimental results showed that the initial rates of 1-hexene disappearance from in the second runs were always larger than those in the first runs. In the later stages, the 1-hexene addition rates required to maintain constant 1-hexene concentration in the gas phase were somewhat lower than those predictions from the first runs.

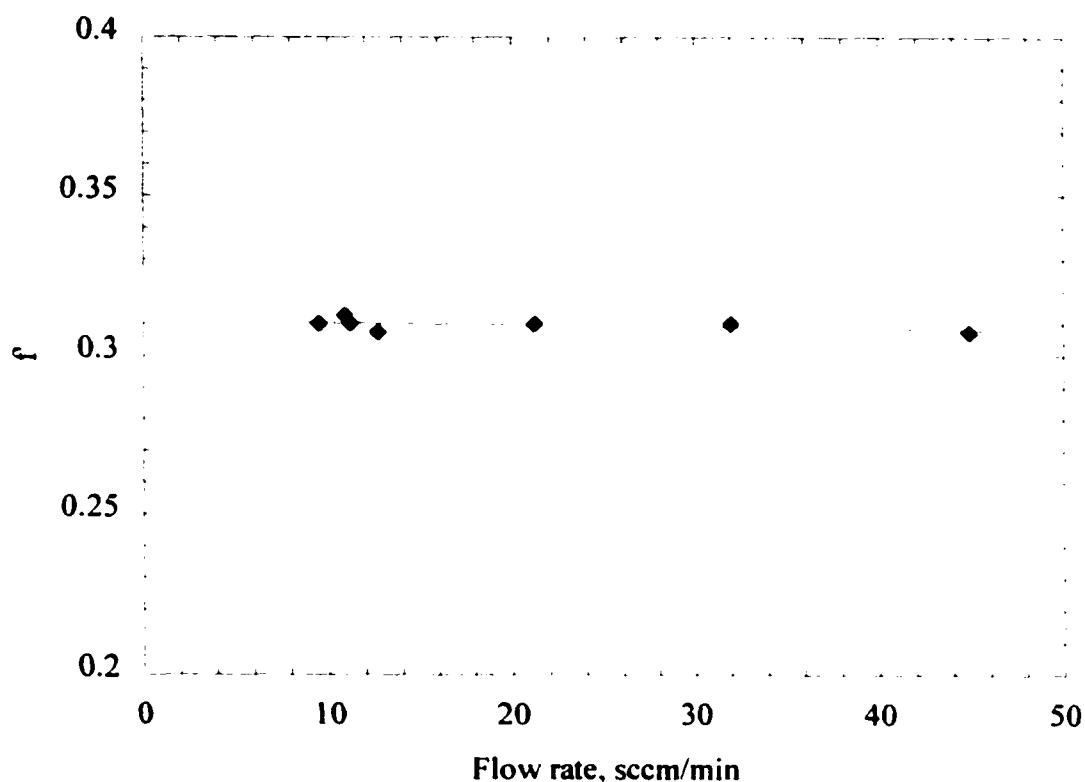


Figure A.1 Dependence of response factor on flow rate of GC sampling gas.

APPENDIX B: 1-HEXENE PHYSICAL AND THERMODYNAMIC PROPERTIES

B.1 Vapor Pressure of 1-Hexene

The vapor pressure of 1-hexene was calculated by Antoine equation. The Antoine coefficients for 1-hexene were obtained from Yaws (1992). The expression is:

$$\begin{aligned} \log P &= A - B/(T + C) \\ A &= 6.8688, \quad B = 1154.646, \quad C = 226.046 \quad (\text{for 1-hexene}) \end{aligned} \quad (\text{B.1})$$

where P is the vapor pressure in mm of Hg and T is the temperature in °C.

B.2 Density of 1-Hexene Liquid

The Rackett equation (Yaws, 1992) was used for liquid density calculations. The Rackett equation is

$$d = A \cdot B^{-(1-T_R)^{2/7}} \quad (\text{B.2})$$

$$A = 0.2416, \quad B = 0.27, \quad T_C = 508.5 \text{ K} \quad (\text{for 1-hexene})$$

where d is the liquid density in g/cm³; T_R is the reduced temperature and $T_R = T/T_C$. At 25°C, the density of 1-hexene is about 0.668 g/cm³.

B.3 PVT Properties of 1-Hexene

Three equations of state were used to compare the predicted P-V-T behavior of 1-hexene, the ideal-gas law, the Redlich-Kwong-Soave equation and the Peng-Robinson equation.

For ideal-gas law

$$PV = nRT \quad (\text{B.3})$$

where V is the volume of reactor, P is the 1-hexene pressure, T is the temperature in reactor and n is the number of moles of 1-hexene.

Redlich-Kwong-Soave equation of state (RKS) is

$$P = \frac{RT}{v-b} - \frac{a(T)}{v(v+b)} \quad (\text{B.4})$$

$$a(T) = a(T_c) \cdot \alpha$$

$$a(T_c) = \frac{0.4278R^2T_c^{2.5}}{P_c}$$

$$\alpha = \left(1 + s(1 - \sqrt{T_r})\right)^2$$

$$s = 0.48508 + 1.55171\omega - 0.15613\omega^2$$

$$b = \frac{0.0867RT_c}{P_c}$$

where v is the molar volume of 1-hexene in m^3/mol ; $P_c=31.6$ bar and $T_c=508.5\text{K}$ for 1-hexene; acentric factor ω is 0.285 for 1-hexene (Yaws, 1992).

Peng-Robinson equation (PR) is similar as RKS equation:

$$P = \frac{RT}{v-b} - \frac{a(T)}{v(v+b) + b(v-b)} \quad (\text{B.5})$$

$$a(T) = a(T_c) \cdot \alpha$$

$$a(T_c) = 0.45724 \frac{RT_c^2}{P_c}$$

$$b = 0.0778 \frac{RT_c}{P_c}$$

$$\alpha = \left[1 + s(1 - \sqrt{T_r})\right]^2$$

$$s = 0.37464 + 1.54226\omega - 0.2699\omega^2$$

Among the above three equations of state, PR and RKS are more suitable for hydrocarbons. The relationships between 1-hexene volume and 1-hexene pressure at 70°C using these three equations are illustrated in Figure B.1. It can be seen that at low pressure, the predictions by the RKS and PR equations are essentially the same and the deviation from ideal-gas law is less than 5%. In this study, the gas-phase composition was calculated by ideal-gas law for both ethylene and 1-hexene during kinetic experiments. Thus, the pressure ratio of ethylene to 1-hexene is equal to the mole ratio of ethylene to 1-hexene.

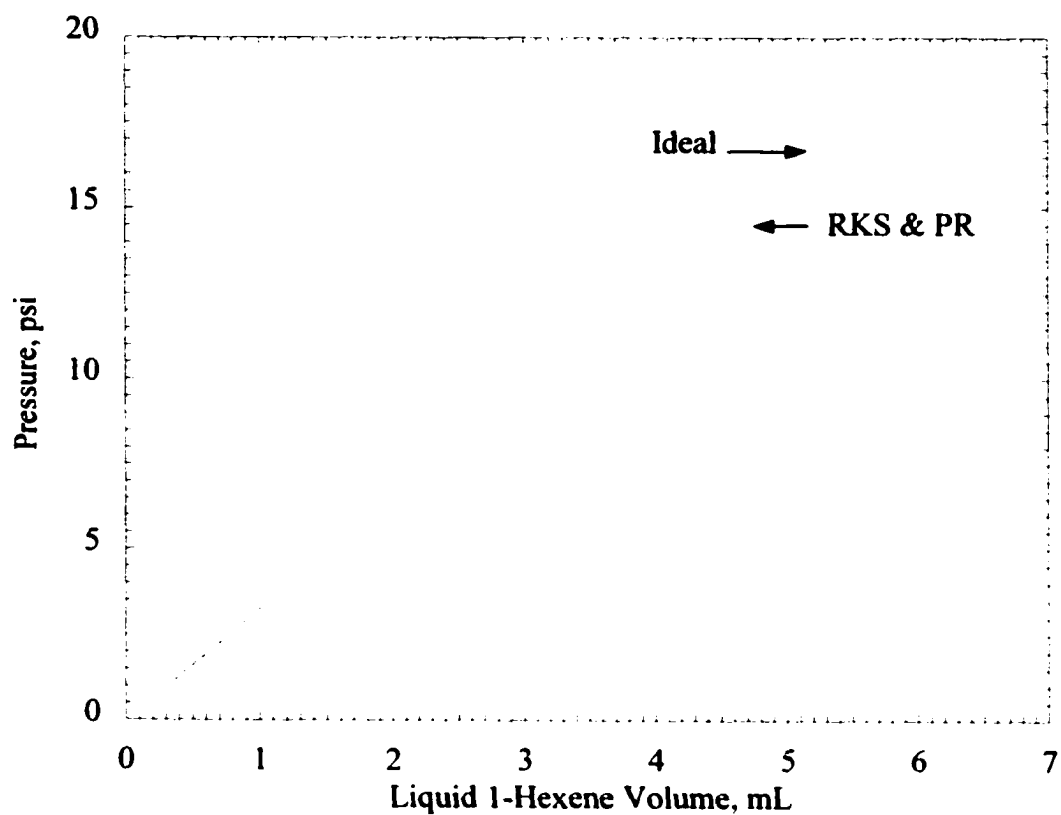


Figure B.1 Comparison of different equations of state (ideal-gas law, PR, RKS) at $T=70^{\circ}\text{C}$.

APPENDIX C: CALCULATION OF 1-HEXENE REACTION RATE

As described in Appendix A, two experiments were carried out to obtain one experiment with controlled gas-phase composition. In the first run, 1-hexene disappearance rate was obtained. In the second the run, 1-hexene was added periodically into the reactor to maintain a constant 1-hexene/ethylene ratio in the gas phase. The amount of 1-hexene added into the reactor is not equal to the 1-hexene incorporation amount into the growing polymer. 1-hexene disappears from the gas phase due to 1-hexene reacted, 1-hexene sorption by the produced polymer and 1-hexene loss in the GC sampling gas. However, the 1-hexene incorporation rate as a function of polymerization time can be estimated from the amount of 1-hexene added at the various times, the measured gas phase 1-hexene/ethylene ratio as a function of time, the polymerization rate as a function of time, the sampling gas flow rate, the 1-hexene content of the final polymer, and the assumption that the solubility of 1-hexene in the growing polymer particle is constant. The 1-hexene content of the final polymer product was obtained by ^{13}C -NMR; all other needed values for the calculation of 1-hexene incorporation rates as a function of polymerization times were measured during each of the copolymerization runs at constant gas-phase composition. The following steps were used in the estimation of 1-hexene incorporation rates as a function of polymerization time for each run:

1. The total amount of 1-hexene in the produced polymer was calculated from mass of polymer made and 1-hexene concentration in the polymer obtained from ^{13}C -NMR measurement (total amount of 1-hexene incorporated = $m_{\text{inc,tot}}$).
2. The total amount of 1-hexene added to the reactor was calculated by summing the various amounts of 1-hexene added during the run (total amount of 1-hexene added = $m_{\text{add,tot}}$).
3. The small change of 1-hexene in the gas phase from beginning to end of run was calculated from the measured 1-hexene/ethylene ratios and the reactor void volume (change in total amount of 1-hexene in gas phase = $\Delta m_{\text{gas,tot}}$).
4. The total amount of 1-hexene removed from the reactor by the sample stream to the GC was calculated from the gas-phase composition and the sample stream flow rate (total amount of 1-hexene to GC = $\Delta m_{\text{samp,tot}}$).

5. The total amount of 1-hexene sorbed by the polymer was calculated from the above quantities, i.e. total amount of 1-hexene sorbed = $m_{\text{sor, tot}} = m_{\text{add, tot}} - m_{\text{inc, tot}} - \Delta m_{\text{gas, tot}} - \Delta m_{\text{samp, tot}}$.
6. The amount of 1-hexene sorbed per gram of polymer was assumed to be constant throughout the experiment and equal to $m_{\text{sor, tot}} / m_{\text{PE, tot}}$, where $m_{\text{PE, tot}}$ is the total amount of polyethylene produced in the run. (This is an approximation since the composition of the polymer varies with time — the amount of 1-hexene sorbed per gram is probably higher at the beginning of the polymerization than at the end since the average 1-hexene content decreases with polymerization time.)
7. The amount of polymer produced as a function of time was obtained by numerical integration of the rate of ethylene addition to the reactor.
8. The amount of 1-hexene incorporated in the time interval between GC analyses, i.e. between additions i-1 and i, was as calculated according to the following equation:

$$m_{\text{inc, i}} = m_{\text{add, i-1}} - \Delta m_{\text{sorp, i}} - \Delta m_{\text{gas, i}} - \Delta m_{\text{samp, i}}$$

Where $m_{\text{add, i-1}}$ = amount of 1-hexene added in addition i-1

$\Delta m_{\text{sorp, i}}$ = amount of 1-hexene sorbed by PE between addition i-1 and i

$\Delta m_{\text{gas, i}}$ = change in amount of 1-hexene in gas phase between addition i-1 and i

$\Delta m_{\text{samp, i}}$ = amount of 1-hexene removed in gas samples stream between addition i-1 and i

9. The average rate of 1-hexene incorporation in the time interval between additions i-1 and i was calculated as

$$r_{\text{c6, avg, i}} = m_{\text{inc, i}} / (t_i - t_{i-1})$$

A sample result of the calculations described above, using the data from Run GasCo40, is shown in Table C.1. The following results for Run GasCo40 were used in the calculations:

The total amount of 1-hexene incorporated into the 9.7 g of PE formed, based on ^{13}C -NMR measurement, was 0.26 g; the decrease in 1-hexene content in the gas phase between the beginning and end of the run was 0.0174 g; and the rate of 1-hexene loss in the gas sampling stream was 0.000825 g/min. The total amount of 1-hexene added during the run was 0.6013 g (see last row in Table C.1). The total amount of 1-hexene sorbed by the PE, according to Step 5 above, is $(0.6013 - 0.26 + 0.0174 - 0.000825 \times 120 =)$ 0.26g. This corresponds to a 1-hexene solubility of 0.027 g C_6/g PE, i.e. 0.26/9.7.

Table C.1 Calculation of 1-Hexene Incorporation Rate of Run GasCo40

Interval Number i	Time min	length of interval $t_i - t_{i-1}$, min	Amount of C ₆ added $m_{add, i}$, g	GC measured C ₆ /C ₂ mole ratio	Increase of C ₆ in gas $\Sigma \Delta m_{gas, i}$, g	Mass PE produced g	C ₆ absorbed by PE $\Sigma \Delta m_{sorp, i}$, g	Cum C ₆ Reacted $\Sigma m_{inc, i}$, g	Amount C ₆ Reacted $m_{inc, i}$, g	Avg. C ₆ React. Rate	
										gC ₆ /h	gC ₆ /gcat-h
0	0	0	0	0.0570	0	0.000	0	0	0	0	0.0
1	1	1	0.1817	0.0560	-0.0109	0.136	0.0036	0.0064	0.0064	0.3853	213.5
2	6	5	0.1313	0.0520	-0.0546	0.805	0.0215	0.2098	0.2034	2.4410	1352.6
3	11	5	0.0606	0.0564	-0.0065	1.484	0.0397	0.2707	0.0609	0.7308	404.9
4	16	5	0.0384	0.0574	0.0043	2.132	0.0570	0.2990	0.0283	0.3391	187.9
5	21	5	0.0242	0.0582	0.0130	2.713	0.0725	0.3090	0.0100	0.1200	66.5
6	26	5	0.0171	0.0582	0.0130	3.254	0.0870	0.3146	0.0056	0.0675	37.4
7	31	5	0.0207	0.0580	0.0109	3.780	0.1010	0.3157	0.0011	0.0126	7.0
8	41	10	0.0179	0.0570	0.0000	4.711	0.1259	0.3140	-0.0016	-0.0098	-5.4
9	51	10	0.0111	0.0564	-0.0065	5.552	0.1484	0.3077	-0.0064	-0.0381	-21.1
10	61	10	0.0207	0.0550	-0.0218	6.334	0.1693	0.3049	-0.0028	-0.0169	-9.4
11	71	10	0.0207	0.0551	-0.0207	7.029	0.1879	0.2976	-0.0073	-0.0436	-24.2
12	81	10	0.0207	0.0553	-0.0185	7.665	0.2049	0.2909	-0.0067	-0.0405	-22.4
13	95	14	0.0182	0.0551	-0.0207	8.476	0.2266	0.2805	-0.0104	-0.0445	-24.7
14	104	9	0.0182	0.0554	-0.0174	8.954	0.2393	0.2751	-0.0053	-0.0355	-19.7
15	120	16	0	0.0554	-0.0174	9.702	0.2593	0.2601	-0.0151	-0.0565	-31.3
Total			0.6013		-0.0174	9.7	0.2593	0.2601			

APPENDIX D: SUMMARY OF SUPPORT AND CATALYST PREPARATIONS AND HOMO- AND CO-POLYMERIZATION RUNS

The preparation conditions and morphology of support particles are summarized in Table D.1. The composition and morphology of the 12 catalysts prepared in this study are given in Table D.2. The summary prepolymerization runs using the 12 catalysts is given in Table D.3. The conditions and results of copolymerization in gas phase are summarized in Table D.4. Table D.5 lists the results of homopolymerization runs and one slurry copolymerization run.

Table D.1 Summary of Support Preparation Conditions

No.	Support name	MgCl ₂ /EtOH	Reaction temp °C	Stirr time min	Stirring rate rpm	Total pressure, bar	Heptane washings °C, times	Mophology Shape and Size (microns)
1	Support-1	3.0	126-131	40	900	4.5	40-60, 15	spheres, irregular and fines, 10-75
2	Support-2	2.9	133	40	1000	4.5	43-48, 18	spheres and fines, 5-70
3	Support-3	3.0	133	N/A	600-850	4.5	50-57,14	spherical and broken particles and fines, 20-90
4	Support-4	3.0	133	45	700-890	4.2	45-60, 15	spheres and fines, 20-90
5	Support-5	3.0	133	60	800-1100	4.5	60-75, 5	spheres and fines, 10-80
6	Support-6	2.9	125-127	50	900	4.5	50-58, 11	spheres and fines, for NOVA
7	Support-7	3.0	122	70	700	5	50-64; 9	spheres and fines, 10-80
8	Support-8	x	x	x	x	x	x	Reactor feeding valve blocked
9	Support-9	3.0	119	160	700	5	55-66, 10	spheres and fines, 10-110
10	Support-10	N/A	111-116	45	700	5	50-66, 16	spheres and fines, 60-130
11	Support-11	3.0	115	120	700	5	46-60, 16	fines, broken and spherical particles, 10-160
12	Support-12	3.2	115	160	700	5	50-64, 18	irregular,spherical and broken particles, 40-120
13	Support-13	x	x	x	x	x	x	Reactor feeding valve blocked
14	Support-14	3.3	120	120	700	6	51-55, 11	spherical and irregular particles and fines,15-110
15	Support-15	3.1	129-130	165	590	6	50,12	spheres and fines,15-80
16	Support-16	3.2	115	230	1000	5.9	54, 12	SEM: spheres and fines, 20-150
17	Support-17	3.5	120	60	900	5	55-60, 12	irregular shape
18	Support-18	2.9	120	20	850	4.5	40-54, 11	most irregular, some spheres
19	Support-19	2.8	131	N/A	820	4.5	40-55, 10	most irregular,some spheres.

Table D.2 Summary of Catalyst Composition and Morphology

Catalyst name	EtOH/Mg Mole Ratio	Ti Addition Procedure		DBP/MgCl ₂ Mole ratio	Ti content wt%*	Morphology observation
		°C	time, h			
Cat-1	1:0.34	-15~-2 110 ml Ti	4.3	0.03	2.1	SEM: spheres and irregular shape and fines. Ti not even distributes
Cat-2	1:1	-20~-5	4.5	0.12	2	Opt: spherical
Cat-3	1:1.4	-22~0	4.5	0.05	4.0	SEM: spheres and irregular shape
Cat-4	1:1.5	-20~0	3.5	0.07	3.5	SEM: spherical; porous inside
Cat-5	1:1.45	-25~-5	5	0.06	3.1	SEM: spheres, some irregular inside solid and porous; 20-100 microns
Cat-6	1:1.8	-15~0	4.5	N/A	5.5	SEM: spheres and fines crack and not smooth, 20-70 microns
Cat-7	1:1.8	-0.3~4.3	1	0	6.5	Opt: spheres, smooth, 25-60 microns
Cat-8	1:1.9	-18~7	2.5	0.08	1.8	SEM: spheres, smooth and cracks outside, some particle broken, 10-80 microns
Cat-9	1:2.5	-4~4	2.5	0.08	1.9	Opt: spheres, broken and fines, 15-50 microns
Cat-10	1:2.8	-15~5	5	0.09	4.3	partially spherical
Cat-11	1:1.8	-15~3	6.2	N/A	4.3	Opt: broken, fine and spherical, 20~60 microns light yellow greenish color, B.D.=0.46 g/cm ³
Cat-12	1:1.9	-16~2.5	2.2	N/A	1.3	Opt: spheres, smooth, 15-50 microns

* Reproducibility of Ti content is within 0.2 wt% Ti.

Note: Opt: optical microscope observation; SEM: SEM observation

Table D.3 Summary of Prepolymerization Runs

Run No.	Run number	Catalyst name	P _{H2} psi	P _{N2} psi	P _{C2H4} psi	Temperature °C	Catalyst amount, g	TEA mL	Time h	Yield g/gcat
1	pre1	Cat-6	16	15	20.5	33	0.082	0.4	2.1	140
2	pre2	Cat-7	16	15	20	30	0.093			no activity
3	pre3	Cat-7	15	15	20	31	0.090	0.415	2.7	83
4	pre4	Cat-7	5	15	10-28	32	0.09	0.4	1.3	166
5	pre5	Cat-7	16	15	6-10-8	29	0.09	0.35	3.0	95
6	pre6	Cat-9	15	16	7	29	0.085	0.38	6.0	32
7	pre7	Cat-6	15	16	5-20	30	0.09	0.35	5	80
8	pre8	Cat-8	15	15	15	31	0.105	0.30	1.4	105
9	pre9	Cat-8	13	14	9	30	0.11	0.21	4.0	90
10	pre10	Cat-8	13	14	9	31	0.11	0.25	3.3	60
11	pre11	Cat-8	15	13	5	30	0.11	0.33	4	83
12	pre12	Cat-5	11	15	15	32	0.126	0.4	3.5	86
13	pre13	Cat-5	11	15	15	31	0.101	0.5	3.9	100
14	pre14	Cat-1	10.8	16	9-7	31	0.1215	0.2	1.8	82
15	pre15	Cat-1	10	16	4-7	31	0.119	0.16	3.5	85
16	pre16	Cat-3	10	15	7-18	30	0.096	0.25	4	74
17	pre17	Cat-4	11	15	8.3	30.5	0.109	0.25	3.5	77
18	pre18	Cat-4	16	15	5-9	30.5	0.1103	0.25	3.8	84
19	pre19	Cat-2	15	16	6	30.3	0.1098	0.25	2.3	72
20	pre20	Cat-2	15	15	6-12	30.3	0.104	0.12	3.0	78
21	pre21	Cat-10	17	28	24	30	0.113	0.50	2.3	73

Table D.4 Summary of Copolymerization Experiments in Gas Phase

No.	Run number	Prepolymer name	prepolym Weight g	P _{H₂} psi	P _{C₂H₄} psi	Initial C ₆ mL(psi)	temp °C	TEA mL	time h	yield, gPE (g PE/(gcat-h))	Morphology, Reaction Condition or Gas Phase Composition (Controlled)	SEC Measurement Mn, Mw
1	GasCo1	pre19	0.155	47	195	6	70	0.27	2	10.1 (2400)	Spherical, B.D.=0.32	27700, 108000
2	GasCo2	pre19	0.149	45	198	6	70	0.27	2	7.1 (1750)	spherical, B.D.=0.32, control gas com	18700, 92400
3	GasCo3	pre18	0.109	50	198	6	70	0.25	2	5.0 (1900)	broken, H ₂ addition before C ₆	12800, 83200
4	GasCo4	pre16	0.150	48	203	6	70	0.28	2	18.1 (4500)	broken, H ₂ addition after C ₆	15400, 101000
5	GasCo5	pre16	0.110	49	198	6	70	0.25	2	6 (2000)	broken, H ₂ addition before C ₆	10700, 90000
6	GasCo6	pre14	0.115	49	198	6	70	0.25	2	4.7 (1700)	broken, H ₂ addition before C ₆	15000, 88000
7	GasCo7	pre4	0.113	46	200	6	70	0.25	2	3.1 (2270)	broken, H ₂ addition before C ₆	16100, 92200
8	GasCo8	pre19	0.120	49	203	6	70	0.25	2	10.5 (3200)	spheres, H ₂ addition after C ₆	21100, 87500
9	GasCo9	pre18	0.110	49	206	6	70	0.25	2	9.1 (3500)	broken, H ₂ addition after C ₆	15200, 81600
10	GasCo10	pre4	0.106	45	200	6	70	0.25	2	3.5 (2700)	broken, H ₂ addition after C ₆	17300, 106000
11	GasCo11	pre18	0.0814	0	195	6	70	0.25	2	21.3 (11000)	broken, no H ₂ test Al/Ti	
12	GasCo12	pre18	0.0392	0	199	6	70	0.25	2	10.7 (11460)	broken, no H ₂ test Al/Ti	
13	GasCo13	pre18	0.1300	0	198	6	70	0.25	2	36.6 (11820)	broken, no H ₂ test Al/Ti	
14	GasCo14	pre18	0.118	0	108	2.3(6.7)	70	0.25	2	14.9 (5300)		
15	GasCo15	pre18	0.120	0	107	2.3	70	0.25	2	14.1 (4930)	[C ₆ /C ₂] _{gas} =0.055; P _{C₆} =5.9 psi	
16	GasCo16	pre18	0.1502	0	61	(3.5)	70	0.27	2	9.5 (2660)		
17	GasCo17	pre18	0.1509	0	61	N/A	70	0.27	2	9.4 (2600)	[C ₆ /C ₂] _{gas} =0.057-0.10; bad control	
18	GasCo18	pre18	0.1500	0	62	1.25	70	0.27	2	8.2 (2300)	[C ₆ /C ₂] _{gas} =0.058; P _{C₆} =3.7 psi	39900, 287000
19	GasCo19	pre18	0.0840	0	150	3(8.7)	70	0.25	2	16.6 (8300)		
20	GasCo20	pre18	0.085	0	151	3	70	0.25	2	15.0 (7400)	[C ₆ /C ₂] _{gas} =0.055; P _{C₆} =8.3 psi	105500, 664000
21	GasCo21	pre18	0.053	0	200	6	70	0.25	2	9.5,7500	catalyst may be poisoned	
22	GasCo22	pre18	0.050	0	200	4.5(12)	70	0.25	2	12.1 (10160)		
23	GasCo23	pre18	0.053	0	200	4.1(11.4)	70	0.25	1	9.2 (14500)		
24	GasCo24	pre18	0.048	0	200	4.3	70	0.25	2	10.7 (9360)	[C ₆ /C ₂] _{gas} =0.057; P _{C₆} =11.5 psi	
25	GasCo25	pre18	0.0535	0	250	5.4(14.2)	70	0.25	2	16.3 (12800)		
26	GasCo26	pre18	0.0532	0	250	5.4	70	0.25	2	17.4 (13700)	[C ₆ /C ₂] _{gas} =0.055; P _{C₆} =13.8 psi	
27	GasCo27	pre18	0.1542	0	60	2.2(6.4)	70	0.27	2	6.1 (1664)		
28	GasCo28	pre18	0.1532	0	60	3.33(9.0)	70	0.27	2	3.2 (878)		
29	GasCo29	pre18	0.1525	0	60	1.85(5)	70	0.27	2	6.6 (1823)	Activity low, no vacuum overnight	
30	GasCo30	pre18	0.1515	0	61	1.5(5.1)	70	0.27	2	8.2 (2265)		
31	GasCo31	pre18	0.1510	0	61	4.05(10.7)	70	0.27	2	2.5 (651)		
32	GasCo32	pre18	0.140	0	61	3.15(7.6)	70	0.27	2	3.2 (960)		

Table D.4 (Cont'd)

No.	Run number	Prepolyme name	prepolym Weight g	P _{H2} psi	P _{Co} psi	Initial C ₀ mL(psi)	temp °C	Teal ml	time h	yield, gPE (g PE/(gcat-h))	Gas Phase Composition (Controlled)	Mn, Mw
33	GasCo33	pre18	0.1535	0	60	2.94(8.3)	70	0.27	2	2.8 (766)		
34	GasCo34	pre18	0.1586	0	60	2.1(6.4)	70	0.27	2	4.5 (1192)	[C ₂ /C ₁] _{gas} =0.105; P _{C₂} =6.3psi	15500, 227000
35	GasCo35	pre18	0.1440	0	60	1.41(4.8)	70	0.27	2	4.5 (1312)	[C ₂ /C ₁] _{gas} =0.085; P _{C₂} =5.1psi	14000, 205000
36	GasCo36	pre18	0.1570	0	62	3.4(9.0)	70	0.27	2	2.6 (695)	[C ₂ /C ₁] _{gas} =0.151; P _{C₂} =9.3psi	9170, 164000
37	GasCo37	pre18	0.1570	0	62	3.15(8.1)	70	0.27	2	2.4 (642)	[C ₂ /C ₁] _{gas} =0.136; P _{C₂} =8.4psi	8550, 157000
38	GasCo38	pre18	0.1922	0	65	4.05(11.4)	70	0.27	2	3.3 (666)	[C ₂ /C ₁] _{gas} =0.18; P _{C₂} =11.5psi	10700, 149000
39	GasCo39	pre18	0.1561	0	60	2.76(7.4)	70	0.27	2	2.3 (619)	[C ₂ /C ₁] _{gas} =0.125; P _{C₂} =7.5psi	7210, 160000
40	GasCo40	pre18	0.1516	0	60	1.16(3.4)	70	0.27	2	9.7 (2611)	[C ₂ /C ₁] _{gas} =0.056; P _{C₂} =3.4psi	26300, 300000
41	GasCo41	pre18	0.097	0	150	4.2(11.5)	70	0.25	2	15.4 (6668)		
42	GasCo42	pre18	0.0973	0	150	4.3(11.7)	70	0.25	2	14.1 (6097)	[C ₂ /C ₁] _{gas} =0.083; P _{C₂} =12.5psi	49900, 248000
43	GasCo43	pre18	0.0891	0	150	2.1(6.9)	70	0.25	2	21.8 (10287)		
44	GasCo44	pre18	0.0700	0	150	2.4(6.5)	70	0.25	2	15.2 (9120)	[C ₂ /C ₁] _{gas} =0.042; P _{C₂} =6.2psi	125000, 666000
45	GasCo45	pre18	0.069	0	150	1.4(3.4)	70	0.25	2	16.4 (9982)	[C ₂ /C ₁] _{gas} =0.022; P _{C₂} =3.2psi	
46	GasCo46	pre18	0.076	0	150	5.2(14)	70	0.25	2	8.0 (4642)	[C ₂ /C ₁] _{gas} =0.093; P _{C₂} =1.4psi	44800, 439000
47	GasCo47	pre18	0.0495	0	250	3.2(8.5)	70	0.24	2	20.8 (17472)		
48	GasCo48	pre18	0.053	0	250	2.8(8.5)	70	0.24	2	20.3 (16086)	[C ₂ /C ₁] _{gas} =0.032; P _{C₂} =8.1psi	
49	GasCo49	pre18	0.056	0	250	3.8(11.4)	70	0.24	2	23.2 (17400)		
50	GasCo50	pre18	0.0532	0	250	5.3(14.1)	70	0.24	2	16.4 (12947)	[C ₂ /C ₁] _{gas} =0.057; P _{C₂} =1.4 psi	
51	GasCo51	pre18	0.0492	0	250	2.2(6.4)	70	0.24	2	20.2 (17243)	[C ₂ /C ₁] _{gas} =0.025; P _{C₂} =6.3psi	
52	GasCo52	pre18	0.0573	0	250	4(11.4)	70	0.24	2	19.7 (14515)	[C ₂ /C ₁] _{gas} =0.047; P _{C₂} =11.7psi	
53	GasCo53	pre18	0.126	0	105	5.5(14)	70	0.27	2	6.45 (2150)	[C ₂ /C ₁] _{gas} =0.134; P _{C₂} =1.4psi	
54	GasCo54	pre18	0.072	0	150	5.4(14)	70	0.25	0.5	3.57 (8330)	[C ₂ /C ₁] _{gas} =9.6%; P _{C₂} =14.4psi	19900, 259000
55	GasCo55	pre18	0.072	0	150	5.3(14)	70	0.25	1	3.98 (4643)		
56	GasCo56	pre18	0.07	0	150	x	70	0.25	0.2	x	Bad control gas phase	
57	GasCo57	pre18	0.079	0	150	5.4(14)	70	0.25	1	5.2 (5530)	[C ₂ /C ₁] _{gas} =0.093; P _{C₂} =1.4psi	40900, 404000
58	GasCo58	pre18	0.069	0	150	5.5(14)	70	0.25	4	8.2 (2495)	[C ₂ /C ₁] _{gas} =0.093; P _{C₂} =1.4psi	58700, 575000
59	GasCo59	pre18	0.116	30	150	4.1(12.5)	70	0.25	2	3.9 (1412)	[C ₂ /C ₁] _{gas} =0.079; P _{C₂} =11.9psi	12500, 103000
60	GasCo60	pre18	0.106	12	150	4.7(12.1)	70	0.25	2	4.5 (1783)	[C ₂ /C ₁] _{gas} =0.08; P _{C₂} =12psi	12900, 131000
61	GasCo61	pre18	0.1035	6	150	4.2(12)	70	0.25	2	7.0 (2846)	[C ₂ /C ₁] _{gas} =0.08; P _{C₂} =12psi	18000, 196000
62	GasCo62	pre18	0.1285	15	150	4.5(12.3)	60	0.25	2	11.2 (3661)	[C ₂ /C ₁] _{gas} =0.078; P _{C₂} =11.8psi	19000, 167000
63	GasCo63	pre18	0.1059	14	150	4.4(12)	80	0.25	2	2.4 (956)		11000, 105000

Table D.4 (Cont'd)

No.	Run number	Prepolymer name	prepolym Weight g	P _{H₂} psi	P _{C₂H₄} psi	Initial C ₆ mL(psi)	temp °C	Teal ml	time h	yield, gPE (g PE/(gcat-h))	Gas Phase Composition (Controlled)	Mn, Mw
64	GasCo64	pre18	0.1100	12	150	4.4(12.1)	80	0.25	2	3.0 (1145)	[C ₂ /C ₁] _{gas} =0.083; P _{C₂} =12.4psi	10400, 108000
65	GasCo65	pre18	0.1190	13	150	4.3(12.1)	90	0.25	2	1.5 (529)	[C ₂ /C ₁] _{gas} =0.083; P _{C₂} =12.4psi	9570, 99200

Table D.5 Summary of Homopolymerization Runs

No.	Run number	Prepolymer name	Mass of pre g	P _{H2} psi	P _{N2} psi	P _{C2H4} psi	temp °C	TEA mL	time h	yield gPE, g/cal/h	Polymer morphology shape, bulk density (g/cm ³) and size (mm)	M _n , M _w
1	GasHo1	pre5	0.15	31	30	50-200	79	0.45	2.2	3.3, 980	spherical and broken, 0.25	
2	GasHo2	pre7	0.19	29	32	50-200	69	0.25	4.2	7.5, 1800	most spherical, 0.36	
3	GasHo3	pre9	0.136	46	20	250	65	0.25	3.1	24.7, 5400	spherical and some irregular, 0.37	
4	GasHo4	pre12	0.153	33	34	196	85	0.11	3.0	3.6, 670	spherical, 0.34	
5	GasHo5	pre12	0.15	30	44	250	70	0.25	5.5	31.5, 3280	broken, 0.33	
6	GasHo6	pre17	0.11	51	15	195	70	0.26	2	10.4, 3700	spherical and broken particles, 0.34	32700, 128000
7	GasHo7	pre18	0.113	53	16	199	70	0.25	1.8	8.9, 3700	spherical, 0.40	27500, 119000
8	GasHo8	pre14	0.129	55	15	200	70	0.26	1.8	6.3, 2200	spherical, 0.33	34100, 137000
9	GasHo9	pre6	0.107	52	14	226	70	0.25	1.5	0.8, 240	spherical, 0.35	
10	GasHo10	pre16	0.112	52	14	206	70	0.25	1.5	8.3, 3500	spherical, 0.38	29900, 113000
11	GasHo11	pre19	0.122	53	14	200	70	0.26	1.5	8.1, 3400	spherical, 0.35	36300, 130000
12	GasHo12	pre12	0.116	52	14	198	70	0.26	1.5	6.3, 3100	spherical, 0.38	30900, 127000
13	GasHo13	pre18	0.094	0	14	198	70	0.21	8	88, 9800	spherical and broken particles	
14	Slu-1	pre13(0.425-0.5)	0.144	40	20	140	70	0.30	2.5	10.7, 3000	spherical, 0.29, 1.73 mm	49000, 196000
15	Slu-2	pre13(0.3-0.35)	0.163	40	20	140	70	0.34	2.5	13.2, 3200	spherical, 0.32, 1.35mm	17300, 149000
16	Slu-3	pre13(0.25-0.3)	0.149	41	21	141	70	0.31	2.5	13.1, 3300	spherical, 0.33, 1.22 mm	43000, 185000
17	Slu-4	pre13(0.21-0.25)	0.150	40	20	141	70	0.31	2.5	13.3, 3500	spherical, 0.34, 1.06 mm	37700, 179000
18	Slu-5	pre13(0.165-0.21)	0.138	39	20	141	70	0.29	2.5	10.4, 2900	spherical, 0.33, 0.89 mm	44100, 167000
19	Slu-6	pre14	0.122	40	22	137	69	0.24	1.9	19.7, 7000	spherical and irregular shape, 0.31	
20	Slu-7	pre16	0.113	39	21	139	70	0.3	2	12.7, 4000	broken	
21	Slu-8	pre18	0.111	40	20	140	70	0.3	2	13.4, 5100	broken	
22	Slu-9	pre18	0.118	40	20	140	70	0.3	2	16.5, 5900	spherical, (C ₆ =5mL, copolymerization)	
2	Slu-10	pre20	0.100	50	25	225	59	0.46	6.5	5.6, 650	broken, 0.35	
23	Slu-11	pre7	0.186	30	22	50-150	69	0.35	3.7	20, 3300	irregular and spherical, 0.31	
24	Slu-12	pre8	0.156	30	30	99	66	0.16	2.0	10.1, 3400	irregular and spherical, 0.31	
25	Slu-13	pre4	0.106	30	20	150	62	0.3	1.6	23.5, 23000	spherical, 0.23	